

**PULSE DOMAIN NOVEL FEATURE
EXTRACTION METHODS WITH APPLICATION
TO ECG BIOMETRIC AUTHENTICATION**

A Thesis Presented to the
**CENTRE FOR EXCELLENCE IN SIGNAL AND IMAGE PROCESSING
DEPARTMENT OF ELECTRONIC AND ELECTRICAL ENGINEERING
UNIVERSITY OF STRATHCLYDE**

In Fulfilment of the Requirements for the Degree of
Doctor of Philosophy

BY
Sairul Izwan Bin Safie

2012

DECLARATION

This thesis is the result of the author's original research. It has been composed by the author and has not been previously submitted for examination which has led to the award of a degree of Doctor of Philosophy. Where appropriate, I have made acknowledgments to the work of others.

The copyright of this thesis belongs to the author under the terms of the United Kingdom Copyright Acts as qualified by University of Strathclyde Regulation 3.50. Due acknowledgement must always be made of the use of any material contained in, or derived from, this thesis.

Signed :

Date :

Copyright © 2012 by

Sairul Izwan Bin Safie

ALL RIGHTS RESERVED

ACKNOWLEDGEMENTS

It has been a very wonderful and valuable three years experience for me working in this research. With strong determination, this thesis is finally compiled. It would not have been possible for me to write this doctoral thesis without the help and support of the kind people around me. It is a pleasure to convey my gratitude to them all in this humble acknowledgment.

First and foremost, I owe my utmost gratitude to my principal supervisor, Prof John J Soraghan for his guidance, sincerity and encouragement from the very early stage of this research. His enthusiasm and expertise in the field of signal processing is unrivalled making him the best idol for me to emulate. His paternalistic advice to me about life as a student, a researcher, a husband and at the same time as a father has facilitated my work and my life at this university. The good advice, support and friendship of my second supervisor, Dr Lykourgos Petropoulakis has been invaluable on both an academic and a personal level, for which I am extremely grateful.

I also like to thank all my friends and colleagues in the Centre for Excellence in Signal and Image Processing (CeSIP), Department of Electronic and Electrical Engineering for creating a very wonderful working and studying atmosphere.

I gratefully thank my sponsor, the Malaysian government, through Majlis Amanah Rakyat (MARA) for giving me the opportunity to pursue my PhD in University of Strathclyde.

To my father, mother, parents-in-law, and my siblings, there are no words that can replace my deep gratitude and thanks for all the support and assistance you have provided to me.

Finally and the most importantly, I would like to express my grateful appreciation to my beloved wife Juliana Dewi whose dedication, love and persistent confidence in me has taken the load off my shoulders. I owe her and my children Safira and Sanie for all the sacrifices they have made, especially of time, emotion, money and pleasure just to satisfy my ambition to hold a PhD degree. I would be lost without their love and support.

Thank you all.

SAIRUL IZWAN BIN SAFIE

UNIVERSITY OF STRATHCLYDE

MARCH 2012

DEDICATION

I would like to dedicate this thesis to:

my wife:

Juliana Dewi

and

my children:

Safira Dhia Irdina

Sanie Isyraq Dawani

ABSTRACT

This thesis presents the concept of representing finite signals in terms of sequential output pulses called pulse domain to extract Electrocardiogram (ECG) features for biometric authentication systems. Two novel methods based on the pulse domain philosophy namely Pulse Active (PA) and Adaptive Pulse Active (APA) techniques are presented in this thesis. A total of 11 algorithms are derived from these two methods and used to generate novel ECG feature vectors. Six algorithms of the PA technique are named as Pulse Active Bit (PAB), Pulse Active Width (PAW), Pulse Active Area (PAA), Pulse Active Mean (PAM), Pulse Active Ratio (PAR) and Pulse Active Harmonic (PAH). Five APA algorithms are named as Adaptive Pulse Active Bit (APAB), Adaptive Pulse Active Width (APAW), Adaptive Pulse Active Area (APAA), Adaptive Pulse Active Mean (APAM) and Adaptive Pulse Active Harmonic (APAH). The proposed techniques are validated using ECG experimental data from 112 subjects. Simulation results indicate that APAW generates the best biometric performance of all 11 algorithms. Selected ranges of PA and APA parameters are determined in this thesis that generates approximate similar biometric performance. Using this suggested range, these parameters are then used as a personal identification number (PIN) which are a part of the proposed PA-APA ECG based multilevel security biometric authentication system.

TABLE OF CONTENTS

DECLARATION.....	I
ACKNOWLEDGEMENTS.....	II
DEDICATION.....	IV
ABSTRACT	V
TABLE OF CONTENTS.....	VI
LIST OF FIGURES	XIII
LIST OF TABLES	XVII
LIST OF ABBREVIATIONS	XVIII
LIST OF SYMBOLS	XX
CHAPTER 1.	1
INTRODUCTION.....	1
1.1. PREFACE	1
1.2. MOTIVATION FOR THIS RESEARCH	2
1.3. SUMMARY OF ORIGINAL CONTRIBUTION	3
1.4. THESIS ORGANIZATION.....	6
CHAPTER 2.	8
BIOMETRIC: SYSTEM, CHARACTERISTIC, ETHICS AND PERFORMANCE	8
2.1. INTRODUCTION	8
2.2. BIOMETRIC SYSTEMS.....	9
2.2.1. <i>Biometric requirements</i>	10

2.2.2.	<i>Overview of a biometric system</i>	10
2.3.	BIOMETRIC CHARACTERISTIC	13
2.3.1.	<i>Overview of biometric characteristic</i>	13
2.3.2.	<i>Behavioural characteristic</i>	14
2.3.3.	<i>External Observable Physiological characteristic</i>	15
2.3.4.	<i>Internal Physiological characteristic</i>	16
2.4.	MULTIMODAL BIOMETRIC	17
2.5.	ETHICAL ISSUE IN BIOMETRIC	18
2.6.	PERFORMANCE EVALUATION	19
2.6.1.	<i>Similarity scores</i>	20
2.6.2.	<i>Confusion matrix</i>	22
2.6.3.	<i>Decision error ratio</i>	23
2.6.4.	<i>Receiver operating characteristic (ROC)</i>	23
2.7.	CONCLUSION	24
 CHAPTER 3.		25
ELECTROCARDIOGRAMS FOR HUMAN RECOGNITION		25
3.1.	INTRODUCTION	25
3.2.	ELECTROCARDIOGRAM	26
3.2.1.	<i>Electrical conductivity of the heart</i>	26
3.2.2.	<i>ECG morphology</i>	27
3.2.3.	<i>Fiducial points and detection</i>	28
3.2.4.	<i>ECG lead configuration</i>	29
3.3.	ECG AS A BIOMETRIC	30
3.3.1.	<i>ECG advantages as biometric</i>	30
3.3.2.	<i>The challenges implementing ECG as a biometric</i>	32
3.3.3.	<i>Processing ECG with noise</i>	33
3.4.	ECG DATABASE	37
3.4.1.	<i>ECG recording requirements</i>	37
3.4.2.	<i>Physikalisch-Technische Bundesanstalt (PTB) database</i>	37
3.4.3.	<i>ECG filtering</i>	39

3.5. ECG BASED FEATURE EXTRACTION TECHNIQUE	39
3.5.1. Characteristic based feature	43
3.5.1.1. Amplitude, duration and slope	43
3.5.1.2. Amplitude and duration	44
3.5.1.3. Temporal Duration	46
3.5.1.4. The whole ECG trace	48
3.5.2. Waveform based feature.....	49
3.5.2.1. Form Factor	49
3.5.2.2. Correlation Coefficient	50
3.5.2.3. Fourier Coefficient	51
3.5.2.4. Combine Waveform and Characteristic features	51
3.5.2.5. Auto Correlation	53
3.5.2.6. Phase Space reconstruction.....	54
3.5.2.7. Wavelet Coefficient	55
3.5.3. Summary and critical evaluation.....	56
3.6. CONCLUSION.....	58

CHAPTER 4. 59

PULSE ACTIVE (PA) FEATURE EXTRACTION TECHNIQUE FOR ECG BIOMETRIC AUTHENTICATION..... 59

4.1. INTRODUCTION	59
4.2. PULSE DOMAIN PHILOSOPHY	60
4.3. FUNDAMENTAL OF PULSE ACTIVE (PA)	60
4.3.1. Pulse Active Topology	61
4.3.2. Pulse Width Modulation	61
4.4. FEATURE EXTRACTION	62
4.4.1. Above Maximum Area (AMA).....	65
4.4.2. First Rise Last Fall (FRLF)	67
4.5. FEATURE LOCATION	68
4.5.1. Single complex	69
4.5.2. Peak R to the next Peak of R	70

4.5.3.	<i>QRS complex</i>	71
4.5.4.	<i>Peak P to Peak T</i>	72
4.6.	FEATURE SELECTION	72
4.6.1.	<i>Pulse Active Bit (PAB)</i>	73
4.6.2.	<i>Pulse Active Width (PAW)</i>	73
4.6.3.	<i>Pulse Active Area (PAA)</i>	74
4.6.4.	<i>Pulse Active Mean (PAM)</i>	75
4.6.5.	<i>Pulse Active Harmonic (PAH)</i>	75
4.6.6.	<i>Pulse Active Ratio (PAR)</i>	78
4.7.	EXPERIMENTAL SETUP	81
4.7.1.	<i>Setting up the training and test databases</i>	81
4.7.2.	<i>Generating matching scores</i>	84
4.7.3.	<i>Simulation Procedure</i>	85
4.8.	EXPERIMENTAL RESULTS	88
4.8.1.	<i>Experiment 1 : Evaluation of extraction locations</i>	88
4.8.1.1.	<i>AUR and EER profile for T_{ECG} between P_s and T_e</i>	88
4.8.1.2.	<i>AUR and EER profile for T_{ECG} between peaks of R</i>	89
4.8.1.3.	<i>AUR and EER profile for T_{ECG} between peaks P and T</i>	91
4.8.1.4.	<i>AUR and EER profile for T_{ECG} within QRS complex</i>	92
4.8.1.5.	<i>Conclusion on the effect of T_{ECG} location</i>	93
4.8.2.	<i>Experiment 2 : The optimum algorithms</i>	94
4.8.3.	<i>Experiment 3 : The optimum similarity measure</i>	97
4.8.4.	<i>Experiment 4 : Optimized PA parameters</i>	99
4.8.4.1.	<i>Effect of varying m_f and m_i</i>	99
4.8.4.2.	<i>Effect of varying O_{max} and O_{min}</i>	104
4.8.4.3.	<i>Effect of varying N</i>	107
4.8.4.4.	<i>Summary of varying PA parameters</i>	108
4.9.	CONCLUSION	111

CHAPTER 5.	112
ADAPTIVE PULSE ACTIVE (APA) FEATURE EXTRACTION TECHNIQUE FOR ECG BIOMETRIC AUTHENTICATION	112
5.1. INTRODUCTION	112
5.2. FUNDAMENTALS OF ADAPTIVE PULSE ACTIVE (APA)	113
5.2.1. <i>Delta Modulation (DM)</i>	113
5.2.2. <i>Adaptive Pulse Active Waveform Generation</i>	115
5.2.2.1. <i>Defining the start and end locations</i>	115
5.2.2.2. <i>Generation of ECG envelopes</i>	116
5.2.2.3. <i>Triangular wave generation</i>	117
5.2.2.4. <i>Extracting Features</i>	118
5.2.3. <i>Adaptive Pulse Active Generalize Equation</i>	121
5.3. APA FOR ECG BIOMETRIC AUTHENTICATION	123
5.4. FEATURE SELECTION	126
5.4.1. <i>Adaptive Pulse Active Bit (APAB)</i>	128
5.4.2. <i>Adaptive Pulse Active Width (APAW)</i>	128
5.4.3. <i>Adaptive Pulse Active Area (APAA)</i>	128
5.4.4. <i>Adaptive Pulse Active Mean (APAM)</i>	129
5.4.5. <i>Adaptive Pulse Active Harmonic (APAH)</i>	130
5.5. EXPERIMENTAL RESULTS	133
5.5.1. <i>Experiment 1: The optimum extraction location</i>	133
5.5.1.1. <i>T_{ECG} between P_s and T_e</i>	134
5.5.1.2. <i>T_{ECG} between P and T</i>	135
5.5.1.3. <i>T_{ECG} within QRS complex</i>	136
5.5.1.4. <i>Summary of T_{ECG} selection using APA</i>	137
5.5.2. <i>Experiment 2 : The optimum algorithms</i>	138
5.5.3. <i>Experiment 3 : The optimum similarity measure</i>	142
5.5.4. <i>Experiment 4 : Optimized APA parameters</i>	144
5.5.4.1. <i>Effect of varying m_f and δ_i</i>	145
5.5.4.2. <i>Effect of varying O_{max} and O_{min}</i>	149
5.5.4.3. <i>Effect of varying N</i>	151
5.5.4.4. <i>Summary of APA optimization study</i>	152

5.6.	CONCLUSION.....	155
CHAPTER 6.....		156
PA-APA ECG BASED MULTILEVEL SECURITY BIOMETRIC AUTHENTICATION SYSTEM.....		156
6.1.	INTRODUCTION.....	156
6.2.	PA AND APA PARAMETER RANGES.....	157
6.3.	MULTILEVEL SECURITY AUTHENTICATION SCHEME.....	158
6.3.1.	<i>Insert card or token</i>	158
6.3.2.	<i>Key in personal identification number (PIN)</i>	158
6.3.2.1.	<i>The first digit p_1</i>	159
6.3.2.2.	<i>The second digit p_2</i>	160
6.3.2.3.	<i>The third digit p_3</i>	160
6.3.2.4.	<i>The fourth digit p_4</i>	161
6.3.3.	<i>Submit ECG as biometric</i>	161
6.4.	PIN: THE FIRST LEVEL OF SECURITY.....	162
6.5.	PERFORMANCE EVALUATION.....	163
6.5.1.	<i>Case 1 : Only ECG is compromised-no breach</i>	166
6.5.2.	<i>Case 2 : Only ECG is compromised- the system is breached</i>	166
6.5.3.	<i>Case 3 : Both PIN and ECG are not compromised – with fraudster attempt</i>	167
6.5.4.	<i>Case 4 : No fraudster attempt</i>	167
6.5.5.	<i>Case 5 : Only PIN is compromised</i>	167
6.5.6.	<i>Results</i>	168
6.6.	DISCUSSION.....	170
6.6.1.	<i>System performance in breach</i>	170
6.6.2.	<i>System performance with noise</i>	170
6.6.3.	<i>Advantages of proposed system</i>	173
6.7.	CONCLUSION.....	174

CHAPTER 7.	175
CONCLUSIONS	175
7.1. THESIS CONCLUSION	175
7.2. FUTURE WORK	178
AUTHOR’S PUBLICATIONS	180
<i>Patent Publication</i>	180
<i>Journal Publications</i>	180
<i>Conference Publications</i>	181
APPENDICES	182
A. <i>Example of generating Receiver Operating Characteristic (ROC) Curve</i>	182
B. <i>Example of generating average ECG signal for databases</i>	192
C. <i>AUR and EER performance for PA feature extraction technique using suggested PA Parameters</i>	202
D. <i>AUR and EER performance for APA feature extraction technique using suggested APA Parameters</i>	207
E. <i>Example of PA and APA performance on non biometric applications</i>	213
REFERENCES	215

LIST OF FIGURES

Figure 2-1 : Basic processing steps in biometric recognition	11
Figure 2-2 : Authentication Mode.....	12
Figure 2-3 : Identification Mode	12
Figure 2-4 : Biometric Operational modes.....	13
Figure 2-5 : Types of biometric characteristic	14
Figure 2-6 : Confusion Matrix	22
Figure 3-1 : Electrical conductivity of the heart	26
Figure 3-2 : Electrocardiogram Complex	27
Figure 3-3 : 10 leads electrode placement in standard 12 Leads configuration.....	29
Figure 3-4 : Einthoven’s triangle	30
Figure 3-5 : Example of Typical ECG recording.....	34
Figure 3-6 : Example of ECG noises	34
Figure 3-7 : Example of typical ECG signal band pass filtered from 2 to 40 Hz	36
Figure 3-8 : Time intervals between recordings	38
Figure 3-9 : Feature Vector used by Biel <i>et al</i> [68] for classification.....	44
Figure 3-10: Feature Vector used by Kyoso <i>et al</i> [69] for classification.....	45
Figure 3-11: Feature Vector used by Gahi <i>et al</i> [73] for classification	46
Figure 3-12: Feature Vector used by Israel <i>et al</i> [70] for classification	47
Figure 3-13: QRS characteristic used by Palaniappan <i>et al</i> [75] to generate feature vector using form factor.....	50
Figure 3-14: QRS characteristic used by Shen <i>et al</i> [66] to generate feature vector using correlation coefficient	51
Figure 3-15: Characteristic features used by Wang <i>et al</i> [109] without PCA and LDA features.....	53
Figure 4-1: Topological Structure of Pulse Active Technique	61

Figure 4-2: Simple Example of PWM Generation.....	62
Figure 4-3: Waveform generation of Pulse Active technique.....	63
Figure 4-4: Pulse Active output generation using AMA without error	66
Figure 4-5: Pulse Active output generation using AMA with error.....	66
Figure 4-6: Pulse Active output generation using FRLF	68
Figure 4-7: ECG extracted from P_s to T_e	69
Figure 4-8: ECG extracted from R to the next R	70
Figure 4-9: ECG extracted within QRS complex	71
Figure 4-10: Waveform generation of Pulse Active Harmonic	77
Figure 4-11: Summary of setting up simulation databases	82
Figure 4-12: Matching Score Process	84
Figure 4-13 : Simulation Procedure	86
Figure 4-14: AUR profile for T_{ECG} location from P_s to T_e	89
Figure 4-15: EER profile for T_{ECG} location from P_s to T_e	89
Figure 4-16: AUR profile for T_{ECG} location from R to the next R	90
Figure 4-17: EER profile for T_{ECG} location from R to the next R	90
Figure 4-18: AUR profile for T_{ECG} location between peaks P and T	91
Figure 4-19: EER profile for T_{ECG} location between peaks P and T	92
Figure 4-20: AUR profile for T_{ECG} location within QRS complex.....	92
Figure 4-21: EER profile for T_{ECG} location within QRS complex.....	93
Figure 4-22: ROC comparison for Healthy Population	95
Figure 4-23: ROC comparison for Arrhythmia Population	95
Figure 4-24: Distance Measurement Comparison For Healthy Population.....	97
Figure 4-25: Distance Measurement Comparison For Arrhythmia Population.....	98
Figure 4-26: AUR profile for PAB	100
Figure 4-27: EER profile for PAB	100
Figure 4-28: AUR profile for PAW, PAA and PAM.....	101
Figure 4-29: EER profile for PAW, PAA and PAM.....	101
Figure 4-30: AUR profile for PAR	102
Figure 4-31: EER profile for PAR	102
Figure 4-32: AUR profile for PAH	103
Figure 4-33: EER profile for PAH.....	103

Figure 4-34: Effects of O_{max} and O_{min} on AUR profiles for PAA and PAM	104
Figure 4-35: Effects of O_{max} and O_{min} on EER profiles for PAA and PAM	105
Figure 4-36: Effects of O_{max} and O_{min} on AUR profiles for PAR	105
Figure 4-37: Effects of O_{max} and O_{min} on EER profiles for PAR	106
Figure 4-38: Effects of N on AUR profiles for PAH	107
Figure 4-39: Effects of N on EER profiles for PAH	107
Figure 5-1 : Block Diagram of DM.....	114
Figure 5-2 : Waveform generation of DM	114
Figure 5-3 : ECG as investigated signal from peak P to peak T	115
Figure 5-4 : ECG envelopes generation	116
Figure 5-5 : Triangular wave generation.....	117
Figure 5-6 : Interception line generation.....	119
Figure 5-7 : Pulse Generation	119
Figure 5-8 : APA Output pulse representation.....	127
Figure 5-9 : Waveform generation of Adaptive Pulse Active Harmonic.....	131
Figure 5-10 : APA profile for T_{ECG} from P_s to T_e	134
Figure 5-11 : APA profile for T_{ECG} from P to T	135
Figure 5-12 : APA profile for T_{ECG} within QRS	136
Figure 5-13 : APA ROC comparison for Healthy Population	139
Figure 5-14 : APA ROC comparison for Arrhythmia Population	140
Figure 5-15: APA feature extraction phenomenon	141
Figure 5-16 : APA distance measurement comparison for healthy population	142
Figure 5-17 : APA distance measurement comparison for Arrhythmia population	143
Figure 5-18 : APAB profile when m_f and δ_i varies.....	145
Figure 5-19 : APAW profile when m_f and δ_i varies	146
Figure 5-20 : APAA profile when m_f and δ_i varies	147
Figure 5-21 : APAM Profile when m_f and δ_i varies	148
Figure 5-22 : APAH profile when m_f and δ_i varies	149
Figure 5-23 : APAA profile when O_{max} and O_{min} vary.....	150
Figure 5-24 : APAM profile when O_{max} and O_{min} vary	151
Figure 5-25 : APAH when N varies	152
Figure 6-1 : Four digit biometric PIN	159

Figure 6-2 : Multilevel Security System Verification.....	165
Figure 6-3 : ROC curve when ECG noise increases	171
Figure 6-4 : AUR and EER profile when ECG noise increases.....	172

LIST OF TABLES

Table 2-1: Advantages and disadvantages of the three main authentication approaches.....	9
Table 2-2 : Distance Based Similarity Measures for Quantitative Variables	21
Table 3-1 : Summary of Important ECG Based Feature Extraction Technique	42
Table 4-1 : Summary of 6 Pulse Active Feature Selection Techniques.....	80
Table 4-2: Summary of AUR performances on different T_{ECG}	94
Table 4-3: Summary of EER performances on different T_{ECG}	94
Table 4-4: ROC AUR and EER values for Healthy and Arrhythmia Populations ...	97
Table 4-5: AUR and EER values using different distance measure	99
Table 4-6: Suggested m_f and m_i settings for PA feature selection.....	104
Table 4-7: AUR and EER profiles for healthy population using general PA parameters	110
Table 4-8: Suggested Ranges, AUR and EER profiles for arrhythmia population.	110
Table 5-1: Summary of 5 Adaptive Pulse Active Feature Selection Technique.....	132
Table 5-2: Summary of AUR performances on different T_{ECG} using APA	137
Table 5-3 : Summary of EER performances on different T_{ECG} using APA.....	137
Table 5-4: APA AUR and EER values for Healthy and Arrhythmia Populations..	140
Table 5-5: APA profile using different distance measure.....	144
Table 5-6 : AUR and EER profiles for healthy population using selected ranges of APA parameters	154
Table 5-7 : AUR and EER profiles for arrhythmia population using selected ranges of APA parameters	154
Table 6-1: PA and APA parameter suggested range.....	157
Table 6-2 : p_l representation for PA and APA algorithms.....	159

LIST OF ABBREVIATIONS

AC	Auto correlation
AMA	Above Maximum Area
APA	Adaptive Pulse Active
APAA	Adaptive Pulse Active Area
APAB	Adaptive Pulse Active Bit
APAH	Adaptive Pulse Active Harmonic
APAM	Adaptive Pulse Active Mean
APAW	Adaptive Pulse Active Width
ATM	Automated teller machines
AUR	Area under ROC curve
AV	Atrioventricular node
AMV	Amplitude Variability
DCT	Discrete Cosine Transform
DM	Delta Modulation
EAST	European ATM Security Team
ECG	Electrocardiogram
EEG	Electroencephalography
EER	Equal Error Ratio

FAR	False Acceptance Ratio
FMR	False Match Ratio
FNMR	False non-match Ratio
FRLF	First Rise Last Fall
FRR	False Rejection Ratio
HRV	Hear Rate Variability
IGR	Information Gain Ratio
LDA	Linear Discriminant Analysis
PA	Pulse Active
PAA	Pulse Active Area
PAB	Pulse Active Bit
PAH	Pulse Active Harmonic
PAM	Pulse Active Mean
PAR	Pulse Active Ratio
PAW	Pulse Active Width
PCA	Principle Component Analysis
PIN	Personal Identification Number
PTB	Physikalisch-Technische Bundesanstalt
PWM	Pulse Width Modulation
ROC	Receiver Operating Characteristic
SA	Sinoatrial node

LIST OF SYMBOLS

A_{ECG}	Maximum amplitude of ECG signal
A_{tri}	Maximum amplitude of the triangular wave
$L_{[2m]}$	Peak location of the triangular period
$L_{[2m+1]}$	Ending point of the triangular period
$L_{[2m-1]}$	Starting point of the triangular period
m_f	Modulation factor
m_i	Modulation index
N	Total harmonic values
$o(t)$	Output pulses
O_{max}	Maximum output pulse
O_{min}	Minimum Output Pulse
P	Peak value of P wave
Pe	End point of P wave
Ps	Starting point of P wave
Q	Starting point of QRS wave
R	Peak value of QRS wave
S	End point of QRS wave
T	Peak value of T wave
$t_{(2m)}$	Even intersection location

$t_{(2m-1)}$	Odd intersection location
t_{+ve}	First intersection from the rising edge of the triangular wave
T_e	Ending point of T wave
T_{ECG}	ECG Duration for extraction
T_{P2R}	ECG duration from the peak of P to the peak of R
T_{P2T}	ECG duration from the peak of P to the peak of T
T_{R2T}	ECG duration from the peak of R to the peak of T
T_s	Starting point of T wave
T_{trans}	Transition state vector
T_{tri}	A period duration of Triangular wave
t_{-ve}	The last intersection from the falling edge
W	Radian transform vector
X	Feature vector
$y_{bottom}(t)$	Bottom replication of the ECG signals
$y_{ECG}(t)$	ECG signal
$y_L(t)$	DC line
$y_{top}(t)$	Top replication of the ECG signals
$y_{tri}(t)$	Triangular wave
δ_i	Deviation index
ΔV	Distance between actual ECG signals and its replication

CHAPTER 1.

INTRODUCTION

1.1. PREFACE

Skimming at automated teller machines (ATMs) is a growing problem throughout the world. Criminals are now using more advance devices which incorporate a micro camera for PIN captures and a skimming device to capture the ATM card data. The European ATM Crime Report published by EAST (the European ATM Security Team) shows a 24% increase for the period January to June 2010 compared with the same period in 2009 in card skimming attacks at European ATMs equivalent to €144 million losses [1].

To counter this problem, biometric ATM has been introduced. Palm and finger vein biometrics are two available technologies incorporated with ATM which have been widely accepted in Japan and Brazil. In Europe, Poland was the first country to trial this technology [2]. Based on this technology, after the ATM card is inserted, hands or fingers are placed over a vein scanner which recognizes a unique data to authorise a transaction. Without entering PIN during the transaction process, capturing the PIN and ATM cards by the skimmers is no longer useful. Unfortunately, a physiological biometric normally cannot be changed. Hence, if it is compromised, it is possible that an authentication can be exposed to fraudulent transactions forever. Thus, in general

consumers still refuse to accept this biometric technology due to the risk of personal data infringements.

Authentication systems using internal body characteristics such as electrocardiograms (ECGs) have attracted significant attention among researchers as ECG based characteristic is difficult to be misrepresented. The ECG represents graphical electrical activity of the heart and is believed to be distinctive among individuals and stable for a long period of time. The main challenge implementing this technology is that the ECG characteristic is time dependent. This makes it difficult to extract the exact same ECG characteristic each time even from the same user. The main source of these variations comes from the effect of heart rate variability (HRV) and amplitude variability (AMV).

1.2. MOTIVATION FOR THIS RESEARCH

This thesis addresses the above shortcomings by developing a new feature extraction technique which can be used for electrocardiograms (ECGs) that increases the security level of a biometric authentication system.

The first objective of the thesis is to develop new feature extraction techniques which

- i. are easy to construct and implement
- ii. are robust to the effect of heart rate and amplitude variability.
- iii. can be used for healthy and arrhythmia subjects.
- iv. keep the health information of the subject private by avoiding the reconstruction of the original ECG signals.

The second objective of the thesis is to develop algorithms to construct an ECG based authentication system which

- i. is capable of increasing the level of security of the authentication system
- ii. give the user the privilege to change their biometric feature vector whenever they feel the security system may be compromised.

Throughout these investigations, a good quality representative ECG data sets is acquired from the public Physikalisch-Technische Bundesanstalt (PTB) database [3].

1.3. SUMMARY OF ORIGINAL CONTRIBUTION

The results, discussion and conclusion detailed in this thesis not only contribute generally to the field of signal processing technology but are directed specifically towards the use of ECG as part of a high level security biometric authentication system. This section summarizes the original contribution of the work reported in this thesis.

The main achievement of this research is the philosophy of representing a signal into pulse domain. Based on this philosophy, it is stated that every signal can be decomposed into a finite set of pulse features. Two architectures successfully developed with respect to this philosophy are named Pulse Active and Adaptive Pulse Active techniques.

1) Pulse Active Feature Extraction Technique

The first novel contribution in this thesis is the development of the Pulse Active (PA) technique. PA is a process of representing an investigated signal into pulse domain based on the concept of Pulse Width Modulation (PWM). A periodic triangular wave

with the same amplitude and period is used to modulate the investigated signal (in this thesis an ECG signal). The output pulse generated signal follows specific intersection rules between the investigated signal and the triangular wave. There are 6 PA variant algorithms developed in this work namely: Pulse Active Bit (PAB), Pulse Active Width (PAW), Pulse Active Area (PAA), Pulse Active Mean (PAM), Pulse Active Ratio (PAR) and Pulse Active Harmonic (PAH).

2) Adaptive Pulse Active Feature Extraction Technique

The second novel contribution in this thesis is the development of Adaptive Pulse Active (APA) technique. APA is a process of representing an investigated signal into output pulses based on the concept of delta modulation. The investigated signal are replicated twice and position on top and bottom (generating an enveloped) of the investigated signal. A periodic triangular wave with the same period but different amplitude is generated within the enveloped. The output pulse generated follows specific intersection rules between the generated triangular wave and a generated DC line. In view of these techniques, 5 different algorithms are developed. These algorithms are named as Adaptive Pulse Active Bit (APAB), Adaptive Pulse Active Width (APAW), Adaptive Pulse Active Area (APAA), Adaptive Pulse Active Mean (APAM), and Adaptive Pulse Active Harmonic (PAH).

3) Performance improvement for ECG Biometric Authentication

The third novel contribution in this thesis is the improvement of the ECG Biometric Authentication works. In this thesis, PA and APA have been used to extract unique ECG features for the use of biometric authentication. The ECG sources used in this work come from the PTB database available freely on-line. The advantage of using this database is that the time intervals between recordings of the same subject available in the database is around 500 days which is very suitable to investigate the effectiveness of the PA and APA algorithms for biometric applications. Using this database, various new innovations which have never been reported in any of the previous work are presented. One of the main innovations is that the capability of the PA and APA algorithms to minimize the effect of HRV and AMV which have been the obstacle of practically implementing ECG as a biometric in current technology. The proposed novel techniques in this work manage to acquire an average

performance of up to 99% while its Equal Error Ratio (EER) manages to be as low as 2%. These results come from the observation and analysis of the Receiver Operating Characteristic (ROC) curves. As a result of investigating these factors, it is discovered in this work that PA and APA are best used to extract ECG information between the peaks of P and T for biometric application. It is also discovered that PAW and APAW remain the best algorithms to generate the best AUR and EER profiles. Investigating the appropriate similarity measures, it is discovered that city block (or Manhattan) and cosine distance based similarity algorithms provide better authentication performance for the PA and APA techniques respectively.

4) Multilevel Security ECG Based Biometric System

The fourth novel contribution in this work is the development of a multilevel security ECG based biometric. The proposed system is developed by combining the PA and APA parameters as a personal identification number (PIN). The novel 11 algorithms developed based on the concept of PA and APA depends on the characteristic of the signal (i.e., amplitude, duration, intersection location) and 6 user defined parameters. Investigating these parameters on all 11 algorithms, it is concluded that different performances in all 11 algorithms can be obtained using specific combination settings of these parameters. Acceptable ranges of these parameters are proposed to generate similar authentication profiles. These acceptable ranges for all parameters are then configured as a PIN. Similar authentication profiles generated using the acceptable parameter ranges are important so that users are not restricted to using specific PIN combinations to achieve the highest authentication performance. In this way, although different feature vectors generated by different PIN may be used even for the same ECG signals, the biometric performance is still acceptably high. Using this system, the authentication process may only proceed when the PIN and correct ECG are used generating a multilevel security authentication system.

1.4. THESIS ORGANIZATION

The remainder of this thesis is organized as follows:

Chapter 2 provides an overview of biometric technology. It includes an introduction of biometric systems and characteristics. The explanation of multimodal biometric systems is then described in this chapter. The ethics on using biometric is discussed next. The final section of this chapter discusses the performance evaluation methods which will be used in this thesis.

Chapter 3 reviews the concept of ECG as a biometric by first describing ECG signals and characteristics. The idea of using ECG as a biometric is described next in this chapter. The ECG sources to be used in this thesis are then discussed. Finally, a review of ECG based feature extraction techniques is provided.

Chapter 4 introduces the novel Pulse Active (PA) feature extraction technique. The chapter begins with the fundamentals of the PA feature extraction technique. This chapter also investigates the best location to extract ECG using the PA technique. Later on in this chapter, 6 PA algorithms are presented based on the method PA features. Finally, results and discussion are given at the end of the chapter.

Chapter 5 introduces a novel Adaptive Pulse Active (APA) feature extraction technique. The fundamentals of APA which include a simple discussion on delta modulation technique are included. A total of 5 APA algorithms are presented in this chapter. Results and discussion on the APA performance concludes the paper.

Chapter 6 presents a novel multilevel security scheme involving PA and APA techniques. A detailed description of the PA-APA ECG based multilevel biometric security system is presented. The performance evaluation and discussion of the proposed scheme is provided in this chapter.

Chapter 7 concludes the thesis along with the discussion on the flexibility of the PA and APA technique to be used not only for ECG biometric application but with extension to other types of signals and applications.

CHAPTER 2.

BIOMETRIC: SYSTEM, CHARACTERISTIC, ETHICS AND PERFORMANCE

2.1. INTRODUCTION

Human authentication technologies have rapidly evolved throughout the years. The main three approaches of these technologies are handheld, knowledge and biometric based as shown in the first column of Table 2-1. The advantages and disadvantages of these 3 main approaches are given in the second and third column of Table 2-1 respectively [4].

As can be seen from the list of disadvantages of all 3 approached in Table 2-1, it can be concluded that using one of these approaches independently would exposed the security system to the threat of fraudulent. The work in this thesis tends to combine two authentication approaches (knowledge and biometric based) from Table 2-1 in order to adapt both advantages of each approaches in the same time minimize their disadvantages when these approaches are considered independently.

Biometric technologies are based on unique physical features of human bodies which are hard to be misrepresented and misplaced. This chapter first discusses the different

categories and requirement of a biometric system. It continues with the description of different types of biometric characteristics, the concept of multimodal biometrics, and the ethical issues with respect to biometrics. Finally, methods to evaluate the performance of a biometric system conclude this chapter.

Table 2-1: Advantages and disadvantages of the three main authentication approaches.

Approaches	Advantages	Disadvantages
Handheld based (card, ID, token, passport, etc)	A new one can be issued. It is quite standard and easy to obtain	It can be stolen or shared. A fake one can be issued. A person can register with different identity
Knowledge based (password, PIN, etc)	It is a simple and economical method. If there are problems, it can be replaced by a new one quite easily.	It can be shared, guessed or cracked. Good passwords are hard to remember. A person can register with different identity
Biometric based (fingerprint, iris, vein, ECG, etc)	It cannot be lost, forgotten, guessed, stolen or shared. It is quite easy to check if someone has multiple identities. It can provide greater security than the other two approaches	In some cases, a fake one can be issued. It is neither replaceable nor secret. If the biometric traits are stolen, it is not possible to be replaced.

2.2. BIOMETRIC SYSTEMS

A biometric system is a system that compares certain characteristics of a person for recognition and/or identification. It started to emerge from a law enforcement application to identify criminals and nowadays is being widely used in civilian applications. Traditionally the features or characteristics of a person are compared visibly by a fully trained person. However, advances in image and signal processing methods in conjunction with the development of sophisticated computers as tools have helped to build automated pattern recognition systems for biometrics.

2.2.1. Biometric requirements

There are 7 requirements that need to be satisfied for a person's characteristic to qualify as a practical biometric system feature [5]. These requirements are listed as follows:

- a) **Universality** : The characteristic should be possessed by every person
- b) **Distinctiveness** : The characteristic should distinguish between any two persons
- c) **Permanence** : The characteristic should be invariant over a period of time
- d) **Collectability** : The characteristic can be measured quantitatively
- e) **Performance** : Relates to the accuracy rate and speed of the recognition process
- f) **Acceptability** : The acceptance of the society to use the biometric characteristic in their daily lives
- g) **Circumvention** : How easy the system can be fooled using fraudulent methods.

Based on these lists, it can be concluded that not every detail in human body can be considered as a biometric trait as not each detail in human body is distinctive, permanent and can be measure quantitatively.

2.2.2. Overview of a biometric system

According to [6], most biometric systems carry out the processes illustrated in Figure 2-1. As can be seen from Figure 2-1, once the biometric characteristic is captured by the sensor, it is pre-processed. In this step, the characteristic is filtered so that noises which were accidentally captured by the sensor can be reduced.

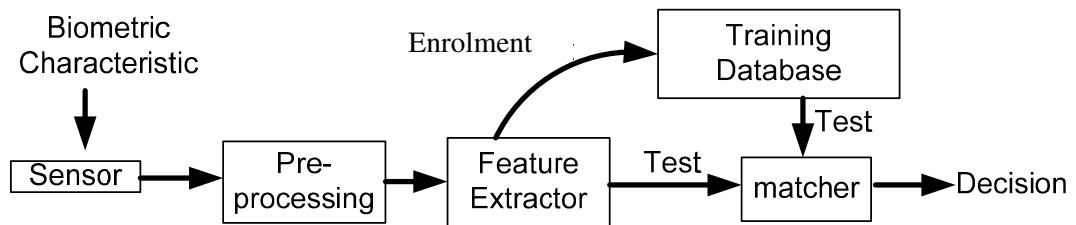


Figure 2-1: Basic processing steps in biometric recognition

The type of noise is dependent on the chosen biometric characteristic. When the characteristic is at its best quality, a feature extraction algorithm or technique is then applied as shown in Figure 2-1 so that the distinctive features that separate one individual from another can be extracted. These features are then used either for enrolment to the training database or for testing the newly submitted identity. Training databases usually store feature vectors of all users recognized by the system. The final stage in biometric recognition process is the matching process which happened in the matcher block as illustrated in Figure 2-1. In this step, the system will match the testing and the training features and decide the identity of the subject.

The biometric system may operate either in identification mode or in authentication mode [4]. In the authentication (or verification) mode, shown in Figure 2-2, the subject claims an identity from a training system database through a user name or a smart card. The aim of the system is to determine whether the subject is who he/she claims to be. The system will search the training database for a template of feature vector of the claim identity. The template is then passed to a matcher block as shown in Figure 2-2. The system will request the user to submit their biometric as test samples at the same time it is collecting the information of the claim identity as shown in Figure 2-2. The test sample is used for feature extraction before sending it to the matching process as shown in Figure 2-2. During the matching process, the system performs a one-to-one comparison between the test and the training feature vectors to decide whether the claim is legitimate or a fraud.

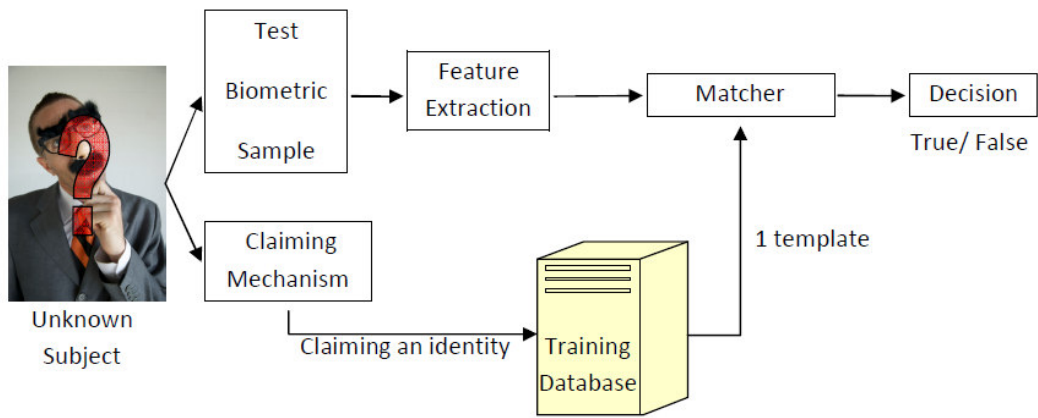


Figure 2-2: Authentication Mode

On the other hand as shown in Figure 2-3, the identification mode operates in the manner, which the test biometric feature vector of a subject is compared with all available feature vectors of in the training database.

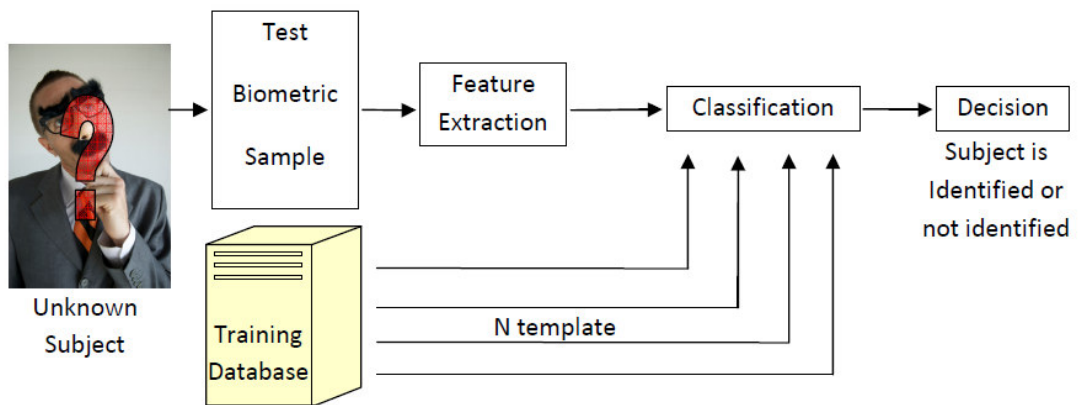


Figure 2-3 : Identification Mode

As can be seen in Figure 2-3, in this approach, no identity is claimed from the user. The user starts the process with submitting their biometric sample for testing. The feature extraction technique is then used to extract unique information from the biometric and send it to a classification stage. In the same time, N available templates of feature vectors from the training database are sent to the classification stage as illustrated in Figure 2-3. In the classification stage, a classifier is used to perform a one-to-many comparison between a single template of the test feature vectors and N available templates of feature vectors from the training database. The classifier then decides if the subject is known to the system.

Figure 2-4 summarizes the overall operation mode of a general biometric system. As can be seen in Figure 2-4, the authentication mode only works in positive recognition while the identification mode may work in positive or negative recognition.

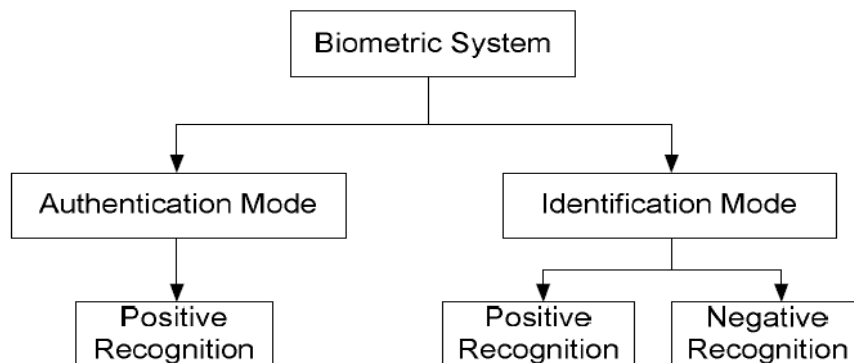


Figure 2-4 : Biometric Operational modes.

In positive recognition, the objective is to prove that the collected biometric samples are known to the system and prevents multiple people from using the same identity. In negative recognition, the system intends to prove whether the person is who they deny to be and prevents a single person to have multiple identities in a single database.

2.3. BIOMETRIC CHARACTERISTIC

2.3.1. Overview of biometric characteristic

In general, biometric characteristics can be divided into two broad categories:- physiological and behavioural as shown in Figure 2-5. Gait[7], signature[8], keystroke[9], voice[10] and grip[11] are examples of behavioural biometric characteristics. Physiological attributes are related to the physical structure of the body. As can be seen from Figure 2-5, these can be further classified into the externally observable characteristics and the internal body characteristics. Facial[12, 13], fingerprint[14, 15], hand geometry[16], iris scanning[17], retina scanning[18]

and footprint recognition[19] are among examples of the external observable physiological biometric characteristics.

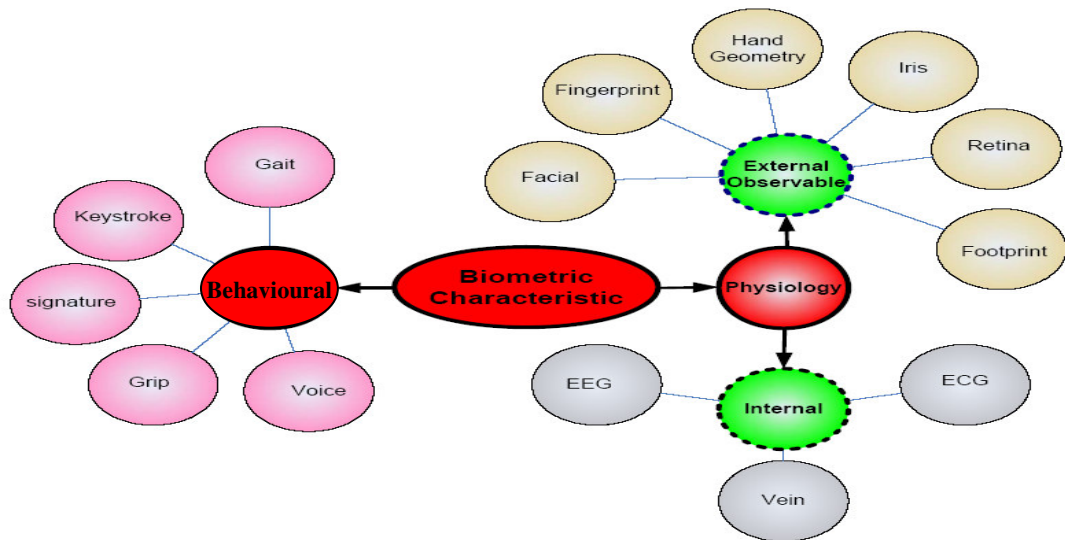


Figure 2-5 : Types of biometric characteristic

The internal physiological biometric characteristics features are always covered by the skin and require invasive methods to misrepresent them. Vein [20, 21], electroencephalography (EEG) [22, 23] and the electrocardiography (ECG) [24, 25] are among examples of internal physiological biometric characteristics given in Figure 2-5. The following subsection will discuss in details these examples of behavioural and physiological characteristics.

2.3.2. Behavioural characteristic

Gait recognition [7] is a method of recognizing a subject based on how they walk. It has an advantage of capturing and analyzing the data from a distance. However it can be imitated and the feature can be covered by the type of clothes the subjects wear. Signature recognition [8] measures handwritten signature of an individual by capturing the shape, acceleration, pressure flow and timing information. It is how the signature is signed that is being measured for discrimination and not how the graphical image is analyzed. Keystroke dynamics [9] is a process that analyzes the

way a user types by monitoring the keyboard inputs in attempt to identify users based on their habitual typing rhythm patterns. The feature is analyzed by measuring the typing tempo, the content and consistency. Speech recognition technology [10] examines the differences in the shape of vocal frequencies and the speaking habits between subjects. However this system can easily be defeated by someone who plays back the recorded voice or imitates a voice. Grip recognition [11], is a new technology implemented in smart gun to detect a gun owner's hand size, strength and the dynamic grip style as a feature. It aims to reduce the misuse of guns by children or felons through the use of embedded smart chips on it.

2.3.3. External Observable Physiological characteristic

Facial recognition [12] is a recognition process that identifies a subject based on the facial characteristics such as nose, lips, eye jaw and cheekbones. These characteristics are extracted from a sequence of images or a video with various facial expressions as references. Nevertheless, the performance of this biometrics trait is affected by the changes in the environmental conditions such as illumination levels [13]. In addition to that, the biometric trait also can be defeated using masks. Fingerprint recognition [14] focuses on the distinctive impression of the ridges and valleys made by an individual's finger. Although this technique can be defeated by using fake fingerprint cast in gel, it has been widely accepted as one of the best known biometric technologies. The fingerprint recognition performance suffers from degraded images due to improper finger placement, skin deformation, slippage and smearing, or sensor noise from wear and tear of surface coatings. For this reasons, current fingerprint recognition technology is moving towards implementation of contactless 3 dimensional fingerprinting to improve the recognition accuracy [15].

Hand geometry recognition [16] captures an image of the hand and measures the length, width, thickness, distance between joint, shapes of the knuckle and surface area of a subject while the hand is guided on a plate. Although the basic shape of the

hand remains stable over its lifetime, natural and environmental factors can cause slight changes.

Iris recognition [17] is a discrimination process based on unique feature of iris pattern possessed by the individual. The features are usually the distinctive coloured ring surrounding the pupil of the eye. This characteristic is reportedly stable through a person's lifetime except in cases of injuries.

Retina recognition [18] has a similar concept as iris recognition by capturing unique features from the eye. However, in this case, the patterns of blood vessels on the back of the eyeball are processed. Although this technology is highly reliable as no two people have the same retinal pattern, it requires high equipment costs and is not user friendly.

Footprint recognition [19] was initially introduced in Japan as it is a part of the Japanese custom that people take off their shoes at the entrance to a dwelling. As a new developed biometric trait, this technology had been suggested as a personal recognition in a small group such as family or roommates.

2.3.4. Internal Physiological characteristic

Vein pattern recognition [20, 21] discriminates images of an individual's vein pattern concentrated either on the face, finger, wrist or hand. Anatomically, the shapes of vascular patterns in the same part of the body are distinct for each person and are very stable over a long period of time. However, for this biometric trait, the success of the system relies on the image acquired. X-ray, ultrasonic and infrared are among the techniques available to generate the best image quality of the vein.

EEG recognition [22, 23] has the advantage of confidentiality and almost impossible to steal as the feature is extracted from the signal coming from the brain. Although a person has the ability to alter most of their brain wave patterns, they cannot alter

what is referred to as their baseline brain wave pattern. Baseline brainwave is specific information stored in a person's brain by measuring electrical brainwave response to words, phrases, or pictures that are presented on a computer screen.

Recent research has shown that ECGs produced by individuals are particularly unique [24, 25]. In ECG recognition, features are extracted from the electrical signal of the heart. Since every individual's heart has a different size, the shape of the electrical signal of the heart measure on the skin is different.

2.4. MULTIMODAL BIOMETRIC

There are no single biometric traits that can be claimed to be the best recognition tool. The choice of selecting the types of characteristics nowadays is more based on how and where it is applied. As the application of using only one single biometric does not always meet the performance requirements, the development of systems that integrate two or more biometrics is emerging as a trend. Such systems are known as multimodal biometric systems [26]. Jain *et al* [5] listed 5 categories of multimodal biometric systems based on how the systems operate.

i. Multiple sensors

Two or more types of sensor are used for the same biometric characteristics. For example using combination of optical and capacitance sensor to capture the same fingerprint characteristics.

ii. Multiple biometrics

Multiple biometric characteristic such as ECG and fingerprinting are combined.

- iii. Multiple unit of the same biometric
The same biometric characteristic, with more than one unit for the same subject, such as 10 fingers or a pair of irises, can be combined.
- iv. Multiple snapshot of the same biometric
The combination of multiple attempts to capture the same features from the same biometric, such as multiple samples of voice or multiple images of faces.
- v. Multiple representations and matching algorithms for the same biometrics.
This involves combining different approaches to extract the feature or features during the classification process.

Most of the work in the multimodal biometric research preferred the used of more than one biometric characteristic during a process of authentication. It is believed that, using more than one biometric trait may help to increase the security of the system. Some of the biometric characteristics are easy to be misused but exhibits a higher degree of discriminative values for example fingerprint. Others might not have a high discriminative value to distinguished individuals, however these characteristics are hard to be misrepresented for example using EEG. Having both types of biometric characteristic at the same time strengthen the system from the fraudster attack.

2.5. ETHICAL ISSUE IN BIOMETRIC

Biometrics raises a number of ethical issues. Privacy is the main issue that needs to be managed accordingly [27]. Data obtained during biometric enrolment, which is provided for a particular purpose could be used for purposes that the individual neither have predicted, nor agreed to. In some cases, misuse of the biometric

information from the people who have gain access to the data storage may be used to locate and harass or harm the user in some manner.

A threat to privacy also comes in the form of unwarranted identification. Facial or gait recognition are among examples of biometrics which can be misused for unauthorized identification since the feature can be extracted from long distance and without the consent of the subject. These lead to a prejudicial system whereby people with criminal or unpleasant background history may be stopped or denied access without considering their initial intention. Safety is another issue in biometrics. If an item is secured through a biometric device, there is a chance that criminals could harm the owner in order to gain access. For example, the owner's finger can be cut if the biometric system uses the fingerprint characteristic as the key.

A new threat on using biometrics as part of a security system is the reconstruction of original biometric characteristics based on the information stored in the security system [28]. It is easier for a fraudster to hack into the security system and obtained information such as the algorithm used and feature vector stored for regeneration of the original biometric characteristics, rather than install special hardware to steal the user biometric. Therefore a user will not be aware their biometric information has been stolen and the fraudster could steal more than one identity from the system. Additionally, biometric characteristics cannot be cancelled or reissued. If the biometric traits are compromised, the effect is a permanent one and could be an issue for the donors for the rest of their lives.

2.6. PERFORMANCE EVALUATION

Theoretically, it is hard to get a perfect match between features due to the imperfection of the sensing conditions during submission of a biometric sample. For

this reason similarity scores are introduced to measure the performance of biometric systems [29].

2.6.1. Similarity scores

Feature vectors are mathematical representations of information extracted from a given sample using a signal processing technique. These feature vectors can be used to build or to compare against the enrolment template stored in the training system. The values returned when the two feature vectors are compared are known as scores.

Similarity scores reflect the strength of a relationship between two feature vectors. Distance measurement is usually used to calculate these similarity scores. Let $\mathbf{q} = [q_1 \ q_2 \ \dots \ q_k]$ and $\mathbf{r} = [r_1 \ r_2 \ \dots \ r_k]$ be an example of two different feature vectors. The most widely used distance measurements between \mathbf{q} and \mathbf{r} are tabulated in Table 2-2. The theoretical assumption for the distance measures in Table 2-2 is that similarity of two items is inversely related to their distance. Two items that are close together will be perceived as similar and those that are far apart will be perceived as dissimilar.

Two types of results obtained from the concept of similarity scores are the ‘Genuine’ score and the ‘Imposter’ score. ‘Genuine’ score refers to the similarity score values of two feature vectors obtained from comparing samples of the same biometric characteristic of the same subject. ‘Imposter’ score on the other hand refers to the similarity score values of two feature vectors obtained from comparing samples of the same biometric characteristic of different subjects.

Table 2-2 : Distance Based Similarity Measures for Quantitative Variables

Similarity Measure	Formula
<i>Euclidean Distance(ED) or 2-norm Distance [30]</i>	$ED(q, r) = \sqrt{\sum_{i=1}^k q_i - r_i ^2} \quad (2-1)$
<i>Manhattan Distance(Man) or 1-norm Distance[31]</i>	$Man(q, r) = \sum_{i=1}^k q_i - r_i \quad (2-2)$
<i>Chebyshev Distance (CHEB) [32]</i>	$CHEB(q, r) = \max_i q_i - r_i \quad (2-3)$
<i>Minkowski Distance (MINK) [31]</i>	$MINK(q, r) = \sqrt[p]{\sum_{i=1}^k q_i - r_i ^p} \quad (2-4)$
<i>Canberra Distance (CANB)[33]</i>	$CANB(q, r) = \sum_{i=1}^k \frac{ q_i - r_i }{ q_i + r_i } \quad (2-5)$
<i>Sorensen Distance (SoR)[34]</i>	$SOR(q, r) = \frac{\sum_{i=1}^k q_i - r_i }{\sum_{i=1}^k (q_i + r_i)} \quad (2-6)$
<i>Cosine distance (CoSd)[35]</i>	$CoSd(q, r) = \frac{\sum_{i=1}^k q_i \cdot r_i}{\sqrt{\sum_{i=1}^k q_i^2 \cdot \sum_{i=1}^k r_i^2}} \quad (2-7)$
<i>Mahalanobis distance (MAHAL)[36]</i>	$MAHAL(q, r) = \sqrt{(q - r) S^{-1} (q - r)'} \quad (2-8)$ with S is a covariance matrix of (q, r)
<i>Correlation (CORR)[37]:</i>	$CORR(q, r) = \frac{\sum_{i=1}^k (q_i - \bar{q})(r_i - \bar{r})}{\sqrt{\sum_{i=1}^k (q_i - \bar{q})^2 \sum_{i=1}^k (r_i - \bar{r})^2}} \quad (2-9)$ with $\bar{q} = \frac{1}{k} \sum_{i=1}^k q_i$ and $\bar{r} = \frac{1}{k} \sum_{i=1}^k r_i$

2.6.2. Confusion matrix

A confusion matrix is a table of two rows and two columns that reports the total value of true acceptance, false acceptance, true rejection and false rejection as shown in Figure 2-6 [38]. In Figure 2-6, a ‘Genuine’ attempt is an attempt by users to match their own training template to generate a ‘Genuine’ score.

		Acceptable Threshold Setting	
		Genuine Score	Imposter Score
Genuine Attempt	True Acceptance	False Rejection	
Imposter Attempt	False Acceptance	True Rejection	

Figure 2-6: Confusion Matrix

If the ‘Genuine’ score falls within the acceptable threshold value, the result is known as true acceptance. If the ‘Genuine’ scores exceed the acceptable threshold value, the result is known as a false rejection. ‘Imposter’ attempt in Figure 2-6 is an attempt by a person to match another person’s training template to generate an ‘Imposter’ score. If an ‘Imposter’ score falls within the acceptable threshold value, the result is known as false acceptance. If the ‘Imposter’ score exceeds the acceptable threshold value, the result is known as true rejection.

2.6.3. Decision error ratio

Biometric performance is normally reported in terms of the decision error ratio which is the false rejection ratio (FRR) and the false acceptance ratio (FAR). FRR reports the degree of expectation for the system to deny a legitimate claim by a ‘Genuine’ user. The transaction may consist of one or more ‘Genuine’ attempts. FRR can be calculated as:

$$FRR = \frac{\text{Total number of False Rejections}}{\text{Total number of 'Genuine' Attempts}} \quad (2-10)$$

FAR reports the degree of expectation of the system to incorrectly accept access of an ‘Imposter’. The transaction may consist of one or more ‘Imposter’ attempts. FAR can be calculated as:

$$FAR = \frac{\text{Total number of False Acceptances}}{\text{Total number of 'Imposter' Attempts}} \quad (2-11)$$

2.6.4. Receiver operating characteristic (ROC)

The receiver operating characteristic (ROC) curves are an accepted method for summarizing the performance of a biometric system [39]. The ROC curve plot, is a function of the decision threshold, which plots the rate of ‘False Acceptance’ (i.e. imposter accepted as genuine) or 1-specificity on the x-axis, against the ‘1-False Rejection’ (i.e. genuine accepted as genuine) or sensitivity on the y-axis. It is also threshold independent, allowing it to be used in comparing different systems under similar settings or a single system under different settings. In order to quantitatively measure the comparison of multiple ROC curve performances, the area under an ROC (AUR) and the Equal Error Ratio (ERR) are used. The AUR calculates the

area under each of the ROC curve. Its value ranges between 0 and 1. The AUR has an important statistical property which is equivalent to an average of the overall performance of the biometric system when all threshold settings generating the ROC curves are considered [40]. The EER is defined as the rate at which the false acceptance ratio equals the false rejection ratio. EER ranges between 0 and 1. A higher AUR value with a lower value of EER is desirable for practical systems. An example of generating the ROC curve, calculating the AUR values and determining the EER values from the ROC curve is given in Appendix A.

2.7. CONCLUSION

This chapter has investigated the theoretical concepts of biometric by discussing an overview of a biometric system followed by a review of various types of biometric traits. This explanation is important to support the justification of selecting electrocardiogram (ECG) as biometric which will be described next in Chapter 3.

CHAPTER 3.

ELECTROCARDIOGRAMS FOR HUMAN RECOGNITION

3.1. INTRODUCTION

Implementing electrocardiograms (ECG) as a biometric trait has become an active research endeavour. This chapter offers an overview of the electrocardiogram process by first explaining the electrical conductivity of the heart, its lead configuration, its morphological structure, ECG fiducial points and methods to detect these points. The concept of an ECG as a biometric is then explored by discussing the advantages and challenges on using ECGs in biometrics. Since experiments using real-time ECG recordings require ethical approval from the authorities, this chapter then explains a strict procedure in using ECG recordings from a publicly available ECG database for all experiments throughout this thesis. A pre-processing technique on these ECG recordings is then described making them ready to be used for feature extraction. Finally, conclusions and discussions on the work of implementing ECGs in biometrics conclude this chapter.

3.2. ELECTROCARDIOGRAM

3.2.1. Electrical conductivity of the heart

An electrocardiogram (ECG) is a graphical representation of the electrical activity of the heart over a period of time. It is recorded using an electrocardiograph machine through a certain configuration of electrode leads placed on the surface skin of the human body. Based on [41], the illustration of the heart and its electrical conduction system is given in Figure 3-1. According to [41], the electrical activity of the heart is spontaneously generated from the Sinoatrial (SA) node towards the Atrioventricular (AV) node. Normal physiology allows the electrical activity further propagates from the AV node to the ventricle or Purkinje Fibers to respective bundle branches and finally fascicles.

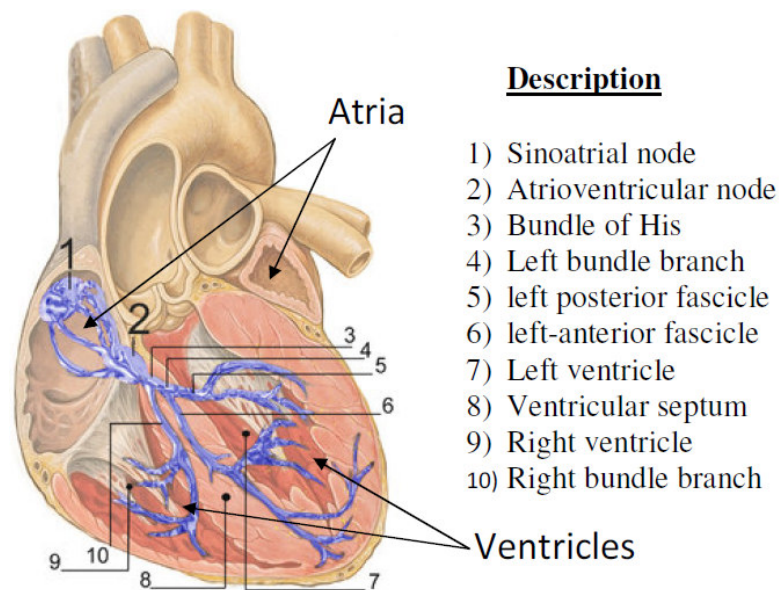
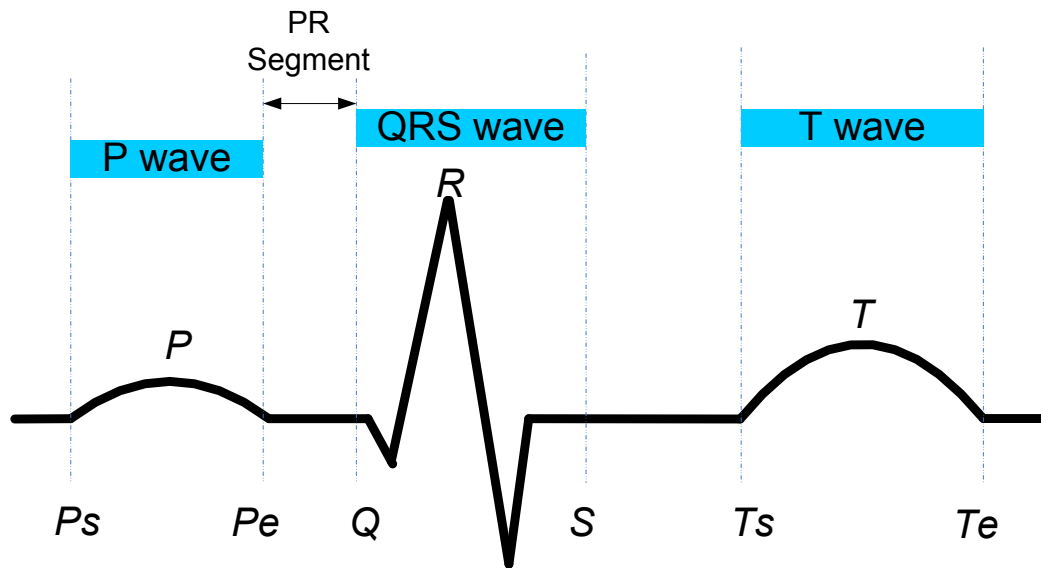


Figure 3-1: Electrical conductivity of the heart

3.2.2. ECG morphology

A healthy heart usually displays 3 main waves in a single ECG complex namely the P wave, QRS wave and the T wave as shown in Figure 3-2 [42]. In Figure 3-2, P wave started from P_s to P_e while T wave starts from T_s to T_e . The QRS wave starts from the location of Q to the location of S. P , R and T in Figure 3-2 represent the respective peak location of the P, QRS and T wave.



P_s :Starting point of P wave	Q : Starting point of QRS wave	T_s : Starting point of T wave
P : Peak value of P wave	R : Peak value of QRS wave	T : Peak value of T wave
P_e : End point of P wave	S : End point of QRS wave	T_e : End point of T wave

Figure 3-2: Electrocardiogram Complex

The nervous system releases adrenaline which starts the electrical activity in the heart specifically in the SA node. The initialization of the electrical activity indicates the starting point of the P wave. This electrical impulse is propagated throughout the right atrium and then throughout the left atrium, stimulating the myocardium (heart muscle) of both atria to contract. The propagation between these atria in ECG represents the P wave. The PR segment on the ECG represents a delay in the AV nodes allowing blood to flow effectively from the atria to the ventricles and avoids

the atria and ventricles to contract at the same time. The spread of electrical activity (depolarization) through the ventricular myocardium produces the QRS wave on the ECG. During depolarization, the sodium and calcium ions stream into the cell while potassium ions stream out of the cell. As blood gets pumped out of the ventricle, ventricular repolarization occurs and the T wave is observed. During repolarization the ion concentration returns to its pre-contraction state.

The heart normally beats at average 72 times per minute and the SA speeds up during exertion, emotional stress, fever, or whenever our body needs an extra boost of blood supply. In contrast, it slows down during rest or under the influence of certain medications. Due to these factors that controlled the generation of the electrical pulses, the intervals between the ends of T wave and the starting point of the next ECG complex can be described as the region which is free from the electrical timing mechanism of the heart [70].

3.2.3. Fiducial points and detection

Fiducial points are the points of interest corresponding to the peaks and boundary locations of the 3 major waves in an ECG complex as illustrated in Figure 3-2. There are 9 fiducial points in an ideal ECG complex. The locations of these fiducial points are affected by the heart rate [43]. In a normal ECG signal, the boundaries of each major wave are not visible to the naked eye. There is no actual definition where each major wave is supposed to start or end. However, there are a number of techniques available to approximately detect these locations including assessment of amplitude, slope and width as proposed by [44] or detecting the local maximum and minimum radius of curvature as mentioned in [45]. A combination of methods is preferred by electrocardiograph manufactures to increase the sensitivity and accuracy of the detection [46]. A widely used available software package for detecting ECG fiducial points is the ECGPUWAVE[47] which can be downloaded freely from Physionet [46, 48]. It is based on the algorithm of Pan and Tompkins [44] with some improvements that make use of slope information [49]. This software would be used

in detecting the fiducial points for all experiments in this thesis as it has sensitivity of 99.69% and a positive prediction of 99.77% [50].

3.2.4. ECG lead configuration

The term ‘lead’ for ECG is referred to two different things. The first term of ‘lead’ corresponds to the electrical cable and wires which connect the electrocardiograph machine with the surface electrode of the user [51]. The second term of ‘lead’ refers to the tracing of the voltage between two points on the human body. To differentiate between these two terms, in this thesis the second term of ‘lead’ will be written starting with a capital letter for example Lead. A Lead is composed of two electrodes of opposite polarity (bipolar) or one electrode and a reference point made up from a signal combination of other electrodes (unipolar) [52]. Different Leads record different aspects (angle) of the heart electrical activity.

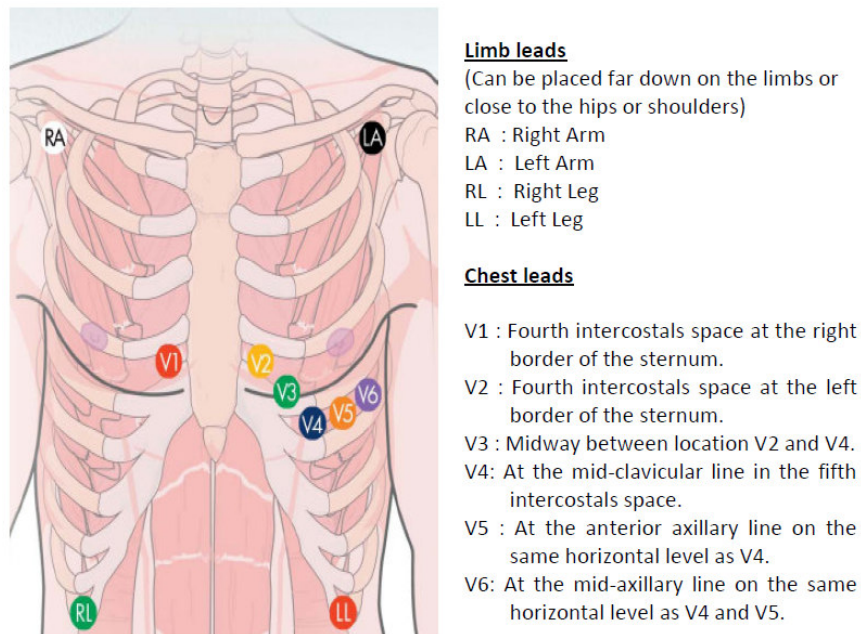


Figure 3-3 : 10 leads electrode placement in standard 12 Leads configuration

There are 10 leads and 12 Leads in a standard surface electrocardiogram. Four of the leads are connected to the limb and six leads are connected to the chest as illustrated in Figure 3-3 from [53]. Each combination of limb leads generates 3 bipolar (I, II and III) and 3 unipolar (aV_R , aV_L and aV_F) Leads as illustrated in Figure 3-4. It is configured based on Einthoven's triangle settings [54] proposed by Willem Einthoven in 1903 [55].

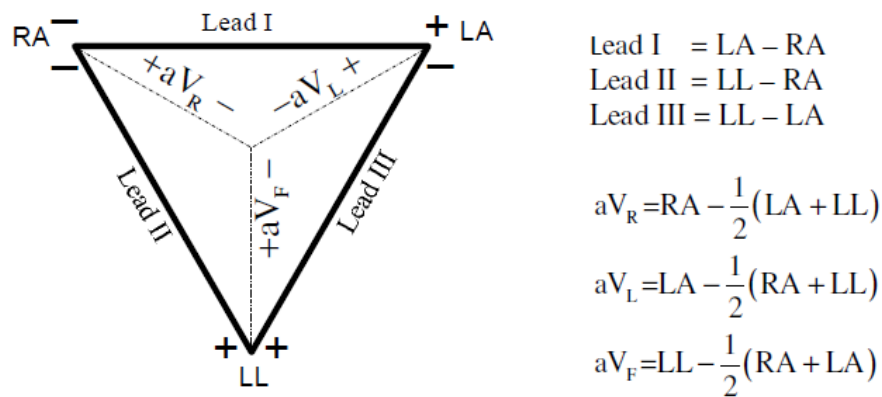


Figure 3-4 : Einthoven's triangle

The rest of the 12 Leads configuration comes from the chest leads. These Leads are unipolar Leads and symbolized by V_1 , V_2 , V_3 , V_4 , V_5 , and V_6 with respect to V_1 , V_2 , V_3 , V_4 , V_5 , and V_6 of the chest leads.

3.3. ECG AS A BIOMETRIC

3.3.1. ECG advantages as biometric

In chapter 2, we discussed 7 requirements that need to be satisfied for a person's characteristic to be considered as a biometric. In this chapter, we will evaluate how ECG fulfils these requirements. These requirements also represent the advantages for ECG implementation in biometric systems.

a) Universality

Electrocardiogram is associated with the electrical activity of the heart. All living humans have a heart which meets the first requirement for ECG to be considered as a biometric.

b) Distinctiveness

ECG inherits the distinctiveness from the individual's DNA [56]. Each human has a unique DNA fingerprint (except for identical twins) [57]. Unlike DNA, ECG distinctiveness also is affected by age, sex, body shape [25], lung-torso, blood mass-torso, torso-air conductivity [58], race [59, 60], and the geometrical shape of the heart [24, 61] making it different between twins.

c) Permanence

According to [62], the permanence characteristic of ECG was studied by a group of PTB researchers [63] by noting that similarity in healthy subjects occurred at different time intervals ranging from 0 to 118 days. In the study, the similarity between those ECGs was observed when they were plotted on top of each other. Despite the fact that ECG shapes do change due to sickness or injuries, these changes are not included in the above study nor will be the concern of this thesis. Zeisler *et al* [64] investigates properties of the ECG in order to classify which properties were invariant. Based on this study, it was concluded that the only known independent invariant properties of the electrocardiogram are its time relations, namely, the sequence of cycles, their rhythm, the temporal duration of the P, QRS, and T waves, and the Q-T, P-R, P-Q and S-T intervals.

d) Collectability

The ECG signals can be recorded, measured and analyzed using electrocardiograph machines. Also, construction of an electrocardiograph machine is cheap [65]. There are various locations of ECG lead placement which can be used to record the ECG signals as mentioned in section 3.2.4. However not all Leads configurations are

practical for a biometric system. According to [66], Leads I configuration is enough to identify individuals. The LA and RA leads can be placed at the tip of the user left hand and right hand fingers respectively as implemented in [67]. This configuration makes the ECG recordings simple and practical.

e) Performance

Research on ECG for human identification performed by [62, 67-97] indicates that ECG has the capability to identify individuals greater than 80% correct classification rates.

f) Acceptability

ECG acceptability by the society is subject to the same issue as other biometric traits - i.e. protecting the privacy of the user. The use of ECG is especially sensitive since ECG signals contain health information relating to the user which some people are reluctant to share. As long as the health information is secure and not divulged by the biometric system, ECG has the potential to be used as a biometric trait.

g) Circumvention

ECG signals are generated based on the activity of the heart. It is practically impossible for a fraudster to duplicate or replicate a user's exact ECG signals. To do so would require access to the heart of the user which is always covered by thorax and skin and requires an invasive method to misrepresent it. This ensures that the legitimate user must always be present during an identification transaction process.

3.3.2. The challenges implementing ECG as a biometric

In the previous subsection, the concept of permanence of ECG for biometrics is explained. Although a healthy individual's ECG shape does not change for a period of time, the temporal duration of the 3 major waves in an ECG complex change with regards to HRV effects. For example, when the heart rate increases, the P and T

waves tends to move towards the peak of R making the whole duration of ECG complex shorter. Another problem that needs to be considered upon implementing ECG as a biometric is the effect of AMV which may contributed by noises. As mentioned in the previous subsection, ECG also holds the user's health information. It is important that the ECG cannot be reconstructed from the feature vector stored in the system, in order to protect user privacy. In order to implement ECG for a practical biometric system, the effects from these three challenges need to be minimized.

3.3.3. Processing ECG with noise

Noise in ambulatory ECG recordings are typically generated from power lines, radio-frequency, electrosurgical noise and instrumentation noise, base line wander, Electromyogram (EMG) and motion artefacts [124, 125]. An example of an ECG signal is shown in Figure 3-5. The ECG shown in Figure 3-5 were recorded with respect to various activities. Regions A, B, C, D, E and F show the Lead I ECG signal when the user is respectively at rest (in a sitting position), slightly moving, opening and closing his/her hands, standing up and sitting down again, pressing both index fingers multiple times and inhaling slowly when breathing. As can be seen from Figure 3-5, the user activity changes the shape of the raw signal. There are 4 main ECG noises that usually reflect these changes which are the baseline wander, power line interference, motion artefacts and EMG as shown in Figure 3-6.

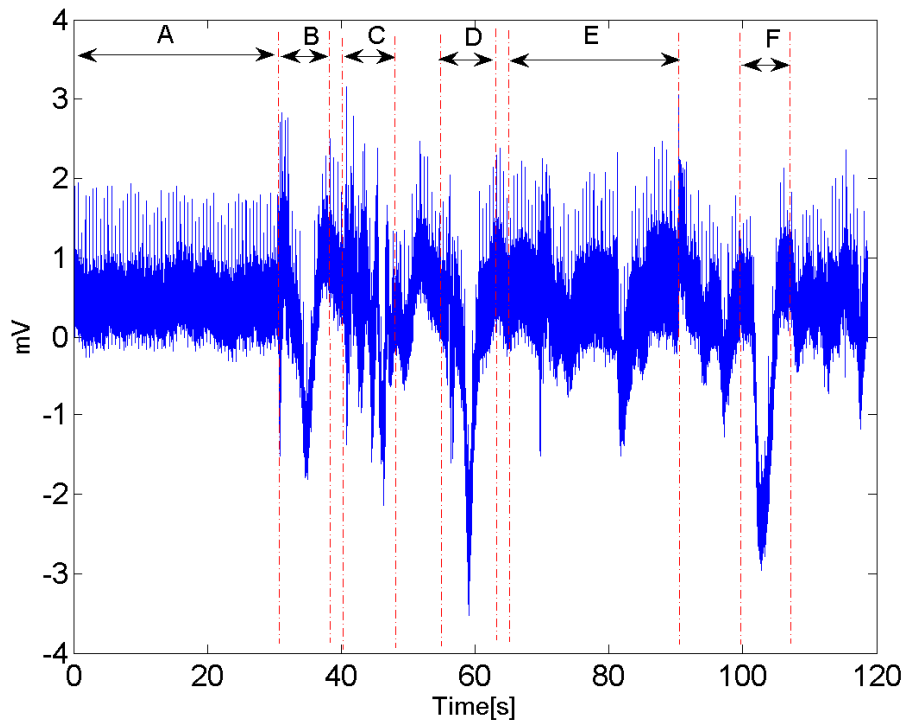


Figure 3-5: Example of Typical ECG recording

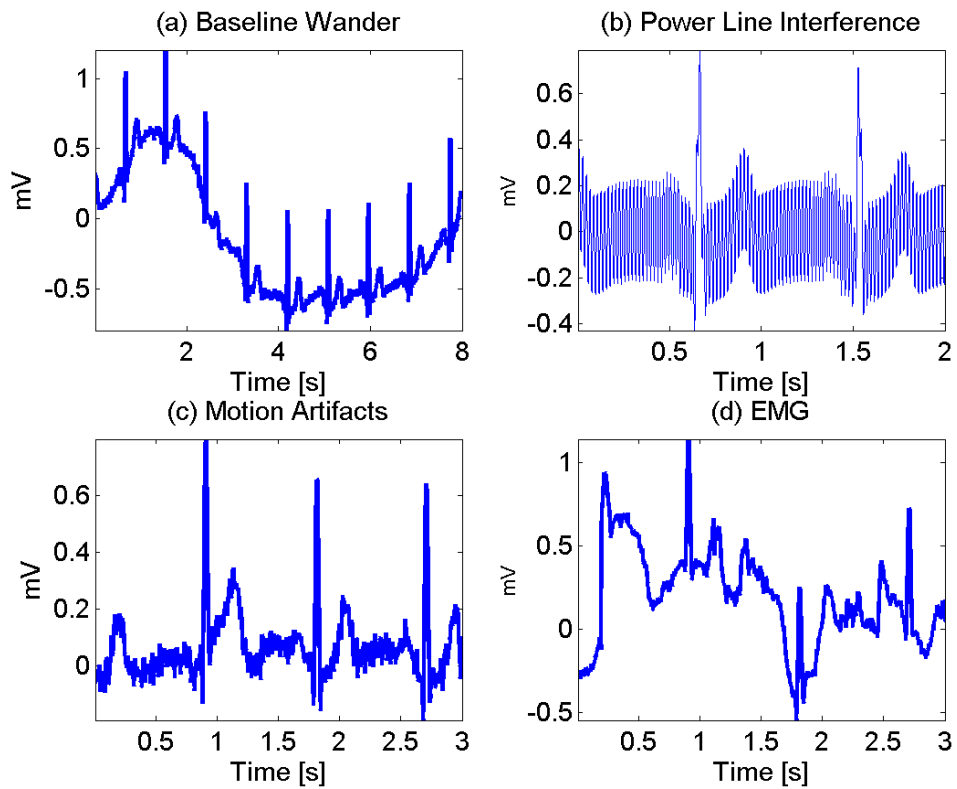


Figure 3-6 : Example of ECG noises

Baseline wander is a low frequency drift range between 0 to 0.5 Hz which can be removed using finite impulse response (FIR) notch filter [126]. Power line interference is a 50 Hz sinusoidal noises come from the power system and also can be removed using notch filter [127]. EMG has a broad bandwidth which sometimes overlaps that of the ECG [128]. Motion artefacts have a spectrum which completely overlaps the spectrum of the ECG [129]. These two types of noise are usually the most difficult forms of noise to eliminate from ambulatory ECG signals and require the use of adaptive filters [128-129]. Removing these noises is very important especially in medical application in order to preserve all accurate information embedded in ECG complexes. Example of designing adaptive filter to remove these noises using artificial neural networks can be found in [133-134].

In this thesis, the design of such filters is not the objective of this research. In ECG biometric application, an accurate reconstruction of ECG signals after filtering process is not that important as in medical application. The main objective of ECG filtering in biometric application is to remove low frequency drift, power line interference in the same time retaining as much as possible unique information from the ECG that can discriminate individuals [70].

Israel *et al* [70] studied the bandpass limits that is capable to retain most of the distinctive individual heartbeat information for identification from 20 000 raw ECG signals. In [70], the initial goal of filtering is to remove the low frequency noises less than 0.06 Hz and 60 Hz noise (US Power Line interference) while retaining the individual heartbeat information between 1.10 Hz and 40 Hz. Their observations indicate that ECG information in the frequency band from 43 Hz to 60 Hz and low frequency band from 0 Hz to 2 Hz changes with HRV of the same individual. Using ECG including these bands will reduce the capability of the biometric system to match different ECGs from the same subject. Their conclusion is that using a frequency bandpass filter between 2 and 40 Hz is practical for biometric applications to minimize the effect of HRV within the same individual.

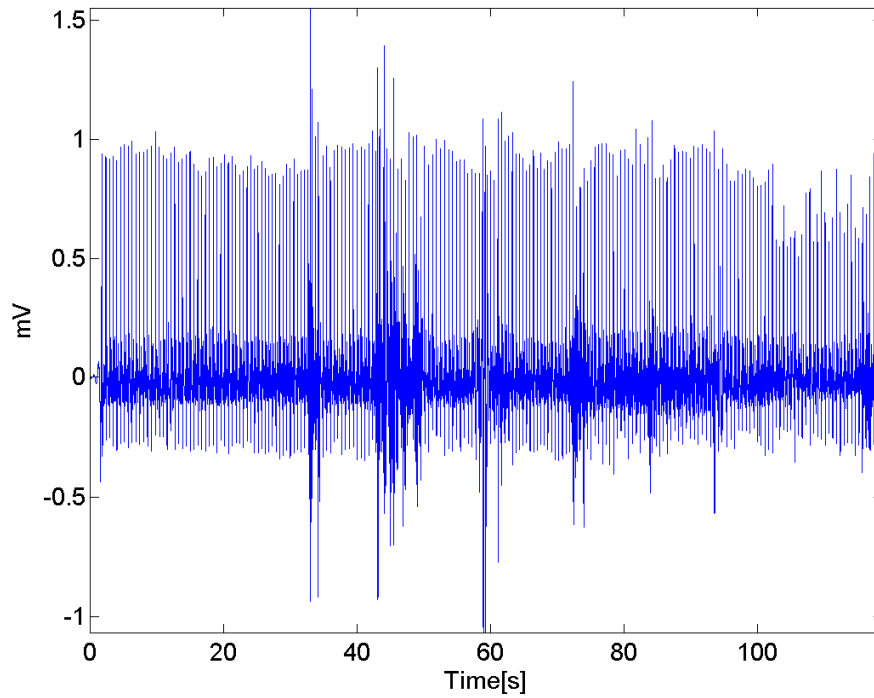


Figure 3-7 : Example of typical ECG signal band pass filtered from 2 to 40 Hz

For ECG biometric application, to minimize the effect of the EMG and motion artefacts in an ECG signals, in this thesis, feature vectors is extracted from an average of multiple ECG complexes instead of considering a complex at a time. In this way, the common attributes of these multiple complex is amplified. The outlier ECG complexes as shown in Figure 3-7 can be removed by introducing acceptable ranges in which an ECG complex can be accepted for averaging.

3.4. ECG DATABASE

All ECG signals in this thesis are taken from a public ECG database available on-line in the Physionet website [3]. This section will explain some strict requirements which must be fulfilled in order to use these ECG recordings for all experiments. These requirements are important so as to generate accurate results which can be compared with real time ECG recordings taken during biometric applications.

3.4.1. ECG recording requirements

ECG recordings taken from the public ECG database available on-line should abide by the following requirements:

- i. Each subject has at least 2 different ECG recordings. One will be used to generate the training database and another to generate the test database.
- ii. The two different recordings are taken in separate sessions, days, months or years apart. This to ensure that the ECG used in the experiment fulfil the permanence concept of a biometric traits.
- iii. The ECG is recorded in a practical manner. In this case, the recordings must come from a Lead I configuration.

3.4.2. Physikalisch-Technische Bundesanstalt (PTB) database

There are many public ECG database available on-line for example the MIT-BIH database [98], the European ST-T database [99], the Physikalisch-Technische Bundesanstalt (PTB) database [100] or taken from Physionet [3]. However, only PTB fulfils the requirements as indicated in subsection 3.4.1.

The PTB is selected because in this database the average time-interval between any two ECG recordings of the same subject is about 500 days [79]. The PTB database includes healthy and arrhythmia beats ECGs. A total of 112 subjects (98 subjects with arrhythmia beats and 14 healthy subjects) have been chosen from the database for all experiments in this thesis based on a requirement that each subject has at least 2 different session ECG recordings.

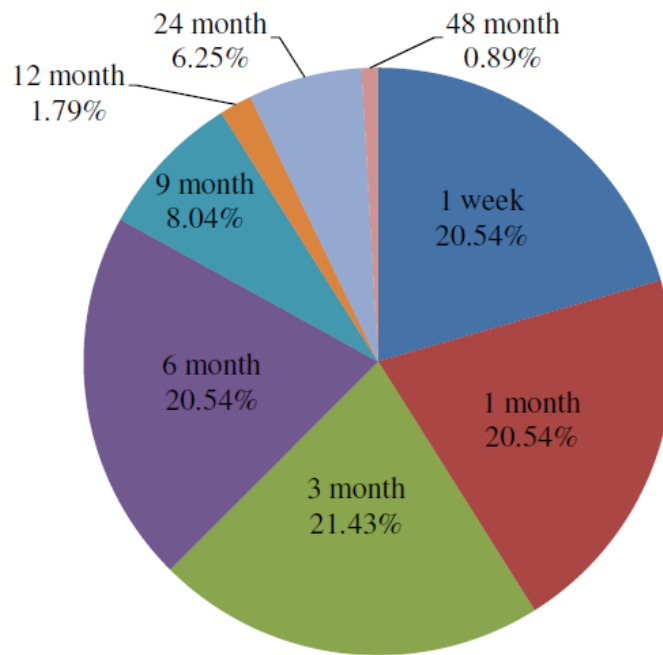


Figure 3-8 : Time intervals between recordings

The PTB database provides a 12 Lead ECG recordings, however only Lead I recordings will be used in all experiments in this thesis. Figure 3-8 illustrates the distribution of the time intervals between two ECG recordings used in this thesis. As can be seen from Figure 3-8 there are 23 pairs of recordings (20.54%) recorded with an interval of less than 1 week, 23 pairs of recordings (20.54%) are recorded with an interval between 1 week to a month, 24 pairs of recordings (21.43%) are recorded between 1 to 3 months, 23 pairs of recording (20.54%) have an interval between 3

and 6 months, 9 pairs of recording (8.04%) are recorded within 6 to 9 months and 10 pairs of recording (8.93%) are recorded with an interval greater than a year.

3.4.3. ECG filtering

ECGs provided from the PTB database are generally raw signals and require pre-processing to ensure that these ECGs are of the highest quality. A filtering process is performed on all ECG recordings so that only ECG components within 2 to 40 Hz are allowed [70] as discussed in section 3.3.3.

There are various digital filters available which generally can be categorized in two: Finite Impulse Response (FIR) and Infinite Impulse Response (IIR) filters. Usually, IIR filters are used when sharp cut off and high throughput are the only main requirement. FIR is used for a system where no phase distortion is acceptable. Since phase distortion has a greater effect on the recorded ECG, in this thesis, FIR filter will be used to ensure the ECG components are within 2 to 40Hz. The FIR filter in this thesis is designed with passband defined from 2 to 40 Hz and two stopbands defined from 1 to 2 Hz and 40 to 41 Hz. The Specification of the passband ripple is 0.1dB and a stopband attenuation of 80dB. In this thesis, a Kaiser Window FIR filter with 5019 taps is designed and implemented.

3.5. ECG BASED FEATURE EXTRACTION TECHNIQUE

There are over 40 publications with respect to the work on implementing ECG as a biometric dating back from the pioneering work of Biel *et al* [68] , Irvine *et al* [85] and Kyoso *et al* [69]. Previous literature works on most of these methods have been widely reported by Nasri *et al* [87] , Sufi *et al* [56] and Chauhan *et al* [82].

Improvement on the ECG based biometric technology reportedly from previous works comes from investigating various factors such as ECG recording technologies [66, 86], feature extraction [68, 70, 71, 76], feature selection [84, 90], classification methods [95, 97] and security system implementations [91].

All studies on using ECG for human identification uses ECG recording based on either single Leads [66, 83, 88, 89, 101], two Leads [81], three Leads [72, 79] or 12 Leads [68, 80]. ECG signals. However, most of the studies concentrate more on using single Leads which is the Lead I of a standard 12 Leads ECG recording to setup their databases. This is because of the practicality on collecting the ECG signals which can come from the finger tips [67] or palms [66, 88, 89, 101] of both individual hands.

Most studies of ECG biometric require the segmentation of ECG recordings into a single complex of ECG signals. However, there are also attempt work on not to segment the ECG recording before extracting the features [71, 76, 80, 93, 94]. The work in [71, 76, 80] generates features based on the auto-correlation of non-overlapping segments of the ECG recording. In [93, 94], the features are generated based on linear frequency cepstral coefficients and linear predictive coding.

The ECG features used for classification in previous studies can be categorized into characteristic features [68, 70] or waveform based features [71, 76, 80]. These categories will be further explains in the following subsection. In general, these features are obtained involving the process of feature extraction and/or feature selection techniques. Some of the studies use directly the immediate features extracted from the ECG signals for classification [79]. Most studies, process the immediate extracted features in order to generate a new set of features. Choices of classifier to be used in recognizing individuals using ECGs involves classification methods such as nearest neighbor [71, 80], Linear Discriminant Analysis [102], Nearest Center [95], neural network [96, 97, 103, 104], support vector machine [93], hidden Markov model [105, 106].

This thesis concentrates in works on improving the feature extraction techniques for ECG biometric authentication. In the literature, it is generally unknown if the good performance comes from using good extracted features, selecting the correct features or using the best classifier. The direction adopted in this thesis is that, if a biometric performance generates the best authentication profile solely due to the feature extraction technique, then this performance can be increased using an appropriate classifier. The main feature extraction techniques from the literature will be described in detail. A summary of the main contributions in the field is tabulated in Table 3-1. In Table 3-1, the 5 characteristic and 9 waveform based feature extraction techniques that are discussed in the following subsection are tabulated. The sample size of the test subjects ranges between 9 and 100 subjects. As can be seen from Table 3-1, these techniques generate identification performance greater than 80% and authentication performance greater than 3 % EER. Nine of the techniques tabulated in Table 3-1 required the detection of ECG fiducial points to generates the characteristic or waveform based features. From Table 3-1, it is also observed that only the methods published in [67, 68, 70, 79] use ECG recordings recorded with more than 24 hours interval.

As mentioned earlier, most ECG based feature extraction techniques can be categorized into either characteristic based or waveform based features. For this section, a description on the main characteristic based feature extraction technique will be presented in the first subsection. The second subsection will cover some of the important waveform based feature extraction techniques. The final subsection will provide summary and critical evaluation of these techniques.

Table 3-1 : Summary of Important ECG Based Feature Extraction Technique

Reference	Total Subject	Recognition Rate (%)		Categories	Fiducial Detection	Mode	ECG Intervals
		I	A				
Biel <i>et al</i> [68]	20	100		C	Yes	I	Multiple days
Kyoso <i>et al</i> [69]	9	99.6		C	Yes	I	Single day
Israel <i>et al</i> [70]	29	100		C	Yes	I	Multiple days
Wubeller <i>et al</i> [79]	74	99	2.8 (EER)	C	No	I A	Multiple days
Gahi <i>et al</i> [73]	24	100		C	Yes	I	Single day
Palaniappan <i>et al</i> [75]	10	97.6		W	Yes	I	Single day
Shen <i>et al</i> [78]	20	100		W	Yes	I	Single day
Seachea <i>et al</i> [77]	35	100		W	Yes	I	Not mentioned
Wang <i>et al</i> [102]	13	97.25		W	Yes	I	Single day
Plataniotis <i>et al</i> [76]	13	99		W	No	I	Single day
Agrafioti <i>et al</i> [71]	27	100		W	No	I	Single day
Fang <i>et al</i> [72]	100	99		W	No	I	Single day
Adrian <i>et al</i> [67]	50	89		W	Yes	I	Three days
Jianchu <i>et al</i> [74]	20		12.50 (FAR) 5.11 (FRR)	W	No	A	Single day

C=characteristic based, W= waveform based, I= Identification, A= Authentication

3.5.1. Characteristic based feature

Characteristic features use the visible information of the ECG characteristic for example amplitudes, temporal duration, slopes or all ECG points in a single complex ECG.

3.5.1.1. Amplitude, duration and slope

In 2001, Biel *et al* [68] demonstrated the possibility of using ECG to identify individuals. By using 12 Lead recordings configuration, ECG measurements are carried out on 20 subjects age between 20 to 55 years using SIEMENS Megacart equipment. The information from the SIEMENS ECG is then converted into 30 usable features which are normally used in the clinical analysis.

A total of 360 features are extracted from all 12 Leads ECG recordings. Their test shows that there are only small differences between using limb leads and the chest leads. For this reason, Lead I configuration has been chosen for further processing due to the simplicity of the electrode attachments. 30 features from Lead I are then reduce to 12 by removing features which are relatively high correlated with the others. After that, further reduction is done based on tests.

The summary of features used in [68] are shown in Figure 3-9. In this work, it is concluded that only 1 lead is enough to identify a person. However, a non-automatic feature detection in this work required special equipment or physician opinion to detect the features. Furthermore, the characteristics chosen were obtained by inspecting the correlation matrix. This limits the selection of features to be related only to the features available in clinical diagnoses of disease.

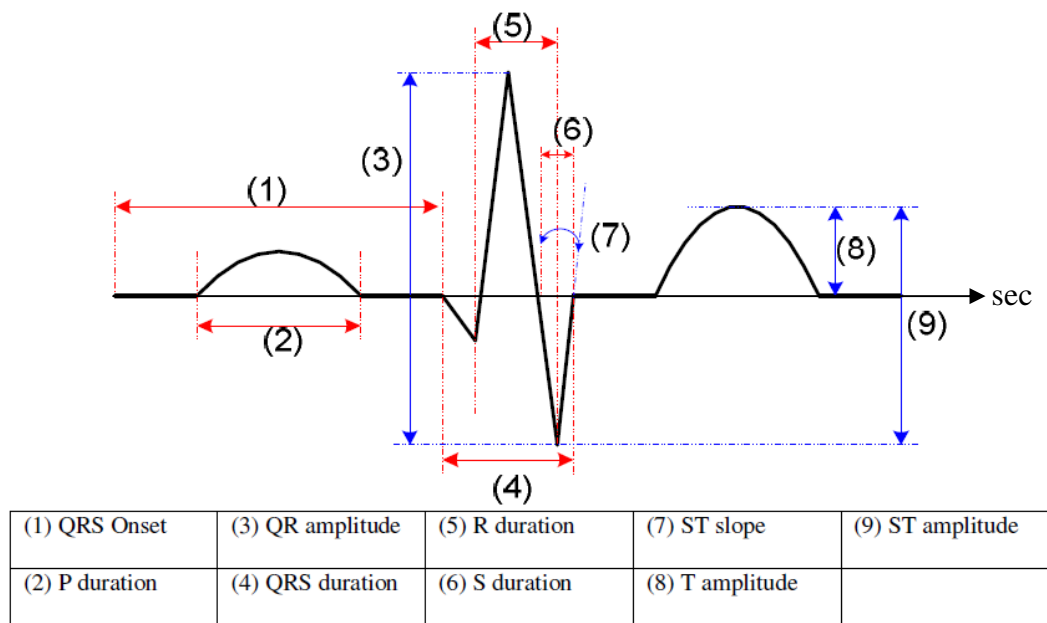


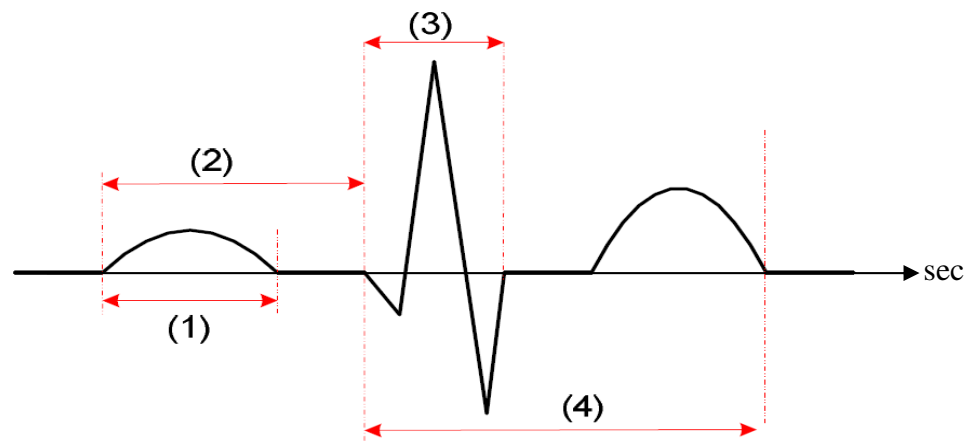
Figure 3-9 : Feature Vector used by Biel *et al* [68] for classification

Soft independent modelling of class analogy (SIMCA) approach is used to classify the person. Using SIMCA, a principle component analysis (PCA) is performed on each class in the data set, and a sufficient number of principal components are retained to account for most of the variation within each class. Various numbers of features have been tested for classification. However, experimental results using 9 features demonstrate the best classification which indicates 100% correct identification rate for a sample of 20 subjects.

In this work also, the best set of features for their observed high identification rates were found experimentally and not proven using a feature selection algorithm

3.5.1.2. *Amplitude and duration*

Kyoso *et al* [69] proposed an alternative method of ECG for identification by using only 4 features based on the duration and intervals of the ECG wave as shown in Figure 3-10. The features used in this technique also related only to the features available in clinical diagnoses of disease.

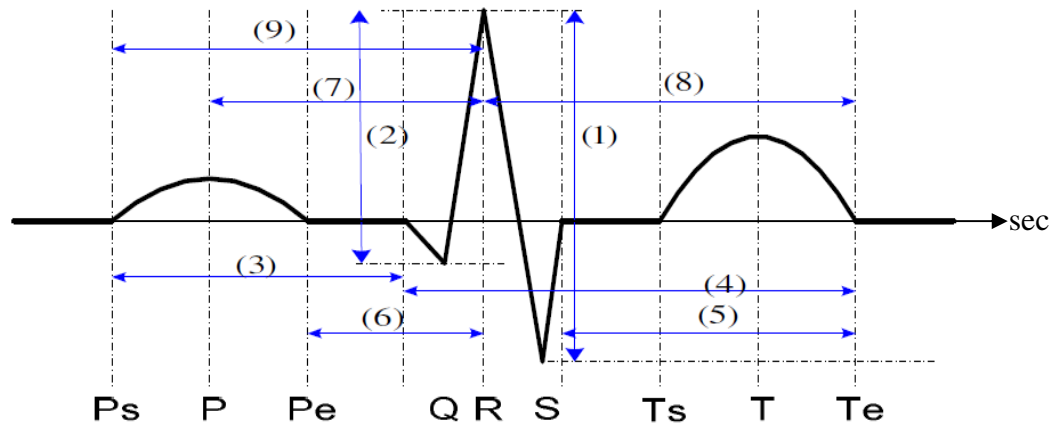


(1) P duration	(2) PQ duration	(3) QRS duration	(4) QT duration
----------------	-----------------	------------------	-----------------

Figure 3-10 : Feature Vector used by Kyoso *et al* [69] for classification

The ECG fiducial points are located using the second order derivative of the original wave. Mahalanobis generalized distance is then used to discriminate the features based on the smallest distance value. Experimental results on 9 subjects indicate that the system may achieve up to 99.6 % correct recognition. Kyoso *et al* only uses 2 dimensional discriminant analysis to discriminate the subject. This affects the accuracy of the system so for some subjects, the accuracy of certain combinations of features is only up to 7.5%

Gahi *et al* [73] reported to capture ECG characteristics using a wireless heart monitor and initially extract 24 features from it. Mean and variance calculations are used to remove the outliers which are not appropriate for training and classification. To select the best features, Information Gain Ratio (IGR) is used to assign score to each individual features. Nine final features, as shown in Figure 3-11, are finally accepted to have the best set of features. Mahalanobis distance based classifier is used to identify the individuals.



(1) RS amplitude	(2) RQ amplitude	(3) PsQ distance	(4) QTe distance	(9) PsR distance
(5) STe distance	(6) PeR distance	(7) PR distance	(8) RTe distance	

Figure 3-11 : Feature Vector used by Gahi *et al* [73] for classification

The experiment is performed on 16 subjects and manages to get 100% correct identification. The features established in this work are found experimentally using IGR. The disadvantage of using IGR to select features is that it computes a weight for a feature without examining other available features [107]. Adding 2 or more random features towards the initial 24 feature will generate different conclusion and reduce the performance of the system.

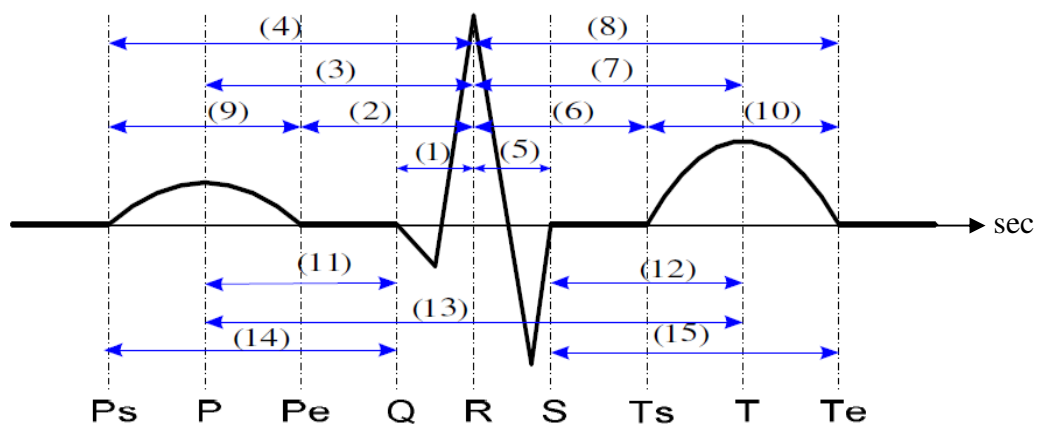
3.5.1.3. Temporal Duration

Israel *et al* [70] reported a more comprehensive study using 15 ECG pulse temporal features for human identification as shown in Figure 3-12. The raw ECG data is first filtered using a bandpass filter between 2 Hz and 40 Hz to remove the noises. The ECG is then broken into single heartbeats and aligned by their R peaks. The ECG fiducial points are then extracted in two steps. First, the peaks position is located by finding the local maximum of the P, QRS and T complexes. Then, the base positions are estimated through the location of the minimum radius of curvature. The features used in their experiment are the temporal distance between the R point and the fiducial points. Normalization process by the period of pulse is carried out so that the features are invariant to heart rate changes. The original 15 features are then reduced

to 12 features using Wilk’s lambda [108]. Classification based on the majority voting is used in this work to assign individuals to the selected classes.

Israel *et al* [70] provide 3 main knowledge contributions in ECG biometric performance, by conducting tests on 29 subjects. Their first experiment shows that their system performance achieves 81% of correct classification with 9% false positives. However, by having the same number of heartbeat for all subjects during the classification process, the performance increased to 87% correct classification with 0% false positives. The research also examined the relationship between identification performance and ECG lead placement.

By observing the ECG data comparing sensor placement between the neck and the chest, they concluded that there is a strong similarity between both sets of data and it is possible to use the neck ECG data as training and the chest data for classification or vice versa. The effect of state anxiety towards the performance of ECG biometrics was also studied in [70].



(1) R-Q distance	(4) R-Ps distance	(7) R-T distance	(10) T wave	(13) P- T distance
(2) R-Pe distance	(5) R-S distance	(8) R- Te distance	(11) P-Q distance	(14) Ps-Q distance
(3) R-P distance	(6) R-Ts distance	(9) P wave	(12) S-T distance	(15) S- Te distance

Figure 3-12 : Feature Vector used by Israel *et al* [70] for classification

Their findings indicate that by normalizing the features extracted from each subject, the performance of ECG biometrics is invariant to the individual's state of anxiety. Although, the methodology used in their experiments offers an automatic recognition for human identification, the accuracy of the system performance is low due to the location of the fiducial points used which are not properly defined or standardized for all subjects.

3.5.1.4. The whole ECG trace

In 2007, Wubbeler *et al* [79] performed an experiment on 74 subjects to investigate the potential of ECG for person recognition. Two dimensional ECG vectors from three Einthoven leads (I, II, III) are used in the experiments by first pre-processing them in terms of correcting the baseline noises, and then filtering them with a cut off frequency of 75 Hz. In this work, instead of extracting the features from the ECGs, a pattern recognition task was performed by comparing the ECG traces themselves. R peaks were determined from the absolute value of the low pass filtered temporal derivative of each ECG trace using a threshold procedure. For classification, 2 disjoint sets were drawn from the test set each containing 74 ECGs representing each subject. Standard nearest neighbour and threshold schemes were used to calculate the error rates.

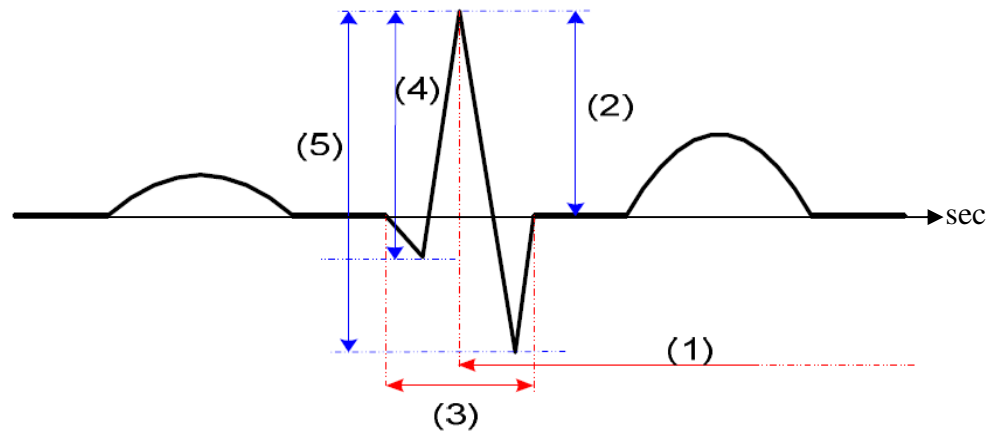
In the verification process, the false match ratio (FMR) was up to 2.5 %, the false non match ratio (FNMR) was up to 10 % and there was 2.8% equal error ratio (EER). The identification process manages to identify 99% of the subjects correctly. Although high authentication and verification results are obtained in their experiment, it is hard to accurately detect the trace boundaries due to the changes of the ECG traces. Using the whole ECG traces instead of extracting features is not practical for a large enrolment database.

3.5.2. Waveform based feature

Waveform based features are generated from a processed ECG waveform using signal processing methods such as correlation coefficient, phase space reconstruction, form factor, auto correlation coefficient, Fourier coefficient, wavelet distance and wavelet coefficients. These features are not visibly observed from the ECG characteristic and required the processing algorithms to explain the information representing the features.

3.5.2.1. Form Factor

Palaniappan *et al* [75], reported a technique to identify individuals using form factor on QRS characteristic as shown in Figure 3-13. In their work, QRS is detected using Pan and Thomkins method [44]. Multilayer Perceptron-Backpropagation (MLP-BP) and Simplified Fuzzy ARTMAP (SFA) have been used for classification. 1000 ECGs from 10 subjects had been tested and their classification results give up to 97.6% correct classification. In this method, a significant amount of distinctive information is excluded by not considering the information of the P wave and the T wave. Furthermore, the inter-beat interval (between the offset of the T wave to the onset of the next P wave) is a transition stage that is independent of the electrical timing mechanism of the heart [70].



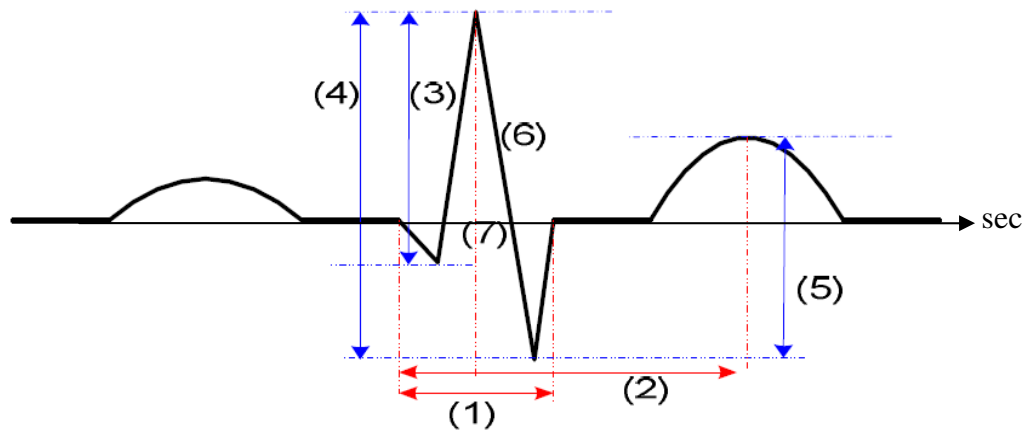
(1) R-R interval	(2) R amplitude	(3) QRS interval	(4) Q-R amplitude	(5) R-S amplitude
------------------	-----------------	------------------	-------------------	-------------------

Figure 3-13 : QRS characteristic used by Palaniappan *et al* [75] to generate feature vector using form factor

This interval can be considered as a random signal which does not represent an electrical activity of the heart and should not be included as a part of human feature vector.

3.5.2.2. Correlation Coefficient

In 2002, Shen *et al* [66] used correlation coefficient of 7 characteristic features from the QRS complex to classify 20 individuals for recognition as shown in Figure 3-14. A template matching is first used to calculate the correlation coefficient among the QRS complexes and a decision based neural network (DBNN) is then used to validate the identity of these 20 subjects. Each subject will submit 20 ECG recording to build up the training set. The correlation coefficient threshold is set to 0.85 in this work. When the average correlation of the 20 ECG recording per subject is less than 0.85, it is concluded that there are no matches between the template and the subject. If the value is greater than 0.85, DBNN will be carried out to determine the identity of the subject. 95% and 80% subject recognition rate were achieved for the template matching and DBNN being performed separately, but the performance achieved 100% when the template matching is done first followed by DBNN as a whole system.



(1) Q-S distance	(3) Q-R amplitude	(5) S-T amplitude	(7) QRS Triangular area
(2) Q-T distance	(4) S-R amplitude	(6) R-S slope	

Figure 3-14 : QRS characteristic used by Shen *et al* [66] to generate feature vector using correlation coefficient

Although the combination of both modules achieved 100% recognition rates for a samples of 20 subjects, using information only related to the QRS complexes discards a lot of information from the ECG recordings which may be useful for a larger training database.

3.5.2.3. Fourier Coefficient

Seachia *et al* [77] proposed a different approached in order to use ECG for identification by using a Fourier transformation. A normalized ECG based on the same heart rate is first divided into 3 subsequences which correspond to P, QRS and T waves. A Fourier transform is taken on these subsequences which later produced a number of Fourier coefficients. Only the significant elements of the Fourier coefficient are selected to be classified using neural networks. Out of 35 subjects being tested, 2.85% were not identified correctly.

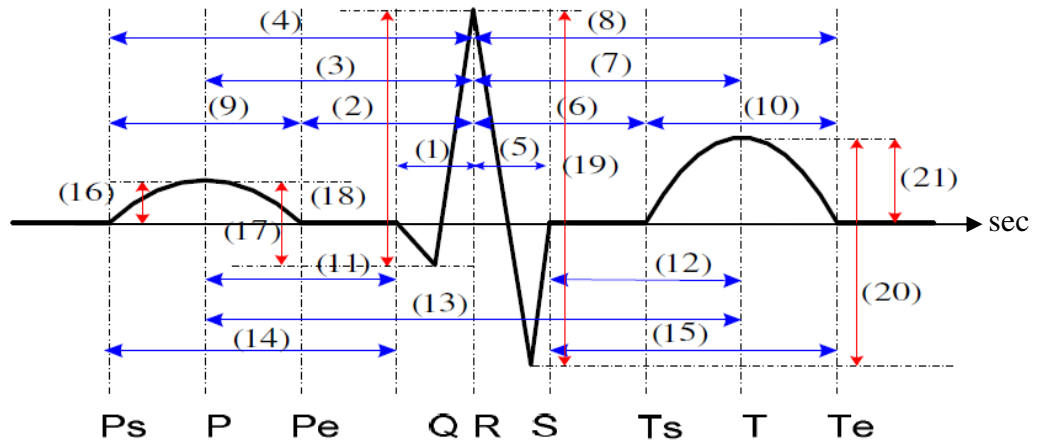
3.5.2.4. Combine Waveform and Characteristic features

In Wang *et al* [109], the waveform features of the ECG trace is captured using Principal Component Analysis (PCA) and Linear Discriminant Analysis (LDA).

These were combined with 21 amplitude and duration features as illustrated in Figure 3-15. ECGPUWAVE is used for detecting peak R of an ECG wave. Then, the heartbeats of a single record are all align by the R peak position and truncated by a window of 800 samples centered at R. QSPT based and peak points were detected in a similar method to that shown in [70] . In order to select a number of features that produced minimum classification error, feature selection method was carried out based on Wilke's lamda in SPSS. The feature vector is compared using the Euclidean distance and clustering was performed based on nearest neighbor and nearest centre techniques.

Experiments are performed based on ECG signal of 13 subjects. Using only distance features, 74.45% of heartbeat identification is achieved. By adding the amplitude features, the heartbeat recognition rate increased to 92.40%. Their comparison result using PCA and LDA with K-nearest Neighbours (KNN) classifier managed to achieve 95.55% and 93.01% identification respectively.

This shows that PCA and LDA are good for human identification from ECG. However, by combining the classification process using the amplitude and distance features with PCA and KNN classifier, the heartbeat recognition accuracy increased to 98.90 %. In this work, the problems in determining the accurate boundaries of the P wave and T wave are still not resolved. This will affect the biometric performance when applied to an ECG with irregularity on the waveform shapes.



(1) RQ distance	(5) RS distance	(9) P wave	(13) PT distance	(17) PQ amplitude
(2) RPe distance	(6) RTs distance	(10) T wave	(14) QPs distance	(18) RQ amplitude
(3) RP distance	(7) RT distance	(11) PQ distance	(15) STe distance	(19) RS amplitude
(4) RPs distance	(8) R Te distance	(12) ST distance	(16) PsP amplitude	(20) ST amplitude
(21) TTe amplitude				

Figure 3-15 : Characteristic features used by Wang *et al* [109] without PCA and LDA features

3.5.2.5. Auto Correlation

In Plataniotis *et al* [76], the ECG is first filtered to remove noise. Every ECG signal must have the same length regardless of the number of ECG complexes contained in that length. Then auto correlation (AC) of the ECG segments is used to capture the essential attributes of the waveform. The number of AC lag (window) depends on a user selection value. To discriminate effectively ECGs from different subjects, a large window length is required. However this will produce high number of features. The Discrete Cosine Transform (DCT) is then applied to reduce the dimensionality and select only useful characteristic for recognition.

To evaluate the performance of the proposed method, normalized Euclidean distance and normalized Gaussian log likelihood had been used for comparison. The method was tested on 14 subjects, the identification performance was 100% for window and subject based recognition. Although the classification result is good, the method is highly dependable to the effectiveness of the filtering process. Any abnormalities

within the ECG length will produce inaccurate AC coefficients within the same subjects. The effect of HRV of the same subject also will produced discrepancy to the AC values prior to the increased or decreased number of ECG complexes per ECG length. In addition to that, even though DCT manages to reduce the dimensionality of the features, the number of features that are capable to produce good discrimination is still large. This will limit the size of the database for any application.

Agrafioti *et al* [71, 110] extended the usage of autocorrelation (AC) for feature selection. The windowing process is first adapted to the ECG signal in order to segment it into non overlapping windows. Then normalized autocorrelation is calculated for every window. Similarly as in the case shown in [76] , the AC process generates a large number of features. Template Matching with the correlation coefficient is performed on the AC coefficient signal. This process is used to shorten the time of the search space by reducing the number of classes so that classification is carried out in a smaller group. Two techniques are highlighted in the work in order to reduce the dimensionality of the features. They are the Discrete Cosine Transform (DCT) and the Linear Discriminant Analysis (LDA). The similarity measure is based on Euclidean distance and nearest neighbour (NN) is used as a classifier.

Experiments are carried out onto 27 subjects. When AC and DCT methods are used, the subject and window recognition rates are 96.3% and 86.3% respectively, while when AC and LDA method are used, the subject and window recognition rates increased to 100% and 95.8% respectively. In this work, the accuracy problem in calculating AC for the same subject, while the heart rate changes, is still not resolved. In this work, inserting additional template matching process compared to the work performs in [76] only reduces the classification processing time. The number of features used for classification is still large.

3.5.2.6. Phase Space reconstruction

Fang *et al* [72] proposed using the whole ECG signal for recognition. The ECG is first filtered using 4th order Butterworth bandpass filter with the pass band from 2 to

50Hz to remove the noises. Then peak R is detected and the waveforms of five consecutive cardiac cycles were averaged with respect to the R peaks. Three dimensional vectors with respect to the average ECG wave are set up using two different ways. The first technique is by embedding 2 different time delays to the original averaged waveform. The other technique is by using 3 different lead configurations denoted as anterior, lateral and posterior leads. The vector is then normalized over the entire cardiac cycle. Spatial correlation (SC) and mutual nearest point distance (MNPD) are used for similarity and dissimilarity measurement. Out of 100 subjects being tested in their experiment, the proposed method manages to achieve 99% sensitivity with 99% accuracy using MNPD and 98% sensitivity with 91% accuracy using SC. In order to get a good classification result, the method needs to evaluate a large number of points or features. The storage of the whole ECG waveform also will create a privacy problem as a lot of personal information can be extracted from the ECG wave.

3.5.2.7. Wavelet Coefficient

Adrian *et al* [67] uses a wavelet distance measure to identify 50 subjects. The ECG data is collected using two Ag-AgCL button electrodes that are held between the thumb and index finger of the user. A 90 seconds ECG data sequence was recorded from each subject for three different sessions. For each data, PQRST complexes were automatically detected using the multiplication of backward difference algorithm [111]. Correlation coefficients were computed between the PQRST complexes. Any PQRST complex with a correlation coefficient below the standard deviation of the mean correlation coefficient will be discarded. The remaining PQRST complexes were then averaged. Discrete wavelet transform coefficients are computed for each average signal using Daubechies scalar wavelet (Db3) with a five level decomposition. The accuracy of this technique is 89%.

In the work of Jiancu *et al* [74], raw ECG signals were decomposed into a structure of coefficients using 'bior1.1' wavelet algorithm at scale 6. This coefficient structure was further extended to a coefficient matrix which principle components were used to discriminate between individuals. This work is performed on 20 different

individuals with 91 % correct classification. In this work, the capability of the technique is reduced by the principle component method since only 40% of ECG information is used.

3.5.3. Summary and critical evaluation

Table 3-1 summarized the important previous work of the characteristic and waveform based feature extracting technique for ECG biometric as described in the previous subsections. As indicated in Table 3-1, most of the methods which manage to achieve 100% correct classification use less than 50 subjects. It is suggested in this thesis that the number of subjects for recognition should be increased to greater than 100. In sections 3.5.1 and 3.5.2, it is shown that most of the works tabulated in Table 3-1 investigate the performance of their feature extraction methods in term of identification modes which require the use of good classifiers. In this study, we focus on investigating the performance of new feature extraction methods for authentication purposes without combining any sophisticated classifier to improve the performance of the biometric system. Comparisons between two ECG recordings of a subject are done based on template matching using simple distance based similarity measures described in section 2.6.1.

In Table 3-1, the characteristic and waveform based feature extraction techniques described in [68-70, 73, 75, 78, 109] use parametric features and require the detection of the 9 fiducial points of the normal ECG signal. Such parametric features associated with the attributes of the ECG may include basic geometric parameters such as length, width, amplitude and/or slope of each wave in an ECG complex. In [68-70, 73, 75, 78, 109], some of the works use these parametric features directly as feature vectors while some require further processing to generate more discriminative features. In section 3.2.2, it has been described that the ECG traces are specifically related to the activity of the ion moving in and out of the cell. For ECG to be used as biometric, it is believed that extracting features based only parametric features discards a lot of information with respect to the ions activities.

The work described in [71, 72, 74, 76, 112] tends to use non parametric features by requiring no ECG fiducial points. As a result, the non parametric features extracted from the ECG signals generate a high number of features thus limiting the storage capacity of the security system. For this reason, these techniques require feature selection or reduction approaches to reduce the dimension of the extracted features. Naturally, additional steps will increase the processing time for the whole system for a large number of subjects. The proposed work which has been carried out in this thesis uses a hybrid concept of parametric and non parametric features. For the proposed technique, more characteristic features are extracted from the ECG signals whereas previous methods have been limited to the use of fiducial locations. However, no data reduction technique is required to reduce the size of the extracted features as it is not that large.

It is also observed that the approaches shown in [71, 72, 74, 76, 112] use feature extraction methods that need to consider more than 1 continuous ECG complex for extraction. Based on section 3.2.2, it has been described that inter beat location between two contiguous ECG complexes is free from the electrical timing mechanism of the heart. It is suggested that the non electric active ECG portion should be excluded for human identification as this region does not reflect the electrical activity of the heart.

As described in section 3.2.3, fiducial locations are related to the heart rate of a person. Not considering these locations as part of the extracted features neglects the issue of HRV. Results presented by [71, 72, 74, 76, 112] do not consider this situation thus raising doubts if these methods can be practically applied when the HRV changes rapidly in general authentication applications.

Evaluating the methods presented in sections 3.5.1, 3.5.2 and Table 3-1, it is observed that the ECG database used only consider ECGs from a healthy subject with a healthy ECG trace. For ECG to be used as biometric in a general population, unhealthy (or arrhythmia) ECG traces need to be consider. By evaluating the arrhythmia ECG trace the biometric performance will be reduce. For practical

implementation, this type of ECG need to be investigates in order to give a concussive overview of the feature extraction performance.

Finally, the methods reviewed on using ECG as a biometric only represents a single level of security. This means that, if the ECG of a user is compromised, the ECG cannot be used any further for biometric authentication. This unacceptable situation will be addressed in the work presented in Chapter 6.

3.6. CONCLUSION

This chapter investigated the concept of using the ECG as a biometric. An overview of electrocardiogram, advantages and challenges of ECGs as biometrics, ECG database and finally ECG based feature extraction techniques are described in this chapter. To implement ECG as a biometric, the effects due to HRV, AMV, and the issues due to the security of the user health information need to be minimized. The next chapter introduces a new feature extraction technique known as Pulse Active technology. This technique has the capability to minimize the effects of HRV, AMV and also secure the health information of the user. The capability of the new feature extraction technique will be investigated by performing authentication mode biometrics.

CHAPTER 4.

PULSE ACTIVE (PA) FEATURE EXTRACTION TECHNIQUE FOR ECG BIOMETRIC AUTHENTICATION

4.1. INTRODUCTION

In chapter 3 it was highlighted that in order to practically use ECG as a biometric, the effects of HRV and AMV need to be minimized. Furthermore, it was indicated that the techniques to extract ECG features for biometric purposes must not allow reconstruction of the original ECG signal based from the information stored in the security system. This chapter introduces a new feature extraction technique named Pulse Active which is capable of minimizing the effect of HRV and AMV. This new technique is also capable of preventing the reconstruction of original ECG signal from the features and algorithms stored in the system thus making it ethically acceptable.

This chapter starts with the definition of Pulse Domain concept. This is followed by the description of a new Pulse Active feature extraction technique. This chapter then discusses various factors on implementing PA for ECG based biometric application. Finally, the performance of the new feature extraction technique will be evaluated for biometric authentication.

4.2. PULSE DOMAIN PHILOSOPHY

The general concept of Pulse Domain is defined with a statement indicating that the relationship between two locations on any given signal can be presented by a simpler signal derived from a simple mathematical function known as a pulse. When multiple pairs of locations on the given signal are taken into consideration, a series of non periodic pulse waveform is generated. There are various available methods which are capable of generating pulse waveforms. The most well known are for example the Pulse Width Modulation (PWM), Delta Modulation (DM), Delta-Sigma Modulation (DSM), Pulse Code Modulation (PCM), Pulse Density Modulation (PDM), Space Vector Modulation (SVM) and Sliding Mode Control (SMC).

The work on Pulse Domain concept in this thesis concentrates mainly on investigating ways of generating a unique pulse waveform in order to represent the original signals. In this thesis, two new methodologies are presented to generate a unique pulse waveform for signal representation named Pulse Active (PA) and Adaptive Pulse Active (APA). This chapter will discuss the PA techniques while the next chapter discusses the APA

4.3. FUNDAMENTAL OF PULSE ACTIVE (PA)

'Pulse Active' refers to a method of transforming a signal into pulse domain based on the concept of Pulse Width Modulation (PWM) technique. PWM has been successfully implemented in many fields such as communication, electronic control, power electronic control and measurement circuits. In this thesis, PWM is modified

to be used as a new feature extraction technique to be used for a novel pattern recognition method.

4.3.1. Pulse Active Topology

The topology structure of the Pulse Active (PA) technique is illustrated in Figure 4-1. The operation of the PA technique, as shown in Figure 4-1, is based on amplitude comparison between the investigated signals (in this thesis an ECG signal) with a triangular wave. When the amplitude of the investigated signal is the same as the amplitude of the triangular wave, the output pulse will start to rise or fall based on certain rules which will be explored further in section 4.4. These transition states of the output pulse are used in the feature extraction process from the investigated signals.

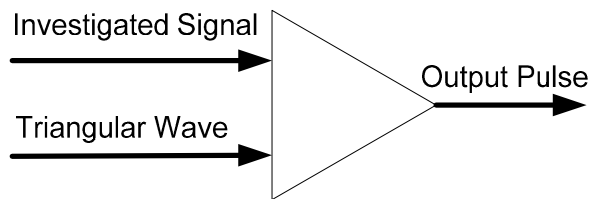


Figure 4-1: Topological Structure of Pulse Active Technique

4.3.2. Pulse Width Modulation

Conventionally, PWM is a process of generating a series of output pulses when an investigated signal is modulated by a modulating signal. Generally, the amplitudes of the investigated signal are represented by variable widths of the output pulse. Figure 4-2 shows a simple method to generate the PWM output pulses. In this example, a sinusoidal wave is chosen to be the investigated signal while a triangular wave is assigned as the modulating signal. Based on the PWM technique, when the

amplitude of the modulating signal is less than the investigated signal, the PWM is in the high state. Otherwise, it is in the lower state

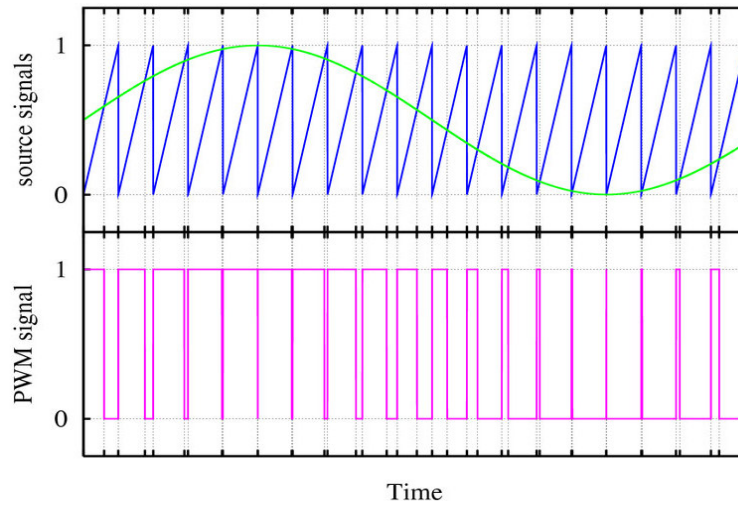


Figure 4-2: Simple Example of PWM Generation

4.4. FEATURE EXTRACTION

The PA technique requires at least two fiducial points to start and end the process. Based from literature discussed in section 3.5, there are 4 common locations to extract ECG features for biometric authentication. However, no matter which location is chosen to start and end the extraction process, the derivation of the generalized PA location will be the same. Further explanation on selection of these locations will be provided in section 4.5. For the purpose of derivation, the peak locations of P and T waves will be defined as the respective starting and ending points of the PA process.

Consider a segmentation of an ECG signal, $y_{ECG}(t)$ for the duration of T_{ECG} from the peak of P to the peak of T with peak-to-peak amplitude of A_{ECG} as shown in Figure 4-3.

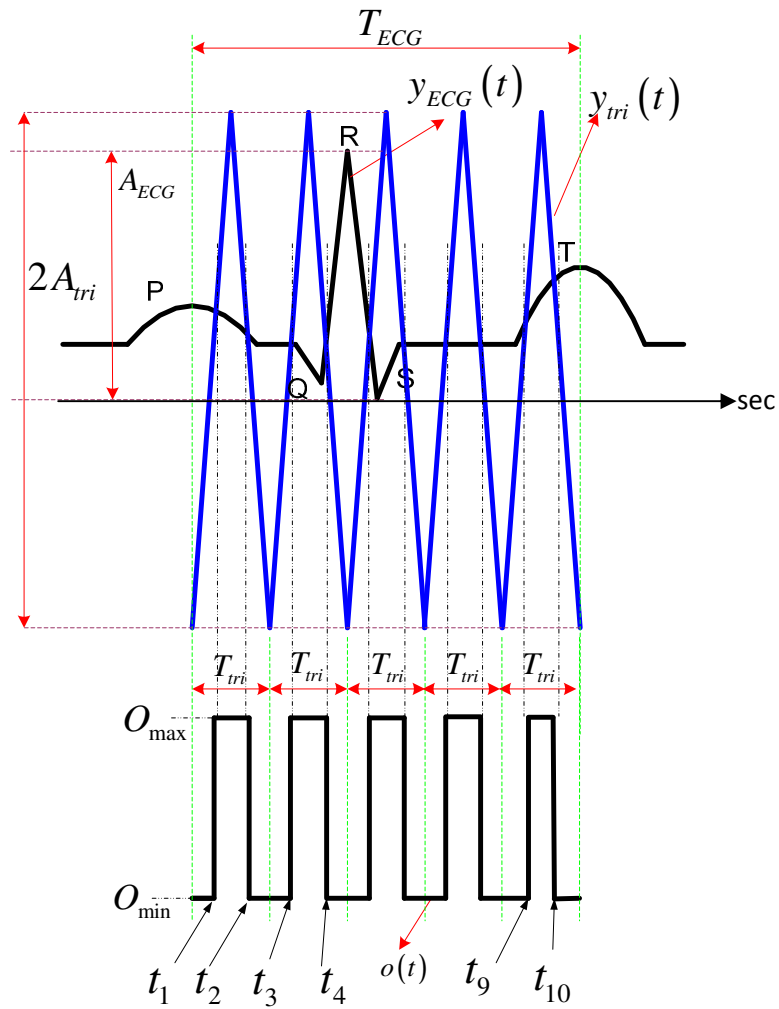


Figure 4-3: Waveform generation of Pulse Active technique

The ECG signal is offset so that its minimum value is equal to zero. The maximum amplitude of $y_{ECG}(t)$ is A_{ECG} . Consider now a periodic triangular waveform $y_{tri}(t)$ of period T_{tri} with maximum amplitude A_{tri} , where $T_{tri} < T_{ECG}$. The latter waveform is superimposed on $y_{ECG}(t)$ as illustrated in Figure 4-3. A modulation factor m_f is introduced and defined as:

$$m_f = \frac{T_{ECG}}{T_{tri}} \quad (4-1)$$

where T_{tri} is selected such that m_f is an integer. In Figure 4-3, $m_f = 5$. The other parameter which also relates $y_{ECG}(t)$ to $y_{tri}(t)$ is the modulation index m_i which is defined as:

$$m_i = \frac{A_{tri}}{A_{ECG}} \quad (4-2)$$

It is important to note that m_f represents the number of periodic triangular waves for $y_{tri}(t)$. As mentioned in the previous chapter, ECG complexes are time varying from one another. This means that it is impossible for two ECG complexes to be exactly the same even though they may come from the same user. Two major contributors to the time varying phenomenon are the HRV and AMV. For example when the heart rate increases the P and T waves of the ECG signals tend to move towards the R making the T_{ECG} duration of the ECG signal shorter. By adjusting the value of m_f , using (4-1), the period of the triangular wave T_{tri} also reduces (to compensate for the reduction of T_{ECG}). Similarly, in cases of AMV, the amplitude of each point in an ECG complex is slightly lower or higher compared to the next ECG complex for similar locations. The rate of variations for these amplitudes is proportional to the values of A_{ECG} . Since the generation of $y_{tri}(t)$ is related to the value of A_{ECG} , adjusting the value of m_i in (4-2), compensates for the reduction of A_{ECG} by ensuring that the amplitude of the triangular period, A_{tri} also reduces.

In Figure 4-3, each period of the periodic triangular waveform, $y_{tri}(t)$ intersects the underlying ECG signal $y_{ECG}(t)$ to generate the output pulses $o(t)$. The max and min of each pulse is O_{max} and O_{min} respectively. To ensure intersections occur between $y_{ECG}(t)$ and $y_{tri}(t)$ within each period, m_i should be selected greater than 1 or $A_{tri} > A_{ECG}$. There are two rules to generate these output pulses. The simplest way is by using the Above Maximum Area (AMA) rule, and the other way is by using the First Rise Last Fall (FRLF) rule. These are now described.

4.4.1. Above Maximum Area (AMA)

The Above Maximum Area (AMA) rule is taken from the concept of the PWM whereby the output pulses $o(t)$ are formed based on amplitude comparison and can be obtained as follows:

$$o(t) = \begin{cases} O_{\max} & y_{ECG}(t) \leq y_{tri}(t) \\ O_{\min} & y_{ECG}(t) > y_{tri}(t) \end{cases} \quad (4-3)$$

for $t = 0 \dots T_{ECG}$, where $[O_{\max}, O_{\min}]$ are user specified values.

Using this rule, the transition state vector T_{trans} is defined as the intersection points where the output pulses change from O_{\max} to O_{\min} or vice versa and can be represented as:

$$T_{trans} = [t_1, t_2, t_3, \dots, t_{2m_f}] \quad (4-4)$$

for $m = 1, 2, 3 \dots m_f$. The odd intersection points refer to the locations where $y_{tri}(t)$ becomes greater or equal than $y_{ECG}(t)$ while the even intersection points are the location when $y_{ECG}(t)$ becomes greater than $y_{tri}(t)$.

As an example Figure 4-4, illustrates the PA output pulse generated from an ECG complex of a subject for m_f setting equal to 6. As can be seen from Figure 4-4, $m_f = 6$ generates 6 output pulses in $o(t)$.

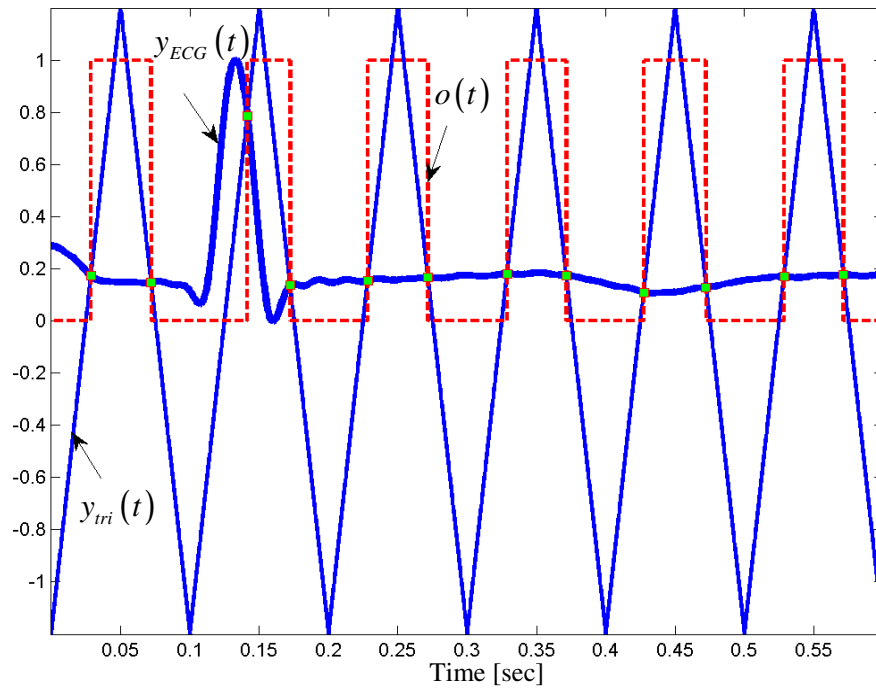


Figure 4-4: Pulse Active output generation using AMA without error

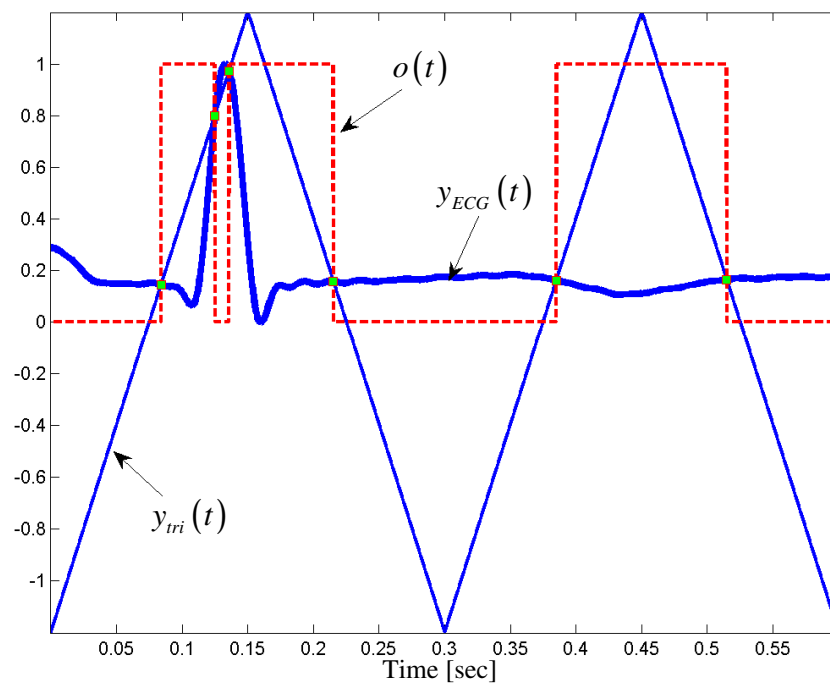


Figure 4-5: Pulse Active output generation using AMA with error

The same ECG complex used in Figure 4-4 is then re-processed using the PA technique with a m_f setting equal to 2. This process is shown in Figure 4-5. From Figure 4-5, it is observed that when m_f is set to 2 for this ECG complex, the number of output pulses generated is equal to 3.

To use PA for ECG biometrics the number of pulses produced represents the dimension of the feature vector extracted. As indicated from the previous two examples the AMA approach does not guarantee a fixed feature vector dimension (number of pulses) for a given ECG complex. Thus AMA based PA using a pulse by pulse comparison cannot be readily used for ECG biometric with application to authentication. For a pulse by pulse comparison, the use of First Rise Last Fall (FRLF) rule for PA techniques is investigated next.

4.4.2. First Rise Last Fall (FRLF)

Based on the First Rise Last Fall (FRLF) rule and with reference to Figure 4-3, for each triangular wave period the location of the first intersection from the rising edge t_{+ve} and the location of the last intersection from the falling edge t_{-ve} are selected as the intersection points for that period. This is defined as the First Rise Last Fall (FRLF) rule. Mathematically, this is described as follows:

$$t_{(2m-1)} = t_{+ve} \quad \text{for} \quad (m-1)T_{tri} \leq t_{(2m-1)} \leq \frac{(2m-1)}{2}T_{tri} \quad (4-5)$$

$$t_{2m} = t_{-ve} \quad \text{for} \quad \frac{(2m-1)}{2}T_{tri} \leq t_{2m} \leq mT_{tri} \quad (4-6)$$

$$\mathbf{T}_{trans} = \left[t_{(2m-1)} \quad t_{2m} \right] \quad \text{for} \quad m = 1, 2, 3, \dots, m_f \quad (4-7)$$

FRLF rules ensure that the total number of output pulses equal the number of the m_f setting. Figure 4-6 illustrates the output pulse generation of the same ECG signal used in Figure 4-4 and Figure 4-5 using m_f equal to 2. As can be seen from Figure 4-6, m_f set to 2 generates two output pulses which are used in a pulse by pulse comparison. Thus, FRLF will be used to generate T_{trans} in all PA algorithm

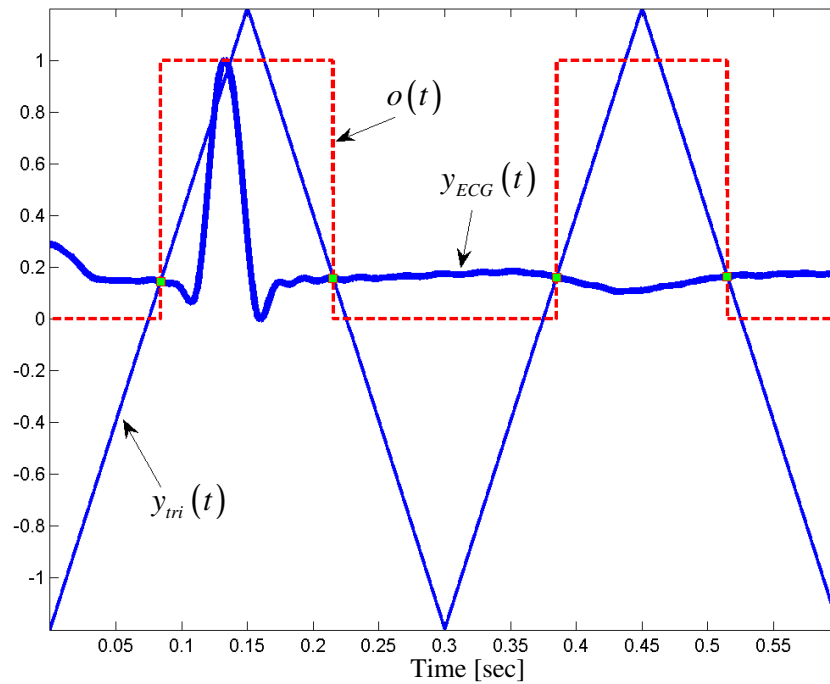


Figure 4-6: Pulse Active output generation using FRLF

4.5. FEATURE LOCATION

Every part within an ECG complex represents different characteristics of the ECG features. This section will describe various locations within ECG traces to be used for feature extraction.

4.5.1. Single complex

As illustrated in Figure 3-2, a complete ECG complex is defined from P_s to T_e (P_sT_e). To ensure that all ECG characteristics are taken into account, the first location of T_{ECG} may be evaluated from these two points as shown in Figure 4-7.

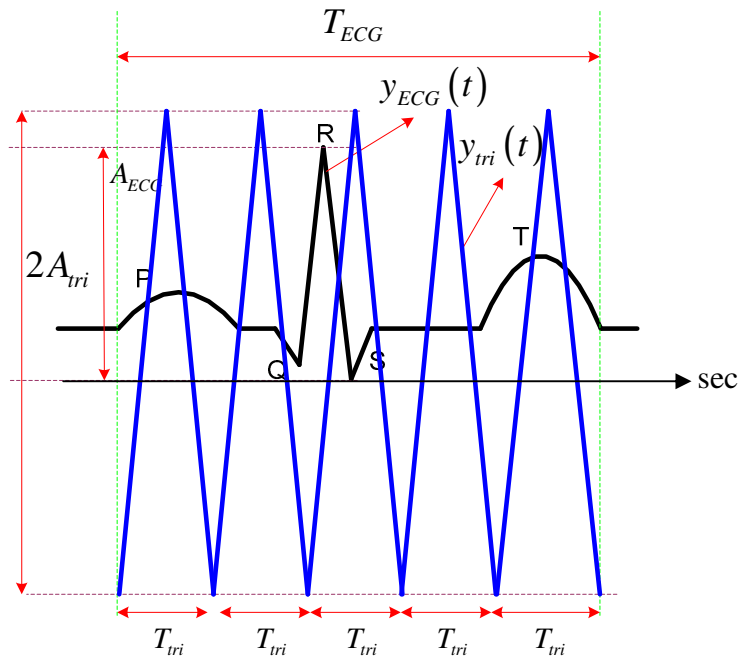


Figure 4-7: ECG extracted from P_s to T_e

An accurate detection on the fiducial points is very crucial when using this location. Using the T_{ECG} location described in Figure 4-7, the theoretical authentication performance should be better since more ECG characteristics are taken into account. However, a reduction in performance is expected based on using this location due to the uncertainties in ECG boundary extraction (i.e. where the 3 major waves within the ECG complex should start and end).

4.5.2. Peak R to the next Peak of R

In some cases, for example where ECG waves exist without P or T waves or where the fiducial detection algorithm fails to detect the fiducial points as described in Figure 3-2 , a peak R to the next peak R (RR') interval can be used to start and end the PA process as shown in Figure 4-8.

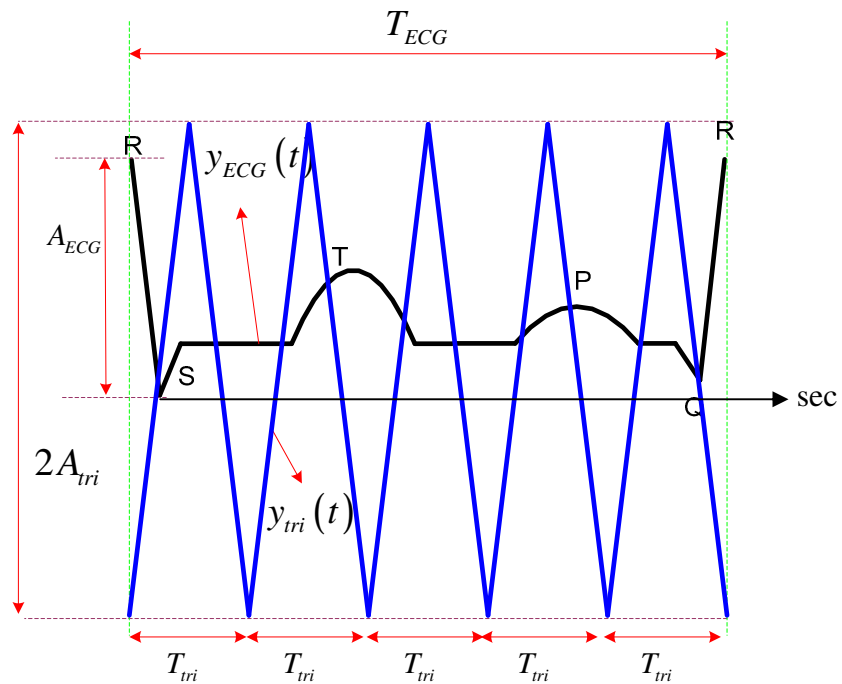


Figure 4-8: ECG extracted from R to the next R

Only 1 fiducial point in each complex, the peak of R, needs to be detected. However, the inter-beat interval (between T_e and the next P_s) might reduce the biometric performance since this location is a transition stage that is independent of the electrical timing mechanism of the heart and can be considered as a random signal [70].

4.5.3. QRS complex

An alternative location to extracting ECG features examined in this section is by taking account of the T_{ECG} region within the QRS complex as shown in Figure 4-9.

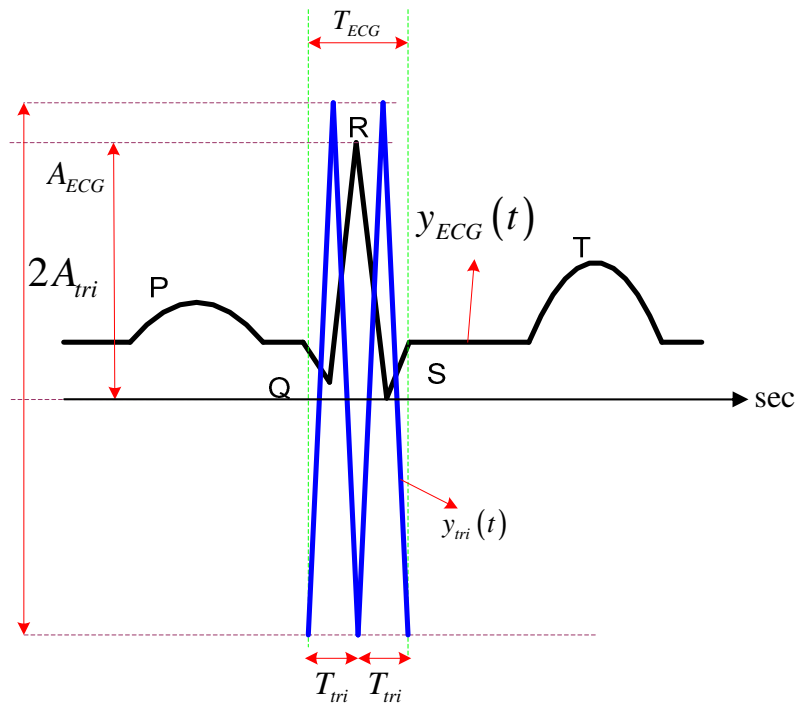


Figure 4-9: ECG extracted within QRS complex

This region is not affected by the HRV [66]. However, not using precise definitions for the QRS boundaries to start and end the PA process can be a problem. The Q and S locations are between the transition of the P wave to the peak R and peak R to T wave respectively. In an ideal ECG signal, the Q and S location can be respectively determined by the locations where the ECG signals start to decrease from a linear zero line to the minimum of the peak P to R waves and the end location at a linear zero line from an increment of the minimum peak R to T waves. However, in actual ECG signals, this linear zero line is not visible making it hard to detect. Furthermore, leaving certain parts of an ECG may leave discriminative features in the P and T wave

4.5.4. Peak P to Peak T

Figure 4-3 shows an ECG extraction location T_{ECG} between the peaks of P and T (PT). This location has the advantage of avoiding the unclear definition of the exact ECG locations where the 3 major waves should start and end (the boundaries locations). The drawback is that when omitting certain parts of an ECG, during a feature extraction process, it may reduce the ability of the biometric to differentiate between individuals. The starting point of P wave to the peak of P and the peak of T to the end of T wave may have embedded some discriminative features which may be useful to discriminate individual.

4.6. FEATURE SELECTION

The foundation of PA relies on the concept that two different ECG complexes with similar morphological shapes would intersect in similar locations generating similar values of (4-7). These similar intersection locations for different heart rates are guaranteed by the changes of the triangular period with a fixed setting of m_f . However, variations in (4-7) between two different ECG complexes from the same subject still occur because these different ECGs consist of signals with different sampling points (for example, the number of sampling points from peak P to peak T) due to the HRV. Two procedures can be used to generate feature vector which may minimize the effect of HRV and at the same time avoid the dependency of T_{trans} on the number of sampling points. The first procedure is based on the concept of normalization while the second is based on the concept of ratio. Using the concept of normalization the duration of ECG complexes within T_{ECG} is normalized to 1 before the ECG features are extracted. Using this approach, T_{trans} in (4-7) is no longer a

function of the ECG sampling points. In this thesis, 6 types of PA algorithm are derived and selected depend on the characteristic types of the output pulses in the following subsection.

The final feature vector \mathbf{X} for all PA algorithms is written in the similar form. Unless otherwise stated, the PA final feature vector is given in the following form:

$$\mathbf{X} = [x(1) \quad x(2) \quad \dots \quad x(m) \quad \dots \quad x(m_f)] \quad (4-8)$$

where $x(m)$ is the individual PA algorithms calculated for $m = 1, 2, \dots, m_f$.

4.6.1. Pulse Active Bit (PAB)

The simplest pulse active feature can be obtained by taken the intersection point of T_{trans} in (4-7) as a feature vector. The term ‘Bit’ in the PAB refers to the bit location where the pulses changes from O_{max} to O_{min} or O_{min} to O_{max} [113]. The PAB feature vector \mathbf{X} is given as:

$$\mathbf{X} = [t_1 \quad t_2 \quad t_3 \quad \dots \quad t_{2m_f}] \quad (4-9)$$

4.6.2. Pulse Active Width (PAW)

The width between two contiguous points of T_{trans} also can be used as feature vector[114]. Thus, the PAW algorithm $x(m)$ is given as:

$$x(m) = t_{2m} - t_{2m-1} \quad (4-10)$$

4.6.3. Pulse Active Area (PAA)

Pulse active area (PAA) uses the width of each pulse as the features. With reference to Figure 4-3, the PAA mathematical expression $x(m)$ can be defined as

$$x(m) = \int_{(m-1)T_{tri}}^{mT_{tri}} o(t) dt \quad (4-11)$$

Expanding (4-11) yields

$$\begin{aligned} x(m) &= \int_{(m-1)T_{tri}}^{t_{2m-1}} O_{\min} dt + \int_{t_{2m-1}}^{t_{2m}} O_{\max} dt + \int_{t_{2m}}^{mT_{tri}} O_{\min} dt \\ &= O_{\min} (t_{2m-1} - t_{2m} + T_{tri}) + O_{\max} (t_{2m} - t_{2m-1}) \\ &= (t_{2m} - t_{2m-1})(O_{\max} - O_{\min}) + O_{\min} T_{tri} \end{aligned} \quad (4-12)$$

Substituting (4-1) to (4-12) yields the final PAA algorithm $x(m)$ as

$$x(m) = (t_{2m} - t_{2m-1})(O_{\max} - O_{\min}) + \frac{O_{\min} T_{ECG}}{m_f} \quad (4-13)$$

It is important to note that the feature vector evaluation using (4-13) involves the transition state vector of (4-7). To ensure the characteristics of the ECG embedded within (4-7) always taken into consideration, O_{\max} should not be set equal to O_{\min} .

4.6.4. Pulse Active Mean (PAM)

The term ‘Mean’ in PAM refers to an averaging process of the output pulses in each period and can be selected as a feature vector[115]. Mathematically, PAM algorithm $x(m)$ can be represented as:

$$x(m) = \frac{1}{T_{tri} (m-1)T_{ri}} \int_{(m-1)T_{ri}}^{mT_{ri}} o(t) dt \quad (4-14)$$

Following to a similar derivation to PAA, the final PAM algorithm $x(m)$ can be written as:

$$x(m) = \frac{m_f}{T_{ECG}} (t_{2m} - t_{2m-1}) (O_{\max} - O_{\min}) + O_{\min} \quad (4-15)$$

Similarly to (4-13) in order to ensure that the ECG characteristics embedded within (4-7) are always taken in to consideration when generating the feature vectors, O_{\max} should not be set equal to O_{\min} .

4.6.5. Pulse Active Harmonic (PAH)

Pulse Active Harmonic (PAH) makes use of the harmonic coefficient of the output pulses as features. The transition state vector as in (4-7) is then transformed to radians as follows:

$$\omega_{(2m-1)} = \frac{t_{(2m-1)} - (m-1)T_{TRI}}{T_{TRI}} \times 2\pi \quad (4-16)$$

$$\omega_{2m} = \frac{t_{2m} - (m-1)T_{TRI}}{T_{TRI}} \times 2\pi \quad (4-17)$$

$$\mathbf{W} = \begin{bmatrix} \omega_{(2m-1)} & \omega_{2m} \end{bmatrix} \quad (4-18)$$

for $m = 1, 2, 3 \dots m_f$.

This forms the output pulse waveform $o(\omega)$ as illustrated in Figure 4-10. Equations (4-16) and (4-17) are used to ensure that each angle within \mathbf{W} , in (4-18) is in the range of 0 to 2π .

The pulse active harmonic (PAH) features are defined as the total harmonic coefficients of the individual pulses in $o(\omega)$. For each output pulse waveform $o(\omega)$ from 0 to 2π , as shown in Figure 4-10, the Fourier coefficients are given as:

$$a_n = \frac{1}{\pi} \int_0^{2\pi} o(\omega) \cos(n\omega) d\omega \quad (4-19)$$

$$b_n = \frac{1}{\pi} \int_0^{2\pi} o(\omega) \sin(n\omega) d\omega \quad (4-20)$$

where n is the order of the harmonic.

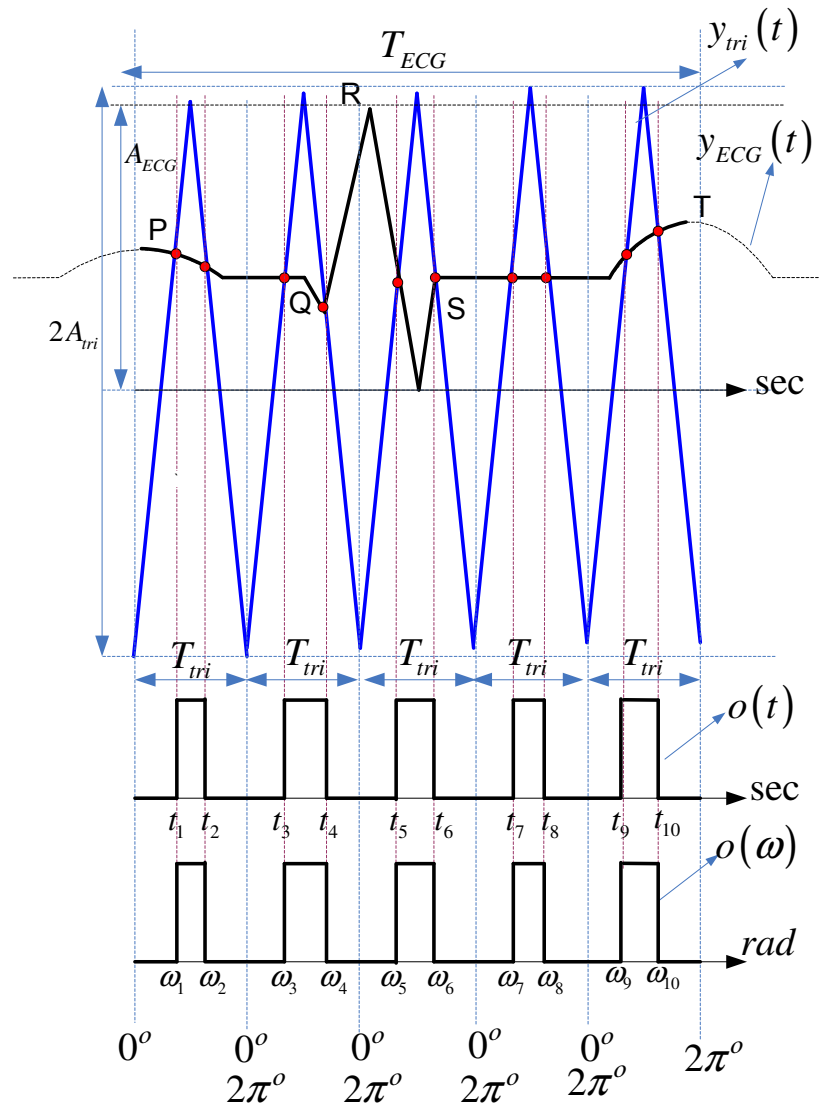


Figure 4-10: Waveform generation of Pulse Active Harmonic

Looking at $o(\omega)$ in Figure 4-10, (4-19) and (4-20) can be written as:

$$a_n = \frac{1}{\pi} \int_{\omega_{(2m-1)}}^{\omega_{2m}} \cos(n\omega) d\omega \quad (4-21)$$

$$b_n = \frac{1}{\pi} \int_{\omega_{(2m-1)}}^{\omega_{2m}} \sin(n\omega) d\omega \quad (4-22)$$

Evaluating (4-21) and (4-22) yields:

$$a_n = \frac{1}{n\pi} \left[\sin(n \cdot \omega_{2m}) - \sin(n \cdot \omega_{(2m-1)}) \right] \quad (4-23)$$

$$b_n = \frac{1}{n\pi} \left[\cos(n \cdot \omega_{(2m-1)}) - \cos(n \cdot \omega_{2m}) \right] \quad (4-24)$$

Based on the PAH definition above, (4-23) and (4-24) are used to generate the PAH feature vector X , as follows:

$$A(n) = \frac{1}{n\pi} \left(\sum_{m=1}^{m_f} \left[\sin(n \cdot \omega_{2m}) - \sin(n \cdot \omega_{(2m-1)}) \right] \right) \quad (4-25)$$

$$B(n) = \frac{1}{n\pi} \left(\sum_{m=1}^{m_f} \left[\cos(n \cdot \omega_{(2m-1)}) - \cos(n \cdot \omega_{2m}) \right] \right) \quad (4-26)$$

$$X = \begin{bmatrix} A(n) & B(n) \end{bmatrix} \quad (4-27)$$

for $n = 1, 2, \dots, N$.

N is the total number of harmonics defined by the user which determines the dimension of the PAH feature vector.

4.6.6. Pulse Active Ratio (PAR)

Subsection 4.6.1 to 4.6.5 normalized ECG complexes first before their features are extracted using the respective equations. PAR does not require the normalization process before the feature extraction process is implemented. PAR feature vector represents the ratio between the area of the output pulse and the area of the triangular wave in each period as illustrated in Figure 4-3 [116, 117]. Mathematically, PAR algorithm $x(m)$ can be presented as:

$$x(m) = \frac{\int_{(m-1)T_{tri}}^{mT_{tri}} o(t) dt}{\frac{1}{2} \times T_{tri} \times 2A_{tri}} \quad (4-28)$$

Expanding (4-28) yields:

$$\begin{aligned} x(m) &= \frac{\int_{(m-1)T_{tri}}^{t_{2m-1}} O_{\min} dt + \int_{t_{2m-1}}^{t_{2m}} O_{\max} dt + \int_{t_{2m}}^{mT_{tri}} O_{\min} dt}{\frac{1}{2} \times T_{tri} \times 2A_{tri}} \\ &= \frac{O_{\min} (t_{(2m-1)} - t_{2m} + T_{tri}) + O_{\max} (t_{2m} - t_{(2m-1)})}{\frac{1}{2} \times T_{tri} \times 2A_{tri}} \\ &= \frac{1}{A_{tri}} \left\{ \frac{1}{T_{tri}} \left[O_{\min} (t_{(2m-1)} - t_{2m}) + O_{\max} (t_{2m} - t_{(2m-1)}) \right] + O_{\min} \right\} \\ &= \frac{1}{A_{tri}} \left\{ \frac{1}{T_{tri}} \left[(t_{2m} - t_{(2m-1)}) (O_{\max} - O_{\min}) \right] + O_{\min} \right\} \end{aligned} \quad (4-29)$$

Substituting (4-1) and (4-2) into (4-29) produces:

$$x(m) = \frac{1}{m_i A_{ECG}} \left\{ \frac{m_f}{T_{ECG}} \left[(O_{\max} - O_{\min}) (t_{2m} - t_{2m-1}) \right] + O_{\min} \right\} \quad (4-30)$$

In (4-30), it is important not to set O_{\max} equal to O_{\min} , to ensure that the ECG characteristic as embedded within (4-7) are always taken into consideration.

The summary all PA algorithms described in section 4.6.1 to 4.6.6 is given in Table 4-1.

Table 4-1 : Summary of 6 Pulse Active Feature Selection Techniques

Name	Criteria	Equation
Pulse Active Bit (PAB)	Intersection locations between triangular wave and ECG signals	$\mathbf{X} = [t_1 \quad t_2 \quad t_3 \quad \dots \quad t_{2m_f}]$
Pulse Active Width (PAW)	Difference between two contiguous points of the intersection locations	$\mathbf{X} = [x(1) \quad x(2) \quad \dots \quad x(m) \quad \dots \quad x(m_f)]$ where $x(m) = [t_{2m} - t_{2m-1}]$
Pulse Active Area (PAA)	The output area of each pulse	$\mathbf{X} = [x(1) \quad x(2) \quad \dots \quad x(m) \quad \dots \quad x(m_f)]$ where $x(m) = (t_{2m} - t_{2m-1})(O_{\max} - O_{\min}) + \frac{O_{\min} T_{ECG}}{m_f}$
Pulse Active Mean (PAM)	The average value of each pulse	$\mathbf{X} = [x(1) \quad x(2) \quad \dots \quad x(m) \quad \dots \quad x(m_f)]$ where $x(m) = \frac{m_f}{T_{ECG}}(t_{2m} - t_{2m-1})(O_{\max} - O_{\min}) + O_{\min}$
Pulse Active Harmonic (PAH)	The total harmonic components of each pulse	$A(n) = \frac{1}{n\pi} \left(\sum_{m=1}^{m_f} [\sin(n \cdot \omega_{2m}) - \sin(n \cdot \omega_{2m-1})] \right)$ $B(n) = \frac{1}{n\pi} \left(\sum_{m=1}^{m_f} [\cos(n \cdot \omega_{2m-1}) - \cos(n \cdot \omega_{2m})] \right)$ $\mathbf{X} = [A(n) \quad B(n)]$
Pulse Active Ratio (PAR)	The ratio between the area of the triangular waves and the area of the output pulse	$\mathbf{X} = [x(1) \quad x(2) \quad \dots \quad x(m) \quad \dots \quad x(m_f)]$ where $x(m) = \frac{1}{m_i A_{ECG}} \left\{ \frac{m_f}{T_{ECG}} [(O_{\max} - O_{\min})(t_{2m} - t_{2m-1})] + O_{\min} \right\}$

for $m = 1, 2, \dots, m_f$ and $n = 1, 2, \dots, N$

4.7. EXPERIMENTAL SETUP

This section described the simulation setup that will be used in this thesis. The same setup will be repeatedly used in chapter 5 and 6. It involves the process of generating the experimental database and matching scores [116]. The procedures on running the experiment will also be covered in this section.

4.7.1. Setting up the training and test databases

As mentioned in section 3.4, the performance of the PA is investigated using a Lead I database of 112 subjects (healthy and arrhythmia) each with at least 2 different recordings from the PTB ECG database which is taken days, months or years apart as described in section 3.4.2. The summary process of setting up the simulation database is given in Figure 4-11. As can be seen from Figure 4-11, there are four major steps to generate databases involving ECG collections, pre-processing, feature extraction and assigning extracted features to the training or test databases.

From Figure 4-11, 2 different ECG recordings are used from 14 healthy and 98 arrhythmia subjects - one recording for the training and one for the test databases. The requirement that need to be fulfilled for ECG sources to be used in biometric applications as described in Section 3.4.1 limit the available ECG signals from the PTB database to 14 healthy subjects. Due to the small sample size, results obtained from ECGs of healthy subjects will only be indicative, and a future simulation set of tests will be required to ascertain statistically significant results. In contrast the sample size of measurements available for arrhythmia subjects can be considered sufficiently large to guarantee statistically significant outcomes.

This procedure generates a total of 224 ECG signals from both databases. The databases are made up by extracting the first 30 seconds of each recording for each subject. Before we can use these 30-second recordings, some pre-processing is needed. This involves filtering all ECG recordings so that only ECG components

within 2 to 40 Hz are allowed [70]. An FIR filter is used to filter the ECGs. ECGPUWAVE [118] is then used to approximate the onset and offset of the P, QRS, and T waves.

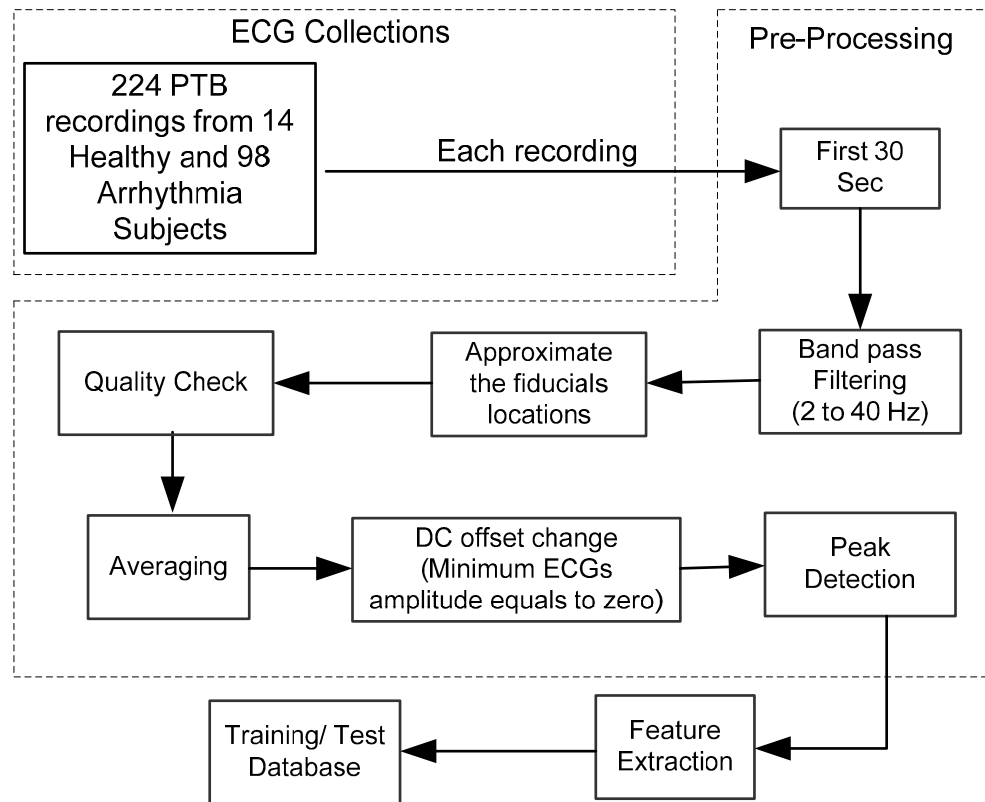


Figure 4-11: Summary of setting up simulation databases

A quality check is performed for each 30-second recording to ensure acceptable quality ECG complexes. A high quality ECG complex in this experiment refers to an ECG morphology, which has visibly clear and apparent P, QRS, and T waves. There are 4 different locations to extract ECG features which will be investigated in this thesis. These are discussed in section 4.5. As for that the quality check process when investigated these locations are done differently. If the extracted locations from the whole ECG complex as described in section 4.5.1 is consider, the quality check is performed by calculating the average distance between the peak of R to the starting and ending point of P and T waves respectively. The first two contiguous ECG complexes of the ECG recording between peaks of R are directly used for extraction if the extracted location is as described in section 4.5.2. For this location, the quality

check and averaging are excluded. This is because of the difficulty of averaging these locations as the inter beat durations between these varies and is independent of electrical heart mechanism activity as explained in section 4.5.2. If the extract locations are within the QRS wave of the ECG complex as described in section 4.5.3 is considered, the quality check is performed by calculating the average distance between the peak of R to the starting and ending point of QRS complex. For extracting ECG locations between the peaks of P and T, the quality check is performed by calculating the average distance between the peak of R to the peaks of P and T waves respectively.

For all averaging process, a tolerance of 50 sampling points is introduced into each average distance values so that the acceptable limits of the peaks and boundaries of the P, QRS and T waves are defined. The first 10 seconds of the 30-second recording is then considered for further processing. All ECG complexes within the 10 seconds recording with a period within the respective acceptable limit are then used for averaging. If there are no good quality ECG complexes within the selected 10-second recording, a new 10-second recording is used. This is made up from the last 9 seconds of the previous 10-second recording plus the recording of the following second. This process continues until good quality ECGs are obtained. Five good quality ECGs in a 10-second period is used in all experiments. These ECGs are averaged to produce smooth ECG signals which magnify the common attributes between complexes and minimize the ripples of the ECGs. The minimum values of the average ECGs are detected and used to change their DC offset to zero. A peak detection algorithm [119] is then used to detect the local maxima of these waves. All averaged ECGs then undergo the feature extraction process. Finally, these feature vectors are assigned to the training and test database respectively. A detail explanation and examples for this process is described in Appendix B.

This process generates 98 feature vectors for each of the arrhythmia training and test databases. For the healthy population, 14 feature vectors are assigned in each of their training and test databases using the same method. Databases for arrhythmia and healthy populations are kept and compared separately. For comparison purposes, the Biel *et al* [68] and Israel *et al* [70] feature extraction techniques as described in

section 3.5.1.1 and 3.5.1.3 respectively are used. The generation of their respective databases follows the procedure as illustrates in Figure 4-11.

4.7.2. Generating matching scores

Using the databases generated as in Figure 4-11, the next process is to generate the genuine and imposter matching scores as illustrated in Figure 4-12. As illustrated in Figure 4-12, for different populations, each feature vector from the test database is compared to all feature vectors in the training database, using similarity measurement as described in subsection 2.6.1 to generate matching scores. If the feature vectors from the test database and training database are from the same subject, the matching score is labeled as the genuine score. Otherwise, the matching score is labeled as an imposter score.

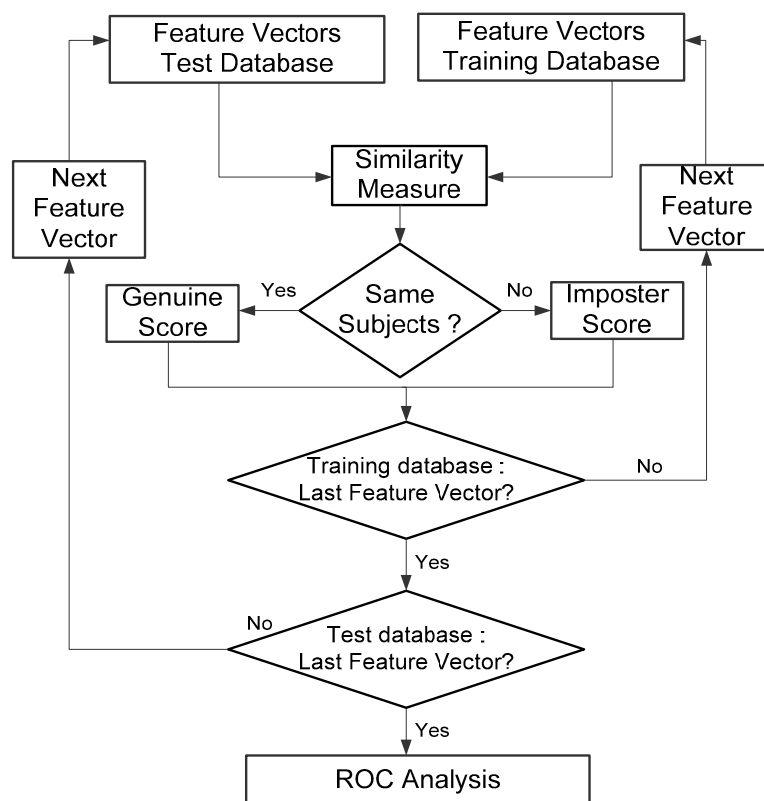


Figure 4-12: Matching Score Process

This process generates 98 values of genuine scores and 9506 values of imposter scores for the arrhythmia population. For the healthy population, the above process generates 14 values of genuine score and 182 values of imposter scores. The score vectors are input to the Receiver Operating Characteristic (ROC) curve processing block.

4.7.3. Simulation Procedure

Based from the description given in section 4.6 there are 6 different PA algorithms namely PAB, PAW, PAA, PAM, PAR and PAH which can be used for feature extraction. It is also can be seen in that section that the feature vector values generated for each algorithms depends on the PA parameters namely modulation index m_i , modulation factor m_f , maximum value of output pulse O_{\max} , minimum value of output pulse O_{\min} and total number of harmonic N .

Unfortunately there are two other factors which need to be considered to obtain these results which are the T_{ECG} location described in section 4.5 and the best similarity measures described in section 2.6.1.

Figure 4-13 illustrates the simulation procedure which will be used in this chapter. As can be seen from Figure 4-13, to evaluate the performance of the proposed method, there are various unknown variables that need to be investigated which includes 4 locations to extract the features, 6 different PA algorithms, 9 types of similarity measures and 5 different PA parameters. The objective of running experiments in this chapter is to compare the performance of all PA algorithms using the optimum settings.

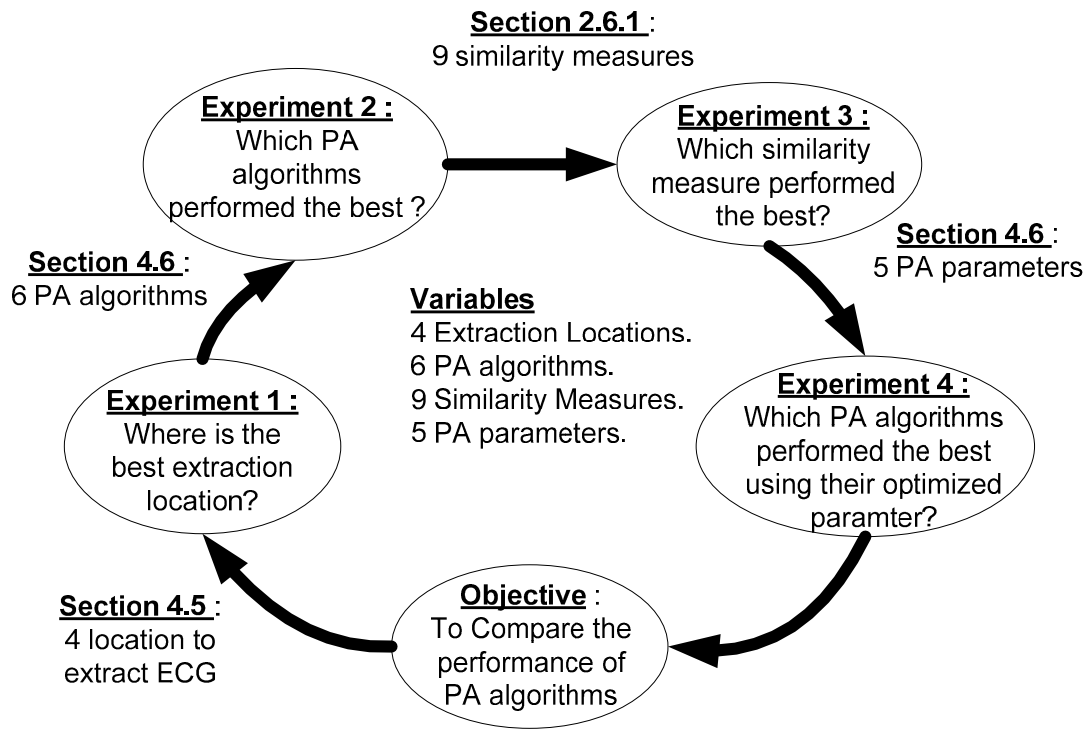


Figure 4-13 : Simulation Procedure

As can be seen from Figure 4-13, the first experiment conducted is to identify the best location of T_{ECG} to be used with PA algorithms as described in section 4.5. Since this would be the first investigation in this chapter, the PA algorithms and similarity measures need to be used with PA algorithms are still unknown. PAR will be initially used as the feature extraction algorithm and the most widely used distance measure namely the Euclidean distance [30] will be used as similarity measures. The results in this experiment will cover various range of m_f and m_i settings while O_{max} and O_{min} are set to be 1 and 0 respectively.

The second experiment in Figure 4-13, compares the performance between the pre-set parameters of PA algorithm (as described in section 4.6) , Biel *et al* [68] (as described in section 3.5.1.1) and Israel *et al* [70] (as described in section 3.5.1.3) feature extraction techniques. Up to this point, the similarities measures need to be used with PA algorithms are still unknown. As for that, the most widely used

similarity measures namely Euclidean distance will be used in the experiment. The best T_{ECG} founded in the first experiment will be used for PA. To allow fair comparison, in this experiment the PA parameters namely m_f, m_i, O_{\max} and O_{\min} are pre-set to be 35, 1.5, 10 and -2 respectively.

Using the T_{ECG} location and the best PA feature selection investigated in the first and second experiments, evaluation of the best distance based similarity measure for PA is performed in the third experiment shown in Figure 4-13. The 9 similarity measures described in section 2.6.1 are compared. The PA parameters used to run the second experiment are reused in this experiment.

Having obtained the best T_{ECG} and similarity measures from the first and third experiments, the optimum PA parameters finally can be investigated in the fourth experiment. The reason to investigate for all PA algorithms is to determine which settings are the best for the specific algorithms. A comparison between algorithms using its optimum PA parameters is also carried out.

4.8. EXPERIMENTAL RESULTS

4.8.1. Experiment 1 : Evaluation of extraction locations

Experiment 1 in this section is to evaluate the best location to extract the ECG signals as explained in section 4.5. As mentioned in the previous section, Euclidean distance will be used first as similarity measures. Pulse Active Ratio (PAR) features as described in section 4.6.6 will be used to compare the performance between these locations using various values of m_i and m_f . The O_{\max} and O_{\min} are set to be 1 and 0 respectively.

4.8.1.1. AUR and EER profile for T_{ECG} between P_s and T_e

Figures 4-14 a) and b) illustrate the AUR performance of the ECG PAR biometric system for various m_f and m_i setting when T_{ECG} is selected from the starting point of the P wave, P_s , to the end of the T wave, T_e , as illustrated in Figure 4-7 for respective healthy and arrhythmia populations. From Figures 4-14 a) and b), it is shown that for m_f greater than 15, lower m_i values projected higher AUR values. As the values of m_i increase, the performance of the authentication process degrades. It is also shown in both figures that when m_f is greater than 15 it does not have much impact towards the authentication performance for a particular setting of m_i . A poor region of the PAR biometric performance is observed for m_f settings less than 5.

Figures 4-15 a) and b) illustrate the EER for healthy and arrhythmia populations when T_{ECG} is selected from P_s to T_e . As can be seen from both figures, lower EER values are obtained by selecting m_i low while the m_f settings do not affect the EER profiles. The EER values increase as the values of m_i increase.

4.8.1.3. AUR and EER profile for T_{ECG} between peaks P and T

The AUR performance when T_{ECG} is selected between the peaks of P and T for healthy and arrhythmia populations are demonstrated in Figure 4-18 a) and b) respectively.

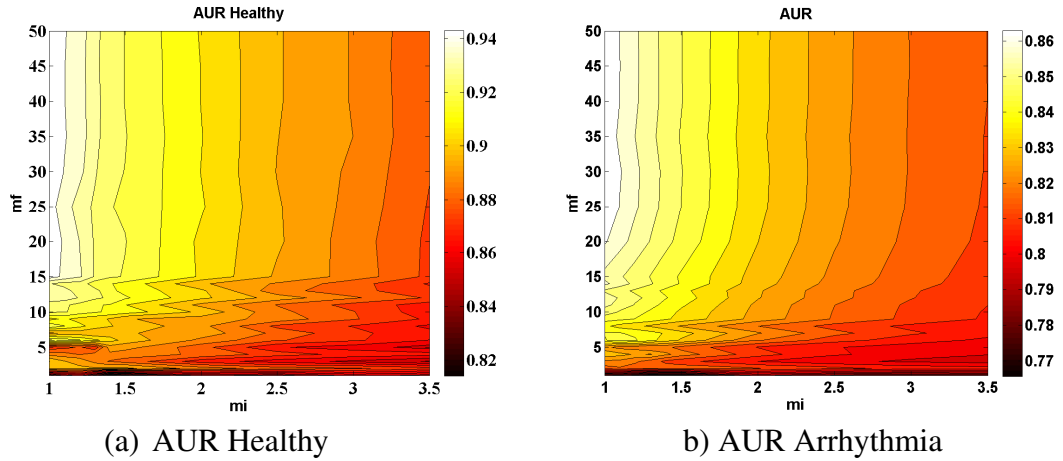
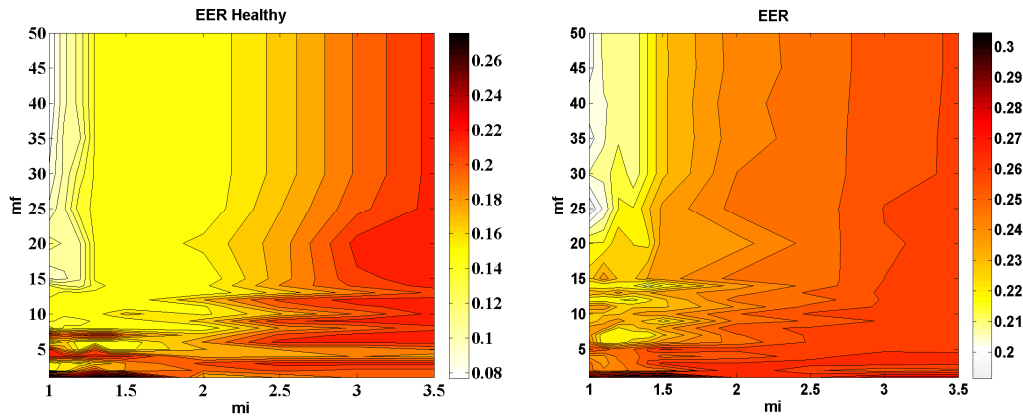


Figure 4-18: AUR profile for T_{ECG} location between peaks P and T

From these figures, it is observed that for m_f greater than 15 and 10 for healthy and arrhythmia population respectively, lower m_i values generate higher values of AUR. It is also observed that the AUR performance is not affected when m_f is greater than these settings for the same setting of m_i .

The EER profiles for healthy and arrhythmia population when T_{ECG} is selected between peaks P and T are shown in Figure 4-19 a) and b) respectively. The figures show that a lower EER value is achieved when m_i is set to 1 with m_f greater than 15 for the healthy population and greater than 20 for the arrhythmia population. As the value of m_i increases, the EER value also increases.



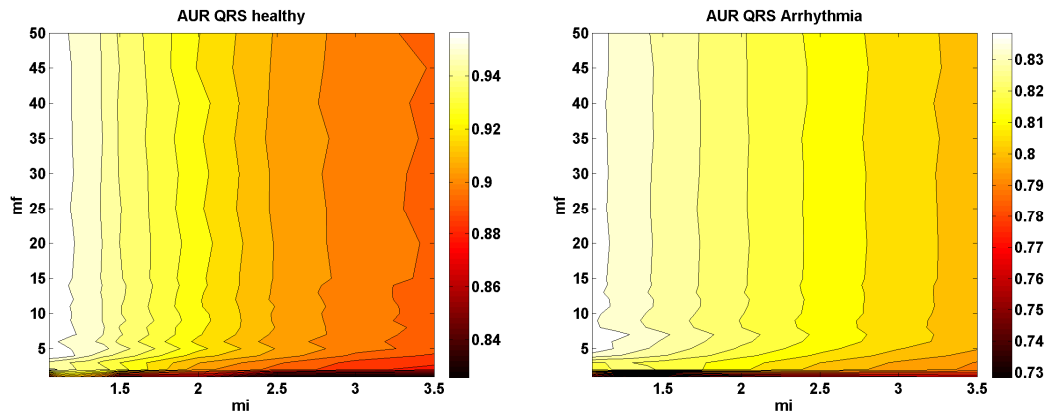
(a) EER Healthy

(b) EER Arrhythmia

Figure 4-19: EER profile for T_{ECG} location between peaks P and T

4.8.1.4. AUR and EER profile for T_{ECG} within QRS complex

By acquiring ECG characteristics within the QRS complex as shown in Figure 4-9, the AUR performances for healthy and arrhythmia populations are given in Figure 4-20 a) and b) respectively.



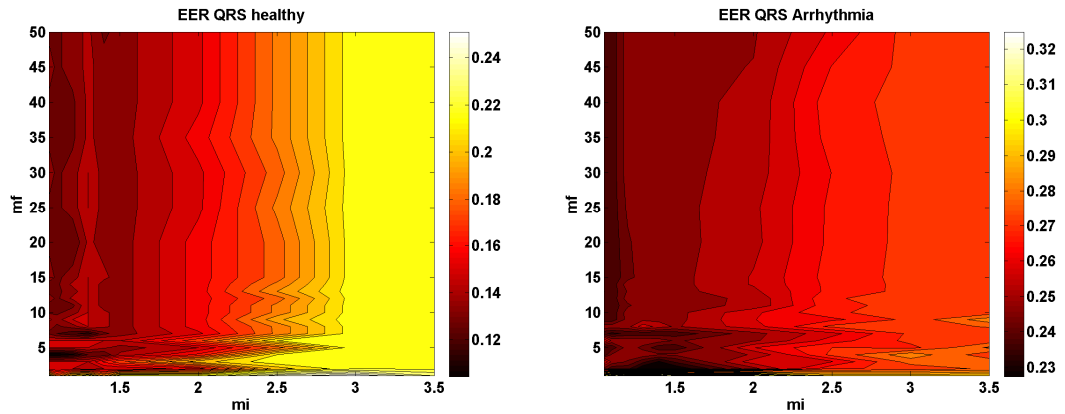
(a) AUR Healthy

(b) AUR Arrhythmia

Figure 4-20: AUR profile for T_{ECG} location within QRS complex

From Figure 4-20 a) and b), it is shown that a lower m_i setting is desirable to achieve a high AUR profile when the m_f setting is greater than 5 for both populations. It is also shown in both figures that m_f is not affecting the authentication performance when it is set greater than 5 for the same setting of m_i . A poor region of AUR profile is observed for both populations when m_f is set to less than 2. Figure 4-21 a) and b)

illustrate the EER profile for the respective healthy and arrhythmia populations when T_{ECG} is selected within the QRS complex. From these figures, it is observed that when the m_i values are close to 1, the EER has its lowest value. As the values of m_i increase, the values of EER increase. It is shown that when m_f is set greater than 7, m_f does not have any impact towards the EER profile for any particular m_i settings.



a) EER Healthy

b) EER Arrhythmia

Figure 4-21: EER profile for T_{ECG} location within QRS complex

4.8.1.5. Conclusion on the effect of T_{ECG} location

Tables 4-2 and 4-3 summarize the AUR and EER performances for all 4 locations. As can be seen from these tables, the maximum AUR with minimum EER values are obtained when T_{ECG} is selected between the peaks of P and T, followed by the QRS locations and then by the RR' intervals. In Table 4-2, it is observed that for healthy populations the AUR profile, when T_{ECG} is selected between the QRS complex, is slightly better compared to the AUR profile when T_{ECG} is selected between the peaks of P and T. However, when the number of subjects with arrhythmia beats increases, the performance degrades. It is concluded in this subsection that, for the ECGs database used in this thesis, T_{ECG} should be selected between peaks P and T to obtain a high AUR and EER profile. As for that, the remaining of this chapter will use T_{ECG} between peaks P and T.

Table 4-2: Summary of AUR performances on different T_{ECG}

T_{ECG}	Population	Optimum m_f range	Optimum m_i range	Maximum AUR	AUR Ranges
Ps	Healthy	>15	<1.5	0.74	0.15
	Arrhythmia	>15	<1.5	0.64	0.06
RR'	Healthy	>5	<1.5	0.91	0.08
	Arrhythmia	$10 < m_f < 35$	<1.2	0.785	0.04
PT	Healthy	>15	<1.2	0.945	0.12
	Arrhythmia	>20	<1.2	0.865	0.09
QRS	Healthy	>5	<1.2	0.96	0.14
	Arrhythmia	>5	<1.2	0.84	0.11

Table 4-3: Summary of EER performances on different T_{ECG}

T_{ECG}	Population	Optimum m_f range	Optimum m_i range	Minimum EER	EER Ranges
Ps	Healthy	>1	<1.5	0.31	0.18
	Arrhythmia	>1	<1.2	0.39	0.09
RR'	Healthy	$25 < m_f < 40$	<1.2	0.16	0.08
	Arrhythmia	$5 < m_f < 30$	<1.2	0.29	0.04
PT	Healthy	>15	<1.2	0.08	0.2
	Arrhythmia	>20	<1.2	0.19	0.12
QRS	Healthy	>10	<1.2	0.1	0.15
	Arrhythmia	>10	<1.2	0.23	0.1

4.8.2. Experiment 2 : The optimum algorithms

Experiment 2 in this subsection is to evaluate the performance of all PA feature selection techniques as explained in section 4.6 compared to the features proposed by Biel[68] and Israel [70] described in section 3.5. In this experiment, T_{ECG} is selected from the peak P to the peak of T . For all PA feature selection techniques, m_f , m_i , O_{max} and O_{min} are set to be 35, 1.5, 10 and -2 respectively. For PAH, N is set to be 7. Figure 4-22 and Figure 4-23 illustrate the ROC comparison for the healthy and

arrhythmia populations respectively. As can be seen from both figures, the ROC curves for all PA feature selection techniques projected higher than the Biel or Israel methods.

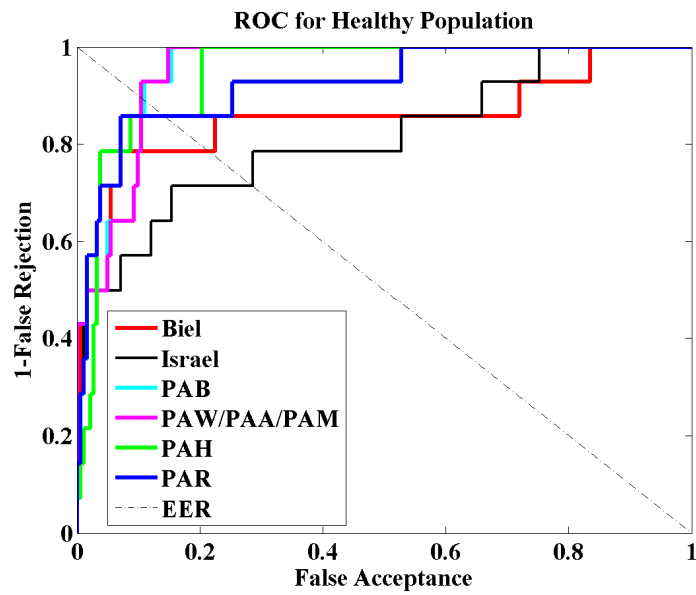


Figure 4-22: ROC comparison for Healthy Population

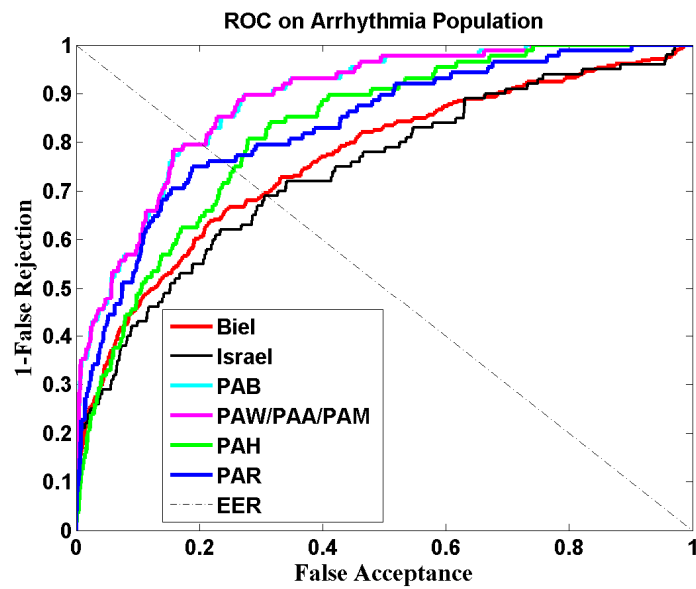


Figure 4-23: ROC comparison for Arrhythmia Population

Simulation results indicate that the PAW, PAA and PAM feature selection techniques share the same ROC performance profile. When T_{ECG} is set to 1, equations (4-10), (4-13) and (4-15) have a linear equation structure given as:

$$X = k \times \Delta_{trans} + c \quad (4-31)$$

where $\Delta_{trans} = t_{2m} - t_{2m-1}$. For PAW, $k = 1$ and $c = 0$. For PAA, $k = (O_{max} - O_{min})$ and $c = \frac{O_{min}}{m_f}$. For PAM, $k = m_f (O_{max} - O_{min})$ and $c = O_{min}$. When comparing two different sets of Δ_{trans} using (4-31), the calculated matching score is also in the form of a linear equation:

$$Score = k \times \Delta_T \quad (4-32)$$

where Δ_T is the difference value between the two sets of Δ_{trans} . The value of k in (4-31) and (4-32) is a constant value predefined by the user. Since the ROC curve is independent of the threshold settings, the generated ROC curves for PAW, PAA and PAM are the same. This leads to similar AUR and EER values. By contrast, although (4-30) seems to exhibit a linear equation structure similar to (4-31), k and c are dependent on individual ECG characteristics, namely A_{ECG} and T_{ECG} . This makes the ROC for PAR different from the ROC for PAW, PAA, or PAM.

From Figures 4-22 and 4-23 it is not clearly visible which PA feature selection technique is better. This is best determined by comparing the AUR and EER values tabulated in Table 4-4. The AUR and EER values in Table 4-4, indicate that the PAW, PAA and PAM generate the highest AUR with the lowest EER values for healthy and arrhythmia populations. This followed by the PAB, PAH and PAR feature selection techniques.

Based from the evaluation in this subsection, it can be concluded that the PAW, PAA and PAM provide the best authentication performance for the healthy and arrhythmia populations used in the simulations based on the given settings. As for that, PAW will be further used to determine the similarity measures.

Table 4-4: ROC AUR and EER values for Healthy and Arrhythmia Populations

	Healthy Population		Arrhythmia Population	
	AUR	EER	AUR	EER
Biel	0.8544	0.2143	0.7630	0.3047
Israel	0.8136	0.2857	0.7420	0.3101
PAB	0.9517	0.1099	0.8864	0.2045
PAW/PAA/PAM	0.9521	0.1044	0.8873	0.2045
PAH	0.9454	0.1429	0.8243	0.2561
PAR	0.9239	0.1429	0.8330	0.2386

4.8.3. Experiment 3 : The optimum similarity measure

As mentioned in subsection 2.6.1, there are 9 widely used distance based similarity measures for quantitative variables. Results generated in all above subsection in this chapter uses ‘Euclidean Distance’ as in (2-1) to be the distance measure to calculate the similarity score. In this subsection, the rest of distance measurements tabulated in Table 2-2 are evaluated.

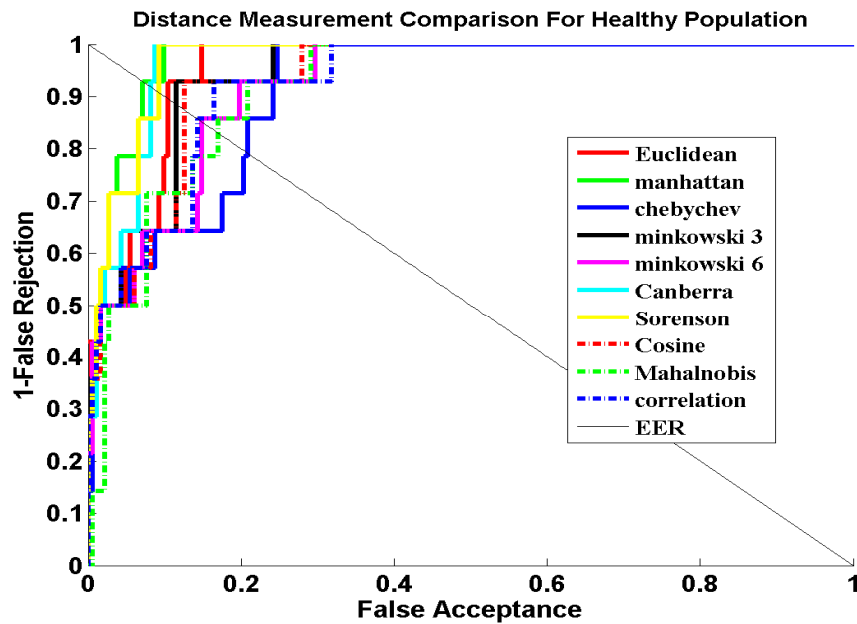


Figure 4-24: Distance Measurement Comparison For Healthy Population

To run this experiment, PAW will be used as the PA feature selection with m_f and m_i set to be 35 and 1.5 respectively. T_{ECG} is set between the peaks of P and T.

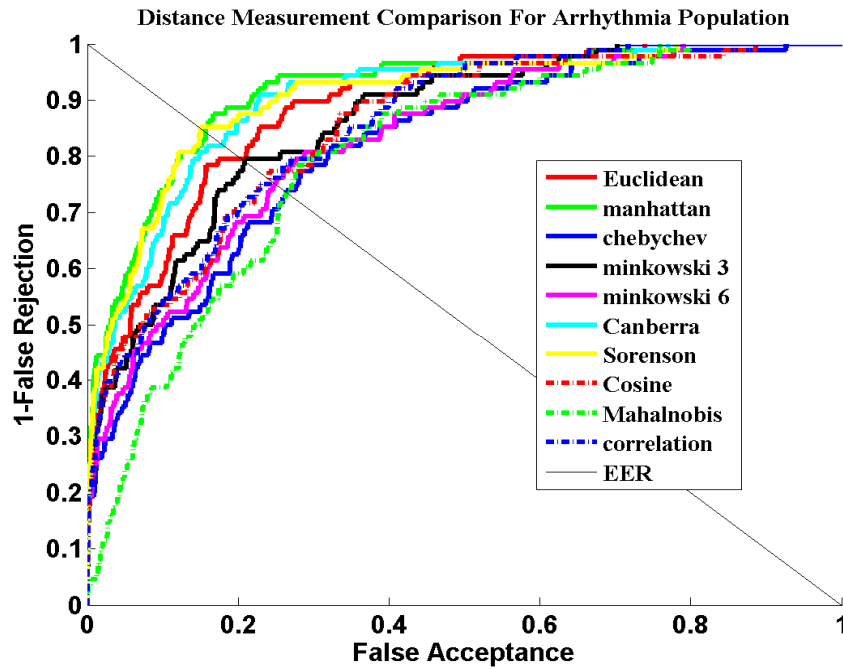


Figure 4-25: Distance Measurement Comparison For Arrhythmia Population

Figures 4-24 and 4-25 illustrate the comparison performance for healthy and arrhythmia population respectively using various distance based similarity measure. It can be seen from these figures that 3 of the highest ROC curve projections are achieved when the distance measurement are using the Manhattan, Canberra and Sorensen distance measure methods. The AUR and EER profile for all distance measures shown in Table 2-2 using PAW are tabulated in Table 4-5.

From Table 4-5, it is shown that the Manhattan distance measure provides the highest AUR and lowest EER values for healthy and arrhythmia populations. Based on these results, the Manhattan distance will be used to obtain the ROC curves throughout this chapter.

Table 4-5: AUR and EER values using different distance measure

Distance		Healthy Population		Arrhythmia Population	
Name	Equation	AUR	EER	AUR	EER
Euclidean	(2.1)	0.9521	0.1044	0.8873	0.2047
Manhattan	(2.2)	0.9733	0.0714	0.9161	0.1573
Chebyshev	(2.3)	0.9097	0.2088	0.8150	0.2640
Minkowski p=3	(2.4)	0.9419	0.1154	0.8600	0.2085
Minkowski p=6	(2.4)	0.9215	0.1484	0.8286	0.2500
Canberra	(2.5)	0.9655	0.0824	0.9017	0.1805
Sorensen	(2.6)	0.9702	0.0934	0.9056	0.1494
Cosine	(2.7)	0.9317	0.1264	0.8490	0.2412
Mahalanobis	(2.8)	0.9168	0.1703	0.7983	0.2637
Correlation	(2.9)	0.9246	0.1484	0.8509	0.2423

4.8.4. Experiment 4 : Optimized PA parameters

In the previous subsection, the performance of each PA feature selection is generated from predefined m_f , m_i , O_{\max} , O_{\min} and/or N values. In this subsection, the biometric performances for all PA feature selection methods are evaluated using various values of m_f , m_i , O_{\max} , O_{\min} and/or N .

4.8.4.1. Effect of varying m_f and m_i

This subsection will look into the effect of varying m_f and m_i for all PA feature selection. PAB would be discussed first, follows by PAW, PAA, PAM, PAR and finally PAH. For PAA, PAM and PAR, O_{\max} and O_{\min} are set to be 10 and -2 respectively. For PAH, N is set to be 7. In all simulation study in this subchapter, m_i varies from 1 to 3.5 while m_f is set between 1 and 50.

Figures 4-26 and 4-27 represent the AUR and EER profile respectively for healthy and arrhythmia population when the ECGs are extracted using PAB.

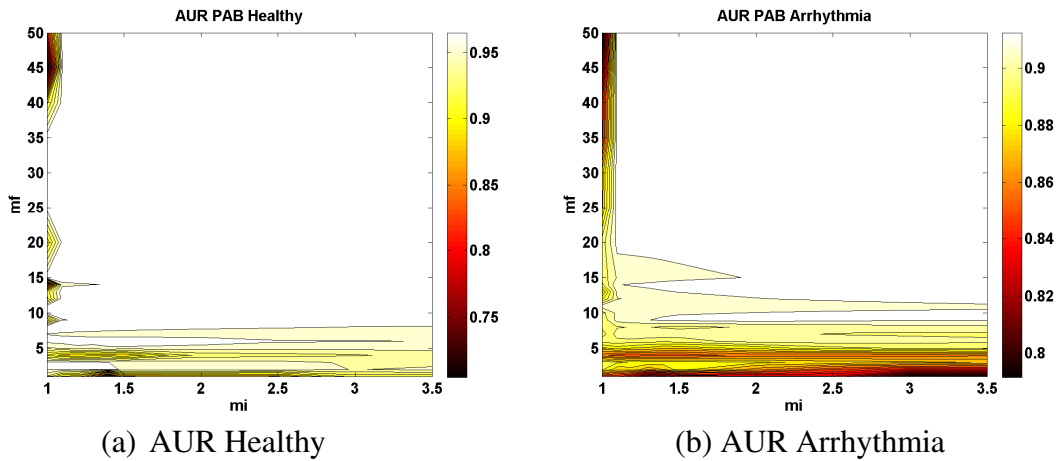


Figure 4-26: AUR profile for PAB

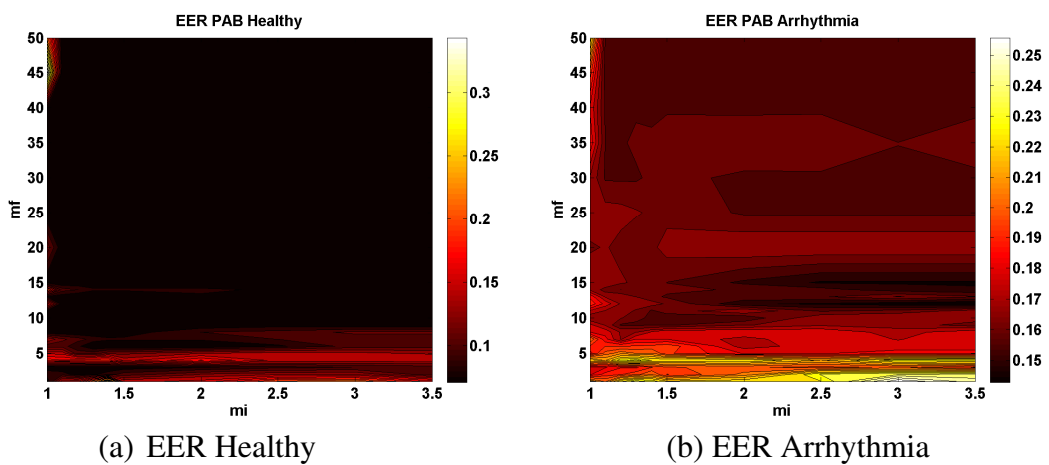


Figure 4-27: EER profile for PAB

For the healthy population, it is observed that the highest AUR value and lowest EER value as shown in Figure 4-26(a) and Figure 4-27 (a) are obtained for m_i values greater or equal to 1.1 while maintaining m_f to be greater than 15. For the arrhythmia population, it is observed that the highest AUR value as shown in Figure 4-26 (b) is obtained for m_i values greater or equal to 1.1 while maintaining m_f to be greater than 20. The lowest EER values as illustrated in Figure 4-27 (b) is in the area when m_i values greater or equal to 1.1 while maintaining m_f to be greater than 8.

Next, the effect of varying m_f and m_i is investigated for PAW, PAA and PAM. As explained in subsection 4.8.2, PAW, PAA and PAM share the same AUR and EER

profile and can be respectively shown in Figures 4-28 and 4-29. Examining the AUR and EER profile for healthy population as illustrated in Figure 4-28 (a) and Figure 4-29 (a), it is discovered that when m_i is set greater than 1 while maintaining m_f greater than 15 gives the highest and lowest EER respectively. For the arrhythmia population, it is observed that the highest AUR value as shown in Figure 4-28 (b) is obtained for m_i values greater or equal to 1.2 while maintaining m_f to be greater than 6. The lowest EER values as illustrated in Figure 4-29 (b) is in the area when m_i values greater or equal to 1.2 while maintaining m_f to be greater than 15.

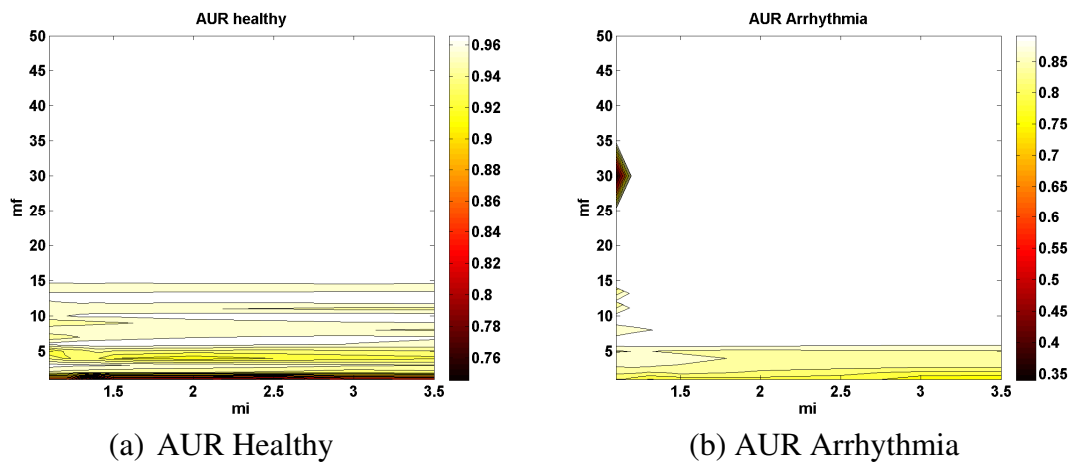


Figure 4-28: AUR profile for PAW, PAA and PAM

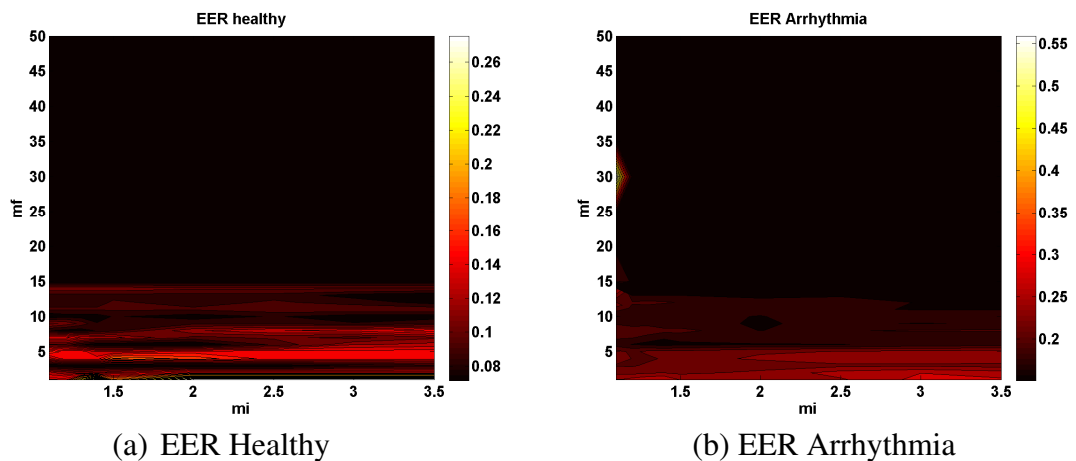


Figure 4-29: EER profile for PAW, PAA and PAM

The effects of varying m_f and m_i towards the AUR and EER profile using PAR algorithm as in (4-9) is shown in Figures 4-30 and 4-31 respectively. From Figure 4-30, it is observed that when m_f is set to be greater than 15 for the healthy population and greater than 10 for the arrhythmia population, the AUR profile decreases as the value of m_i increases. Similar phenomenon is observed on the EER profile in Figure 4-31. In the figure, it is shown that when m_f is set to be greater than 15 for both populations, the EER value increases as the value of m_i increases.

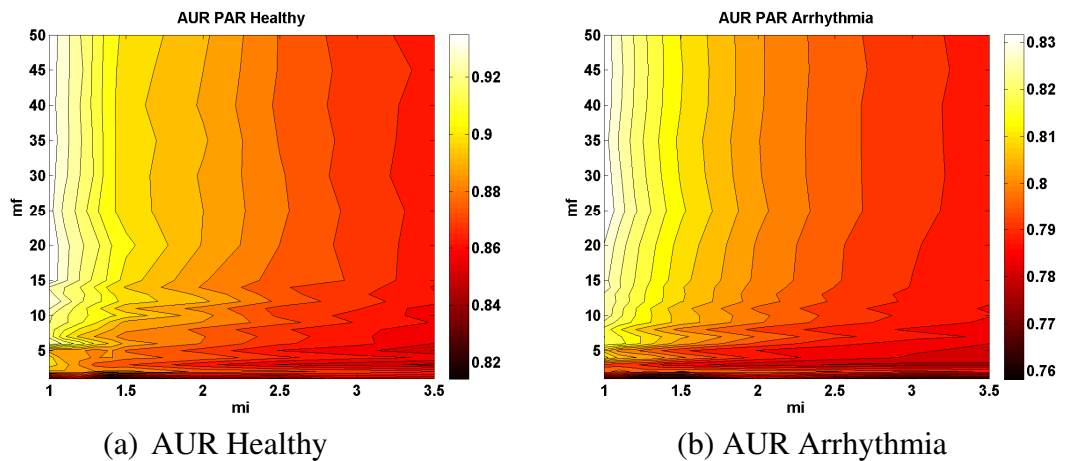


Figure 4-30: AUR profile for PAR

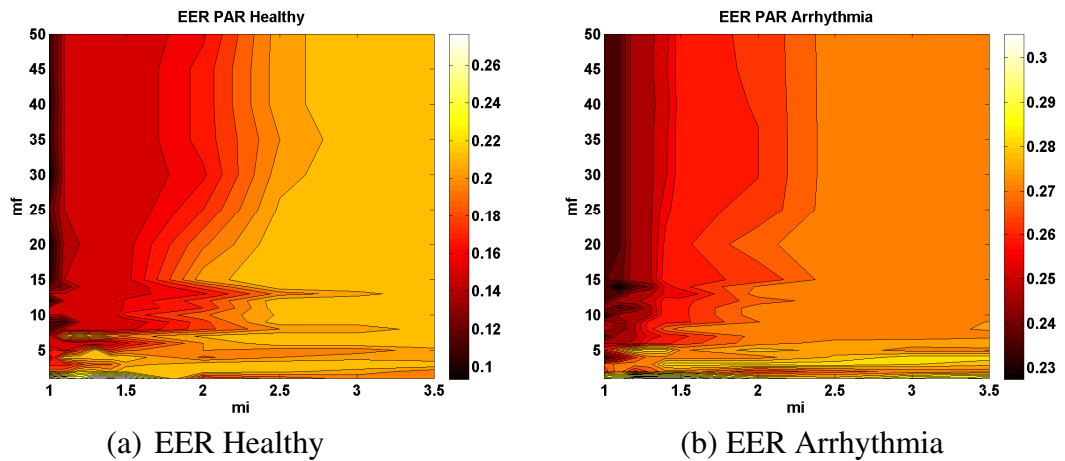


Figure 4-31: EER profile for PAR

The AUR and EER profile for healthy population using PAH are respectively shown in Figure 4-32(a) and Figure 4-33(a). Examining these figures, it can be concluded that the highest AUR and lowest EER are achievable when the values of m_i is low

while maintaining the value of m_f greater than 15. For the arrhythmia population, the AUR and EER profile of PAH as illustrated in Figure 4-32 (b) and Figure 4-33(b) indicates that the highest AUR and lowest EER profile is achievable when m_i is set less than 2.5 while m_f greater than 15.

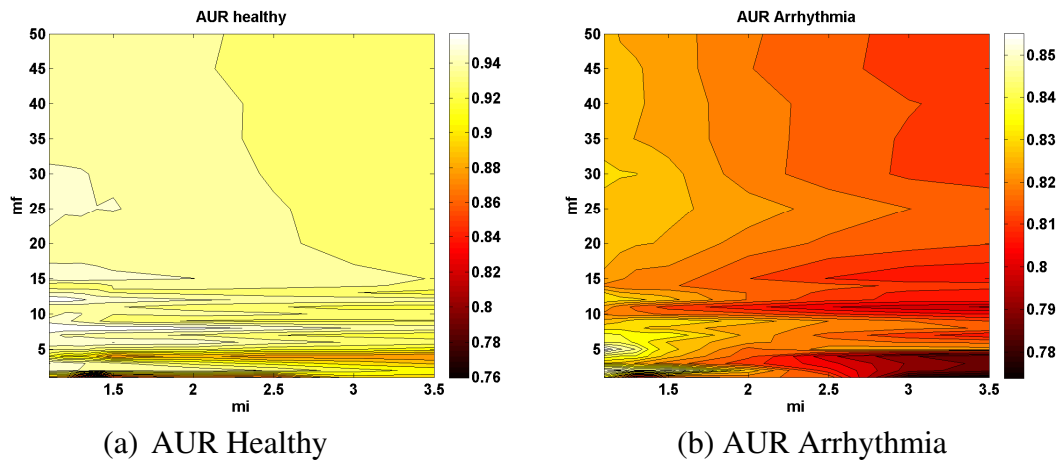


Figure 4-32: AUR profile for PAH

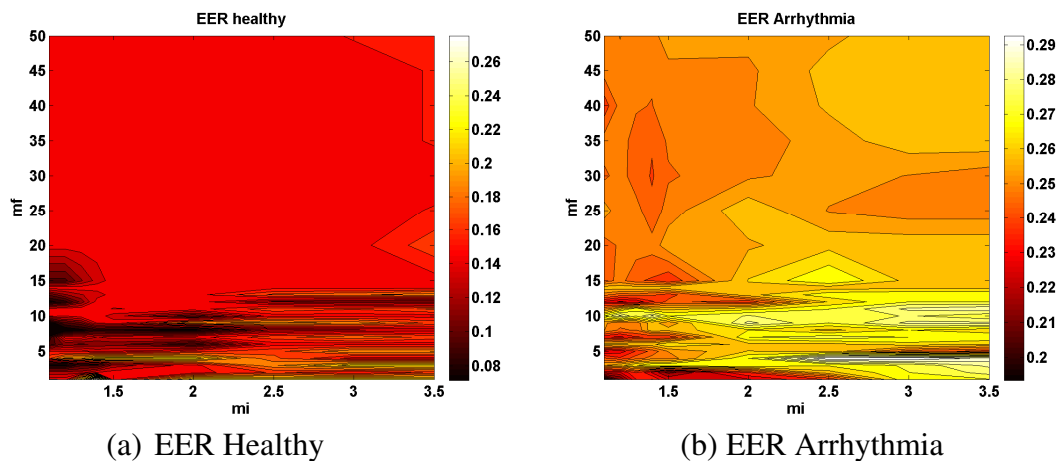


Figure 4-33: EER profile for PAH

From this subsection, it can be concluded that selecting the correct value of m_i and m_f may be helpful in generating the best AUR and EER profile. Table 4-6 summarized the m_i and m_f setting which produced the highest AUR values and in the same time having the lowest EER profile discussed in this subsection.

Table 4-6: Suggested m_f and m_i settings for PA feature selection

	Healthy		Arrhythmia	
	m_i	m_f	m_i	m_f
PAB	≥ 1.1	> 15	≥ 1.1	> 20
PAW	≥ 1	> 15	≥ 1.2	> 15
PAA	≥ 1	> 15	≥ 1.2	> 15
PAM	≥ 1	> 15	≥ 1.2	> 15
PAR	≤ 2.5	> 15	≤ 2.5	> 15
PAH	≤ 2.5	> 15	≤ 2.5	> 15

For a general PA settings, from Table 4-6, it can be conclude that m_i should be set between 1.1 and 2.5 while m_f should be set greater than 20.

4.8.4.2. Effect of varying O_{max} and O_{min}

This subsection will now evaluate the effects of changing O_{max} and O_{min} towards the AUR and EER values. Based from Table 4-1, O_{max} and O_{min} exists in the final equations of PAA, PAM and PAR. To run this experiments, m_f and m_i are set to be 30 and 1.2 respectively. O_{max} varies between 1 and 50 while O_{min} varies between -50 and 50.

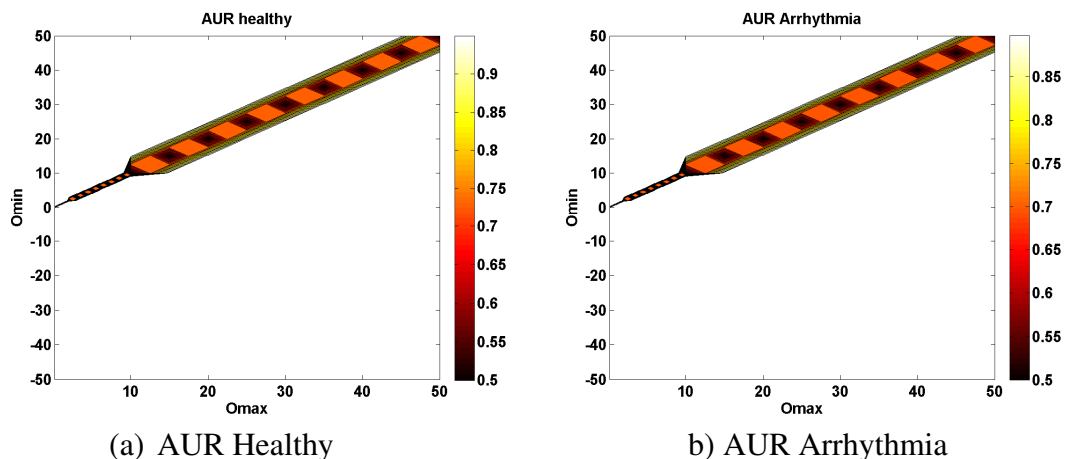
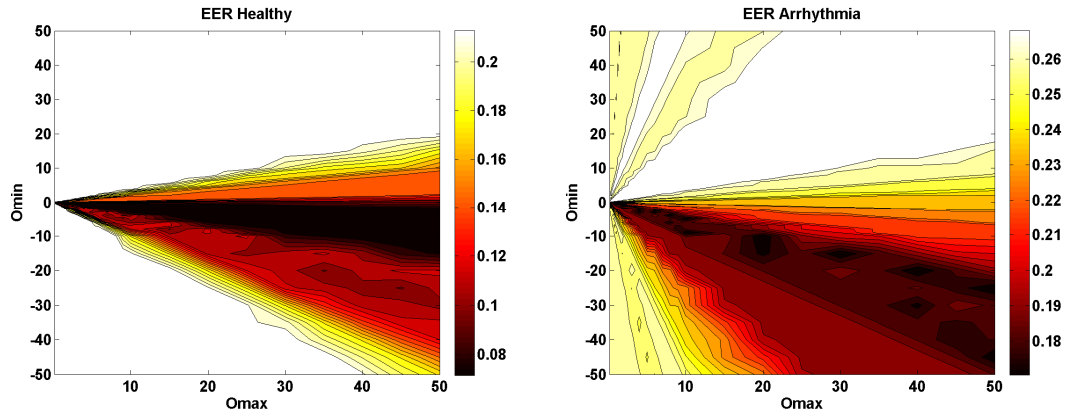


Figure 4-34: Effects of O_{max} and O_{min} on AUR profiles for PAA and PAM



(a) EER Healthy (b) EER Arrhythmia

Figure 4-37: Effects of O_{max} and O_{min} on EER profiles for PAR

In section 4.6 it has been repeatedly highlighted that O_{max} should not be set equal to O_{min} when the PAA, PAM or PAR algorithms are used to generate feature vectors. Another consideration which needs to be taken into account when setting the values of O_{max} and O_{min} is that the output pulse area generated must not be equal to zero. In (4-13), (4-15) and (4-30), the multiplication process of $(O_{max} - O_{min})$ with $(t_{2m} - t_{2m-1})$ represents the area of each pulse. To ensure that the pulse area is not zero the following condition must hold:

$$\int_{(m-1)T_{iri}}^{t_{2m-1}} O_{min} dt + \int_{t_{2m-1}}^{t_{2m}} O_{max} dt + \int_{t_{2m}}^{mT_{iri}} O_{min} dt \neq 0 \quad (4-33)$$

Equation (4-33) can be rearranged as follows:

$$O_{max} \neq O_{min} \left(1 - \frac{T_{iri}}{(t_{2m} - t_{2m-1})} \right) \quad (4-34)$$

Substituting (4-1) into (4-34) generates:

$$O_{max} \neq O_{min} \left(1 - \frac{T_{ECG}}{m_f (t_{2m} - t_{2m-1})} \right) \quad (4-35)$$

Regions of very poor performance are seen in Figures 4-34 to 4-37 correspond to values of O_{max} which produce zero or very small pulse areas, as suggested in (4-35).

4.8.4.3. Effect of varying N

The effect of another PA parameters needs to be evaluate is the total harmonic values, N in PAH. Figure 4-38 shows the AUR profile for healthy and arrhythmia populations when N varies between 1 and 50. In this simulation, m_i and m_f are set to be 1.2 and 15 respectively. Observing the figure, it is shown that similarly high AUR values can be achieved when N is between 3 and 20.

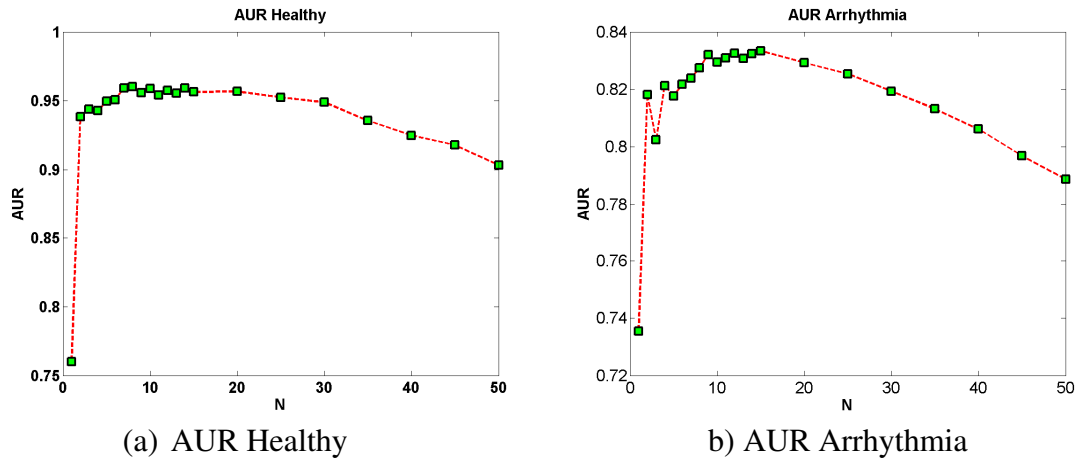


Figure 4-38: Effects of N on AUR profiles for PAH

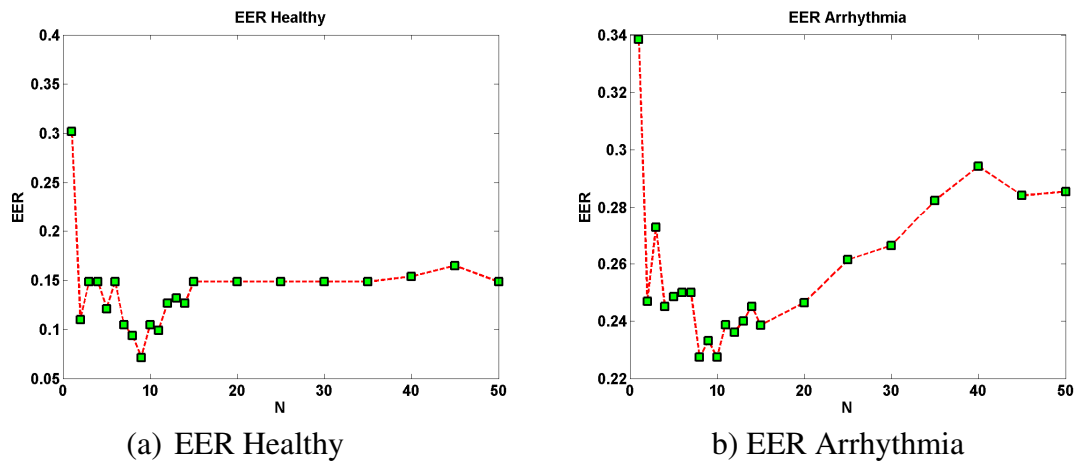


Figure 4-39: Effects of N on EER profiles for PAH

Figures 4-39 a) and b) show the EER profiles for healthy and arrhythmia populations respectively when N varies between 1 and 50. The values of m_i and m_f are also set to be 1.2 and 15 respectively. In these figures, it is observed that when N is set between 2 and 20, the EER value are similarly low. The tolerance for healthy

population is around ± 0.08 whilst for the arrhythmia population, the EER tolerance is around ± 0.03 .

4.8.4.4. Summary of varying PA parameters

For non-biometric applications, the requirement of selecting ECG sources as described in section 3.4.1 can be reduced to using ECG measurements from healthy populations that may come from the same recording and be collected with any Lead configuration. The performance of such application using 58 healthy subjects is shown in Appendix E where it is seen that the PAW still manages to generate ROC curves with high AUR and low EER which are respectively equal to 0.953 and 0.1210.

In the applications of biometric authentication, the study conducted in subsections 4.8.4.1 to 4.8.4.3 suggested that common PA parameters, namely m_f , m_i , O_{\max} , O_{\min} and N can be assigned to obtain a similar AUR and EER performance. The ranges extracted are from the statistically significant arrhythmia subjects. It is noted that using these ranges produces acceptable results for the healthy subjects used in the simulations. From subsection 4.8.4.1, it has been shown that a similar high AUR and low EER profile can be achieved using:

$$20 \leq m_f \leq 50 \quad (4-36)$$

$$1.2 \leq m_i \leq 2.5 \quad (4-37)$$

From subsection 4.8.4.2, it can be concluded that PAA, PAM and PAR will have the similar highest AUR and lowest EER profile by setting O_{\min} and O_{\max} as follows:

$$O_{\min} < 0 \quad (4-38)$$

$$O_{\max} = -0.4 \times O_{\min} \quad (4-39)$$

The N parameter as studied in subsection 4.8.4.3 reveals that the highest AUR and EER profile can be achieved using

$$2 \leq N \leq 20 \quad (4-40)$$

The graphical representation of the AUR and EER performances based on the general PA parameters setting given from (4-36) to (4-40) are shown in Appendix C. From Appendix C, the maximum and minimum values of AUR and EER for healthy populations using these settings are tabulated in Table 4-7. The maximum and minimum values of AUR and EER for arrhythmia populations using these settings are tabulated in Table 4-8.

Observing Appendix C, Table 4-7 and Table 4-8, it can be seen that, in general, when m_f is set as (4-36) and m_i set as (4-37), the AUR profiles for healthy and arrhythmia populations vary around ± 0.05 and ± 0.015 respectively for all PA feature selection techniques. The EER profiles for similar settings vary by ± 0.07 and ± 0.025 for the healthy and arrhythmia population respectively. Setting O_{\max} and O_{\min} as in (4-38) and (4-39) vary the AUR and EER values by ± 0.085 for both populations.

Finally, by setting N as in (4-40) the AUR and EER tolerances for both populations are around ± 0.035 and ± 0.08 respectively. These tolerances, using the suggested PA parameters range, indicate that a similar biometric authentication performance, using the different settings, is achievable and that it will be advantageous to set up a doubly secure ECG-based biometric system as explained in chapter 6.

Table 4-7: AUR and EER profiles for healthy population using general PA parameters

PA Feature Selection	AUR		EER	
	max	min	max	Min
PAB(m_f and m_i varies)	0.974	0.9695	0.0765	0.0715
PAW (m_f and m_i varies)	0.9735	0.97	0.0765	0.0715
PAA (m_f and m_i varies)	0.9735	0.97	0.0765	0.0715
PAM (m_f and m_i varies)	0.9735	0.97	0.0765	0.0715
PAR (m_f and m_i varies)	0.925	0.88	0.22	0.15
PAH(m_f and m_i varies)	0.948	0.934	0.145	0.145
PAA (O_{\max} and O_{\min} varies)	0.97	0.97	0.07	0.07
PAM (O_{\max} and O_{\min} varies)	0.97	0.97	0.07	0.07
PAR (O_{\max} and O_{\min} varies)	0.965	0.88	0.21	0.07
PAH (N varies)	0.96	0.938	0.15	0.07

Table 4-8: Suggested Ranges, AUR and EER profiles for arrhythmia population

PA Feature Selection	AUR		EER	
	max	min	max	Min
PAB(m_f and m_i varies)	0.918	0.915	0.17	0.158
PAW (m_f and m_i varies)	0.9185	0.9135	0.169	0.156
PAA (m_f and m_i varies)	0.9185	0.9135	0.169	0.156
PAM (m_f and m_i varies)	0.9185	0.9135	0.169	0.156
PAR (m_f and m_i varies)	0.825	0.705	0.272	0.25
PAH(m_f and m_i varies)	0.83	0.816	0.262	0.242
PAA (O_{\max} and O_{\min} varies)	0.91	0.91	0.17	0.17
PAM (O_{\max} and O_{\min} varies)	0.91	0.91	0.17	0.17
PAR (O_{\max} and O_{\min} varies)	0.89	0.82	0.255	0.17
PAH (N varies)	0.835	0.8	0.275	0.225

4.9. CONCLUSION

This chapter has introduced a new feature extraction technique named Pulse Active. The fundamental concept of the Pulse Active technique was first introduced in this chapter by deriving the general topology of the Pulse Active feature extraction technique which leads to six different feature selection mechanisms. Various locations within the ECG, from where features can be extracted, have also been examined in this chapter. Simulations on these techniques suggested the optimized ranges of each feature selection algorithm. In chapter 6 these ranges will be revisited and reused to set up the multilevel security ECG-based authentication system. The next chapter will describe an alternative way to generate pulse domain output pulses named as Adaptive Pulse Active technique.

CHAPTER 5.

ADAPTIVE PULSE ACTIVE (APA) FEATURE EXTRACTION TECHNIQUE FOR ECG BIOMETRIC AUTHENTICATION

5.1. INTRODUCTION

In Chapter 4, the PA technique used a triangular wave which is then superimposed on to the ECG signal and the intersection locations between both signals will determine the on-set and off-set of the output pulses based on certain rules. It was shown that the ECG peak-to-peak amplitude A_{ECG} and temporal duration T_{ECG} characterize the shape of the triangular wave used in PA. The maximum amplitude of the triangular wave A_{tri} , for each period of the triangular wave T_{tri} , is the same throughout the T_{ECG} . In this chapter, a new feature extraction technique named the Adaptive Pulse Active (APA) is developed and used for biometric authentication. APA also transforms the investigated signals into a series of output pulses similar to PA with three fundamental differences which define the term ‘Adaptive’ in APA. These differences are:

- i. The maximum amplitude of the triangular wave in each period is not the same.
- ii. The output pulse generation is not based on the intersection location between the triangular wave and the ECG signals, but it is solely based on the

characteristics of the generated triangular waves.

iii. APA is developed based on the concept of delta modulation (DM)

This chapter will first introduce the fundamentals of APA by briefly discussing the concept of DM. This is followed by the development of a generalized scheme of the APA feature extraction technique. Four types of APA feature selection methods are then discussed and, finally, the optimization of the APA parameters is presented.

5.2. FUNDAMENTALS OF ADAPTIVE PULSE ACTIVE (APA)

The APA approach is developed based on Delta Modulation (DM) in PA. In order to introduce APA, the operation principle of DM is first presented in this subsection. This is then followed by the concept and mathematical derivation of the APA technique.

5.2.1. Delta Modulation (DM)

The block diagram of delta modulation (DM) and its waveform operational principle are illustrated in Figures 5-1 and 5-2 respectively. As shown in Figure 5-1, the input signal $V_i(t)$ is subtracted from the feedback signal $V_F(t)$ to generate an error signal $V_{err}(t)$. The error signal is then quantized commonly using a hysteresis comparator with level $\pm\Delta V$ to generate a series of modulated output pulses $V_m(t)$ which are then integrated to generate the output signal $V_F(t)$. The closed loop configuration of the DM ensures that the polarity of each output pulse $V_m(t)$ is adjusted according to the sign of $V_{err}(t)$.

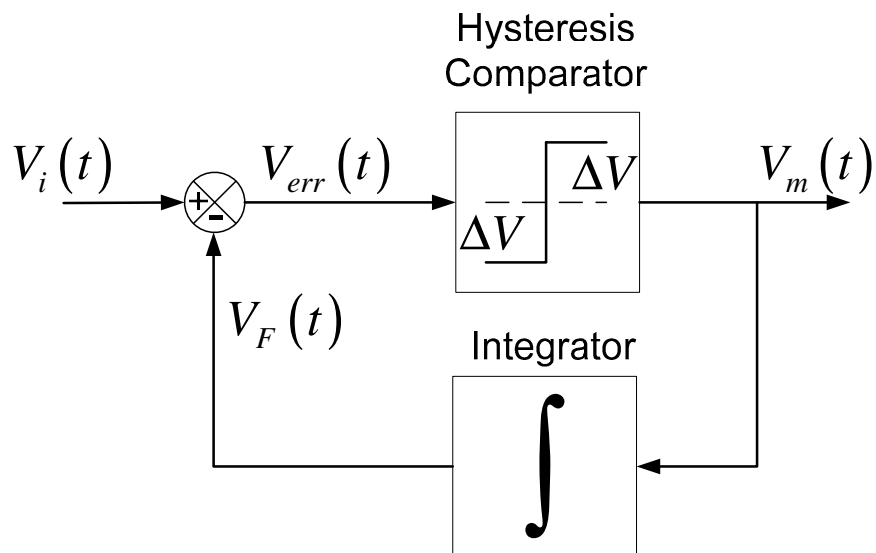


Figure 5-1 : Block Diagram of DM

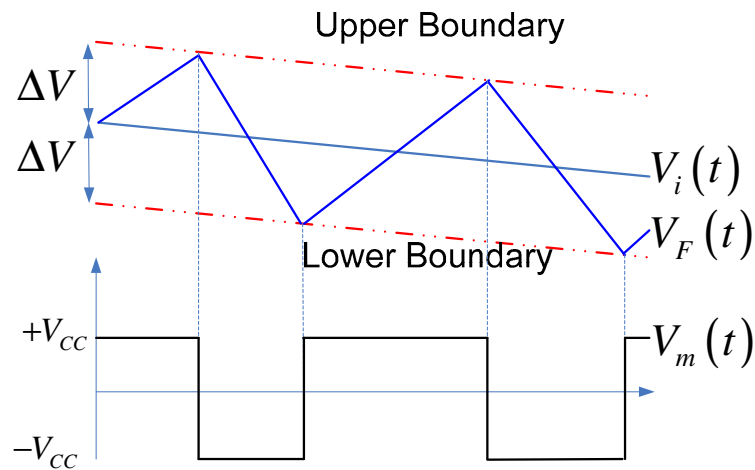


Figure 5-2 : Waveform generation of DM

Figure 5-2 illustrates typical waveforms $V_i(t)$, $V_F(t)$, $V_m(t)$ and the hysteresis band ΔV process based on the concept of DM shown in Figure 5-1. The initial value of $V_F(t)$ is 0. Using this value, the generated $V_{err}(t)$ has a positive value. $V_{err}(t)$ is fed into the hysteresis comparator. With a positive $V_{err}(t)$, the $V_m(t)$ will also generate a positive value. The positive $V_m(t)$ value is fed into an integrator.

Integrating any positive value would generate a positive slope of $V_F(t)$ which will increase the stepwise value of $V_F(t)$. This process continues until $V_F(t)$ reaches the upper level of ΔV and consequently results in a negative $V_m(t)$.

5.2.2. Adaptive Pulse Active Waveform Generation

The development of the APA feature extraction technique on ECG signals includes 4 stages:

- i) Defining the start and end locations of the APA process
- ii) Generation of ECG envelopes
- iii) Triangular waves generation
- iv) Extracting APA features

5.2.2.1. *Defining the start and end locations*

Similar to PA, APA requires the detection of 2 fiducial points to start and end the process. For the implementation on ECG signals, the APA process can start and end anywhere between these two fiducial points by employing any standard fiducial detection algorithm.

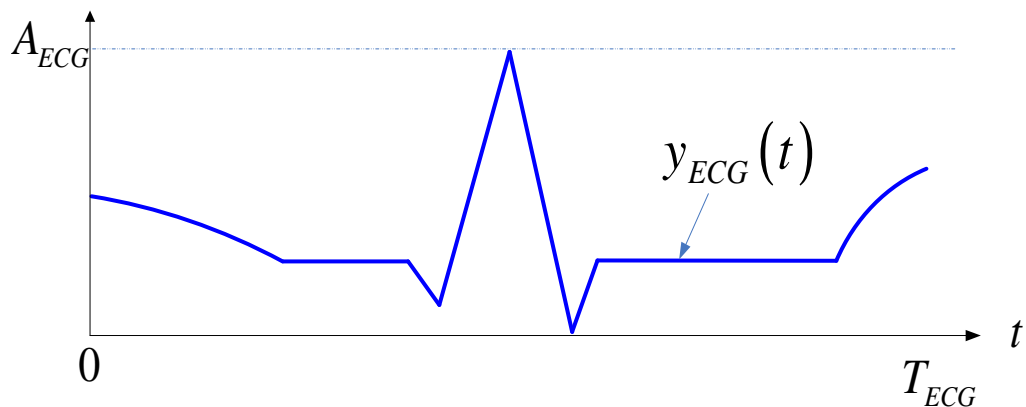


Figure 5-3 : ECG as investigated signal from peak P to peak T

This location is denoted as T_{ECG} . Consider an ECG signal $y_{ECG}(t)$ from the peak of P to the peak of T. This temporal T_{ECG} duration has peak to peak amplitude A_{ECG} as shown in Figure 5-3. The ECG signal is offset so that its minimum value is equal to zero.

5.2.2.2. Generation of ECG envelopes

Next, $y_{ECG}(t)$ is replicated twice and the replicates are positioned a distance ΔV above and below the original $y_{ECG}(t)$ as shown in Figure 5-4. The top replication of the ECG signal is labeled $y_{top}(t)$ while the bottom replication of the ECG signal is labeled $y_{bottom}(t)$. The signals $y_{top}(t)$ and $y_{bottom}(t)$ work like an envelopes on the $y_{ECG}(t)$ for the distance ΔV . A constant, known as the deviation index δ_i , is introduced and defined as:

$$\delta_i = \frac{\Delta V}{A_{ECG}} \quad (5-1)$$

where δ_i is a user defined value.

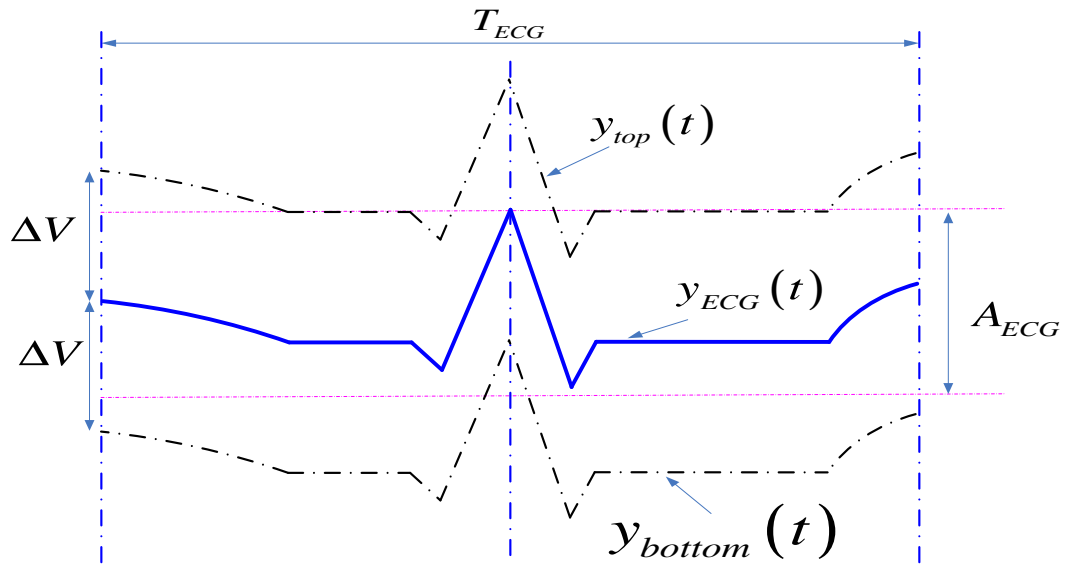


Figure 5-4 : ECG envelopes generation

This constant allows us to control the level between replicates and underlying signal. It also allows us to cope with the degree of amplitude variations.

5.2.2.3. Triangular wave generation

The next process is to generate triangular waves $y_{tri}(t)$ within the $y_{ECG}(t)$ envelope as shown in Figure 5-5. As can be seen from Figure 5-5, the triangular waves do not have the same peak to peak values, however, the duration for each period of the triangular wave is the same, i.e. T_{tri} . The modulation factor m_f , used earlier in (4-1), is redefined here as:

$$m_f = \frac{T_{ECG}}{T_{tri}} \quad (5-2)$$

In Figure 5-5 m_f is set to 4. Each period of the triangular waves would have three important points which represent the starting point $L_{[2m-1]}$, the peak, $L_{[2m]}$ and the end point $L_{[2m+1]}$ of the triangular period.

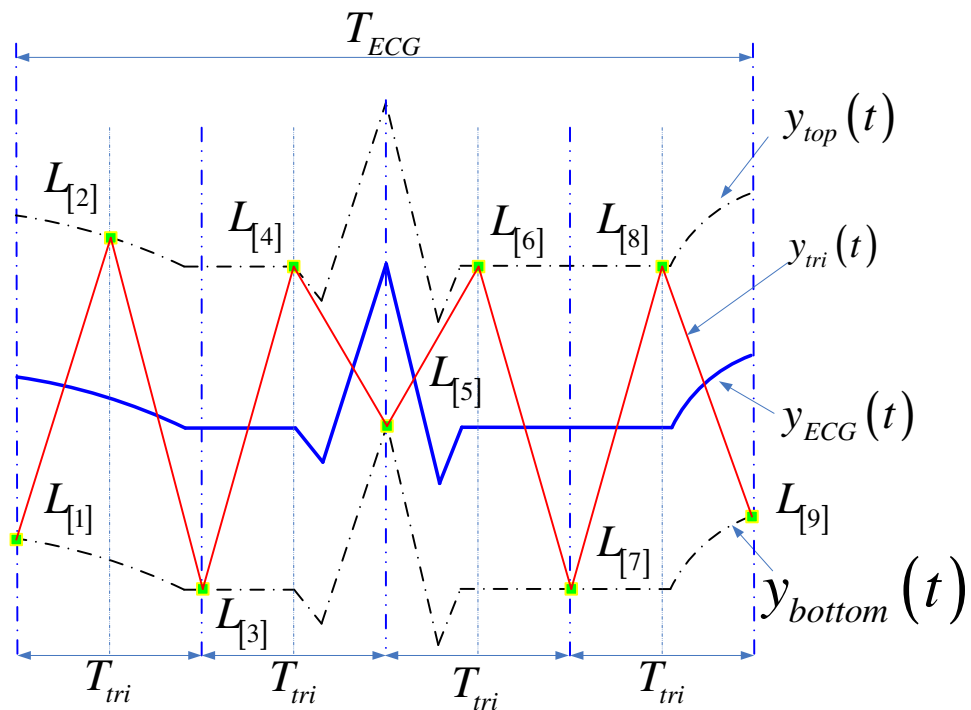


Figure 5-5 : Triangular wave generation

These locations are denoted as location vectors and can be mathematically described as follows:

$$L_{[2m-1]} = (m-1)T_{tri} \quad (5-3)$$

$$L_{[2m]} = (m-0.5)T_{tri} \quad (5-4)$$

$$L_{[2m+1]} = mT_{tri} \quad (5-5)$$

for $m = 1, 2, 3 \dots m_f$.

$y_{tri}(t)$ is then generated using the following rules:

$$y_{tri}(t) = \left(\frac{y_{top}(L_{[2m]}) - y_{bottom}(L_{[2m-1]})}{L_{[2m]} - L_{[2m-1]}} \right) (t - L_{[2m-1]}) + y_{bottom}(L_{[2m-1]}) \quad (5-6)$$

for $(m-1)T_{tri} \leq t \leq (m-0.5)T_{tri}$ and $m = 1, 2, 3 \dots m_f$,

and

$$y_{tri}(t) = \left(\frac{y_{bottom}(L_{[2m+1]}) - y_{top}(L_{[2m]})}{L_{[2m+1]} - L_{[2m]}} \right) (t - L_{[2m]}) + y_{top}(L_{[2m]}) \quad (5-7)$$

for $(m-0.5)T_{tri} \leq t \leq mT_{tri}$ and $m = 1, 2, 3 \dots m_f$.

5.2.2.4. *Extracting Features*

The next step is to extract the APA features from the generated triangular signal $y_{tri}(t)$. To do this, an interception line, $y_L(t)$ is defined. As illustrated in Figure 5-6, this is a DC line that runs across T_{ECG} and is generated as follows:

$$y_L(t) = \frac{\min(y_{top}(t)) - \max(y_{bottom}(t))}{2} + \max(y_{bottom}(t)) \quad (5-8)$$

for $(m-1)T_{tri} \leq t \leq mT_{tri}$.

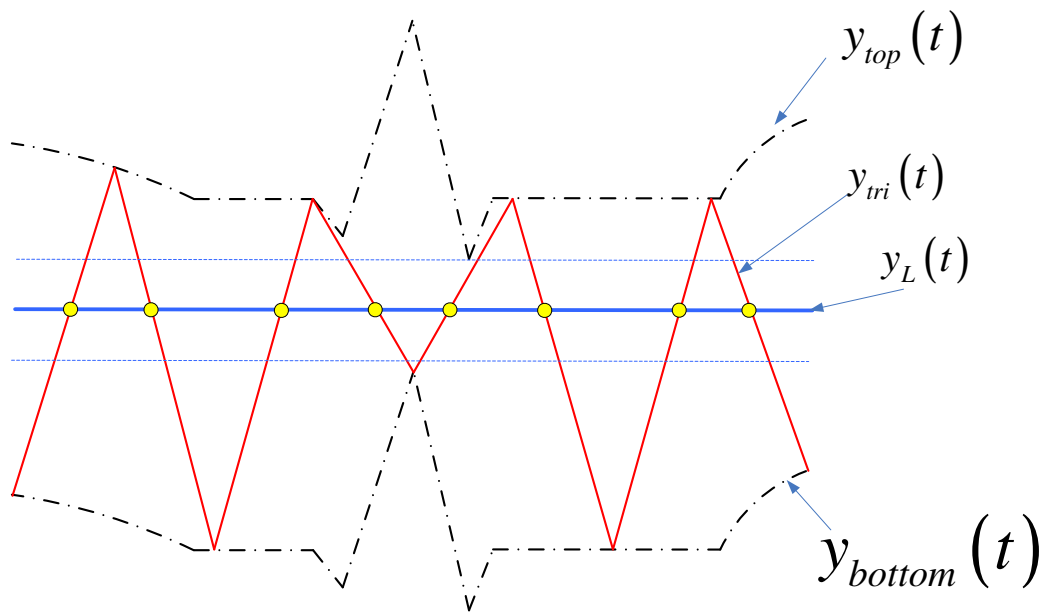


Figure 5-6 : Interception line generation

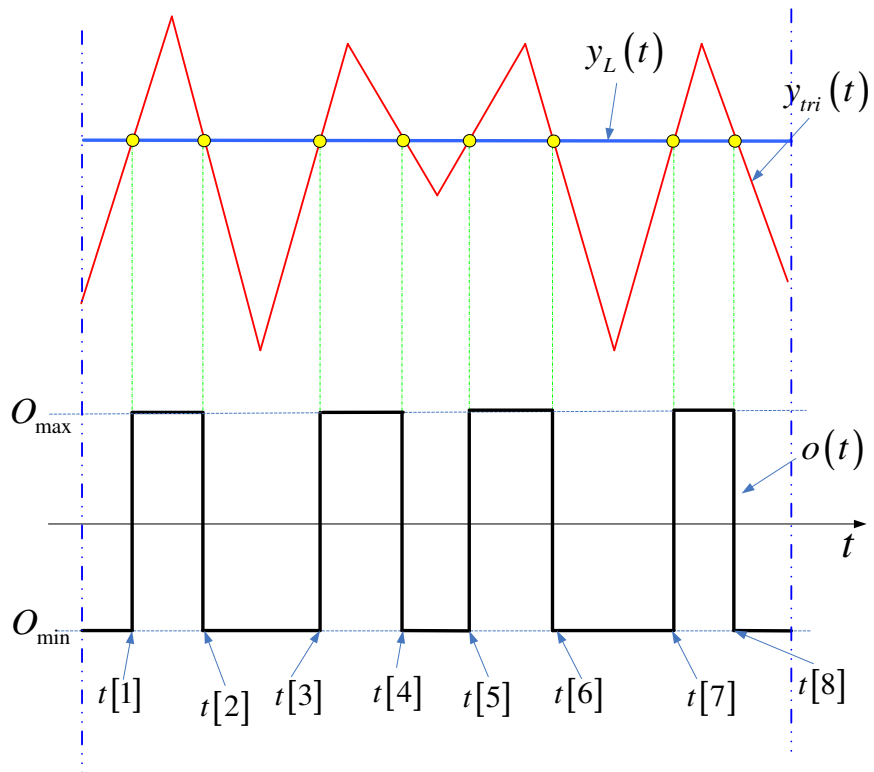


Figure 5-7 : Pulse Generation

To ensure that the minimum value of $y_{top}(t)$ is always greater than the maximum value of $y_{bottom}(t)$ the value of the deviation index δ_i , given in (5-1), must be greater than 0.5. This will ensure that each triangular period is intersected by the DC line $y_L(t)$ in two places (one for the positive edge and one for the negative edge).

As illustrated in Figure 5-7 the output pulses $o(t)$ are formed as follows:

$$o(t) = \begin{cases} O_{\max} & y_{tri}(t) \geq y_L(t) \\ O_{\min} & y_{tri}(t) < y_L(t) \end{cases} \quad (5-9)$$

for $t = 0 \dots T_{ECG}$

For each triangular wave period, the location $t_{[2m-1]}$ where the DC line $y_L(t)$ intersects with the positive slope, and the location $t_{[2m]}$ where the DC line $y_L(t)$ intersects with the negative slope are selected as the intersection points for that period. These intersection locations are defined as a transition state vector and can be written as:

$$\begin{bmatrix} T_{trans}(2m-1) \\ T_{trans}(2m) \end{bmatrix} = \begin{bmatrix} t_{[2m-1]} \\ t_{[2m]} \end{bmatrix} \quad (5-10)$$

for $m = 1, 2, 3 \dots m_f$. T_{trans} also corresponds to the location where the output pulse, $o(t)$ state changes.

5.2.3. Adaptive Pulse Active Generalize Equation

In the previous subsection the process of obtaining T_{trans} was shown graphically. In this subsection, the derivation of a generalized T_{trans} algorithm is presented. Recall the algorithm to generate the triangular wave as indicated in (5-6) and (5-7). Based on Figure 5-4 it is evident that

$$y_{top}(t) = y_{ECG}(t) + \Delta V \quad (5-11)$$

$$y_{bottom}(t) = y_{ECG}(t) - \Delta V \quad (5-12)$$

Substituting (5-11) and (5-12) into (5-6) and (5-7) yields

$$y_{tri}(t) = \left(\frac{y_{ECG}(L_{[2m]}) - y_{ECG}(L_{[2m-1]}) + 2\Delta V}{L_{[2m]} - L_{[2m-1]}} \right) (t - L_{[2m-1]}) + y_{ECG}(L_{[2m-1]}) - \Delta V \quad (5-13)$$

for $(m-1)T_{tri} \leq t \leq (m-0.5)T_{tri}$ and $m = 1, 2, 3 \dots m_f$,

$$y_{tri}(t) = \left(\frac{y_{ECG}(L_{[2m+1]}) - y_{ECG}(L_{[2m]}) - 2\Delta V}{L_{[2m+1]} - L_{[2m]}} \right) (t - L_{[2m]}) + y_{ECG}(L_{[2m]}) + \Delta V \quad (5-14)$$

for $(m-0.5)T_{tri} \leq t \leq mT_{tri}$ and $m = 1, 2, 3 \dots m_f$.

Substituting (5-11) and (5-12) into (5-8) yields

$$y_L(t) = \frac{\min(y_{ECG}(t)) - \max(y_{ECG}(t)) + 2\Delta V}{2} + \max(y_{ECG}(t)) - \Delta V \quad (5-15)$$

Since $\min(y_{ECG}(t)) = 0$ and $\max(y_{ECG}(t)) = A_{ECG}$, expanding (5-15) generates

$$y_L(t) = \frac{1}{2} A_{ECG} \quad (5-16)$$

Based on subsection 5.2.2.4, T_{trans} is the location vector where the triangular waves $y_{tri}(t)$ intersect the DC line $y_L(t)$. Mathematically, this is written as

$$y_{tri}(t) = y_L(t) \quad (5-17)$$

Substituting (5-16), (5-13) and (5-14) into (5-17) yields

$$\left(\frac{y_{ECG}(L_{[2m]}) - y_{ECG}(L_{[2m-1]}) + 2\Delta V}{L_{[2m]} - L_{[2m-1]}} \right) (t_{[2m-1]} - L_{[2m-1]}) + y_{ECG}(L_{[2m-1]}) - \Delta V = \frac{A_{ECG}}{2} \quad (5-18)$$

$$\left(\frac{y_{ECG}(L_{[2m+1]}) - y_{ECG}(L_{[2m]}) - 2\Delta V}{L_{[2m+1]} - L_{[2m]}} \right) (t_{[2m]} - L_{[2m]}) + y_{ECG}(L_{[2m]}) + \Delta V = \frac{A_{ECG}}{2} \quad (5-19)$$

for $m = 1, 2, 3 \dots m_f$.

Solving $t_{[2m-1]}$ in (5-18) yields

$$t_{[2m-1]} = \left(\frac{A_{ECG}}{2} + \Delta V - y_{ECG}(L_{[2m-1]}) \right) \left(\frac{L_{[2m]} - L_{[2m-1]}}{y_{ECG}(L_{[2m]}) - y_{ECG}(L_{[2m-1]}) + 2\Delta V} \right) + L_{[2m-1]} \quad (5-20)$$

Solving $t_{[2m]}$ in (5-19)

$$t_{[2m]} = \left(\frac{A_{ECG}}{2} - \Delta V - y_{ECG}(L_{[2m]}) \right) \left(\frac{L_{[2m+1]} - L_{[2m]}}{y_{ECG}(L_{[2m+1]}) - y_{ECG}(L_{[2m]}) - 2\Delta V} \right) + L_{[2m]} \quad (5-21)$$

Substituting (5-3), (5-4) and (5-5) into (5-20) and (5-21) generates

$$t_{[2m-1]} = \frac{T_{tri}}{4} \left\{ \frac{A_{ECG} + \Delta V(8m-6) + (2-4m)y_{ECG}((m-1)T_{tri}) + (4m-4)y_{ECG}((m-0.5)T_{tri})}{y_{ECG}((m-0.5)T_{tri}) - y_{ECG}((m-1)T_{tri}) + 2\Delta V} \right\} \quad (5-22)$$

$$t_{[2m]} = \frac{T_{tri}}{4} \left\{ \frac{A_{ECG} + (2-8m)\Delta V - (4m)y_{ECG}((m-0.5)T_{tri}) + (4m-2)y_{ECG}(mT_{tri})}{y_{ECG}(mT_{tri}) - y_{ECG}((m-0.5)T_{tri}) - 2\Delta V} \right\} \quad (5-23)$$

Substituting (5-1) and (5-2) into (5-22) and (5-23) yields

$$t_{[2m-1]} = \frac{T_{ECG}}{4m_f} \left\{ \frac{A_{ECG} \cdot (1 + \delta_i \cdot (8m - 6)) + (2 - 4m) \cdot y_{ECG} \left(\frac{(m-1)}{m_f} T_{ECG} \right) + (4m - 4) \cdot y_{ECG} \left(\frac{(m-0.5)}{m_f} T_{ECG} \right)}{y_{ECG} \left(\frac{(m-0.5)}{m_f} T_{ECG} \right) - y_{ECG} \left(\frac{(m-1)}{m_f} T_{ECG} \right) + 2\delta_i A_{ECG}} \right\} \quad (5-24)$$

$$t_{[2m]} = \frac{T_{ECG}}{4m_f} \left\{ \frac{A_{ECG} \cdot (1 + \delta_i \cdot (2 - 8m)) - (4m) \cdot y_{ECG} \left(\frac{(m-0.5)}{m_f} T_{ECG} \right) + (4m - 2) \cdot y_{ECG} \left(\frac{m}{m_f} T_{ECG} \right)}{y_{ECG} \left(\frac{m}{m_f} T_{ECG} \right) - y_{ECG} \left(\frac{(m-0.5)}{m_f} T_{ECG} \right) - 2\delta_i A_{ECG}} \right\} \quad (5-25)$$

$$m = 1, 2, 3 \dots m_f .$$

From this derivation, it can be seen that APA transition state vector \mathbf{T}_{trans} can also be generated using equations (5-24) and (5-25) by first measuring A_{ECG} and T_{ECG} of the ECG signals and setting the APA parameters such δ_i and m_f .

5.3. APA FOR ECG BIOMETRIC AUTHENTICATION

In subsection 5.2.2.3, it was highlighted that the generation of the triangular wave supposed to be within the $y_{ECG}(t)$ envelope prior to the original concept of DM. In Figure 5-5, it was shown that, the signal length between peaks P and R, T_{P2R} is the

same with the signal length between peaks R and T, T_{R2T} . Thus the triangular wave generated is connected at peak R of $y_{bottom}(t)$ and the triangular wave successfully generated within the $y_{ECG}(t)$ envelope. In an actual ECG signals, T_{P2R} and T_{R2T} are not the same. This will make the triangular wave generated outside the $y_{ECG}(t)$ envelope if T_{tri} is the same throughout the ECG signals. To fix this fundamental flaw during the implementation of ECG biometric authentication, APA will extract ECG features within T_{P2R} and T_{R2T} separately with the following conditions:

- i. The number of periodic triangular waves within T_{P2R} and T_{R2T} is the same. This is done by using the same value of m_f in both processes.
- ii. The envelope characteristic generated within T_{P2R} and T_{R2T} using the same parameters. This is done by using the same A_{ECG} and δ_i as defined in subsection 5.2.2.2.
- iii. The interception lines $y_L(t)$ generated within T_{P2R} and T_{R2T} are the same. This is done by using (5-8) for the overall signals.

Let $y_{P2R}(t)$ and $y_{R2T}(t)$ represent ECG signals within T_{P2R} and T_{R2T} respectively. The location $t_{P2R[2m-1]}$ and $t_{P2R[2m]}$ where the DC line $y_L(t)$ intersects with the positive slope, and the negative slope respectively within T_{P2R} can be written as:

$$t_{P2R[2m-1]} = \frac{T_{P2R}}{4m_f} \left\{ \frac{A_{ECG} \cdot (1 + \delta_i \cdot (8m - 6)) + (2 - 4m) \cdot y_{P2R} \left(\frac{(m-1)}{m_f} T_{P2R} \right) + (4m - 4) \cdot y_{P2R} \left(\frac{(m-0.5)}{m_f} T_{P2R} \right)}{y_{P2R} \left(\frac{(m-0.5)}{m_f} T_{P2R} \right) - y_{P2R} \left(\frac{(m-1)}{m_f} T_{P2R} \right) + 2\delta_i A_{ECG}} \right\} \quad (5-26)$$

$$t_{P2R[2m]} = \frac{T_{P2R}}{4m_f} \left(\frac{A_{ECG} \cdot (1 + \delta_i \cdot (2 - 8m)) - (4m) \cdot y_{P2R} \left(\frac{(m-0.5)}{m_f} T_{P2R} \right) + (4m-2) \cdot y_{P2R} \left(\frac{m}{m_f} T_{P2R} \right)}{y_{P2R} \left(\frac{m}{m_f} T_{P2R} \right) - y_{P2R} \left(\frac{(m-0.5)}{m_f} T_{P2R} \right) - 2\delta_i A_{ECG}} \right) \quad (5-27)$$

for $m = 1, 2, 3 \dots m_f$.

The location $t_{R2T[2m-1]}$ and $t_{R2T[2m]}$ where the DC line $y_L(t)$ intersects with the positive slope, and the negative slope respectively within T_{R2T} can be written as:

$$t_{R2T[2m-1]} = \frac{T_{R2T}}{4m_f} \left(\frac{A_{ECG} \cdot (1 + \delta_i \cdot (8m-6)) + (2-4m) \cdot y_{R2T} \left(\frac{(m-1)}{m_f} T_{R2T} \right) + (4m-4) \cdot y_{R2T} \left(\frac{(m-0.5)}{m_f} T_{R2T} \right)}{y_{R2T} \left(\frac{(m-0.5)}{m_f} T_{R2T} \right) - y_{R2T} \left(\frac{(m-1)}{m_f} T_{R2T} \right) + 2\delta_i A_{ECG}} \right) \quad (5-28)$$

$$t_{R2T[2m]} = \frac{T_{R2T}}{4m_f} \left(\frac{A_{ECG} \cdot (1 + \delta_i \cdot (2 - 8m)) - (4m) \cdot y_{R2T} \left(\frac{(m-0.5)}{m_f} T_{R2T} \right) + (4m-2) \cdot y_{R2T} \left(\frac{m}{m_f} T_{R2T} \right)}{y_{R2T} \left(\frac{m}{m_f} T_{R2T} \right) - y_{R2T} \left(\frac{(m-0.5)}{m_f} T_{R2T} \right) - 2\delta_i A_{ECG}} \right) \quad (5-29)$$

for $m = 1, 2, 3 \dots m_f$.

The final transition state vector T_{trans} can be written as:

$$\begin{bmatrix} T_{trans}(2m-1) \\ T_{trans}(2m) \end{bmatrix} = \begin{bmatrix} t_{P2R[2m-1]} \\ t_{P2R[2m]} \end{bmatrix} \quad (5-30)$$

$$\begin{bmatrix} T_{trans}(2m-1+2m_f) \\ T_{trans}(2m+2m_f) \end{bmatrix} = \begin{bmatrix} t_{R2T[2m-1]} \\ t_{R2T[2m]} \end{bmatrix} \quad (5-31)$$

for $m=1,2,3\dots m_f$. T_{trans} also corresponds to the location where the output pulse, $o(t)$ state changes.

5.4. FEATURE SELECTION

The features extracted using APA are in the form of generated output pulse $o(t)$. Each pulse within each period of the triangular wave $y_{tri}(t)$ is the ECG feature extracted within that period. In general, the representation of each output pulse is illustrated in Figure 5-8.

From Figure 5-8, there are 5 different types of features can be selected from $o(t)$. The selections of features in each algorithm depend on the characteristic types of the output pulses. Since the triangular wave generated in each period does not have a similar base, the area of the triangular waves is difficult to calculate. This prevent the used of ratio as described in section 4.5 to be selected as features. As explained in section 4.6, to avoid the dependency of T_{trans} on the number of sampling points, the time durations for $y_{P2R}(t)$ and $y_{R2T}(t)$ are normalized to 1.

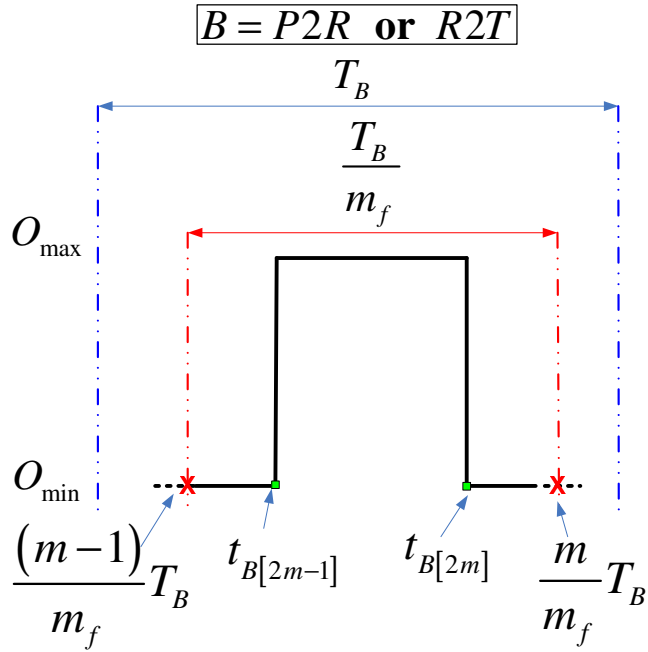


Figure 5-8 : APA Output pulse representation

For ECG biometric application, the final feature vector \mathbf{X} for all APA algorithms is written in the similar form. Unless it is stated otherwise, the APA final feature vector is given in the following form:

$$\mathbf{X} = \begin{bmatrix} x_{P2R}(1) & x_{P2R}(2) & \dots & x_{P2R}(m) & \dots & x_{P2R}(m_f) & x_{R2T}(m_f+1) \\ & & & & & & x_{R2T}(m_f+2) & \dots & x_{R2T}(m_f+m) & \dots & x_{R2T}(2m_f) \end{bmatrix} \quad (5-32)$$

where $x_{P2R}(m)$ and $x_{R2T}(m+m_f)$ are the individual APA algorithms calculated for $m = 1, 2, \dots, m_f$.

5.4.1. Adaptive Pulse Active Bit (APAB)

Similar as in subsection 4.6.1, the simplest way to select $o(t)$ features is by using T_{trans} in (5-30) and (5-31) as a feature vector. The term ‘Bit’ in the APAB refers to the bit location where the pulses changes from O_{max} to O_{min} or O_{min} to O_{max} . The APAB feature vector X is given as:

$$X = \begin{bmatrix} t_{P2R[1]} & t_{P2R[2]} & \cdots & t_{P2R[m]} & \cdots & t_{P2R[2m_f]} \\ t_{R2T[1]} & t_{R2T[2]} & \cdots & t_{R2T[m]} & \cdots & t_{R2T[2m_f]} \end{bmatrix} \quad (5-33)$$

for $m = 1, 2, 3 \dots 2m_f$.

5.4.2. Adaptive Pulse Active Width (APAW)

The width between two contiguous points of T_{trans} also can be used as feature vectors. The APAW algorithm can be calculated as follows:

$$x_{P2R}(m) = t_{P2R[2m]} - t_{P2R[2m-1]} \quad (5-34)$$

$$x_{R2T}(m + m_f) = t_{R2T[2m]} - t_{R2T[2m-1]} \quad (5-35)$$

for $m = 1, 2, 3 \dots m_f$.

5.4.3. Adaptive Pulse Active Area (APAA)

APAA uses the width of each pulse as the features. With reference to Figure 5-8, the APAA mathematical expression can be defined as

$$x_{P2R}(m) = \int_{\frac{(m-1)T_{P2R}}{m_f}}^{\frac{mT_{P2R}}{m_f}} o(t) dt \quad (5-36)$$

$$x_{R2T}(m + m_f) = \int_{\frac{(m-1)T_{R2T}}{m_f}}^{\frac{mT_{R2T}}{m_f}} o(t) dt \quad (5-37)$$

for $m = 1, 2, \dots, m_f$

Following the similar derivation steps as shown in (4-12), (5-36) and (5-37) can be written as

$$x_{P2R}(m) = (t_{P2R[2m]} - t_{P2R[2m-1]})(O_{\max} - O_{\min}) + O_{\min} \frac{T_{P2R}}{m_f} \quad (5-38)$$

$$x(m + m_f) = (t_{R2T[2m]} - t_{R2T[2m-1]})(O_{\max} - O_{\min}) + O_{\min} \frac{T_{R2T}}{m_f} \quad (5-39)$$

for $m = 1, 2, \dots, m_f$

It is important for the feature vectors evaluated using (5-38) and (5-39) involves the transition state vectors of (5-30) and (5-31). To ensure the characteristic of the ECG embedded within (5-30) and (5-31) always taken into consideration, O_{\max} should not be set equal to O_{\min} .

5.4.4. Adaptive Pulse Active Mean (APAM)

The term ‘Mean’ in APAM refers to an averaging process of the output pulses in each period and can be selected as feature vector. Mathematically, APAM can be presented as:

$$x(m) = \frac{m_f}{T_{P2R}} \int_{\frac{(m-1)T_{P2R}}{m_f}}^{\frac{mT_{P2R}}{m_f}} o(t) dt \quad (5-40)$$

$$x(m + m_f) = \frac{m_f}{T_{R2T}} \int_{\frac{(m-1)T_{R2T}}{m_f}}^{\frac{m}{m_f}T_{R2T}} o(t) dt \quad (5-41)$$

for $m = 1, 2, \dots, m_f$

Following the similar derivation to APAA, the mathematical expression of APAM can be written as:

$$x_{P2R}(m) = \frac{m_f}{T_{P2R}} (t_{P2R[2m]} - t_{P2R[2m-1]}) (O_{\max} - O_{\min}) + O_{\min} \quad (5-42)$$

$$x(m + m_f) = \frac{T_{R2T}}{m_f} (t_{R2T[2m]} - t_{R2T[2m-1]}) (O_{\max} - O_{\min}) + O_{\min} \quad (5-43)$$

for $m = 1, 2, \dots, m_f$

Similar as in (5-38) and (5-39) to ensure the ECG characteristics embedded within (5-30) and (5-31) are always taken in to consideration during generating the APAM feature vectors, O_{\max} should not be set equal to O_{\min} .

5.4.5. Adaptive Pulse Active Harmonic (APAH)

Adaptive Pulse Active Harmonic (APAH) make used the harmonic coefficient of the output pulses as features similar like the Pulse Active Harmonic described in subsection 4.6.5. The transition state vectors as in (5-30) and (5-31) are then transformed to radians as follows:

$$\omega_{P[2m-1]} = \frac{m_f t_{P[2m-1]} - (m-1)T_P}{T_P} \times 2\pi \quad (5-44)$$

$$\omega_{P[2m]} = \frac{m_f t_{P[2m]} - (m-1)T_P}{T_P} \times 2\pi \quad (5-45)$$

for $m=1,2,3\dots m_f$ and $P=P2R$ or $R2T$. This forms the output pulse waveform $o(\omega)$ as illustrated in Figure 5-9.

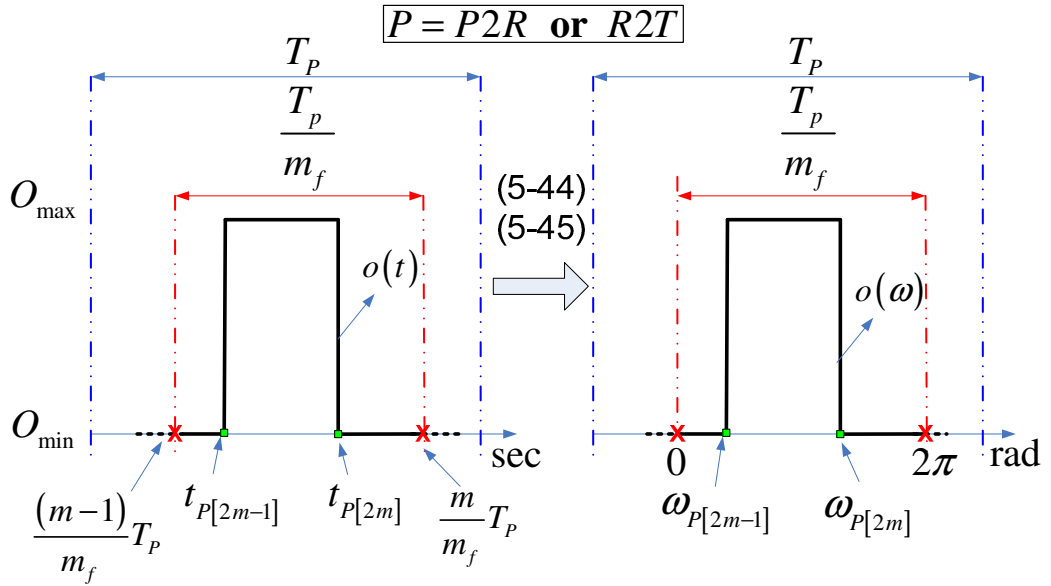


Figure 5-9 : Waveform generation of Adaptive Pulse Active Harmonic

The radian transform vector \mathbf{W} are then defined as

$$\begin{bmatrix} \mathbf{W}(2m-1) \\ \mathbf{W}(2m) \end{bmatrix} = \begin{bmatrix} \omega_{P2R[2m-1]} \\ \omega_{P2R[2m]} \end{bmatrix} \quad (5-46)$$

$$\begin{bmatrix} \mathbf{W}(2m-1+2m_f) \\ \mathbf{W}(2m+2m_f) \end{bmatrix} = \begin{bmatrix} \omega_{R2T[2m-1]} \\ \omega_{R2T[2m]} \end{bmatrix} \quad (5-47)$$

for $m=1,2,3\dots m_f$

Following the similar procedure as listed in (4-19) to (4-27), the final APAH equation can be written as:

$$A(n) = \frac{1}{n\pi} \left(\sum_{k=1}^{2m_f} [\sin(n \cdot \mathbf{W}(2k)) - \sin(n \cdot \mathbf{W}(2k-1))] \right) \quad (5-48)$$

$$B(n) = \frac{1}{n\pi} \left(\sum_{k=1}^{2m_f} [\cos(n \cdot \mathbf{W}(2k-1)) - \cos(n \cdot \mathbf{W}(2k))] \right) \quad (5-49)$$

Table 5-1: Summary of 5 Adaptive Pulse Active Feature Selection Technique

Name	Criteria	Equation
Adaptive Pulse Active Bit (APAB)	Intersection locations between generated triangular wave and DC line	$\mathbf{X} = \begin{bmatrix} t_{P2R[1]} & t_{P2R[2]} & \dots & t_{P2R[m]} & \dots & t_{P2R[2m_f]} \\ t_{R2T[1]} & t_{R2T[2]} & \dots & t_{R2T[m]} & \dots & t_{R2T[2m_f]} \end{bmatrix}$ <p>for $m = 1, 2, 3 \dots 2m_f$.</p>
Adaptive Pulse Active Width (APAW)	Difference between two contiguous points of the intersection locations	$\mathbf{X} = \begin{bmatrix} x_{P2R}(1) & x_{P2R}(2) & \dots & x_{P2R}(m) & \dots & x_{P2R}(m_f) & x_{R2T}(m_f + 1) \\ & & & & & & x_{R2T}(m_f + 2) & \dots & x_{R2T}(m_f + m) & \dots & x_{R2T}(2m_f) \end{bmatrix}$ <p>with</p> $x_{P2R}(m) = t_{P2R[2m]} - t_{P2R[2m-1]}$ $x_{R2T}(m + m_f) = t_{R2T[2m]} - t_{R2T[2m-1]}$
Adaptive Pulse Active Area (APAA)	The output area of each pulse	$\mathbf{X} = \begin{bmatrix} x_{P2R}(1) & x_{P2R}(2) & \dots & x_{P2R}(m) & \dots & x_{P2R}(m_f) & x_{R2T}(m_f + 1) \\ & & & & & & x_{R2T}(m_f + 2) & \dots & x_{R2T}(m_f + m) & \dots & x_{R2T}(2m_f) \end{bmatrix}$ <p>with</p> $x_{P2R}(m) = (t_{P2R[2m]} - t_{P2R[2m-1]})(O_{\max} - O_{\min}) + O_{\min} \frac{T_{P2R}}{m_f}$ $x(m + m_f) = (t_{R2T[2m]} - t_{R2T[2m-1]})(O_{\max} - O_{\min}) + O_{\min} \frac{T_{R2T}}{m_f}$
Adaptive Pulse Active Mean (APAM)	The average value of each pulse	$\mathbf{X} = \begin{bmatrix} x_{P2R}(1) & x_{P2R}(2) & \dots & x_{P2R}(m) & \dots & x_{P2R}(m_f) & x_{R2T}(m_f + 1) \\ & & & & & & x_{R2T}(m_f + 2) & \dots & x_{R2T}(m_f + m) & \dots & x_{R2T}(2m_f) \end{bmatrix}$ <p>with</p> $x_{P2R}(m) = \frac{m_f}{T_{P2R}} (t_{P2R[2m]} - t_{P2R[2m-1]})(O_{\max} - O_{\min}) + O_{\min}$ $x(m + m_f) = \frac{T_{R2T}}{m_f} (t_{R2T[2m]} - t_{R2T[2m-1]})(O_{\max} - O_{\min}) + O_{\min}$
Adaptive Pulse Active Harmonic (APAH)	The total harmonic components of each pulse	$A(n) = \frac{1}{n\pi} \left(\sum_{k=1}^{2m_f} [\sin(n \cdot W(2k)) - \sin(n \cdot W(2k-1))] \right)$ $B(n) = \frac{1}{n\pi} \left(\sum_{k=1}^{2m_f} [\cos(n \cdot W(2k-1)) - \cos(n \cdot W(2k))] \right)$ $\mathbf{X} = \begin{bmatrix} A(n) & B(n) \end{bmatrix}$

for $m = 1, 2, 3 \dots m_f$ and $n = 1, 2, \dots, N$

$$\begin{bmatrix} X(n) \\ X(n+N) \end{bmatrix} = \begin{bmatrix} A(n) \\ B(n) \end{bmatrix} \quad (5-50)$$

for $n=1,2,\dots,N$. N is the total number of harmonics defined by the user which determines the dimension of the APAH feature vector. Table 5-1 summarizes the 5 APA general equations discussed in this section.

5.5. EXPERIMENTAL RESULTS

A simulation setup as described in section 4.7 is also used in this section to find the best T_{ECG} location, similarity measures technique and APA parameters for ECG biometric application.

5.5.1. Experiment 1: The optimum extraction location

As described in section, 4.4, there are 4 locations related to fiducial points commonly used to extract ECGs. These locations are the whole ECG complex (from starting point of P wave to the ending point of T wave), from peak to R to the next peak of R, within the QRS complex and between peaks of P and T. However, not all locations can be used for APA. The implementation of APA for ECG biometric authentication requires the ECG signals to be separated at the peak of R to ensure the triangular wave is generated within the ECG envelopes as described in section 5.3. For this reason, investigation of the optimum extraction location in Experiment 1 only considers 3 extraction locations. In this experiment, APAW will be used to extract ECG features from the starting point of the P wave to the ending point of the T wave, within the QRS complex and between the peaks of P and T. Euclidean distance will be used as the similarity measure.

5.5.1.1. T_{ECG} between P_s and T_e

Figure 5-10 shows the AUR and EER profile of the ECG APAW biometric system for various m_f and δ_i setting when T_{ECG} is selected from the starting point of the P wave, P_s , to the end of the T wave, T_e for both healthy and arrhythmia populations. Comparing AUR profile in Figures 5-10 (a) and (b) and the EER profile in Figures 5-10 (c) and (d), it is shown that the selection of δ_i generates an opposite profile between the healthy and arrhythmia population. This phenomenon may occur due to the abnormalities of the ECG signals for the arrhythmia population.

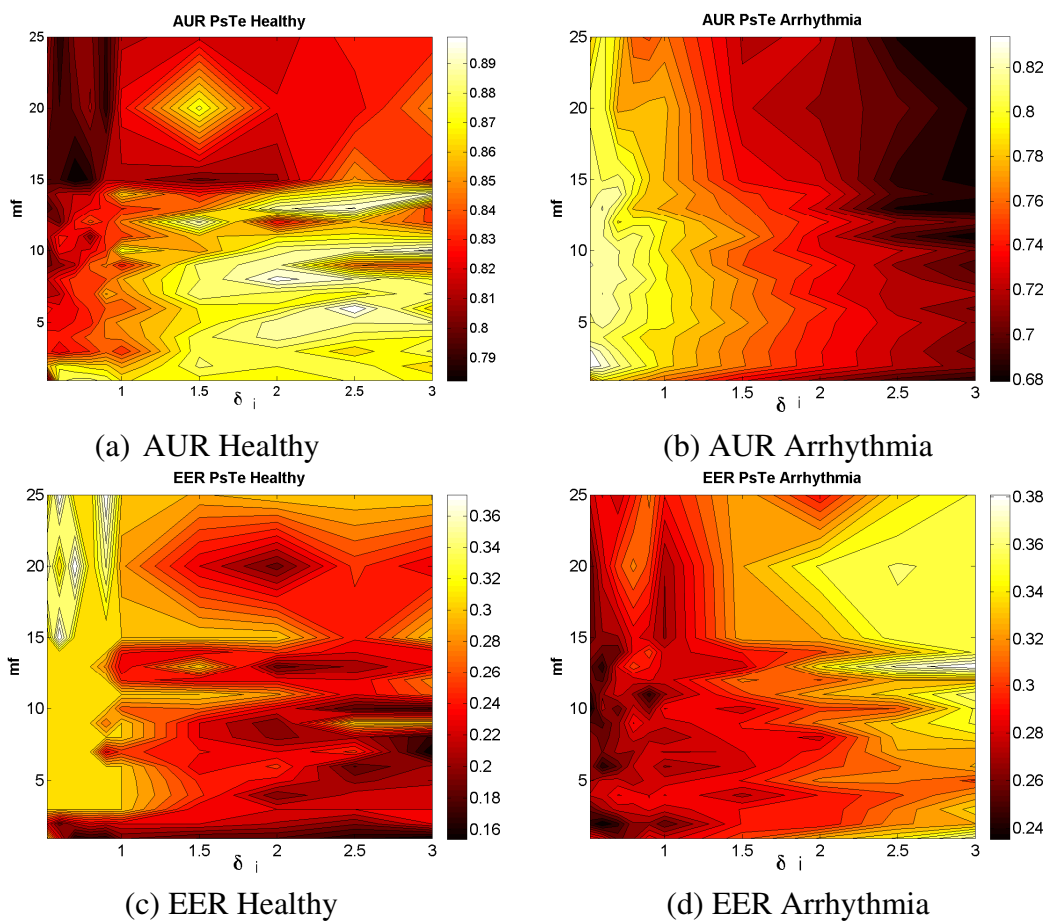


Figure 5-10 : APA profile for T_{ECG} from P_s to T_e

For the healthy population, it can be seen from Figures 5-10 (a) and (c) that the acceptable high AUR and low EER value are generated when m_f between 3 and 15 while δ_i is between 1.5 and 3. For the arrhythmia population, it can be seen from

Figures 5-10 (b) and (d) that the acceptable high AUR and low EER value are generated when m_f between 5 and 15 while δ_i is between 0.5 and 1. From this observation, it can be concluded that specific range of m_f and δ_i which are applicable for both healthy and arrhythmia population is not available.

5.5.1.2. T_{ECG} between P and T

Figure 5-11 illustrates the AUR and EER profile for healthy and arrhythmia population when T_{ECG} is selected between the peak of the P wave, P and the T wave, T .

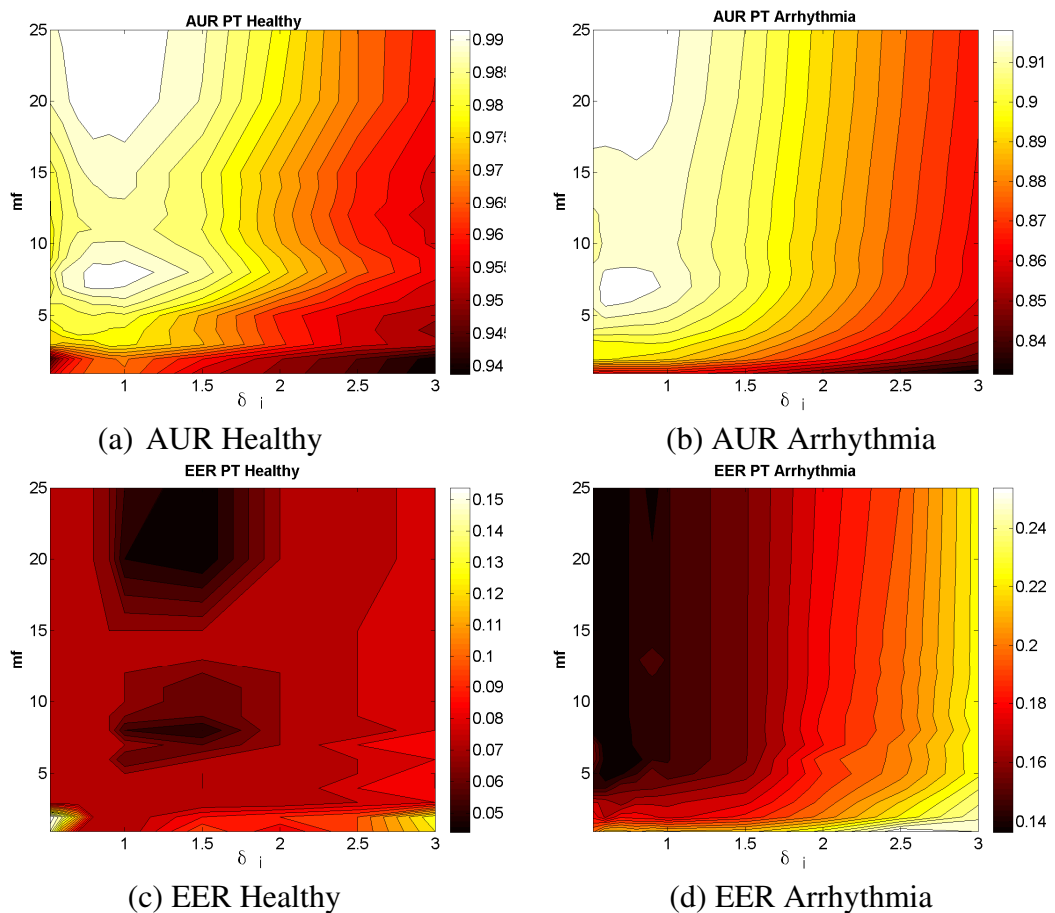


Figure 5-11 : APA profile for T_{ECG} from P to T

As can be seen from Figures 5-11 (a) and (b), the acceptable high AUR value can be obtained from the healthy and arrhythmia population when m_f is set greater than 6

while δ_i is between 0.5 and 1.5. The EER profile for healthy and arrhythmia population as shown in Figure 5-11 (c) and (d) indicates that an acceptable low value can be obtained when m_f is set greater than 6 for both population while δ_i is from 1 to 2 for the healthy population and between 0.5 and 1 for the arrhythmia population.

5.5.1.3. T_{ECG} within QRS complex

Figure 5-12 shows the AUR and EER profile for healthy and arrhythmia population when T_{ECG} is selected within QRS complex.

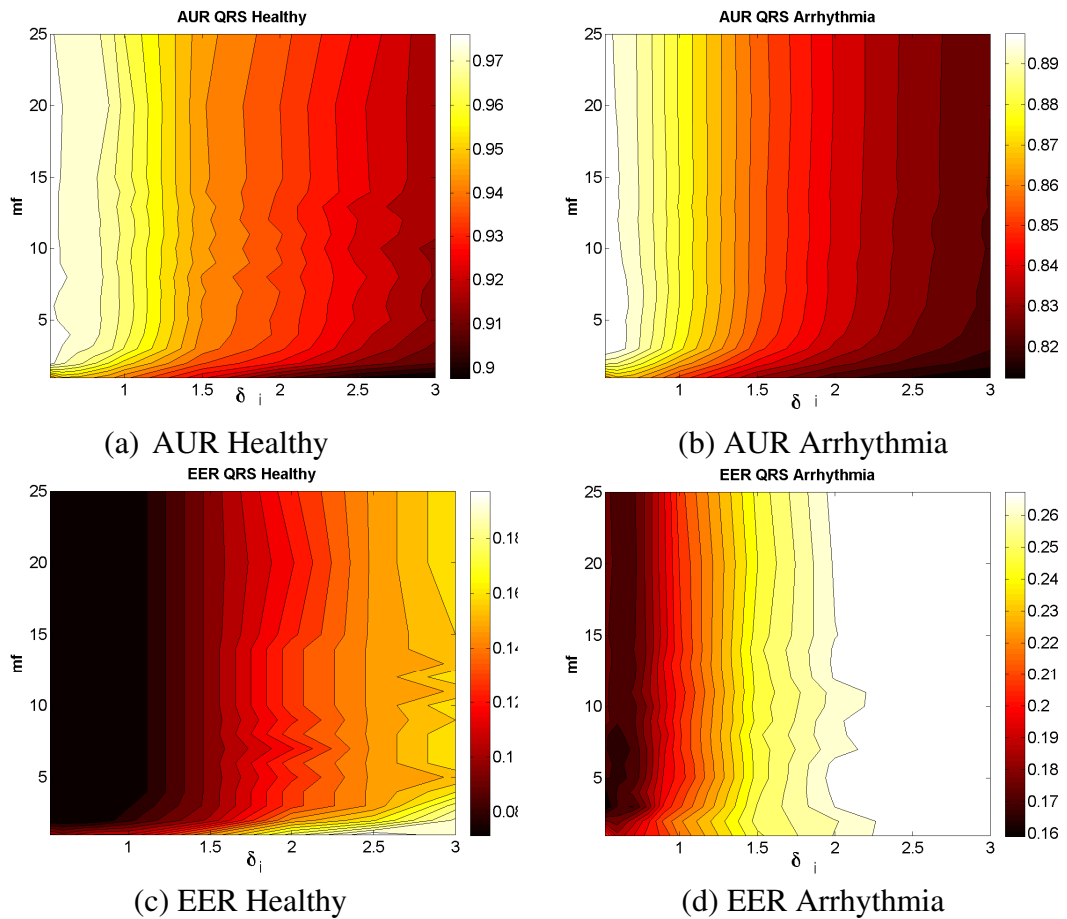


Figure 5-12 : APA profile for T_{ECG} within QRS

As can be seen from Figure 5-12, a high value of AUR and low value of EER are obtained for healthy and arrhythmia subjects when m_f greater than 3 while δ_i is between 0.5 and 1.

5.5.1.4. Summary of T_{ECG} selection using APA

Tables 5-2 and 5-3 tabulate the summary of AUR and EER performances respectively on different T_{ECG} using APA.

Table 5-2: Summary of AUR performances on different T_{ECG} using APA

T_{ECG}	Population	Optimum m_f range	Optimum δ_i range	Maximum AUR	AUR Ranges
P_s T_e	Healthy	$3 \leq m_f \leq 15$	$1.5 \leq \delta_i \leq 3$	0.9	0.12
	Arrhythmia	$5 \leq m_f \leq 15$	$0.5 \leq \delta_i \leq 1$	0.84	0.16
PT	Healthy	$m_f \geq 6$	$0.5 \leq \delta_i \leq 1.5$	0.99	0.05
	Arrhythmia	$m_f \geq 6$	$0.5 \leq \delta_i \leq 1.5$	0.92	0.1
QRS	Healthy	$m_f \geq 3$	$0.5 \leq \delta_i \leq 1$	0.975	0.075
	Arrhythmia	$m_f \geq 3$	$0.5 \leq \delta_i \leq 1$	0.9	0.09

Table 5-3 : Summary of EER performances on different T_{ECG} using APA

T_{ECG}	Population	Optimum m_f range	Optimum δ_i range	Minimum EER	EER Ranges
P_s T_e	Healthy	$3 \leq m_f \leq 15$	$1.5 \leq \delta_i \leq 3$	0.155	0.21
	Arrhythmia	$5 \leq m_f \leq 15$	$0.5 \leq \delta_i \leq 1$	0.24	0.14
PT	Healthy	$m_f \geq 6$	$1 \leq \delta_i \leq 2$	0.04	0.12
	Arrhythmia	$m_f \geq 6$	$0.5 \leq \delta_i \leq 1$	0.14	0.12
QRS	Healthy	$m_f \geq 3$	$0.5 \leq \delta_i \leq 1$	0.07	0.12
	Arrhythmia	$m_f \geq 3$	$0.5 \leq \delta_i \leq 1$	0.16	0.12

Notice that the optimum range selected from the statistically reliable arrhythmia population contains the range of the healthy subjects as a subset. As can be seen from these tables, the maximum AUR with minimum EER values are obtained when T_{ECG} is selected between the peaks of P and T, followed by the QRS locations and then

from P_s to T_e . It can be concluded from this evaluation that APA would generate a better discriminative performance when the ECG is extracted between the peaks of P and T. This location will be used for the rest of the chapters.

5.5.2. Experiment 2 : The optimum algorithms

In Experiment 2 described in this section, the performance of all APA feature selection techniques as explained in section 5.4 are compared with Biel *et al* [68] , Israel *et al* [70] and PA feature selection techniques described in section 4.6. For all PA feature selection techniques, PA parameters namely m_f , m_i , O_{\max} , O_{\min} and N are set to 35, 1.5, 10, -2 and 7 respectively. Meanwhile the APA parameters, namely m_f , δ_i , O_{\max} , O_{\min} and N , are set as 8, 0.8, 10, -2 and 7 respectively. From evaluation in section 5.5.1 T_{ECG} is best selected between the peak of P and the peak of T. Euclidean distance is used as the similarity measures in this experiment.

Figures 5-13 and 5-14 illustrates the ROC comparison for healthy and arrhythmia populations. As can be seen from both figures, the ROC curves trajectories for APAW, APAA and APAM were higher than the rest of feature selection techniques investigated in this section. It is not visibly clear which of these three APA feature selection technique is the best, and comparison can only be made by using the AUR and EER values as tabulated in Table 5-4.

It is also observed in Figures 5-13 and 5-14 that the ROC profile for APAB and APAH is projected lower than for all the PA and the rest of the APA feature selection techniques. By including Biel and Israel features, APAH generate the worst ROC performance.

The AUR and EER values in Table 5-4 indicate that for healthy population, APAW generates the highest AUR and the lowest EER with values of 0.9929 and 0.0714 respectively. For arrhythmia populations, APAM generates the highest AUR and the

lowest AUR with values of 0.9278 and 0.1364 respectively. Comparing all feature extraction techniques, APAH has the poorest authentication performance and generates the lowest AUR with the highest EER.

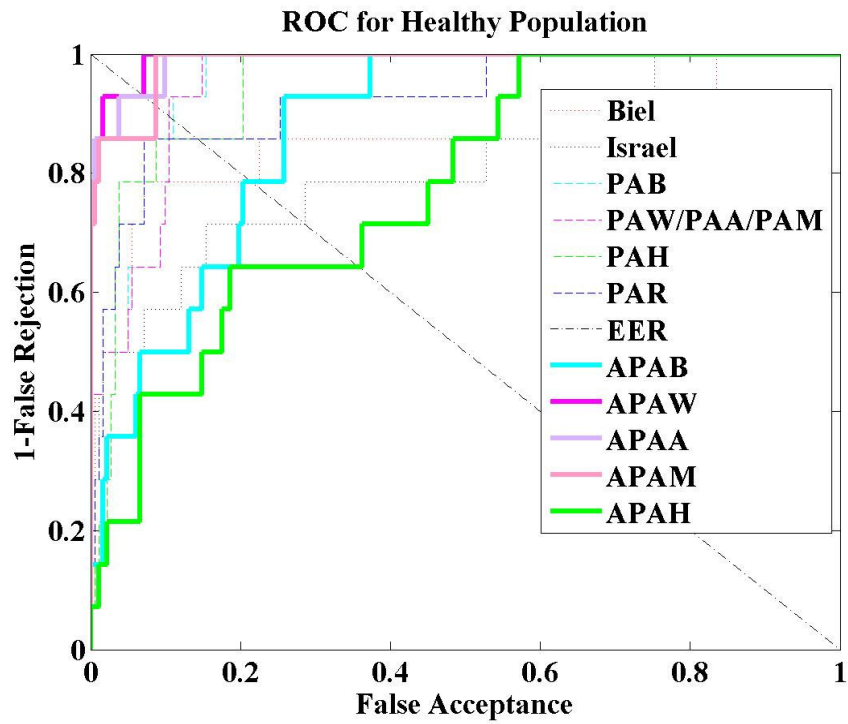


Figure 5-13 : APA ROC comparison for Healthy Population

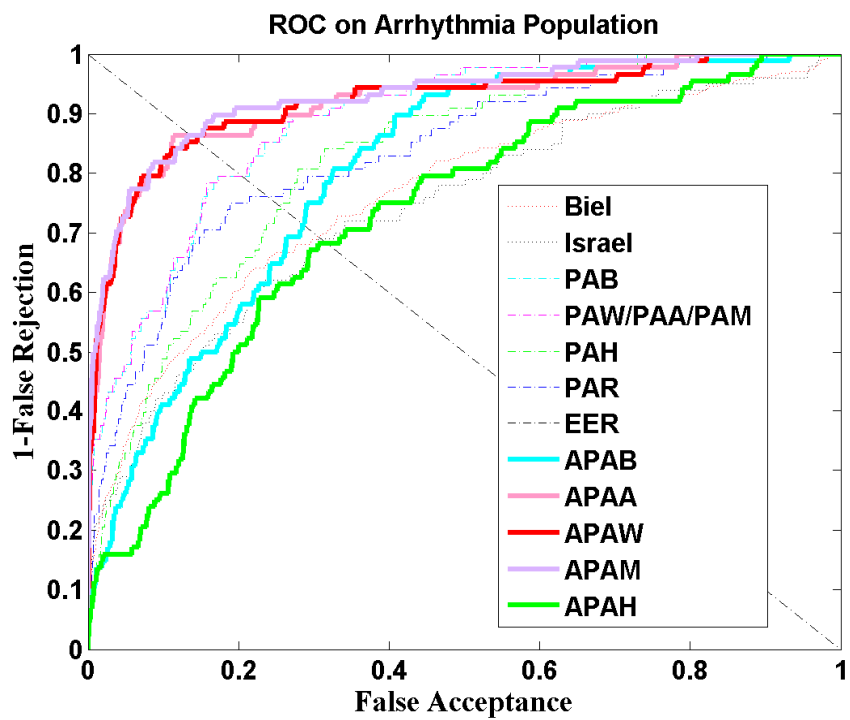


Figure 5-14 : APA ROC comparison for Arrhythmia Population

Table 5-4: APA AUR and EER values for Healthy and Arrhythmia Populations

	Healthy Population		Arrhythmia Population	
	AUR	EER	AUR	EER
Biel	0.8544	0.2143	0.7630	0.3047
Israel	0.8136	0.2857	0.7420	0.3101
PAB	0.9517	0.1099	0.8864	0.2045
PAW/PAA/PAM	0.9521	0.1044	0.8873	0.2045
PAH	0.9454	0.1429	0.8243	0.2561
PAR	0.9239	0.1429	0.8330	0.2386
APAB	0.8748	0.2198	0.8023	0.2853
APAW	0.9929	0.0714	0.9188	0.1455
APAA	0.9898	0.0714	0.9179	0.1364
APAM	0.9863	0.0879	0.9278	0.1364
APAH	0.7747	0.3571	0.7280	0.3183

The APA feature extraction technique extracts information from the generated triangular waves. Compared to the PA, the triangular wave generated using APA appears to exhibit a unique representation of the investigated signal.

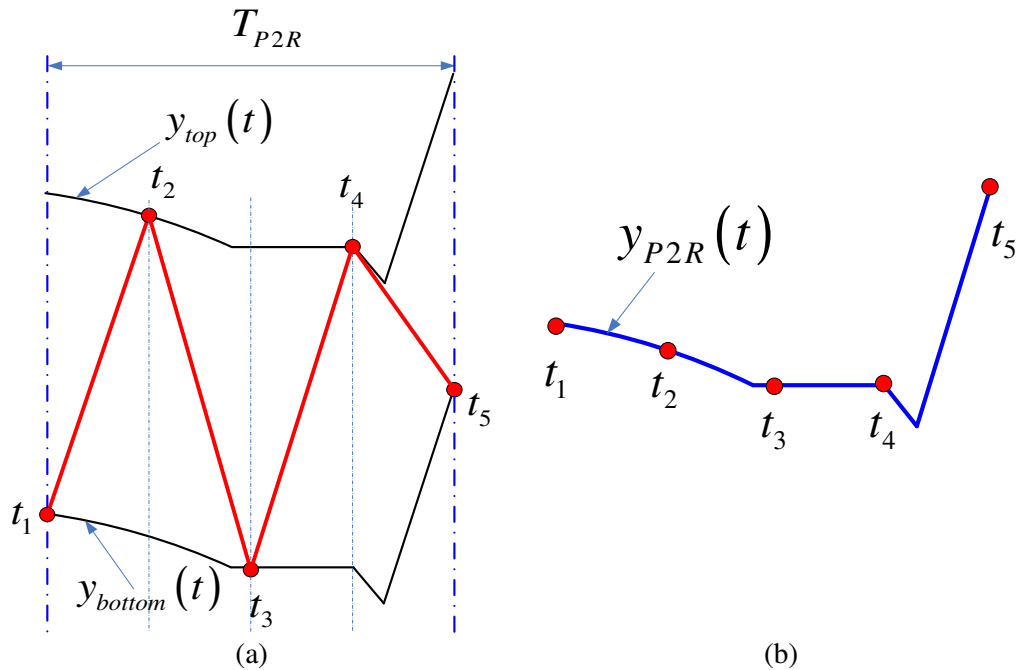


Figure 5-15: APA feature extraction phenomenon

$y_{top}(t)$ and $y_{bottom}(t)$ in Figure 5-15 (a) are the ECG envelopes ECG signal from peak P to R, $y_{P2R}(t)$ of Figure 5-15 (b). In Figure 5-15 (a), the location vectors t_1 to t_5 are similar unique points of the original signal $y_{P2R}(t)$ as presented in Figure 5-15 (b). When features are intended to be extracted between location vectors, for example between t_1 and t_2 in Figure 5-15 (b), APA transforms the original information between these two points into a straight line (in this example becomes a positive slope of the triangular waves) as shown in Figure 5-15 (a). The use of a DC line to intersect the transformed straight lines in the next APA procedure represents an extraction process of a unique characteristic between the two locations. Thus, information between two contiguous location vectors is finally transformed into a single value. In order to accurately characterize a signal, feature selection process between three contiguous locations give a better representation of the investigated signal compared to only using two contiguous locations. This conclusion is based on

a low performance of APAB and APAH profile shown in Table 5-4 whereby the feature vector which represents the investigated signal comes from features selected between two contiguous points at a time. However, when three contiguous locations are considered at a time, a more accurate signature is extracted. This is reflected by the good performance of APAW, APAA and APAM shown in Table 5-4.

5.5.3. Experiment 3 : The optimum similarity measure

Subsection 5.5.1 and 5.5.2 respectively concludes that T_{ECG} is best selected between the peaks of P and T and APAW is the best feature selection technique. Experiment 3 in this subsection will next investigate the best distance measure to be used with APA similar as carried out in section 4.8.3 . The APAW parameters namely m_f and δ_i are set to be 20 and 0.8 respectively. Figures 5-16 and 5-17 illustrate the comparison performance for healthy and arrhythmia population respectively using various distance based similarity measure.

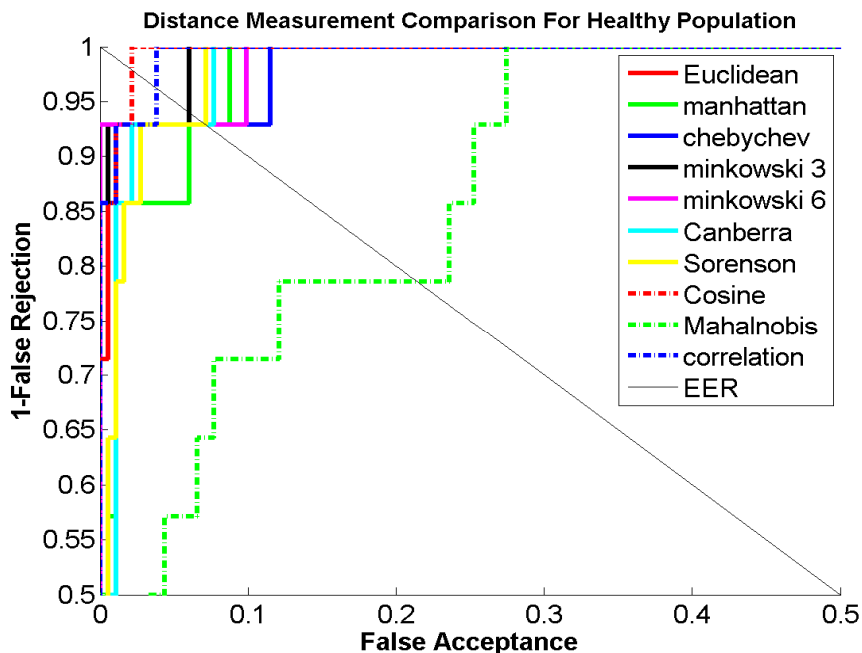


Figure 5-16 : APA distance measurement comparison for healthy population

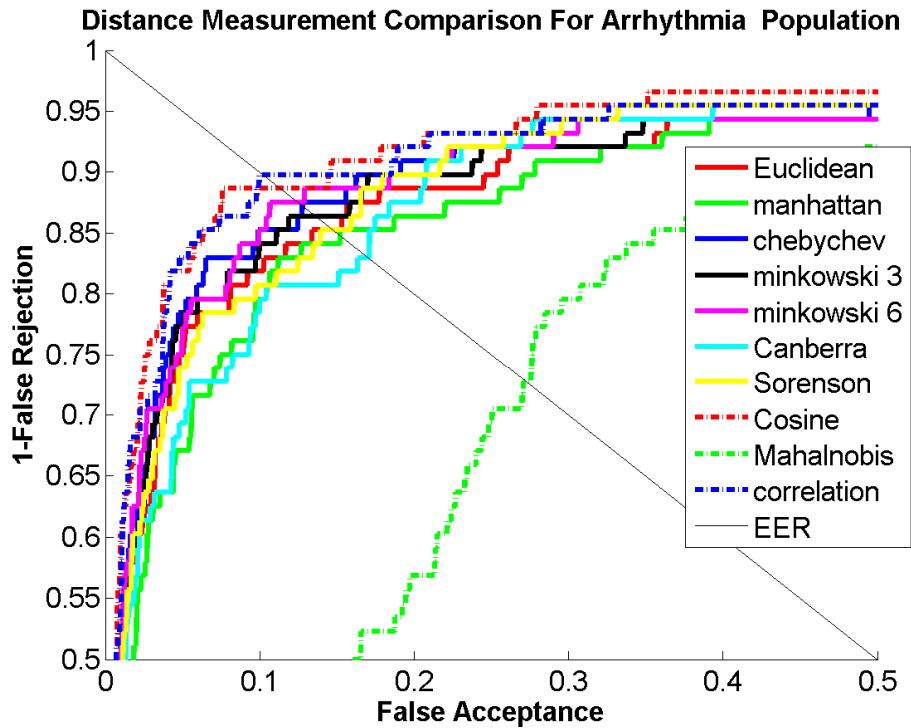


Figure 5-17 : APA distance measurement comparison for Arrhythmia population

As can be seen from these figures, the ROC curve for most of the similarity measures are very closed to each other except Mahalanobis distance measure. It can be seen from these figures that 2 of the highest ROC curve projections are achieved when the distance measurement are using the Cosine and Correlation distance measure methods. Thus, analytical comparison to determine the best similarity measure between these two cannot be determined from the graph and can only be compared using their AUR and EER profile tabulated in Table 5-5.

Table 5-5: APA profile using different distance measure

Distance		Healthy Population		Arrhythmia Population	
Name	Equation	AUR	EER	AUR	EER
Euclidean	(2.1)	0.9933	0.0714	0.9201	0.1477
Manhattan	(2.2)	0.9855	0.0714	0.9112	0.1520
Chebyshev	(2.3)	0.9918	0.0714	0.9265	0.1276
Minkowski p=3	(2.4)	0.9953	0.0604	0.9232	0.1364
Minkowski p=6	(2.4)	0.9929	0.0714	0.9253	0.1250
Canberra	(2.5)	0.9886	0.0714	0.9216	0.1705
Sorensen	(2.6)	0.9886	0.0714	0.9292	0.1477
Cosine	(2.7)	0.9969	0.0220	0.9432	0.1138
Mahalanobis	(2.8)	0.9141	0.2198	0.8021	0.2727
Correlation	(2.9)	0.9965	0.0385	0.9378	0.1024

From Table 5-5, it is shown that the Cosine distance measure provides the highest AUR and lowest EER values for healthy population. For arrhythmia populations, Cosine distance measure generates the highest AUR values while correlation distance measure generates the lowest EER values. Based on these results, the Cosine distance measure would be used to obtain the ROC curves throughout this chapter.

5.5.4. Experiment 4 : Optimized APA parameters

Results indicating APAW as the best feature selection technique as shown in subsection 5.5.2 are based from a preset value. Experiment 4 presented in this subsection investigates the biometric performances for all APA feature selection methods are evaluated using various values of m_f , δ_i , O_{\max} , O_{\min} and/or N .

5.5.4.1. Effect of varying m_f and δ_i

The first two parameters that would be investigated in this subsection are the m_f and δ_i . O_{\max} , O_{\min} and N are respectively set to be 1, 0 and 7. All APA feature selection technique requires the information from these two variables.

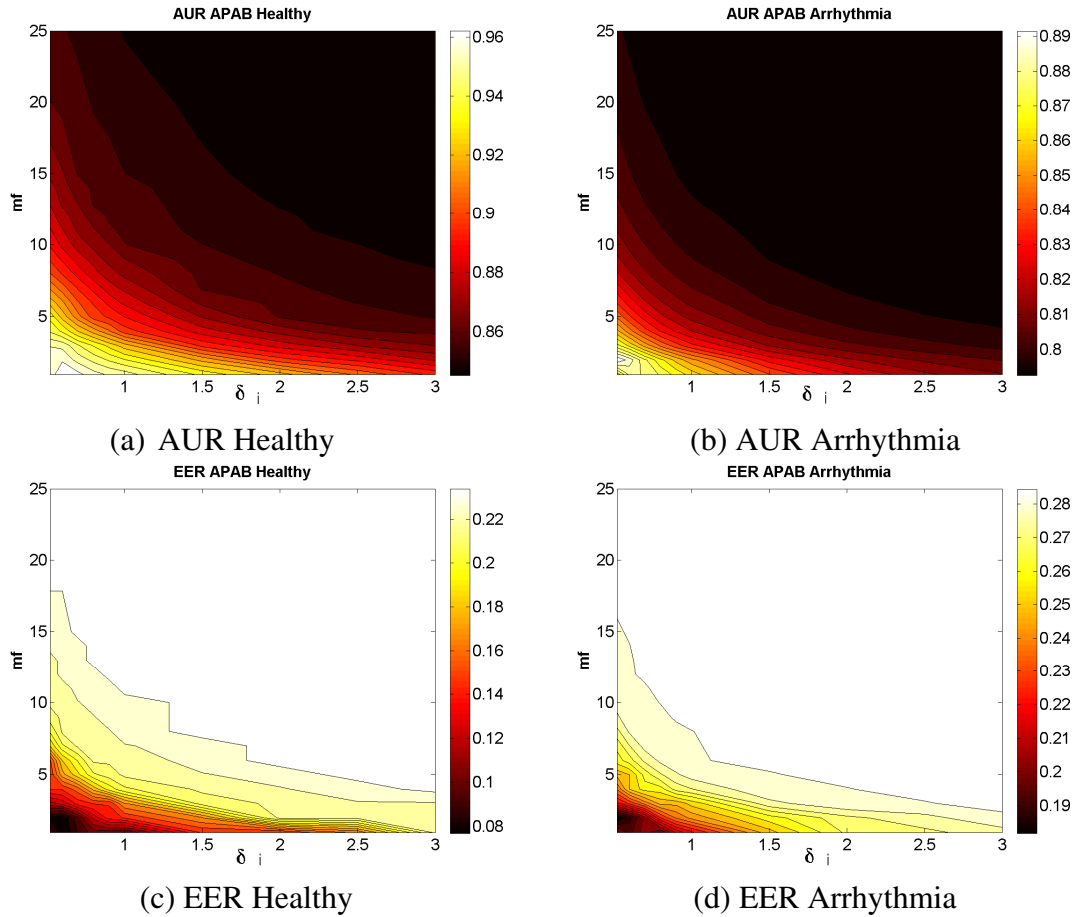


Figure 5-18 : APAB profile when m_f and δ_i varies

Figure 5-18 illustrates the AUR and EER profile for healthy and arrhythmia population when δ_i and m_f parameters varies using APAB. From this figure, it indicates that a higher AUR and lower EER are obtained with a low settings of δ_i and m_f . As the value of δ_i and m_f increases, the authentication performance is decreased.

Figure 5-19 illustrates the AUR and EER profile for healthy and arrhythmia population when δ_i and m_f parameters varies using APAW.

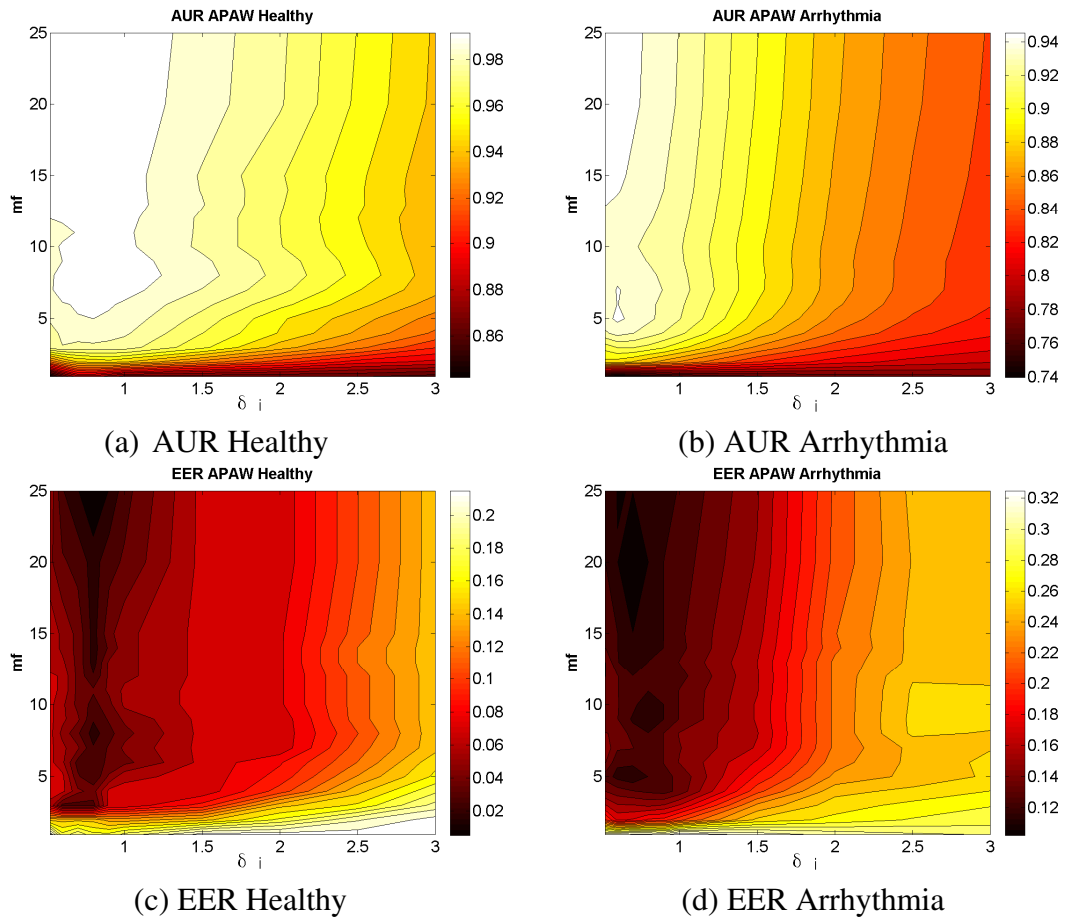


Figure 5-19 : APAW profile when m_f and δ_i varies

For healthy population as shown in Figures 5-19 (a) and (c), a high AUR and low EER can be obtained by setting m_f greater than 3 and δ_i between 0.5 and 1.5. For the arrhythmia population as shown in Figures 5-19 (b) and (d), a high AUR and low EER can be obtained by setting m_f greater than 3 and δ_i from 0.5 to 1.

Figure 5-20 shows the AUR and EER profile for healthy and arrhythmia population when δ_i and m_f parameters varies using APAA.

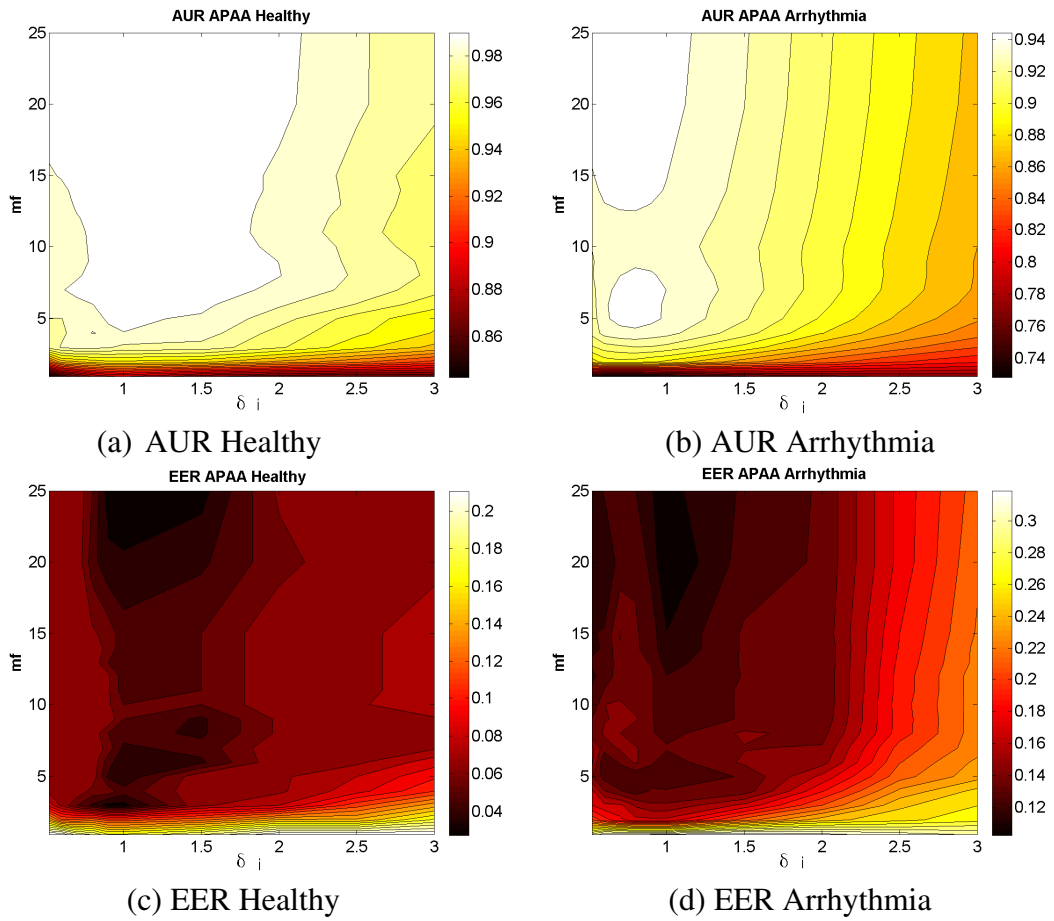


Figure 5-20 : APAA profile when m_f and δ_i varies

For healthy population as shown in Figures 5-20 (a) and (c), a high AUR and low EER can be obtained by setting m_f greater than 3 and δ_i between 0.5 and 2. For the arrhythmia population as shown in Figures 5-20 (b) and (d), a high AUR and low EER can be obtained by setting m_f greater than 5 and δ_i from 0.5 to 1.5.

Figure 5-21 shows the AUR and EER profile for healthy and arrhythmia population when δ_i and m_f parameters varies using APAM.

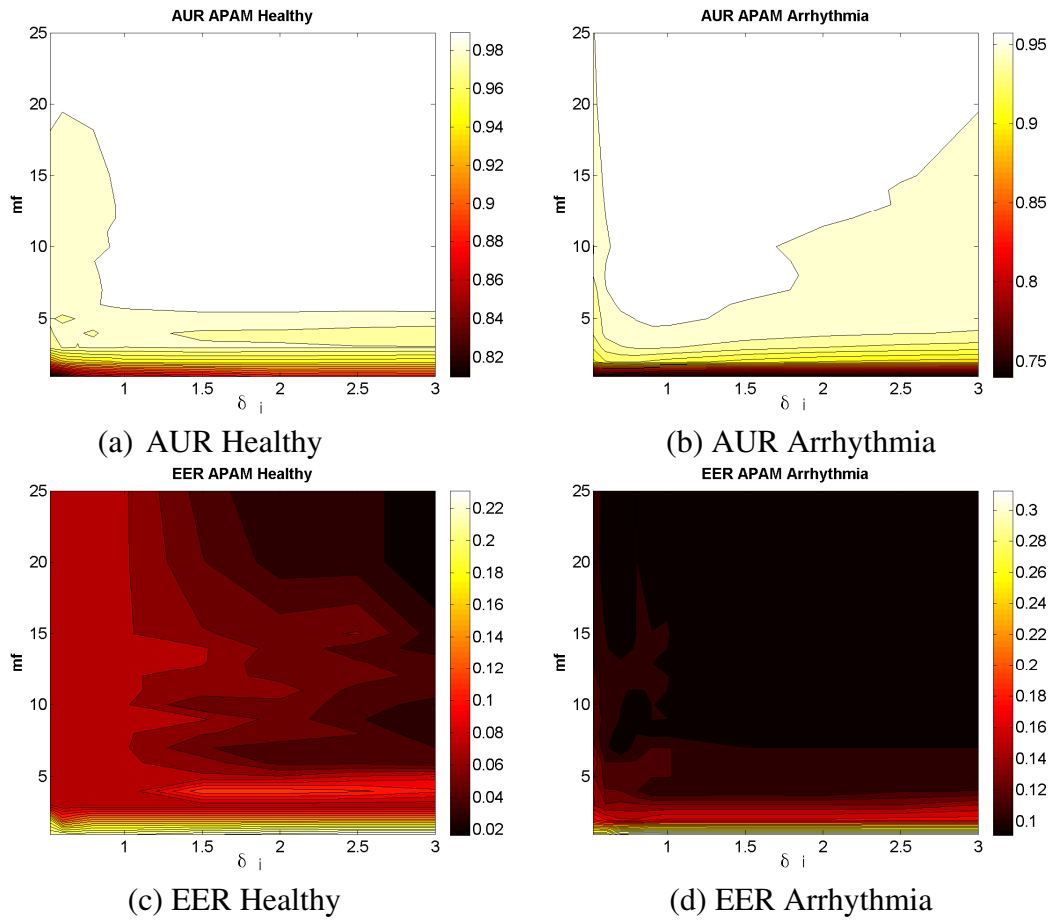


Figure 5-21 : APAM Profile when m_f and δ_i varies

Figures 5-21 (a) and (c) indicates that a high AUR and low EER for healthy population can be obtained when m_f greater than 3 and δ_i greater than 1. In Figures 5-21 (b) and (d), a high AUR and low EER for arrhythmia population can be obtained when m_f greater than 3 and δ_i greater than 0.5.

Figure 5-22 illustrates the AUR and EER profile for healthy and arrhythmia population when δ_i and m_f parameters varies using APAH.

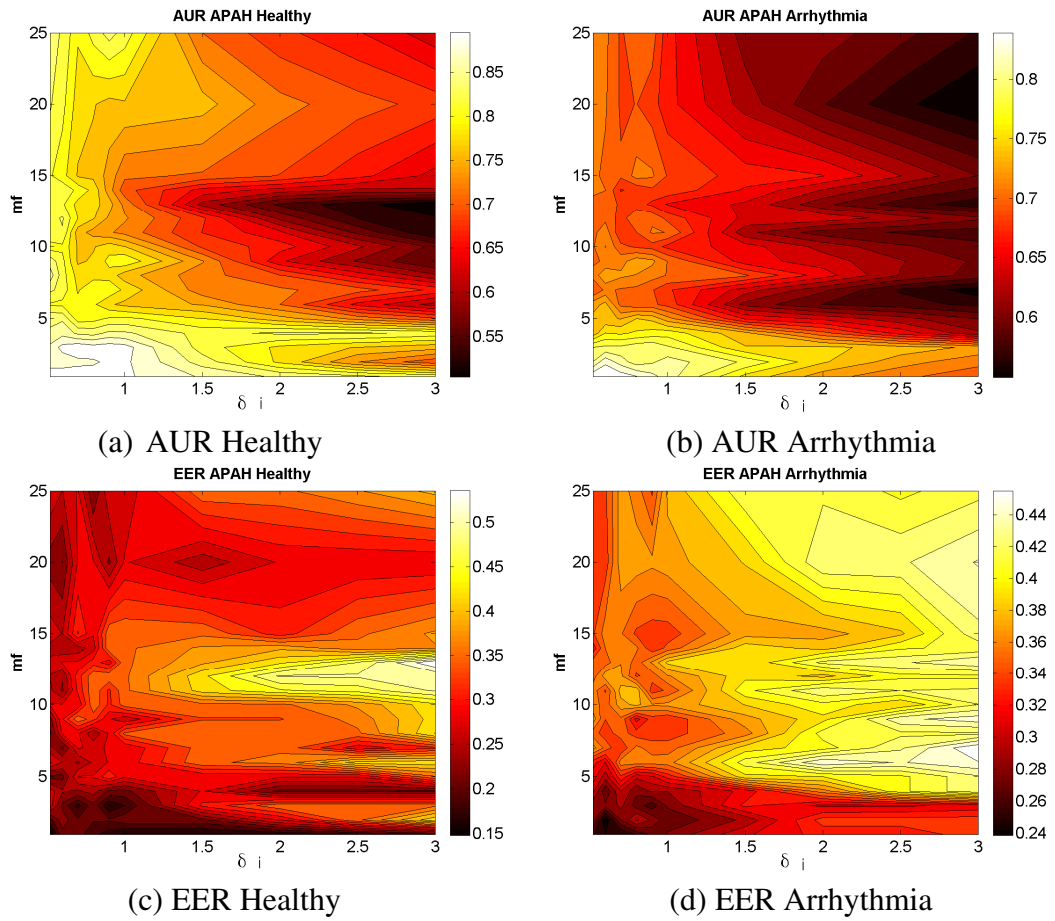


Figure 5-22 : APAH profile when m_f and δ_i varies

From this figure, it is observed that that a higher AUR and lower EER for both healthy and arrhythmia population are obtained with a low settings of δ_i and m_f .

5.5.4.2. Effect of varying O_{max} and O_{min} .

The next two variables that would be investigated in this subsection are the O_{max} and O_{min} . Other variables such as m_f and δ_i are set to be 7 and 0.8 respectively. Figure 5-23 illustrates the AUR and EER profile for healthy and arrhythmia population when O_{max} and O_{min} parameters varies using APAA.

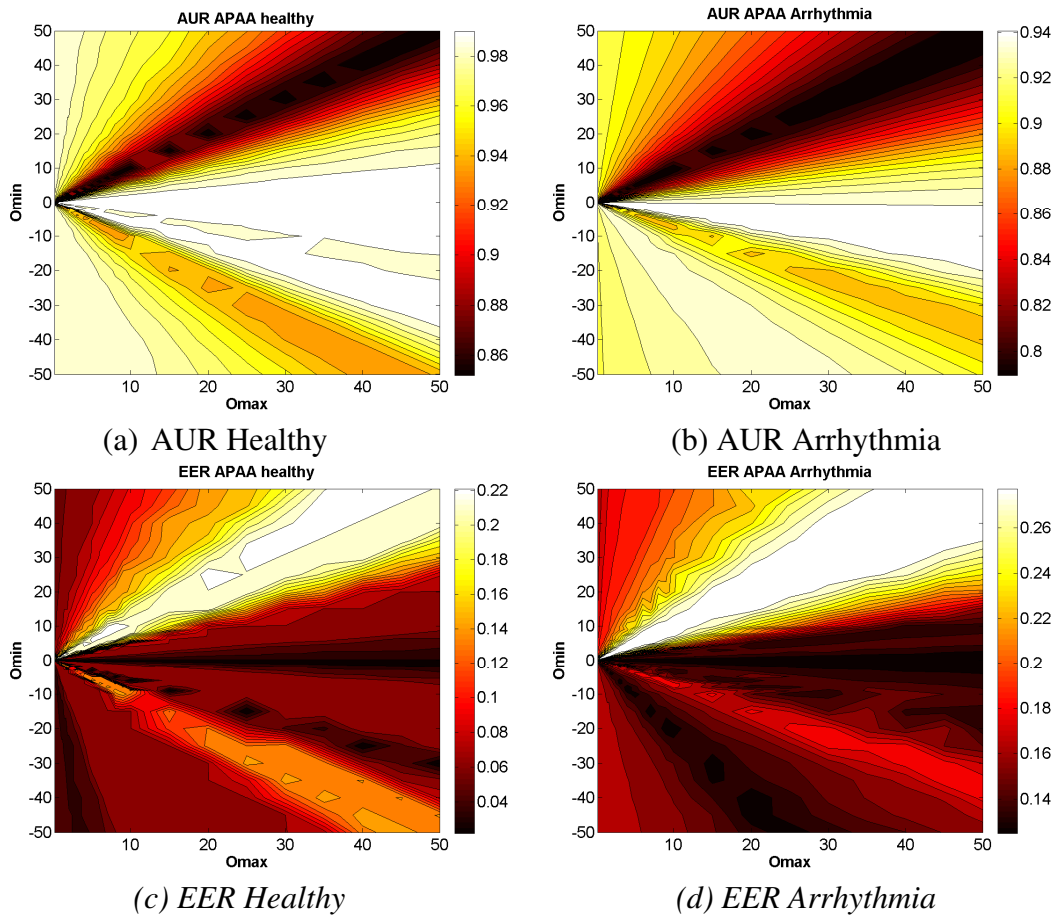


Figure 5-23: APAA profile when O_{max} and O_{min} vary

As can be seen from all figures in Figure 5-23 the high AUR and low EER values is obtained for any value of O_{max} greater than 0 while setting O_{min} to be zero.

Figure 5-24 shows the AUR and EER profile for healthy and arrhythmia population when O_{max} and O_{min} parameters varies using APAM. Based from all figures shown in Figure 5-24, the high AUR and low EER values is obtained for any value of O_{max} greater than 0 while setting O_{min} to be zero.

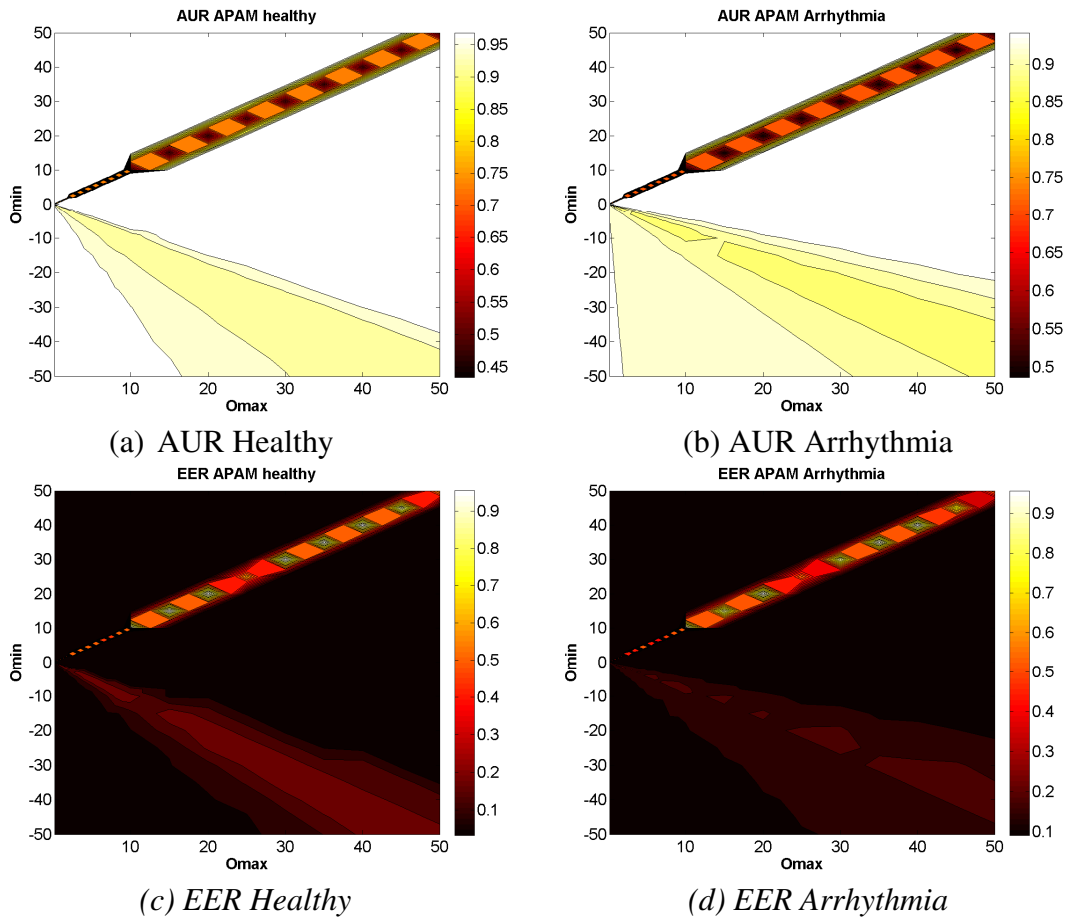


Figure 5-24: APAM profile when O_{max} and O_{min} vary

5.5.4.3. *Effect of varying N .*

The final variable that would be investigated in this subsection is the effect of changing the total harmonic values, N for APAH. The AUR and EER profile for healthy and arrhythmia population when N varies are shown in Figure 5-25. Figures 5-25 a) and (c) illustrate the AUR and EER profile for healthy population. As can be seen from these figures, when N is greater than 10, AUR is greater than 0.85 while EER is less than 0.2. The AUR and EER profile for arrhythmia population is respectively shown in Figures 5-25 (b) and (d). From these figures, it is observed that when N is greater than 15, AUR is greater than 0.75 while EER is less than 0.3.

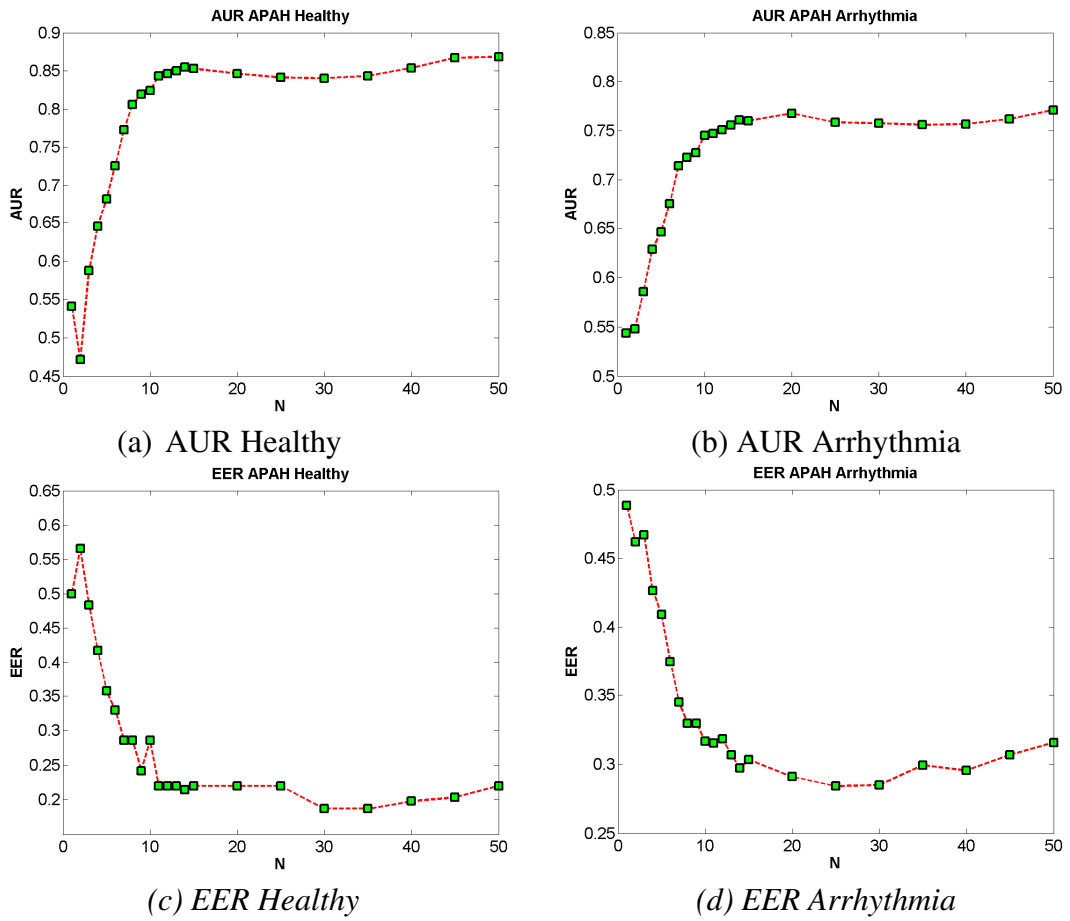


Figure 5-25 : APAH when N varies

5.5.4.4. Summary of APA optimization study

The performance for a non-biometric ECG data set using 58 healthy subjects is shown in Appendix E where it is seen that the APAW still manages to generate ROC curves with a high AUR and low EER which are, respectively, equal to 0.948 and 0.1210.

In the applications of biometric authentication, the study conducted in subsections 5.5.4.1 to 5.5.4.3 suggested that different APA feature selection techniques react differently using specific ranges of APA parameters namely m_f , δ_i , O_{\max} , O_{\min} and N in terms of AUR and EER performance. For example, APAB and APAH performs better when both m_f and δ_i values are low. APAM on the other hand gives a better

authentication performance when both m_f and δ_i values are high. Despite of these observations, a common ranges of m_f and δ_i may be suggested for all APA feature selections technique as certain ranges generates almost similar performance in terms of AUR and EER as shown in Appendix D. From Appendix D, it is shown that a similar high AUR and low EER profile can be achieved using:

$$5 \leq m_f \leq 15 \quad (5-51)$$

$$0.6 \leq \delta_i \leq 1.5 \quad (5-52)$$

It also have been shown in this section that when O_{\max} is set greater than 0 while setting O_{\min} to be zero generates the best AUR and EER profile for APAA and APAM. In Appendix D, it is shown that similar AUR and EER profile for healthy and arrhythmia population are achieved using APAA and APAM when

$$O_{\min} = 0 \quad (5-53)$$

$$5 \leq O_{\max} \leq 25 \quad (5-54)$$

From subsection 5.5.4.3, it also have been shown that when N is greater than 15 both healthy and arrhythmia population generates a high AUR and EER values. In Appendix D, the AUR and EER profile when N is range greater than 15. From Appendix D, the maximum and minimum values of AUR and EER for healthy populations using these settings are tabulated in Table 5-6. The maximum and minimum values of AUR and EER for arrhythmia populations using these settings are tabulated in Table 5-7.

From Tables 5-6 and 5-7, it is observed that when APA parameters set as in (5-51) to (5-54), the AUR for APAA, APAA and APAM for healthy population are greater than 0.99 while for the arrhythmia population, the AUR is greater than 0.94.

Table 5-6 : AUR and EER profiles for healthy population using selected ranges of APA parameters

APA Feature Selection	AUR		EER	
	max	min	max	Min
APAB(m_f and δ_i varies)	0.92	0.85	0.24	0.175
APAW (m_f and δ_i varies)	0.996	0.974	0.07	0.02
APAA (m_f and δ_i varies)	0.996	0.982	0.07	0.03
APAM (m_f and δ_i varies)	0.994	0.978	0.07	0.05
APAH(m_f and δ_i varies)	0.85	0.6	0.42	0.22
APAA (O_{\max} and O_{\min} varies)	0.996	0.996	0.03	0.03
APAM (O_{\max} and O_{\min} varies)	0.993	0.993	0.07	0.07
APAH (N varies)	0.87	0.87	0.22	0.185

The EER for healthy and arrhythmia populations for APAW, APAA and APAM are respectively less than 0.05 and 0.1. APAB is then included in the comparison for healthy and arrhythmia population, it is observed that the AUR and EER varies ± 0.1 and ± 0.2 respectively between APAB, APAW, APAA and APAM. However, the performance of APAH is differ largely compare to the rest of APA feature selection technique

Table 5-7 : AUR and EER profiles for arrhythmia population using selected ranges of APA parameters

APA Feature Selection	AUR		EER	
	max	min	max	Min
APAB(m_f and δ_i varies)	0.835	0.795	0.29	0.255
APAW (m_f and δ_i varies)	0.945	0.89	0.2	0.11
APAA (m_f and δ_i varies)	0.945	0.92	0.145	0.115
APAM (m_f and δ_i varies)	0.965	0.95	0.12	0.09
APAH(m_f and δ_i varies)	0.62	0.74	0.42	0.3
APAA (O_{\max} and O_{\min} varies)	0.94	0.94	0.125	0.125
APAM (O_{\max} and O_{\min} varies)	0.963	0.963	0.115	0.115
APAH (N varies)	0.772	0.756	0.315	0.28

5.6. CONCLUSION

This chapter has presented a new feature extraction technique named Adaptive Pulse Active (APA). The chapter started by explaining the fundamental concept of APA feature extraction technique. Five different feature selection algorithms, namely APAB, APAW, APAA, APAM and APAH are derived from the APA concept. Various locations within the ECG, from where features can be extracted using APA, have also been examined in this chapter. In this chapter, the performance comparison for all APA feature selection algorithms is performed. The performance comparison also includes all PA feature selection algorithms described in chapter 4. To improve the biometric performance profile, the best distance similarity measure to be used with APA has also been investigated in this chapter. Finally, this chapter evaluated the optimum APA parameters and suggests acceptable ranges for these parameters to generate similar authentication performance. The next chapter will use a hybrid PA and APA methods to set up multilevel security system.

CHAPTER 6.

PA-APA ECG BASED MULTILEVEL SECURITY BIOMETRIC AUTHENTICATION SYSTEM

6.1. INTRODUCTION

The Pulse Active (PA) and Adaptive Pulse Active (APA) feature extraction techniques for ECG biometric authentication were explored extensively in chapters 4 and 5 respectively. In those chapters, it was shown that PA and APA parameters performed differently depending on their 5 user defined parameters. However, specific ranges of these parameters may generate similar AUR and EER performances. The suggested ranges for PA and APA parameters were provided in subsection 4.8.4.4 and 5.5.4.4 respectively. In this chapter, the PA and APA suggested parameters will be used to integrate the knowledge and biometric based security approached as explain in Table 2-1 into a new concept of multilevel security system. Based on this new concept of security system, PA and APA parameters will be designed to be a 4 digit PIN of the system which then used to generate unique ECG biometric features. Both PIN and ECG need to be correctly submitted to allow the system to pass.

This chapter started with an overview of PA and APA parameters ranges which produce a similar biometric performance. A similar biometric performance is important for the system to avoid every user to use the same PIN which generates the highest biometric performance. Next the PA-APA ECG based multilevel security biometric authentication system. The advantage of a PIN as the first level of security is then discussed. Then the simulation setup to verify the performance of the proposed system is then follows. Results and discussion are given next. Finally the conclusion of the proposed scheme is given by the end of the chapter.

6.2. PA and APA parameter ranges

It has been shown that when PA and APA are set within the ranges shown in Table 6-1, their AUR and EER profiles varies by up to ± 0.1 and ± 0.15 respectively.

Table 6-1: PA and APA parameter suggested range

Parameters	PA Ranges		APA Ranges	
	Maximum	Minimum	Maximum	Minimum
m_f	50	20	15	5
m_i	2.5	1.5	Not Available	
δ_i	Not Available		1.5	0.6
O_{\max}	$-0.4 \times O_{\min}$		25	5
O_{\min}	< 0		0	
N	20	2	≥ 15	

In this chapter, the PA and APA parameters listed in Table 6-1 will be used to set up the PA-APA ECG based multilevel security biometric authentication system. As mentioned previously, a total of 11 PA and APA algorithms are available to be used for ECG biometric authentication system as listed in Tables 4-1 and 5-1. To setup the proposed security system, only 10 of these algorithms which have the highest AUR

and lowest EER are used. They are the APAW, APAA, APAM, APAB, PAW, PAA, PAM, PAR, PAB and PAH.

6.3. MULTILEVEL SECURITY AUTHENTICATION SCHEME

The proposed PA-APA ECG based multilevel security biometric authentication system involves 3 steps [115, 120]:

- i. Insert card or token
- ii. Key in personal identification number (PIN)
- iii. Submit ECG for authentication

6.3.1. Insert card or token

A user is required first to insert a card or token to claim an identity in the security system. Next, the system will request the user to provide two security parameters. i.e. a PIN and an ECG signal.

6.3.2. Key in personal identification number (PIN)

This step is the first level of security whereby the user is required to key in a four digit PIN as shown in Figure 6-1. If the PIN inserted is the same as the PIN stored in the system, the first level of security is verified and the user can proceed to step 3.

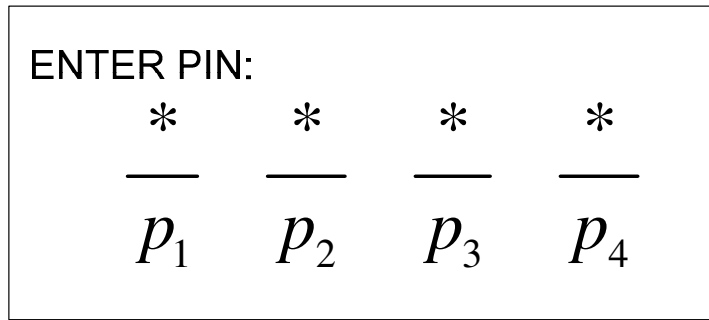


Figure 6-1 : Four digit biometric PIN

There are only 10 possible values for each digit which are 0 to 9. The proposed relationships between p_1 , p_2 , p_3 and p_4 with the PA and APA parameters are given in the following subsection.

6.3.2.1. The first digit p_1 .

This digit selects the specific PA or APA algorithms (either APAW, APAA, APAM, APAB, PAW, PAA, PAM, PAR, PAB or PAH) used to extract the ECG features. The substitution of the 10 digits that represents PA or APA algorithm is given in Table 6-2. Although these algorithms generate similar AUR and EER profiles, the values for each feature vector are different even though the values of PA or APA parameters are the same in all cases.

Table 6-2 : p_1 representation for PA and APA algorithms

p_1	Algorithm	p_1	Algorithm
0	APAA	1	APAM
2	APAW	3	APAB
4	PAB	5	PAW
6	PAA	7	PAM
8	PAR	9	PAH

The fact that the user is able to select the type of algorithm to extract the ECG features introduces added security safeguards giving the user 9 alternative procedures if one is ever compromised.

6.3.2.2. The second digit p_2 .

This digit is related to the value of m_f . From Table 6-1, it is observed that PA and APA have different ranges of m_f . The proposed relationship between p_2 and m_f depends on the selection value of p_1 . Furthermore, m_f is required to be an integer to ensure that a complete triangular period is generated. The relationship between p_2 and m_f is given as follows:

$$p_2 = \begin{cases} m_f - 5 & \text{if } p_1 \leq 3 \\ \frac{1}{3}(m_f - 20) & \text{if } p_1 \geq 4 \end{cases} \quad (6-1)$$

Equation (6-1) is used to generate the value of m_f from the user selection value of p_2 . The values for these variables are: p_2 ranges between 0 and 9, $p_1 \leq 3$, m_f ranges between 5 and 14. $p_1 \geq 4$, and m_f ranges between 20 and 47. PAR, PAW, PAA and PAM all have the same size of feature vector as m_f , while the size of the PAB, APAW, APAA and APAM feature vector is twice the size of m_f . The size of APAB on the other hand is 4 times the size of m_f . Although the same algorithm is used, when comparing two feature vectors with different m_f values, the matching score between those two vectors will still be high. Two different feature vector sizes can be accommodated by adding zeros at the end of the smaller size feature vector to match the larger size feature vector. This represents an additional level of security to the system when the matching score exceeds the threshold setting.

6.3.2.3. The third digit p_3 .

This digit is related to the value of m_i for PA and δ_i for APA. It also depends on the selected value of p_1 . From Table 6-1, the relationships between p_3 and m_i and δ_i are given as follows:

$$p_3 = \begin{cases} 10\delta_i - 6 & \text{if } p_1 \leq 3 \\ 10m_i - 15 & \text{if } p_1 \geq 4 \end{cases} \quad (6-2)$$

Equations (6-2) is used to generate the value of m_i and δ_i from the user selection value of p_3 . Since p_3 is ranges between 0 and 9, for $p_1 \leq 3$, δ_i ranges between 0.6 and 1.5 while for $p_1 \geq 4$, m_i ranges between 1.5 and 2.4.

6.3.2.4. The fourth digit p_4 .

This digit corresponds to the value of O_{\max} and O_{\min} for APAA, APAM, PAR, PAA and PAM the range of N for PAH or just a random number for APAB, APAW, PAB and PAW. The relationships between p_4 and the PA or APA parameters are given as follows:

$$p_4 = \begin{cases} 0.5 \times O_{\max} - 2.5 & \text{if } p_1 \leq 2 \\ 0 \times O_{\min} & \text{if } p_1 \leq 2 \\ \text{random} & \text{if } 3 \leq p_1 \leq 4 \\ 2.5 \times O_{\max} - 1 & \text{if } 5 \leq p_1 \leq 8 \\ -O_{\min} - 1 & \text{if } 5 \leq p_1 \leq 8 \\ 0.5 \times N - 1 & \text{if } p_1 \geq 9 \end{cases} \quad (6-3)$$

Equations (6-3) is used to generate the value of O_{\max} , O_{\min} and N from the user selection value of p_4 . Here p_4 ranges between 0 and 9, $p_1 \leq 2$, O_{\max} ranges between 5 and 23, while O_{\min} is always zero. For $3 \leq p_1 \leq 4$, the value of p_4 is just a random number. For $5 \leq p_1 \leq 8$, O_{\max} ranges between 0.4 and 4 while O_{\min} always ranges between -1 and -10. For $p_1 \geq 9$, N ranges between 2 and 20.

6.3.3. Submit ECG as biometric

Once the PIN is verified and the values of the PA and APA parameters are calculated using equations (6-1) to (6-3) the feature extraction process can commence. The calculated feature vector value is compared to the value of the stored feature vector. If the difference between the two is within the acceptable threshold setting, the authentication is verified. This represents the next level of security in this system. It is first required to insert a card or token to claim an identity in the security system.

Next, the system will request the user to provide two security parameters. i.e. a PIN and an ECG signal.

6.4. PIN: THE FIRST LEVEL OF SECURITY

Personal identification numbers (PIN) or passwords remain the widely used authentication means around the world. On the downside, the PIN can be accidentally or deliberately compromised, e.g. a micro camera can be used to obtain the PIN without user consent. However, a PIN can always be changed whenever the user requires or when it has been compromised [121]. For a 4 digit PIN, there are 10000 possible combinations of numbers which make it hard to guess. The odd for a fraudster to guess these PIN numbers is 1 in 10000 or 0.0001 %. Many PIN verification systems allow 3 wrong PIN attempts, thereby giving a fraudster a 0.003% probability of guessing the correct PIN before the authentication process is blocked. Furthermore, some security system do not allowed PIN to be numbers where all digits are identical (such as 1111 or 2222) or consecutive (1234 or 2345) as these PIN are easy to guess [122]. For this reason, the probability of guessing a PIN increases. In 2002, Bond *et al* [123], discovered a security flaw in the PIN generation system of the IBM 3624, which was duplicated in most later hardware. Known as the decimalization table attack, the flaw would allow someone who has access to a bank's computer system to determine the PIN for an ATM card in an average of 15 guesses. Yet again, the chances of guessing the PIN increase.

A 4 digit PIN described in the proposed PA-APA ECG based multilevel security biometric authentication system do not have any limitation on the choice of number intended for PIN making the chance of guessing the PIN up to 0.0001%. Integrating the PA and APA ECG based parameters as a part of the PIN increase the level of security of the system making the fraudster PIN guessing effort useless.

In a practical biometric systems, after an identity is claimed by a user (either using token or card), the next step is to submit the PIN. If the PIN is not correct, even if a fraudster has managed to obtain the legitimate ECGs, the system will automatically terminate the transaction without extracting any features. In some cases, for example in the event of a software attack by the fraudster or a glitch in the system, a system may allow a user to proceed to the next step of submitting an ECG thus extracting the ECG features. In this situation when the 1st level of security is breached, a wrong PIN will generate a different set of feature vectors. Comparing two different sets of feature vectors will subsequently generate a high imposter matching scores and prevent authentication.

6.5. PERFORMANCE EVALUATION

To test the performance of the proposed PA-APA ECG based multilevel security biometric authentication system, the 112 processed average ECG training and test databases set up in chapter 4 and 5 are reused in this study. As mentioned in chapter 2, the ROC curve requires two sets of matching scores known as ‘Genuine Scores’ and ‘Imposter Scores’. Five different cases are simulated in this study to generate the ‘Genuine’ and ‘Imposter’ scores as illustrated in Figure 6-2.

Two terms will be repeatedly used when describing each case. The first term is ‘Only ECG is compromised’. This term means that a fraudster managed to obtained or reconstruct the original ECGs of a user. When this happens, the system would not be able to distinguish whether the newly submitted ECG comes from a legitimate user or a fraudster. Using the training and test databases, this situation is simulated by comparing the same subject between these databases.

The second term is ‘Only PIN is compromised’. This term reflects a situation where the system could not differentiate between the correct PIN keyed in by the legitimate

user and the correct PIN keyed in by a fraudster. In the simulation setup, this situation is simulated by using the same PIN for the training and test databases.

Since similarity measurement for PA is the best using Manhattan distance, while for APA the best similarity measure is the Cosine distance, the best similarity score used in this experiment is still unknown. Based from Figures 4-24, 4-25, 5-16 and 5-17, it is observed that Cosine and Manhattan distance do not working very well for PA and APA respectively. As for that the widely used similarity measures namely Euclidean distance will be used in this experiment to generate the scores.

In the PA-APA ECG based biometric system, there are 2 types of information stored in the security system. These are the PIN and the ECG feature vectors. The matching scores processed in Figure 6-2 started after a user claimed an identity from the system. Once the identity is recognized by the system, the first step is to compare the stored and newly submitted PIN.

There are only two outcomes from a PIN comparison, either they are the same or different. If the two compared PIN numbers are the same, then either the legitimate user has key in the PIN correctly or a fraudster has managed to obtain the correct PIN and keyed it into the system. The ECGs are then the second level of security.

Using the proposed PA-APA ECG based biometric authentication, a feature vector is generated from the submitted ECG using the settings obtained from the PIN. The generated feature vector is then compared with the stored feature vector from the system. As we are using ECGs from the training and test databases setup in Chapter 4, the name of the ECG sources for both databases are known. In Figure 6-2 the ECG sources for the stored ECG feature vectors come from the training database while the sources for the newly submitted ECGs come from the test database.

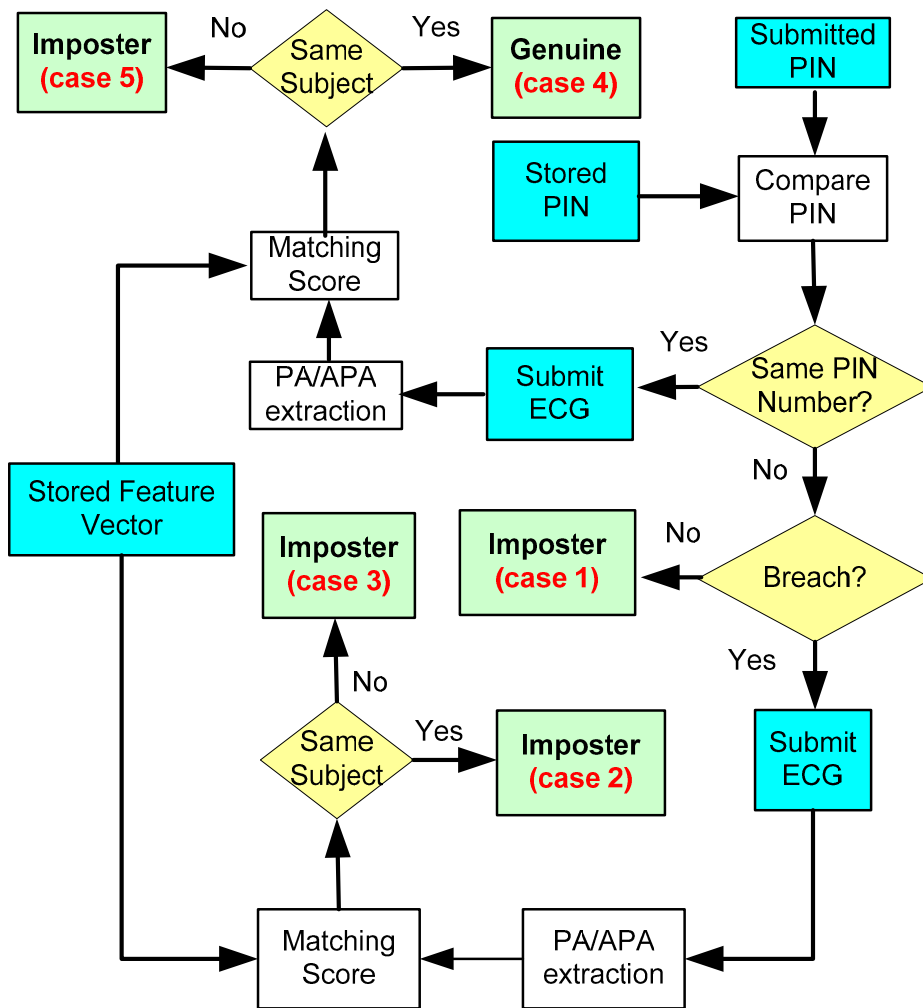


Figure 6-2 : Multilevel Security System Verification

Hence, as described in Figure 6-2, since the both compared feature vector are from the same subject, the matching scores between these feature vectors are labelled as ‘Genuine’. We categorize this as Case 4 where both PIN and ECG in the databases come from the same subject. If the compared feature vectors are from different subjects, the matching scores between these feature vectors are labelled as ‘Imposter’. We categorize this as Case 3 in where the same PIN is used to extract ECG features from different subjects from the training and test databases.

In the process of generating the ROC curve, any matching scores generated using two different PIN will be labelled as ‘Imposter’. There are 3 cases, namely Case 1, Case 2 and Case 3, which generate matching scores labelled as ‘Imposter’. In the experiment illustrated in Figure 6-2, we evaluate two scenarios when different PINs

are compared. The first scenario is that there is no breach in the system. We categorize this as Case 1. In Case 1, the system will automatically terminate the transaction if the submitted and stored PINs are not the same. The second scenario is studied by considering that there is a breach in the system. Cases 2 and 3 reflect this scenario. In these cases, although the PIN inserted is not the same, the user is still allowed to submit their ECG for feature extraction. If the ECG used to generate the matching score comes from the same subject, we categorize this as Case 2. Otherwise, the matching score will be categorized as Case 3.

In running this simulation, two different PINs might generate feature vectors with two different sizes. To make sure that comparison can be performed for these vectors, the smaller size feature vector will be filled with zero to obtain the size exhibited by the larger feature vector.

The following sections will describe in detail simulation procedure for all 5 cases.

6.5.1. Case 1 : Only ECG is compromised-no breach

Referring to Figure 6-2, the first case explained in this subsection is by considering that only the ECG is compromised with no security breach. Practically, when the PIN submitted is not the same with the one stored, the system will automatically reject the authentication process. Thus no 'Imposter' scores are generated.

6.5.2. Case 2 : Only ECG is compromised- the system is breached

Case 2 considers only the ECG is compromised when the system is breached. .As shown in Figure 6-2, for case 2, it is assumed that the user is allowed to move to the next step of submitting their ECGs although the PIN inserted is not the same as that stored. It is also assumed that the security system will only allow a wrong PIN to be inserted a maximum of 3 times before the transaction is blocked as explained in section 6.4.

6.5.3. Case 3 : Both PIN and ECG are not compromised – with fraudster attempt

The third case as illustrates in Figure 6-2, considers that both PIN and ECG are not compromised. The purpose of this simulation is to generate ‘Imposter’ scores by assuming that the ECGs and the PIN are not compromised i.e. fraudster attempt. This means that the comparisons will not involve two ECGs with the same PIN from the same subject and all measures will be relatively high.

6.5.4. Case 4 : No fraudster attempt

The fourth case presented in Figure 6-2 is by considering no fraudster attempt. This simulation study generates ‘Genuine Scores’ by assuming that the PIN and the ECGs are not compromised and that no attempts to gain fraudulent access have been made. Since the comparisons are only done for ECGs from the same subject with the same PIN, all matching scores calculated in this case are labelled as ‘Genuine Scores’ and will be relatively low.

6.5.5. Case 5 : Only PIN is compromised

The fifth case illustrates in Figure 6-2 considers the situation which only the PIN is compromised. In this simulation, the purpose is to generate ‘Imposter Scores’ by assuming that the PIN is compromised but the ECG is not. In this case the Imposter scores will be relatively high.

6.5.6. Results

As mentioned in previous section, there are no ‘Imposter’ scores generated due to Case 1. However, to include the effect of rejection for this case in the ROC curve, this thesis intentionally represents the rejection with a high value. To obtain this high value, a different randomly PIN are used to extract feature vector from the test and training database. The feature vector from the test and training database are compared to generate matching scores. The maximum matching scores values from these comparisons is defined as the high value. Matching process of Case 1 generates 112 high value ‘Imposter’ scores. These scores come from comparing the same subject from the training and test database. Since the PINs are not the same, matching scores generated from these comparisons are replaced by the high value.

For Case 2, to ensure the simulation runs in a controlled environment, all ECGs from the training database are extracted using the same PIN for example in this experiment PIN 8827 is used to extract feature vectors from all subjects in the training database. The feature vectors extracted from this PIN is defined as the ‘Stored Feature Vector’ described in Figure 6-2. Each ECG from the test database will be extracted repeatedly using 3 different sets of PIN numbers. To ensure the simulation runs in a controlled environment, the three randomly chosen PINs are selected as 9470, 2334 and 5549. Feature vectors extracted using these three PINs are defined as ‘Submitted Feature Vector’. Each Stored Feature Vector will be compared to all Submitted Feature Vector to generate the ‘Imposter’ scores. Matching process of Case 2 generates 336 ‘Imposter’ scores. These scores come from comparing generated feature vectors of the same subject from the test and training databases using the respective PIN.

For case 3, each subject in the training database is compared with different subjects in the test database (ECGs used in comparison come from different subjects to reflect situation in which the ECG is not compromised). To reflect cases where the PIN numbers are not compromised, the same PIN used to extract feature vectors from the training and the test databases, described in Case 2, are reused. Matching process of

Case 3 generates a total of 37 296 ‘Imposter’ scores (12 432 ‘Imposter’ scores for each submitted PIN).

Case 4 can be simulated by ensuring that all ECGs compared from the training and test databases belong to the same subject. In this case, the same PIN is used to extract ECG features from both test and training databases. In this simulation, a random PIN 4470 is chosen to extract the features. Matching process of Case 4 generates 112 ‘Genuine’ scores.

In Case 5, the same PIN is used for different subjects in the test and training databases. In this study, a random PIN 0334 will be used to extract ECG features from both the training and test databases. Matching process of Case 5 generates 12 432 ‘Imposter’ scores.

All matching scores for cases 1 to 5 are then combined to generate the ROC curves of the PA-APA ECG based multilevel security authentication system. The ROC curve for healthy and arrhythmia populations in this experiment generates an ideal case of authentication performance. In actual cases, the 1st level of security (which is the PIN) will always terminate a transaction if the keyed in PIN is not the same as the one stored.

Since the Euclidean distance used as the similarity measures described in section 6.5 generates an ideal ROC performance, the rest of similarity measure would not be evaluated in this section.

6.6. DISCUSSION

6.6.1. System performance in breach

Cases 1, 2 and 3, explained in section 6.5, consider situations in which the PIN numbers are unknown to the fraudster. The proposed system performance, with respect to the capability of the system to automatically terminate the transaction if the submitted PIN is not correct as described in case 1, has been discussed in section 6.4. However, the objective of simulating case 1 in section 6.5.1 was to include the imposter matching scores for the ROC curves in the situation when the system is not breached. In a practical system, cases 2 and 3 are rarely to be found as most of the time the system will terminate the transaction if the submitted PIN is not the same as the one stored.

Cases 4 and 5 explained in section 6.5 consider situations which the PIN numbers are known to the fraudster. Since the PIN is the combination of the PA and the APA algorithms and parameters, as described in section 6.3.2, the general biometric performance when only cases 4 and 5 are considered have been shown in sections 4.8.4.4 and 5.5.4.4. In those sections, the suggested range of PA and APA for all algorithms used which relate to the PIN technology in section 6.3.2 have been compared with ECGs from the same subject (Case 4) and different subject (Case 5).

6.6.2. System performance with noise

This subsection discusses the effect of noises as explained in subsection 3.3.3 on the proposed system performance when the level of noises in the raw ECGs increases. The noise sources to test the system are:

- a) 50 Hz sinusoidal interference with peak to peak amplitudes equals to a quarter of the peak to peak amplitude of the 30 second ECG recordings.

- b) White Gaussian noise to model muscle EMG noise

- c) Low Frequency drift generated using a noise generator designed by [130] that consists of baseline wander taken from the MIT-BIH Noise Stress Test Database [3].

All 28 PTB ECG recordings of the 14 healthy subjects described in Figure 4-11 will be combined additively with the noise described above. The white Gaussian noise will be added with SNR equal 0dB, 15dB, 45dB and 60dB. For the purpose of this study, an arbitrary PIN 5207 will be used to extract feature vector for the training and test databases..

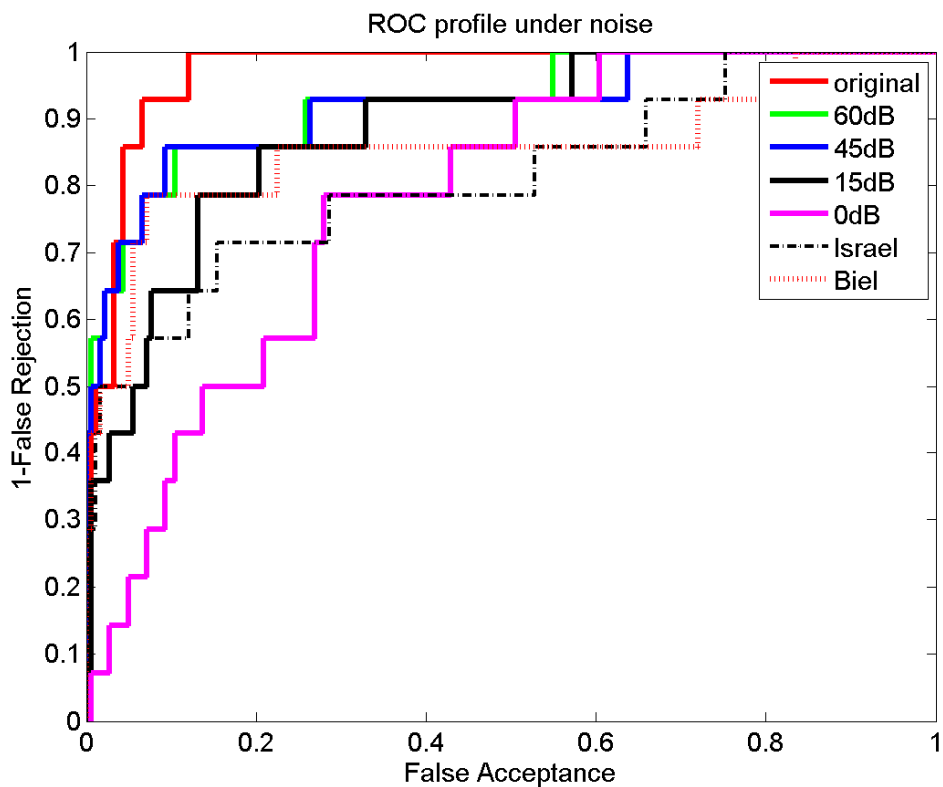


Figure 6-3 : ROC curve when ECG noise increases

Figure 6-3 illustrates the ROC curve when all ECG signal are contaminated with various noises. In Figure 6-3, the ROC curves for Biel [68], Israel[70] and feature vector generated using PIN 5207 without adding the white Gaussian noise are also presented.

As can be seen from Figure 6-3, the ROC profile for noise SNR greater than 45dB is better than Biel [68] and Israel [70] feature extraction techniques without adding the white Gaussian noise. The AUR and EER profiles for these noisy ECG signals are shown in Figure 6-4.

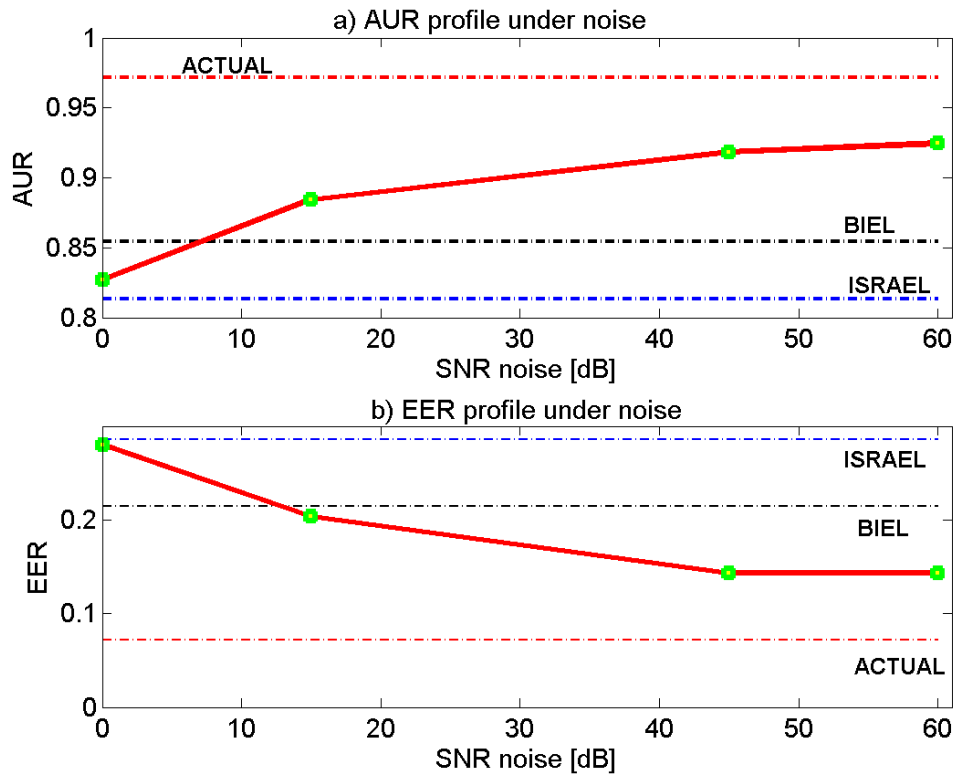


Figure 6-4 : AUR and EER profiles when ECG noise increases

In Figure 6-4, the AUR and EER profiles for the noisy ECG signals are respectively higher and lower than Biel[68] and Israel[70] feature extraction techniques if the noise SNR is greater than 12dB.

For all SNR noise, the AUR and EER profiles are better than the Israel feature extraction technique. From this observation, it is shown that the proposed method manages to generate useful authentication profiles under the influence of heavy noises. The AUR and EER performances reduce by up to 14% when 0dB SNR noise is added to the ECG signals.

6.6.3. Advantages of proposed system

The proposed PA-APA ECG based multilevel security authentication system has the following advantages:

- i. If the PIN is compromised, the fraudster still cannot access the system, as the correct ECGs are also required.
- ii. If the ECGs are compromised, the user can change the PIN number so that the extracted features stored in the system change and hence it will reject an attempted authentication process by a fraudster.
- iii. The user must be alive and present during the transaction process.
- iv. The proposed system is safe from invertibility attacks such as those aiming to recover the original ECG by looking for information such as PIN, algorithm and feature vector stored in the system database. To regenerate the original ECG a high number of T_{trans} is required which is not presented by the user during the enrolment process. Prediction on the next intersection point within a T_{trans} is hard to acquire since the original ECG morphology of a human is determined by factors such as health, condition, sex and the shape of an individual's heart.
- v. Using a different PIN to change feature vectors stored in the system is easy to perform. Users have the flexibility to change the PA or APA settings. Unlike combining smartcard or randomly coded tokens with a biometric trait, only specialized persons with certain type of hardware have the capability to change the algorithm parameters.

6.7. CONCLUSION

A multilevel security PA-APA ECG based biometric authentication system using new signal processing technology name as pulse active (PA) and adaptive pulse active (APA) was presented. It was shown that the first level of security for a biometric system is the 4 digit PIN that represents the PA or APA parameters. The feature vectors of the ECG wave generated by 10 different PA and APA algorithms become the secondary level of security. Through experiments using the ECG dataset, it was shown that the proposed PIN range of the generalized PA-APA ECG based biometric system generates a good performance as a multilevel security authentication system.

CHAPTER 7.

CONCLUSIONS

7.1. THESIS CONCLUSION

The work presented in this thesis explored a new concept of representing a signal into pulse domain for ECG authentications. A highly level security system is very important nowadays to protect consumers' money and property. Experts in the field of security believe that biometrics is the answer. Yet, consumers refuse to use the technology due to fear of personal data infringements. The significance of using biometrics, advantages and challenge were presented in Chapter 2 of this thesis.

In chapter 2, the advantages and disadvantages of the three main authentication approaches namely handheld based, knowledge based and biometric based systems were discussed. Each authentication approach has its own strengths and weaknesses. This leads to an idea of combining more than one approaches to increase the security of the authentication system as presented in this thesis. Most of the biometric system involves the process of collecting data, pre-processing, feature extraction, and classification. Improvement on the biometric performance may come from one of these steps. The scope of the work in this thesis is limited to improving the feature extraction techniques for biometric application.

In Chapter 2, the difference between authentication and identification biometric security systems is discussed. As discussed in chapter 2, the authentication system compared 1 to 1 template feature vectors to validate the claim of a subject. Thus, no advance classifier was used in the system. The capability of the authentication system depends mainly on the capability of the feature extraction technique to extract distinct features. For this reason, the need to have a good feature extraction method has motivated the research work in this thesis. Comparison between the training and test databases in this work is done using a simple template matching technique involving similarity distance measure. Nine widely used similarity measure are described in Chapter 2. To analyze the performance of the proposed technique in this thesis, the receiver operating characteristic (ROC) curve is used. ROC curve provide 2 important information of the biometric system which is the overall performance of the system which is measured by the area under the ROC (AUR) and the equal error rates of false acceptance and false rejection.

This thesis focused on the use of ECG as biometric trait. As explained in Chapter 3, ECG represents electrical activity of the heart and is believed to be unique among individuals. In chapter 3, the main feature extraction techniques in the literature which can be categorized into characteristic and waveform based were discussed. Many of these techniques reported a perfect classification using their methods. However, it is unknown from which step (feature extraction or classification) of the biometric system contribute to the perfect classification. The general hypothesis in this thesis claims that a better authentication can be achieved using any classifier using a good discriminative features. For this reason, extensive works have been done in this thesis to improve the feature extraction technique for ECG based biometric authentication system.

Practical implementation of ECG for authentication is effected by placing the ECG electrodes using Lead I configuration so as to measure the voltage between two points on the human body (typically between the left and right hand of the user). In these measurements, the electrocardiograph current must propagate from one hand, through the heart and exit at the other hand to generate the ECG signals. As explained in Chapter 3, different Lead configurations examine the heart at different

angle, thus the ECG generated will not be the same. It is suggested that any recognition performance of the ECG based biometric which are not using Lead I configuration are not practical to be consider as general ECG based biometric performance. An ECG signal cannot be falsified in the same way as iris or fingerprint information can to allow unauthorized. However, in the future, when an ECG biometrics technology has been widely accepted as an authentication means, there will always be possibility of ECG recordings used without consent by the fraudster for authentication purposes. Another major challenge on implementing ECG as a biometric is the effect of HRV and AMV which have been discussed in chapter 3.

These issues motivated the research to develop novel techniques named Pulse Active (PA) and Adaptive Pulse Active (APA) to solve the problem. The PA and APA are derived from the concept of representing a signal into pulse domain. The philosophy behind this is that, all signals can be presented by a finite sequence of pulses. Different parts of the signals would generate different width of the pulses based on the amplitude and duration of the signals.

The fundamental of Pulse Active (PA) techniques was discussed in chapter 4. This technique is developed based on the concept of Pulse Width Modulation (PWM). In the area of pattern recognition, the concept of PWM to extract features is relatively new. This chapter systematically explains the PA techniques to generate unique ECG features for biometric purposes. 6 new PA based algorithms were derived from this concept. The key advantage of this technique is that the features extracted from the ECG signal not only consists the information of the signal but also embedded user knowledge information represented by 5 PA unique parameters. Altering these parameters will change the value of feature vectors. In this research, the simulations carried out in the thesis focused on finding the optimal range of the PA parameters. There are two other factors which need to be considered when PA is used to extract ECG features for biometric application. These factors are the location of extraction and the best similarity measures. In chapter 4, these factors have been investigated. Comparing all PA techniques developed in chapter 4, PAW, PAA and PAM generates the best authentication profile which manage to obtain 97% AUR and 7% EER.

The alternative technique to PA is the Adaptive Pulse Active (APA) discussed in chapter 5. The APA technique is developed based on the concept of delta modulation (DM). 5 different algorithms based on this technique are derived. This chapter investigated the optimum of 5 APA parameters by considering first the extracted location and selecting the best similarity measure. Comparing all APA algorithms in this chapter, it is shown that APAW methods generates the best authentication profile which manage to obtain 99% AUR and 2% EER authentication performance.

In general, chapters 4 and 5 in this thesis have shown how these techniques generate good authentication results whilst, at the same time, they deal with the HRV and AMV problems. In the future, simulation studies with larger number of healthy subjects needs to be conducted in order to produce statistically significant results for biometric authentication. The concern of a fraudulent uses of recorded ECGs as a means of authentication is solved by introducing a PIN related technology into the developed algorithms as discussed in chapter 6. The optimum ranges used to configure the PIN in this thesis are all based on the statistically significant arrhythmia result that contains the range of the 14 healthy subjects as a subset. The PIN will generate different feature vectors based on a selected algorithm. The PIN will generate different feature vectors based on a selected algorithm. Embedding the PIN and ECG biometric as part of an authentication process requires both the active presence of the user and knowledge of the PIN.

7.2. FUTURE WORK

The success of implementing the new algorithms on ECG signal for authentication generates a lot of potential for future work. The algorithms developed namely the PA and APA techniques are not limited to the use of ECG biometric authentication. By using fixed PA and APA parameters these techniques can be used for clinical application such as detecting abnormal ECG complexes within ECG recordings. A

typical example would be detection of sleep Apnea. The PA and APA algorithms can also be used for a non ECG signals such as speech, electromyography (EMG) and Electroencephalography (EEG) which have amplitude and time scaling variation issues.

Feature vectors generated based on PA and APA is extracted from unique locations of the original signal. Different PA and APA parameters will generate different feature vectors. When multiple feature vectors (various PA and APA parameters) are considered, numerous locations on the original signal are taken into account. Combinations of these feature vectors will generate signature of the signals.

In terms of transforming a signal in pulse domain, the PA and APA techniques transformed the original signals in the form of unipolar pulses with two output states. The PA and APA techniques can be further expended to form bipolar output pulses with three output states in pulse domain. A multilevel output pulse also can be developed to represent the features of the signal. Finally, the philosophy of transforming a signal into pulse domain can be extended to transform an image (2-D) or video (3-D) into pulse domain.

AUTHOR'S PUBLICATIONS

The following lists the author's publications in reverse chronological order

Patent Publication

- [P1] Safie, S.I.; Soraghan, J.J.; Petropoulakis, L.; , "Pulse Domain Feature Extraction Technique with Application to ECG Biometric Authentication," *UK Patent* , filed March 2012

Journal Publications

- [J1] Safie, S.I.; Soraghan, J.J.; Petropoulakis, L.; , " Bipolar Pulse Active Cumulative Transform (BPACT) Signature Extraction," *Signal Processing, IEEE Transactions on* (submitted February 2012)
- [J2] Safie, S.I.; Soraghan, J.J.; Petropoulakis, L.; "PA-ECG Based Multilevel Security Biometric Authentication System," *Information Forensics and Security, IEEE Transactions on* (submitted February 2012).
- [J3] Safie, S.I.; Soraghan, J.J.; Petropoulakis, L.; "Electrocardiogram (ECG) Biometric Authentication Using Pulse Active Ratio (PAR)," *Information Forensics and Security, IEEE Transactions on*, vol.6, no.4, pp.1315-1322, Dec. 2011
- [J4] Safie, S.I.; Soraghan, J.J.; Petropoulakis, L.; " Pulse Active Harmonic (PAH) Features for ECG Biometric Authentication," *IET Information Security*. (submitted June 2011).

Conference Publications

- [C1] Safie, Sairul I.; Soraghan, John J.; Petropoulakis, Lykourgos; , "Pulse Active Mean (PAM): A PIN supporting feature extraction algorithm for doubly secure authentication," *Information Assurance and Security (IAS), 2011 7th International Conference on* , vol., no., pp.210-214, 5-8 Dec. 2011
- [C2] Sairul I Safie, John J Soraghan, and Lykourgos Petropoulakis, "Pulse Active Ratio (PAR):A New Feature Extraction Technique for ECG Biometric Authentication" *2011 International Conference on Signal and Image Processing Applications (ICSIPA 2011)*, pp 16-20, November 16-18, 2011.
- [C3] Safie, S.I.; Soraghan, J.J.; Petropoulakis, L.; , "ECG biometric authentication using Pulse Active Width (PAW)," *Biometric Measurements and Systems for Security and Medical Applications (BIOMS), 2011 IEEE Workshop on* , vol., no., pp.1-6, 28-28 Sept. 2011
- [C4] Sairul I Safie, John J Soraghan, and Lykourgos Petropoulakis "ECG Based Biometric for Doubly Secure Authentication" *19th European Signal Processing Conference, EUSIPCO 2011*, pp 2274-2278 , 29Aug-2Sept 2011,
- [C5] Safie, S.I.; Soraghan, J.J.; Petropoulakis, L.; , "Pulse Active Bit (PAB) feature extractor for ECG biometric authentication," *Systems, Signals and Image Processing (IWSSIP), 2011 18th International Conference on* , vol., no., pp.1-4, 16-18 June 2011.

APPENDICES

A. Example of generating Receiver Operating Characteristic (ROC) Curve

Let Tables A-1 and A-2 represent the respective training and test database of 4 subjects. S1, S2, S3 and S4 in both tables represents the name of the subjects while X[1], X[2], X[3], X[4] and X[5] are the value of feature vector X.

Table A-1: Example feature vectors from the training database

	X[1]	X[2]	X[3]	X[4]	X[5]
S1	3	9	9	6	2
S2	4	1	7	9	4
S3	6	5	8	4	4
S4	5	1	6	1	2

Table A-2 : Example feature vectors from test database

	X[1]	X[2]	X[3]	X[4]	X[5]
S1	4	9	6	7	4
S2	2	3	5	6	2
S3	4	3	2	8	5
S4	3	3	6	3	9

The feature vectors of all subjects in the training database are compared to generate matching scores with the feature vectors of all subjects in the test database. In this example, Euclidean Distance is used as the similarity measures. Table A-3 tabulated the matching scores of this comparison.

Table A-3: Example of matching score results

Subject Name		Authentication		Subject Name		Authentication	
Train	Test	Actual	Score	Train	Test	Actual	Score
S1	S1	Positive	3.87	S2	S1	Negative	8.31
	S2	Negative	7.28		S2	Positive	5.00
	S3	Negative	9.95		S3	Negative	5.57
	S4	Negative	10.15		S4	Negative	8.19
S3	S1	Negative	5.74	S4	S1	Negative	10.25
	S2	Negative	6.08		S2	Negative	6.24
	S3	Positive	7.81		S3	Negative	8.89
	S4	Negative	6.56		S4	Positive	7.81

The 1st and 6th column in Table A-3 indicates the name of subjects from the training database while the 2nd and 7th column represent the name of the subjects from the test database. The 3rd and 8th column indicates the Actual authentication results between the training and test database while the 4th and 9th column represents its matching scores. Next, all matching scores are normalized to 1 which the closest distance is near to 1. Table A-4 shows the normalized matching scores of Table A-3 using (A.1). In this example, the normalizing process is performed by using the maximum information from Table A-3 as follows:

$$\text{Normalize Score} = 1 - \frac{\text{Score}}{\text{Maximum Score}} \quad (\text{A.1})$$

Table A-4: Example of normalized matching score results

Subject Name		Authentication		Subject Name		Authentication	
Train	Test	Actual	Score	Train	Test	Actual	Score
S1	S1	Positive	0.62	S2	S1	Negative	0.19
	S2	Negative	0.29		S2	Positive	0.51
	S3	Negative	0.03		S3	Negative	0.46
	S4	Negative	0.01		S4	Negative	0.20
S3	S1	Negative	0.44	S4	S1	Negative	0.00
	S2	Negative	0.41		S2	Negative	0.39
	S3	Positive	0.24		S3	Negative	0.13
	S4	Negative	0.36		S4	Positive	0.24

It is observed in Tables A-3 and A-4 that there should be 4 positive authentication (PA) results and 12 negative authentication (NA) results. ROC curve is generated based on a selection of all available thresholds in the system and compared to the matching score in Table A-4. In this example, the values of thresholds are selected from 0.1 to 0.9 in the step of 0.1. Table A-5 represents the authentication results when the selected threshold values are used to authenticate the matching score of Table A-4. In Table A-5, the actual authentication (AA) and matching score (MS) comes from Table A-4. The selected threshold values are then compared to the value of matching scores from Table A-4. If MS is greater than the threshold values, the 'system authentication based on the threshold' (TA) will generate PA. Otherwise TA will generate NA. Table A-5 (a) shows the example of TA when threshold is set as 0.4

Table A-5 (a): Threshold value = 0.4

AA	MS	TA	AA	MS	TA	AA	MS	TA	AA	MS	TA
PA	0.62	PA	NA	0.19	NA	NA	0.44	PA	NA	0.00	NA
NA	0.29	NA	PA	0.51	PA	NA	0.41	PA	NA	0.39	NA
NA	0.03	NA	NA	0.46	PA	PA	0.24	NA	NA	0.13	NA
NA	0.01	NA	NA	0.20	NA	NA	0.36	NA	PA	0.24	NA

From Table A-5 (a), it is shown that there are 2 true positive (TP) and 3 false positive (FP) authenticated when the threshold is set to 0.4. This process is continue for the selected threshold values and their results are presented in Tables A-5 (b) to A5 (i).

Table A-5 (b) : Threshold = 0.9

AA	MS	TA	AA	MS	TA	AA	MS	TA	AA	MS	TA
PA	0.62	NA	NA	0.19	NA	NA	0.44	NA	NA	0.00	NA
NA	0.29	NA	PA	0.51	NA	NA	0.41	NA	NA	0.39	NA
NA	0.03	NA	NA	0.46	NA	PA	0.24	NA	NA	0.13	NA
NA	0.01	NA	NA	0.20	NA	NA	0.36	NA	PA	0.24	NA

Table A-5 (c) : Threshold = 0.8

AA	MS	TA	AA	MS	TA	AA	MS	TA	AA	MS	TA
PA	0.62	NA	NA	0.19	NA	NA	0.44	NA	NA	0.00	NA
NA	0.29	NA	PA	0.51	NA	NA	0.41	NA	NA	0.39	NA
NA	0.03	NA	NA	0.46	NA	PA	0.24	NA	NA	0.13	NA
NA	0.01	NA	NA	0.20	NA	NA	0.36	NA	PA	0.24	NA

Table A-5 (d) : Threshold = 0.7

AA	MS	TA	AA	MS	TA	AA	MS	TA	AA	MS	TA
PA	0.62	NA	NA	0.19	NA	NA	0.44	NA	NA	0.00	NA
NA	0.29	NA	PA	0.51	NA	NA	0.41	NA	NA	0.39	NA
NA	0.03	NA	NA	0.46	NA	PA	0.24	NA	NA	0.13	NA
NA	0.01	NA	NA	0.20	NA	NA	0.36	NA	PA	0.24	NA

Table A-5 (e) : Threshold = 0.6

AA	MS	TA	AA	MS	TA	AA	MS	TA	AA	MS	TA
PA	0.62	PA	NA	0.19	NA	NA	0.44	NA	NA	0.00	NA
NA	0.29	NA	PA	0.51	NA	NA	0.41	NA	NA	0.39	NA
NA	0.03	NA	NA	0.46	NA	PA	0.24	NA	NA	0.13	NA
NA	0.01	NA	NA	0.20	NA	NA	0.36	NA	PA	0.24	NA

Table A-5 (f) : Threshold = 0.5

AA	MS	TA	AA	MS	TA	AA	MS	TA	AA	MS	TA
PA	0.62	PA	NA	0.19	NA	NA	0.44	NA	NA	0.00	NA
NA	0.29	NA	PA	0.51	PA	NA	0.41	NA	NA	0.39	NA
NA	0.03	NA	NA	0.46	NA	PA	0.24	NA	NA	0.13	NA
NA	0.01	NA	NA	0.20	NA	NA	0.36	NA	PA	0.24	NA

Table A-5 (g): Threshold = 0.3

AA	MS	TA	AA	MS	TA	AA	MS	TA	AA	MS	TA
PA	0.62	PA	NA	0.19	NA	NA	0.44	PA	NA	0.00	NA
NA	0.29	NA	PA	0.51	PA	NA	0.41	PA	NA	0.39	PA
NA	0.03	NA	NA	0.46	PA	PA	0.24	NA	NA	0.13	NA
NA	0.01	NA	NA	0.20	NA	NA	0.36	PA	PA	0.24	NA

Table A-5 (h): Threshold = 0.2

AA	MS	TA	AA	MS	TA	AA	MS	TA	AA	MS	TA
PA	0.62	PA	NA	0.19	NA	NA	0.44	PA	NA	0.00	NA
NA	0.29	PA	PA	0.51	PA	NA	0.41	PA	NA	0.39	PA
NA	0.03	NA	NA	0.46	PA	PA	0.24	PA	NA	0.13	NA
NA	0.01	NA	NA	0.20	PA	NA	0.36	PA	PA	0.24	PA

Table A-5 (i): Threshold = 0.1

AA	MS	TA	AA	MS	TA	AA	MS	TA	AA	MS	TA
PA	0.62	PA	NA	0.19	PA	NA	0.44	PA	NA	0.00	NA
NA	0.29	PA	PA	0.51	PA	NA	0.41	PA	NA	0.39	PA
NA	0.03	NA	NA	0.46	PA	PA	0.24	PA	NA	0.13	PA
NA	0.01	NA	NA	0.20	PA	NA	0.36	PA	PA	0.24	PA

Using the TP and FP values obtained from Tables A-5 (a) to (i), the False Acceptance Ratio (FAR) and False Rejection Ratio (FRR) can be calculated using equations 2.2 and 2.3. The results of FAR and FRR is shown in Table A-6.

Table A-6: FAR and FRR Calculation

Threshold	Total		Total		$\frac{TP}{P}$	$\frac{FP}{N}$	1-FRR	FAR
	PA	NA	TP	FP				
0.9	4	12	0	0	0	0	0	0
0.8	4	12	0	0	0	0	0	0
0.7	4	12	0	0	0	0	0	0
0.6	4	12	1	0	0.25	0	0.25	0
0.5	4	12	2	0	0.5	0	0.5	0
0.4	4	12	2	3	0.5	0.25	0.5	0.25
0.3	4	12	2	5	0.5	0.42	0.5	0.42
0.2	4	12	4	7	1	0.58	1	0.58
0.1	4	12	4	9	1	0.75	1	0.75

Finally, the ROC curve can be projected based on the FAR and 1-FRR values tabulated in Table A-6 as shown in Figure A-1.

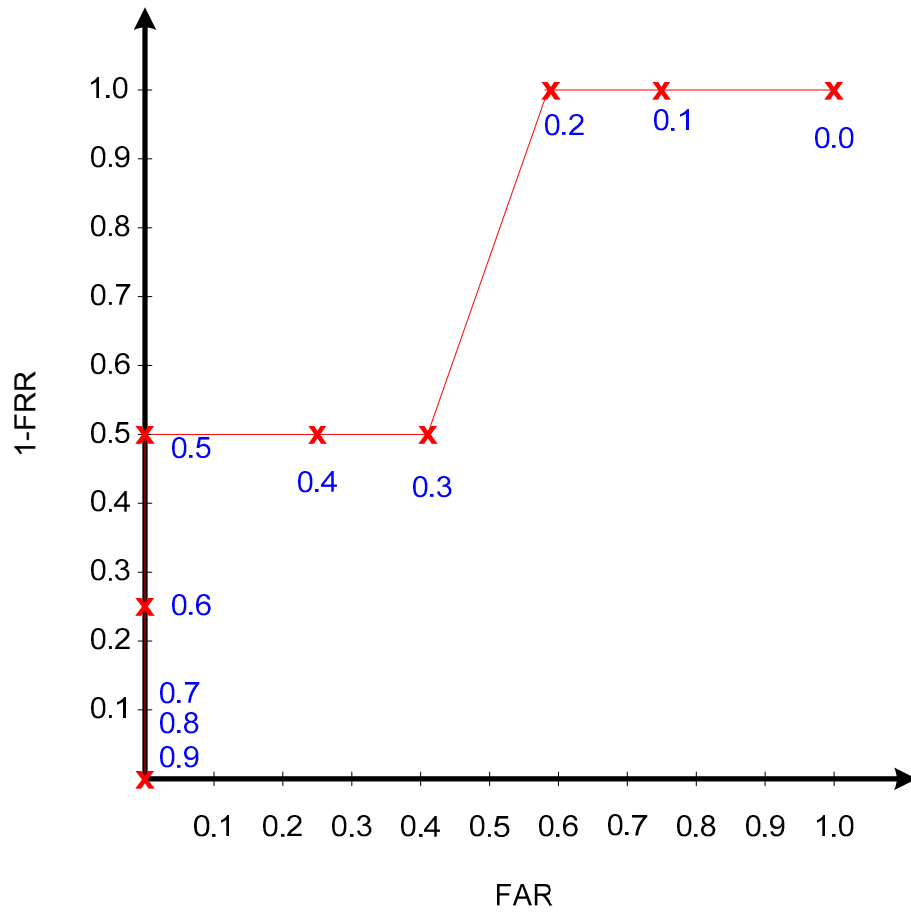


Figure A-1: Examples of ROC curve generation

The ROC curve illustrated in Figure A-1 can be smoothed by increasing the value of the threshold settings. The area under ROC (AUR) can be calculated by the area under the ROC curve as shown in Figure A-2.

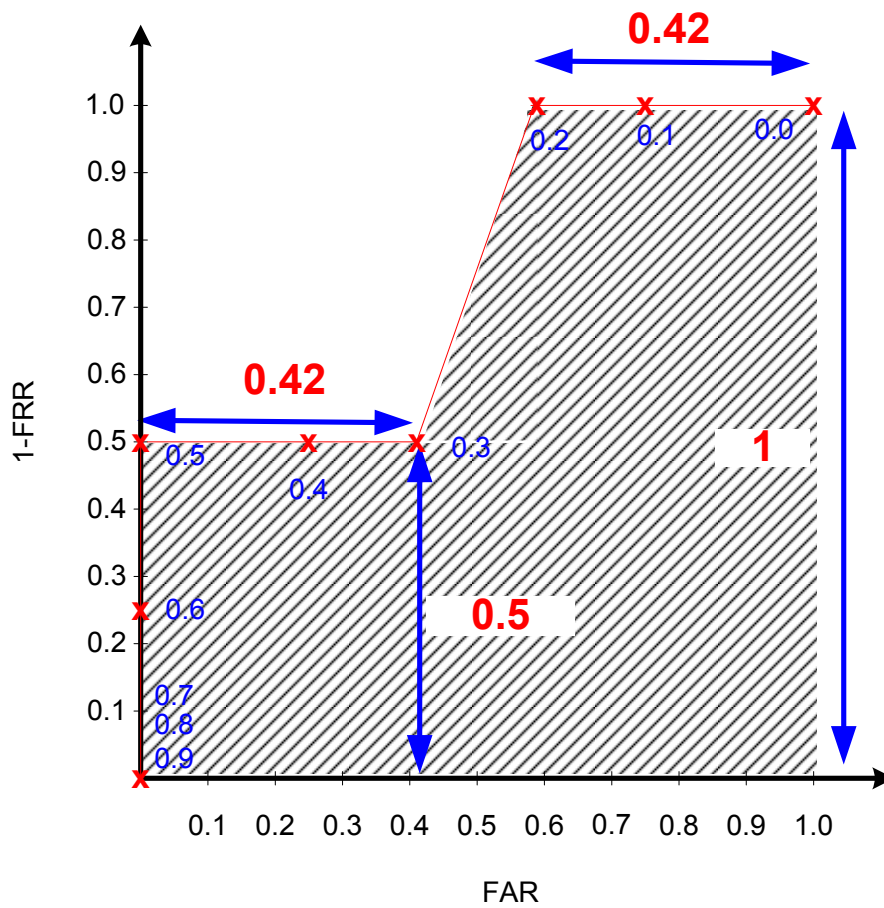


Figure A-2: Examples of AUR Calculation

The AUR calculation for the example ROC curve in Figure A-2 is shown as follows:

$$\begin{aligned}
 \text{AUR} &= (0.42 \times 0.5) + \left(\frac{1}{2} \times 0.16 \times 0.5 \right) + (1 \times 0.42) \\
 &= 0.21 + 0.04 + 0.42 \\
 &= 0.67
 \end{aligned}$$

The equal error ratio is observed from the ROC curve which the FRR equals FAR. This value is equal to the intersection of a decreased linear line with the ROC curve as shown in Figure A-3. From Figure A-3, the EER observed is equal to 0.48

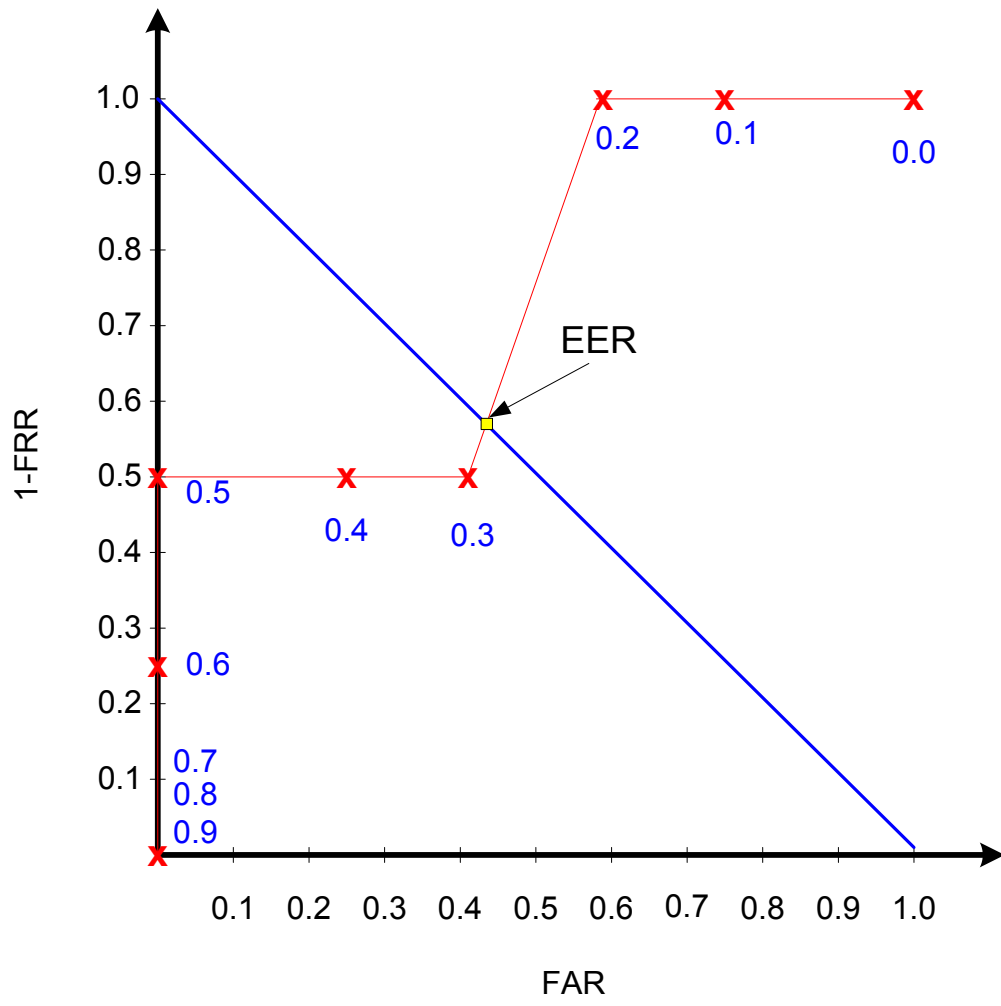


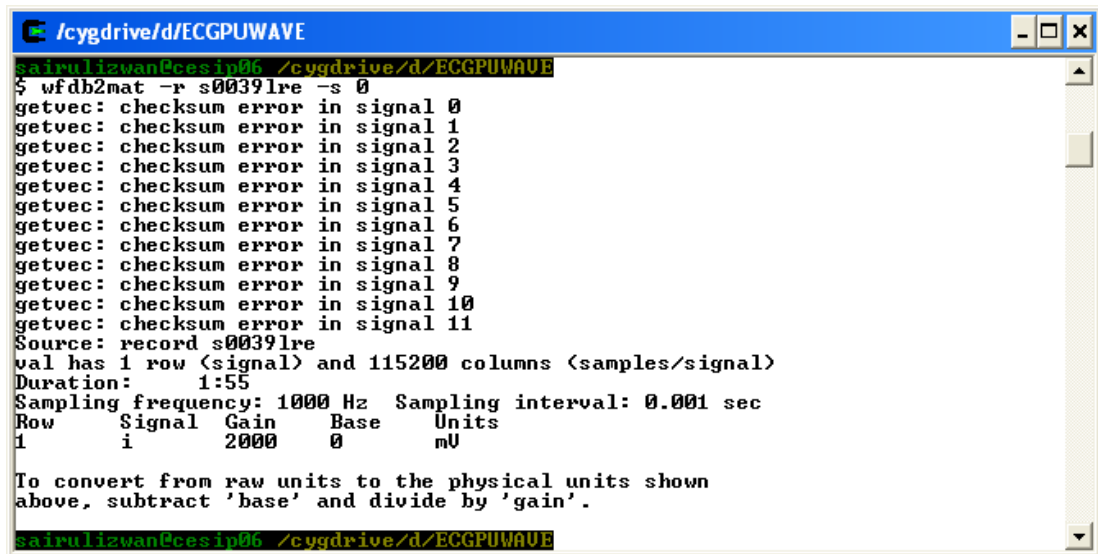
Figure A-3: Examples of EER determination from the ROC curve

B. Example of generating average ECG signal for databases

This appendix provides an example of a step by step description of generating the average ECG signal used in the setup of training and test database

B1. ECG signals from the PTB database.

ECG signals from the PTB database can be obtained in the Physionet website: <http://www.physionet.org/physiobank/database/ptbdb/>. There are two types of files for every subject that must be downloaded. The extensions of the files are *.dat* and *.hea* for example 's0039lre.dat' and 's0039lre.hea'. Using Cygwin software, these file are then used to generate the MATLAB data file (*.mat*) for the particular subject. The Cygwin instruction to convert the original data to MATLAB is `wfdb2mat`.



```
Cygdrive/d/ECGPUWAVE
sairulizwan@cesip06 /cygdrive/d/ECGPUWAVE
$ wfdb2mat -r s0039lre -s 0
getvec: checksum error in signal 0
getvec: checksum error in signal 1
getvec: checksum error in signal 2
getvec: checksum error in signal 3
getvec: checksum error in signal 4
getvec: checksum error in signal 5
getvec: checksum error in signal 6
getvec: checksum error in signal 7
getvec: checksum error in signal 8
getvec: checksum error in signal 9
getvec: checksum error in signal 10
getvec: checksum error in signal 11
Source: record s0039lre
val has 1 row (signal) and 115200 columns (samples/signal)
Duration: 1:55
Sampling frequency: 1000 Hz Sampling interval: 0.001 sec
Row Signal Gain Base Units
1 i 2000 0 mV

To convert from raw units to the physical units shown
above, subtract 'base' and divide by 'gain'.
```

Figure B-1: Cygwin response during the conversion of *.dat* file to *.mat*

The output from the Cygwin would be as shown in Figure B-1. From Figure B-1, it is observed that converted 's0039lre.mat' signals have 115200 samples for the duration of 1 minute and 55 seconds. The sampling frequency of the converted signal is 1 kHz. The actual unit of the converted signals can be obtained based on information described in Figure B-1 using the following equation:

$$\text{Actual signal} = \frac{\text{converted signal} - \text{Base}}{\text{Gain}}$$

B.1

Figure B-2 shows the ECG graph for 's00391re.mat' in mV obtained from the Cygwin.

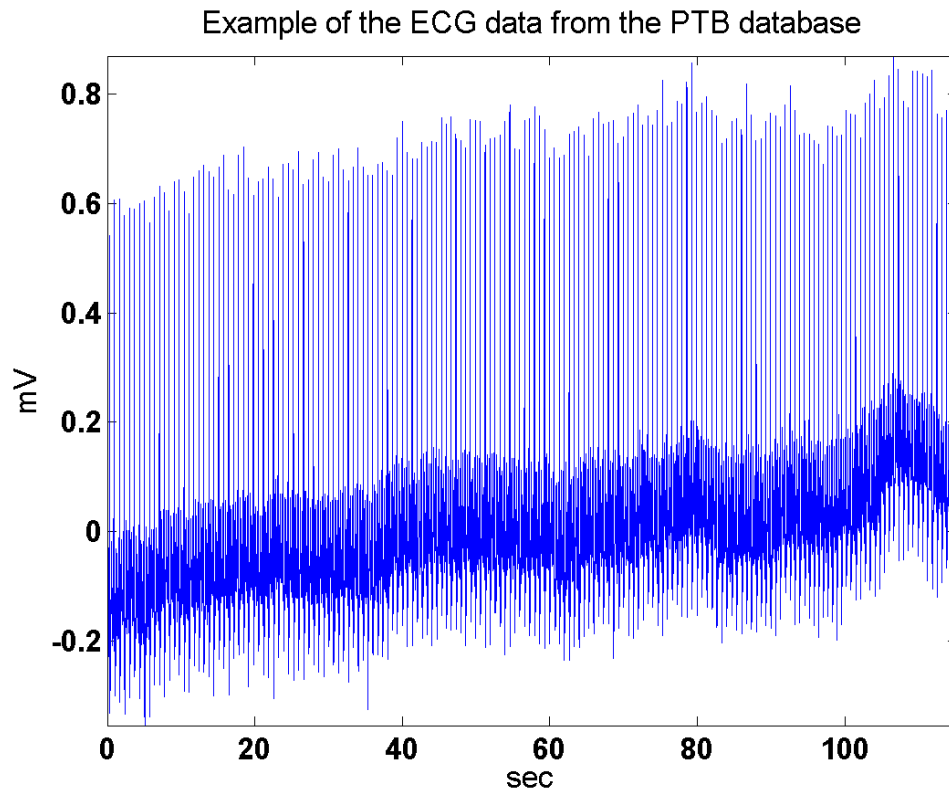


Figure B-2: Example of the raw ECG signal from the PTB database

The next step as described in Figure 4-11 is to extract the first 30 seconds of the signals. Figure B-3 illustrates the 30 seconds recording of the ECG signals shown in Figure B-2.

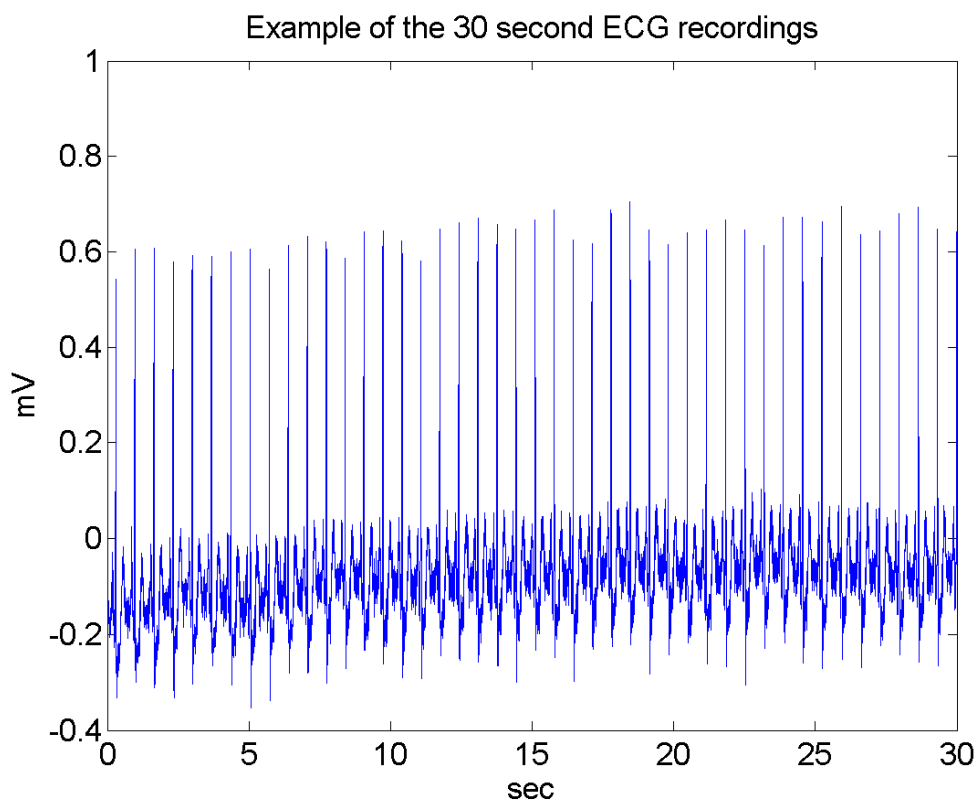


Figure B-3: Example of the 30 seconds ECG recordings

B2. Filtering the ECG signals

The next process as described in Figure 4-11 is to filter the 30 seconds ECG recordings. As explained in section 4.7.1, in this thesis, an FIR filter is used to filter all ECG recordings so that only ECG components within 2 to 40 Hz are allowed. There are various digital filters available which generally can be categorized in two: Finite Impulse Response (FIR) and Infinite Impulse Response (IIR) filters. Usually, IIR filters are used when sharp cut off and high throughput are the only main requirement. FIR is used for a system where NO phase distortion is acceptable. Since phase distortion has a greater effect on the recorded ECG, in this thesis, FIR filter will be used to ensure the ECG components are within 2 to 40Hz. The FIR filter in this thesis is designed with Passband defined from 2 to 40 Hz and two Stopbands defined from 1 to 2 Hz and 40 to 41 Hz.

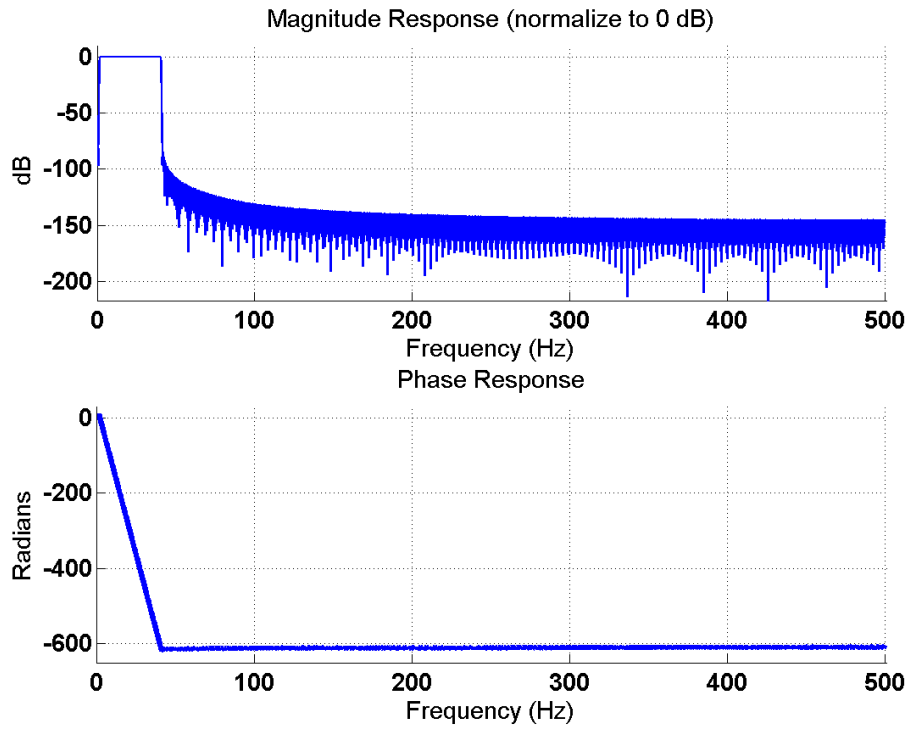


Figure B-4: Magnitude and Phase Response of the design filter

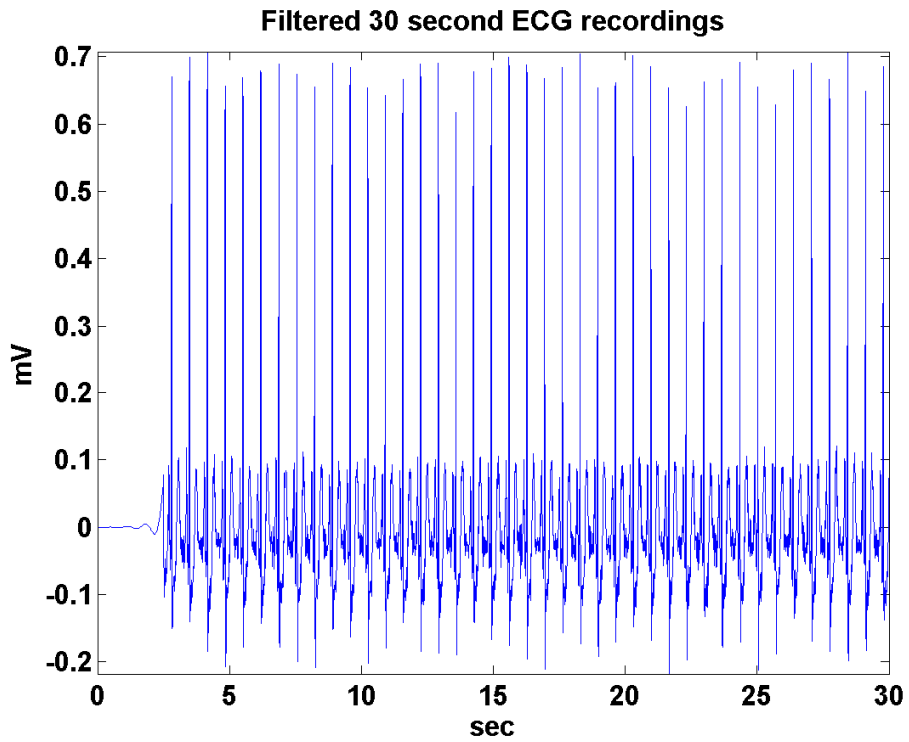


Figure B-5: Filtered 30 Second ECG signals

Specification of the Passband ripple is 0.1dB and a Stopband attenuation of 80dB. The magnitude and frequency response of the designed filter is shown in Figure B-4. In this thesis, a Kaiser window FIR filter is designed through MATLAB using the '**kaiserord**' instruction. Given a set of specifications in the frequency domain, '**kaiserord**' estimates the minimum order of the FIR filter that will approximately meet the specification. The minimum order generated using this instruction for the given specification is 5019. Although this filter specification is not practical for hardware development, for the simulation work in this thesis, it is acceptable. Figure B-5 illustrates the filtered ECG signals of the 30 seconds ECG recording shown in Figure B-3. The filtered ECG values are saved as MATLAB *.mat* files.

B3. Approximate the fiducial points

ECGPUWAVE can only detect the fiducial points of the ECG source if the ECG source is in the WFDB format.

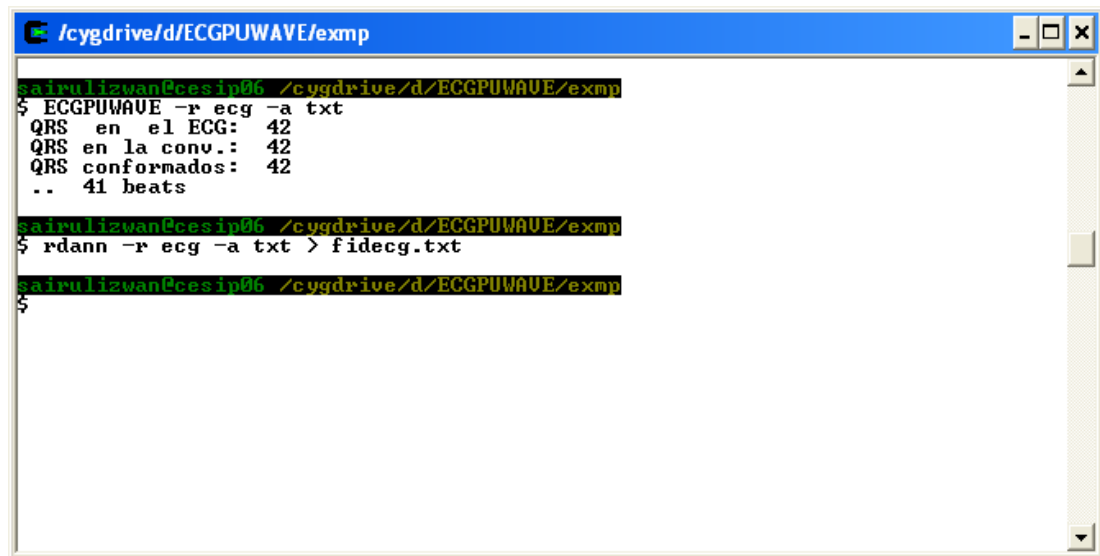
B3.1 Converting the filtered ECG signals into WFDB format.

The next step is to detect the fiducial locations of the ECG signals. The first step is to generate the original ECG signal ('s003911re.dat') in *.txt* format using **rdsamp** through Cygwin. Rename the generated *.txt* file as *samples.txt*. Using MATLAB, convert the filtered ECG signals into *.txt* following the format in '*samples.txt*'. The new converted file is name as '*myfile.txt*'. Next using Cygwin, convert the *myfile.txt* file into WFDB format.

B3.2 ECGPUWAVE

As shown in Figure B-6, **ECGPUWAVE** is used to analyses an ECG signal from the specified record, detecting the QRS complexes and locating the beginning, peak, and end of the P, QRS, and ST-T waveforms. The fiducial locations of the filtered ECG

are in the *.txt* format. In this example, we name the fiducial locations file as 'fidecg.txt'.



```

/cygdrive/d/ECGPUWAVE/exmp
sairulizwan@cesip06 /cygdrive/d/ECGPUWAVE/exmp
$ ECGPUWAVE -r ecg -a txt
QRS en el ECG: 42
QRS en la conv.: 42
QRS conformados: 42
.. 41 beats
sairulizwan@cesip06 /cygdrive/d/ECGPUWAVE/exmp
$ rdann -r ecg -a txt > fidecg.txt
sairulizwan@cesip06 /cygdrive/d/ECGPUWAVE/exmp
$

```

Figure B-6 : ECGPUWAVE fiducial detection process

Figure B-7 shows an example of the fidecg.txt output file between 2.67 and 3.149 seconds. As can be seen from Figure B-7, the first and second column indicates the fiducial locations in time and sampling point. The third column indicates the types of fiducial detected in those locations which are either the peaks of P wave ("p"), T wave ("t") or QRS wave ("N"). For example, in Figure B-7, it is shown that the peak of the P wave occurs at 2.698 seconds or 2698 sampling intervals after the beginning of the ECG recording. In using the **ECGPUWAVE**, the fourth and fifth columns are unused. The last column is called **num** and indicates specific information of the detected fiducial. **ECGPUWAVE** classifies each T wave as type 0 (normal), 1 (inverted), 2 (positive monophasic), 3 (negative monophasic), 4 (biphasic negative-positive), or 5 (biphasic positive-negative); this numeric classification is written into the **num** field each TWAVE row. The P, QRS, and T waveform onsets and ends are marked in the output annotation file using WFON ("(") and WFOFF (")") annotations. The **num** field of each WFON and WFOFF annotation designates the type of waveform with which it is associated: 0 for a P wave, 1 for a QRS complex, or 2 for a T wave.

0:02.670	2670	(0	0	0
0:02.698	2698	p	0	0	0
0:02.740	2740)	0	0	0
0:02.763	2763	(0	0	1
0:02.807	2807	N	0	0	0
0:02.833	2833)	0	0	1
0:02.956	2956	(0	0	2
0:03.065	3065	t	0	0	0
0:03.149	3149)	0	0	2

Figure B-7: ECGPUWAVE output file

B3. Quality Check, Averaging and Changing the DC offset

As explain in section 4-7-1, quality check is performed on each 30 second recordings to obtain a high quality ECG complex. This is done by calculating the average distance between the peak of R to the peak of P and T defined in the pre-processing step for the duration of the 30-second recordings. A tolerance of 50 sampling points is introduced into both average distance value so that the acceptable limit of all peaks locations is defined. There are 42 ECG complexes detected using ECGPUWAVE in previous steps. Figure B-8 illustrates the fiducial locations of the example ECG source detected using ECGPUWAVE.

The next step as described in Figure 4-11 is the quality check process. This process is to ensure that the ECG complex segmented from the ECGPUWAVE are within the acceptable heart rate that exhibits visibly clear and apparent P, QRS, and T waves.

The fiducial points are then used to break the ECG recording into single complexes as shown in Figure B-9. As explained in section 4.7.1, only the first 5 ECG complexes are considered. Since in there are 4 different extracted locations intended for extraction as described in section 4.5, the breaking up process for these locations are done separately.

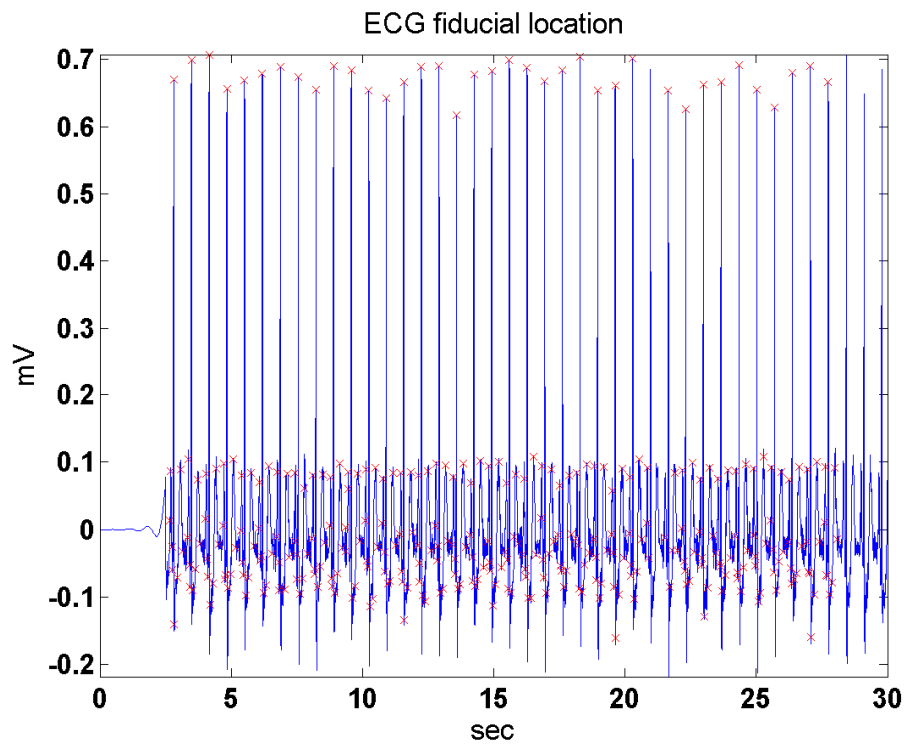


Figure B-8: Fiducial Locations

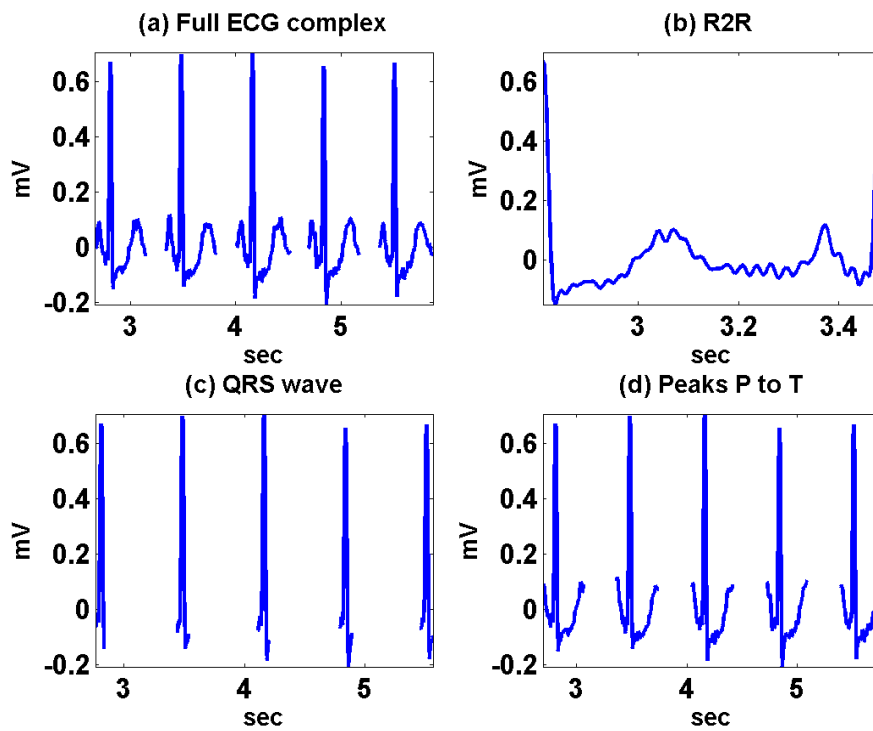


Figure B-9: Segmentation of ECG

Except ECG signals taken between peaks R to the next peaks of R, these ECG segments are averaged. This is done by aligning these ECG at the peaks of R before averaging them. Figure B-10 illustrates the average ECG of 5 ECG complexes.

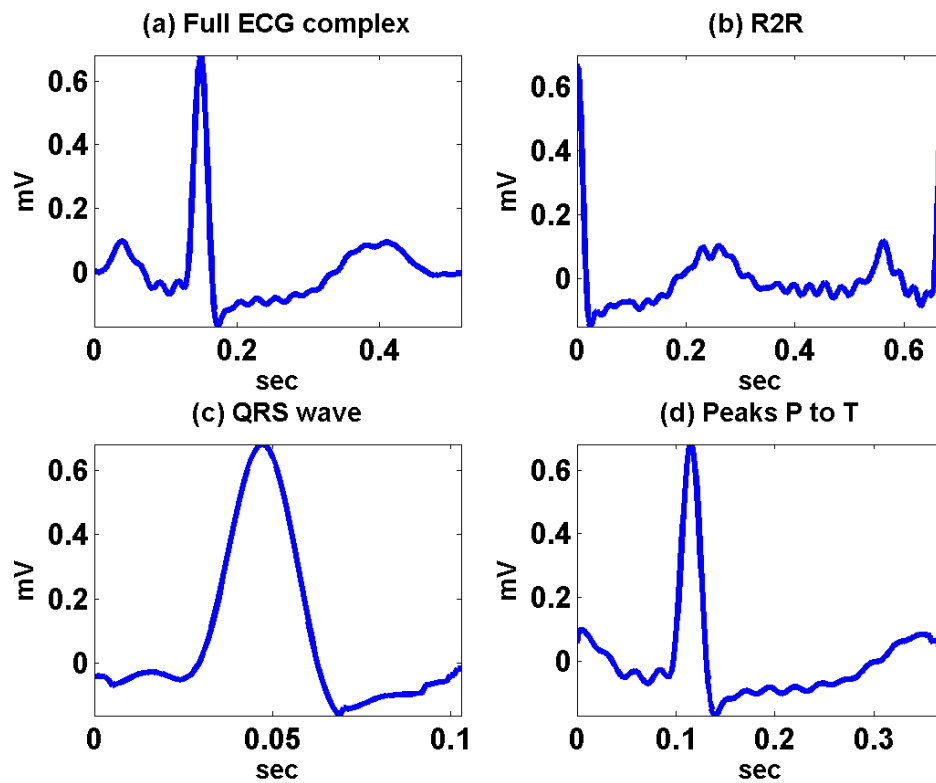


Figure B-10: Average ECG signals

As can be seen from Figure B-10, the starting and ending points of the average ECG signals are as defined as in section 4.5 expect in Figure B-10 d). To ensure the ECG signals as shown in Figure B-10 d) follow the definition of peaks P to T, the minimum values of the average ECGs are detected and used to change their DC offset to zero. A peak detection algorithm by Billauer [119] is then manually used to correct the peaks location of ECG signal in Figure B-10 d). The final ECG signals used to setup the training or test database are shown in Figure B-11.

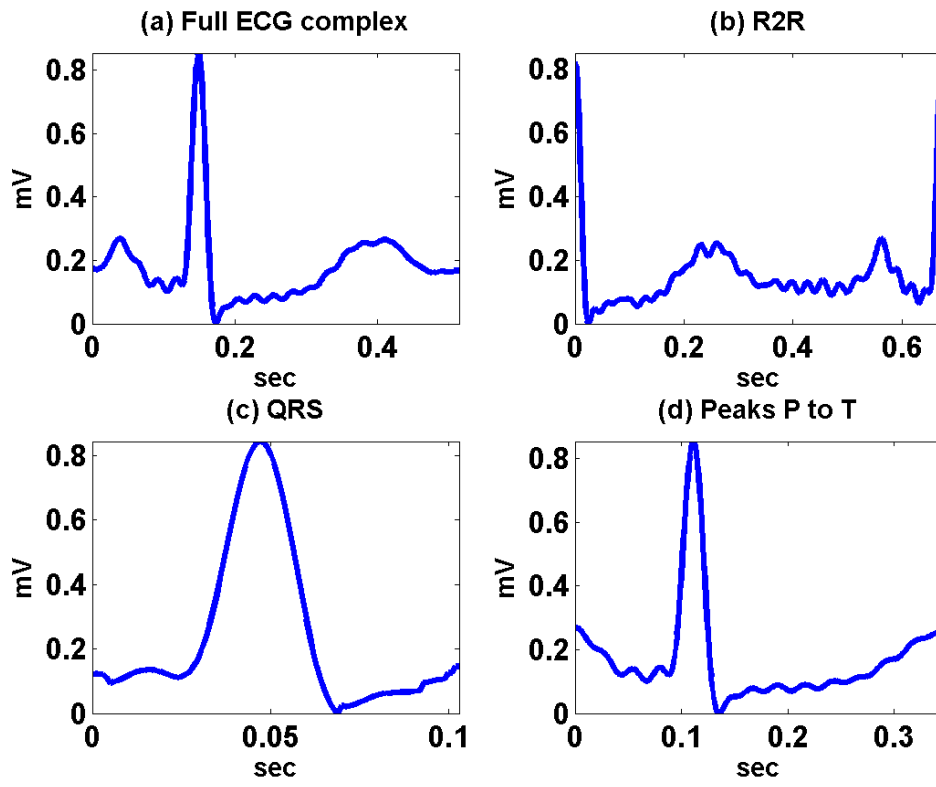
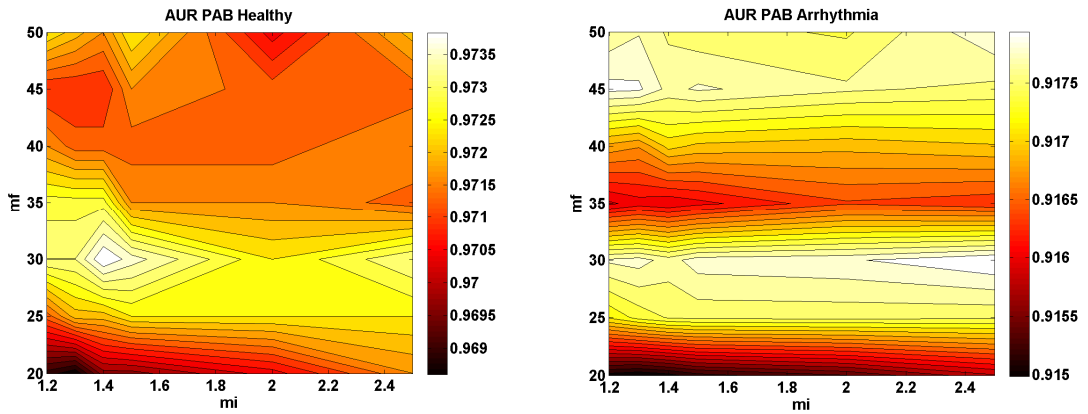


Figure B-11 : Final ECG signals for t

C. AUR and EER performance for PA feature extraction technique using suggested PA Parameters

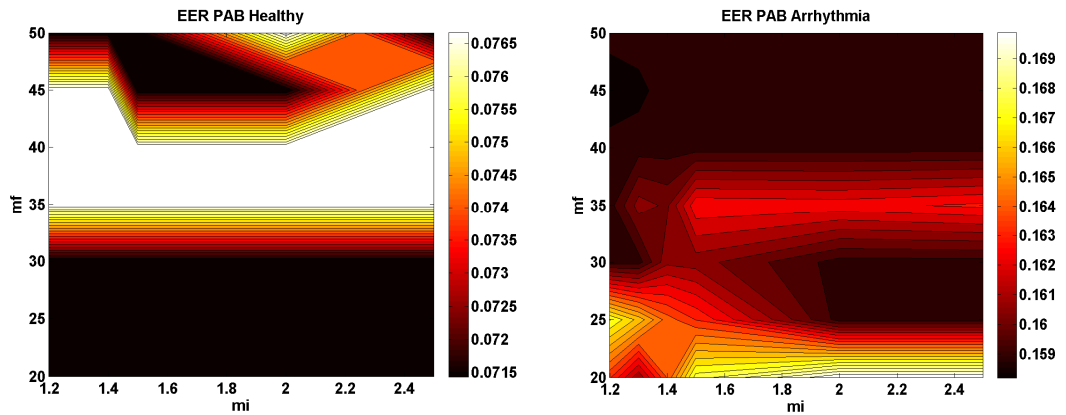
Figure C-1 to C-A14 illustrates the AUR and EER profile for PA feature selection technique when PA parameters are set as suggested from (4-36) to (4-40).



(a) AUR Healthy

(b) AUR Arrhythmia

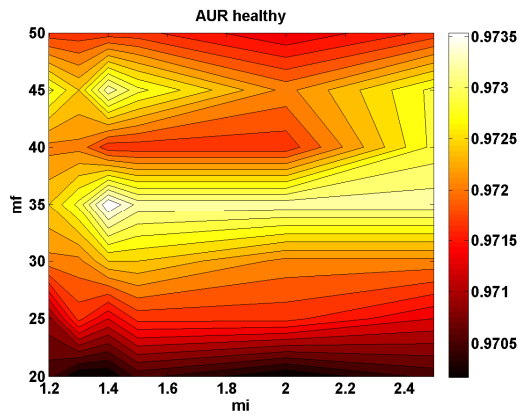
Figure C-1: AUR profile for PAB when m_f and m_i vary



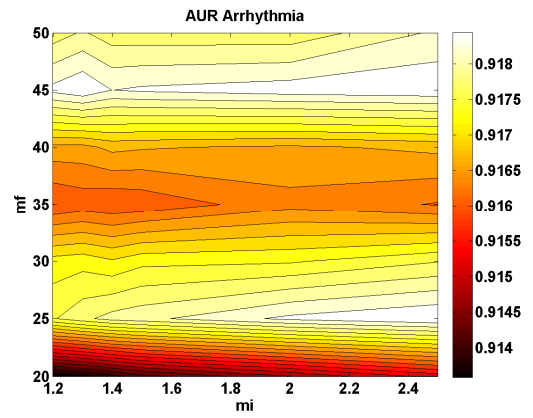
(a) EER Healthy

(b) EER Arrhythmia

Figure C-2: EER profile for PAB when m_f and m_i vary

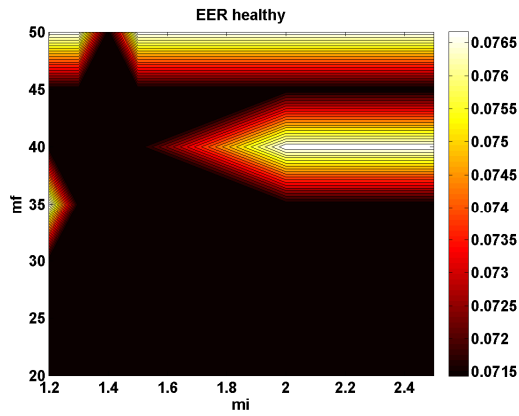


(a) AUR Healthy

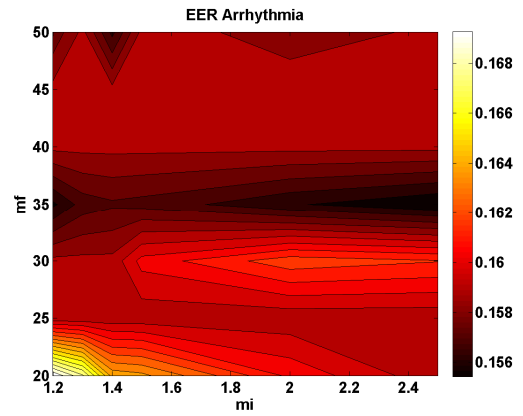


(b) AUR Arrhythmia

Figure C-3: AUR profile for PAW, PAA and PAM when m_f and m_i vary

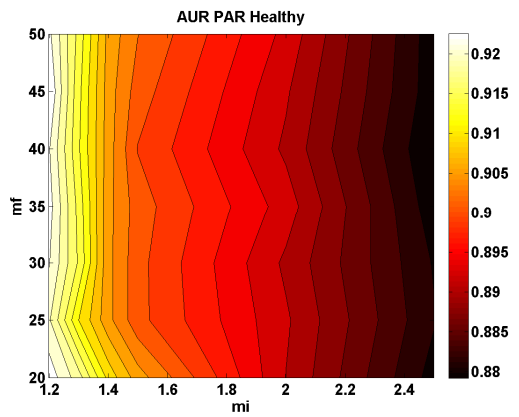


(a) EER Healthy

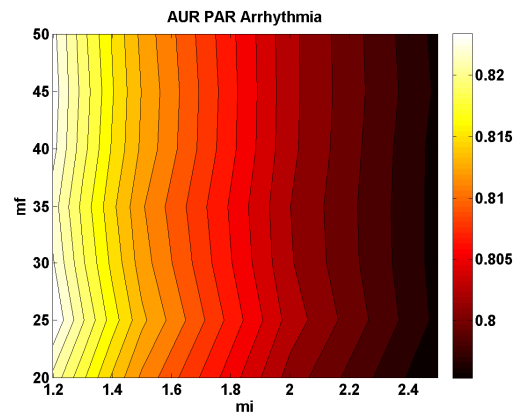


(b) EER Arrhythmia

Figure C-4: EER profile for PAW, PAA and PAM when m_f and m_i vary

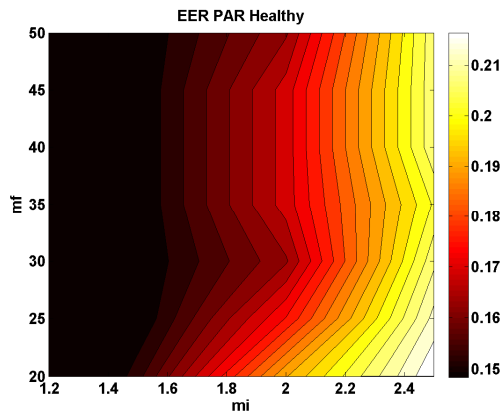


(a) AUR Healthy

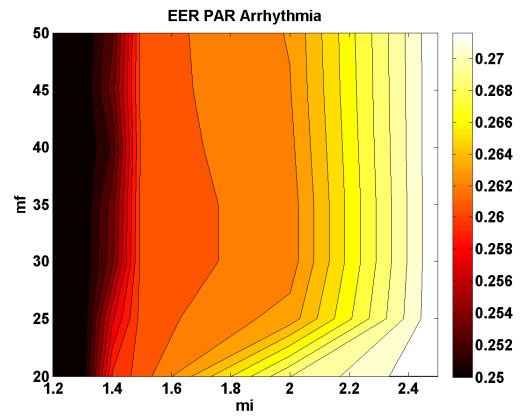


(b) AUR Arrhythmia

Figure C-5: AUR profile for PAR when m_f and m_i vary

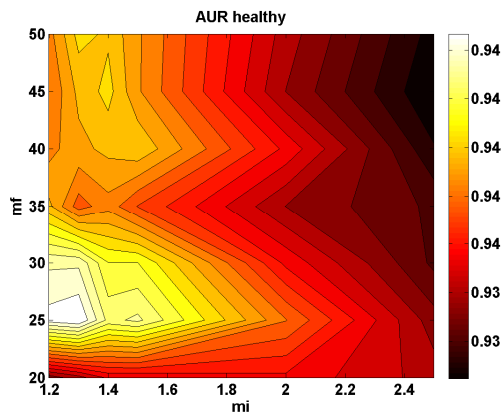


(a) EER Healthy

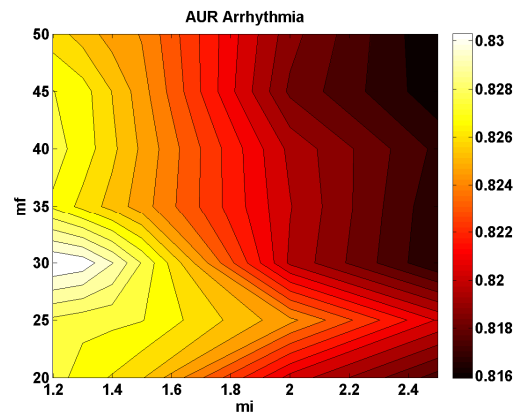


(b) EER Arrhythmia

Figure C-6: EER profile for PAR when m_f and m_i vary

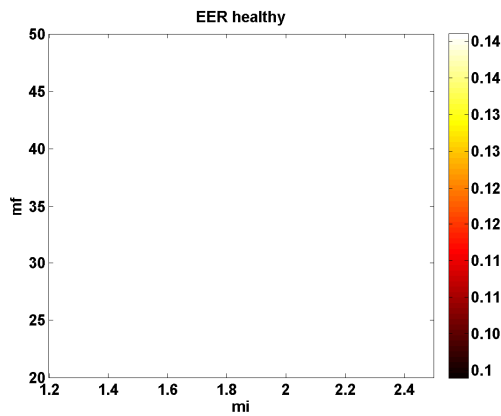


(a) AUR Healthy

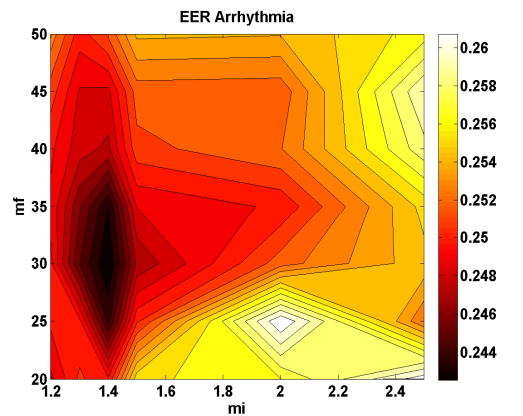


(b) AUR Arrhythmia

Figure C-7: AUR profile for PAH when m_f and m_i vary

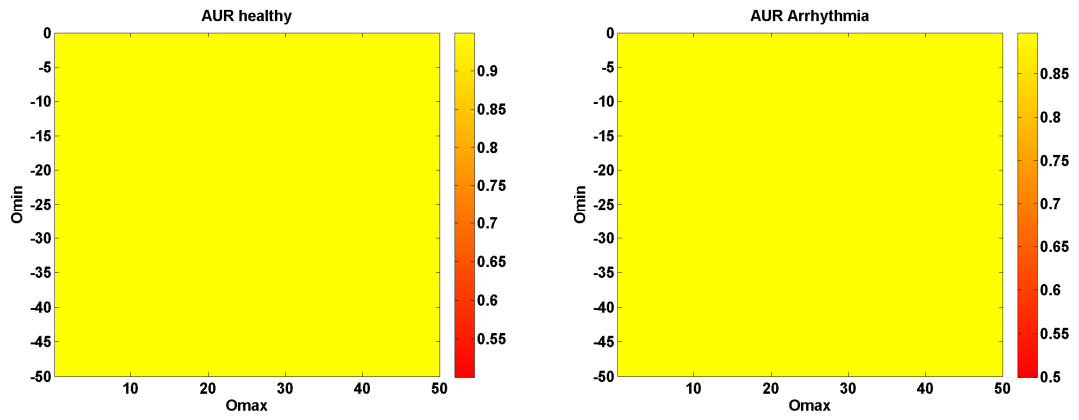


(b) EER Healthy

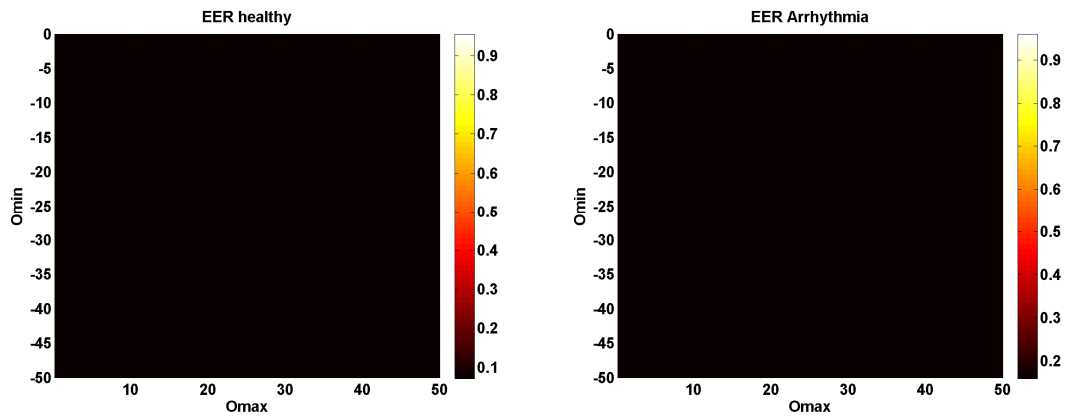


(b) EER Arrhythmia

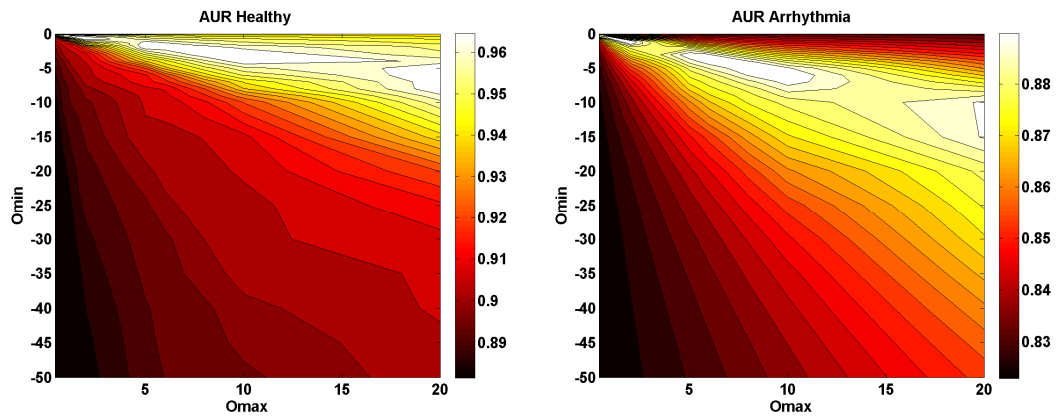
Figure C-8: EER profile for PAH when m_f and m_i vary



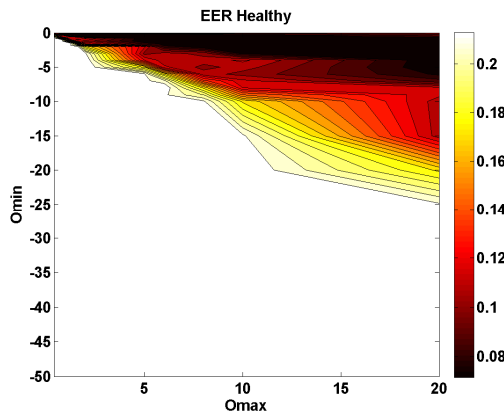
(a) AUR Healthy (b) AUR Arrhythmia
 Figure C-9: AUR profile for PAA and PAM when O_{\max} and O_{\min} vary



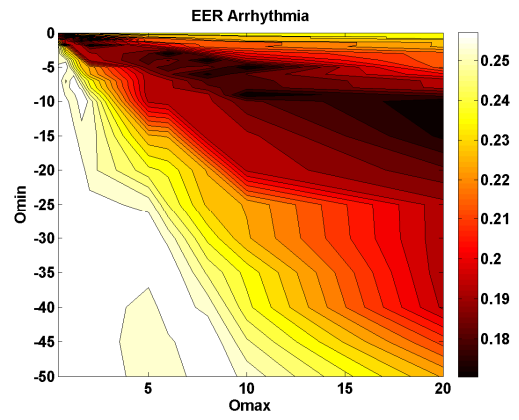
(a) EER Healthy (b) EER Arrhythmia
 Figure C-10: EER profile for PAA and PAM when O_{\max} and O_{\min} vary



(a) AUR Healthy (b) AUR Arrhythmia
 Figure C-11: AUR profile for PAR when O_{\max} and O_{\min} vary

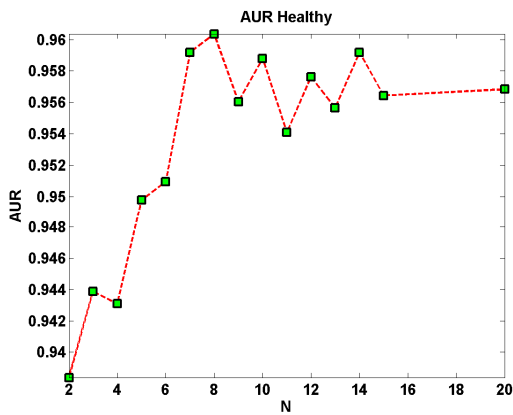


(a) EER Healthy

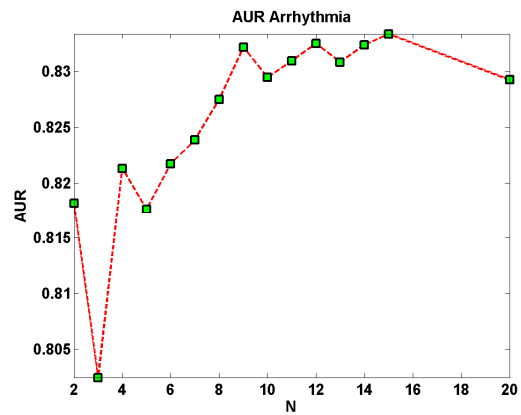


(b) EER Arrhythmia

Figure C-12: EER profile for PAR when O_{max} and O_{min} vary

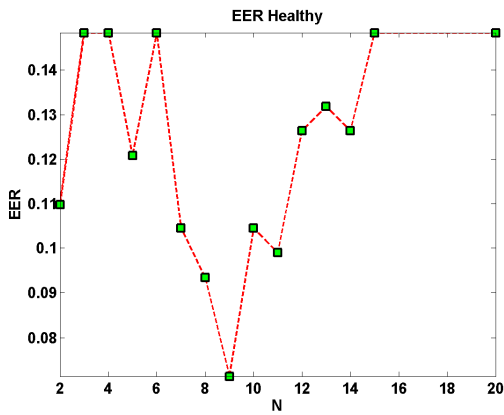


(a) AUR Healthy

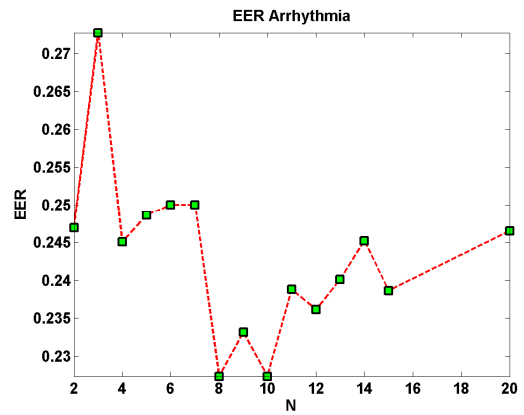


(b) AUR Arrhythmia

Figure C-13: AUR profile for PAH when N varies



(b) EER Healthy



(b) EER Arrhythmia

Figure C-14: EER profile for PAH when N varies

D. AUR and EER performance for APA feature extraction technique using suggested APA Parameters

Figure D-1 to D-16 illustrates the AUR and EER profile for APA feature selection technique when APA parameters are set as suggested from subsection 5.5.4.4

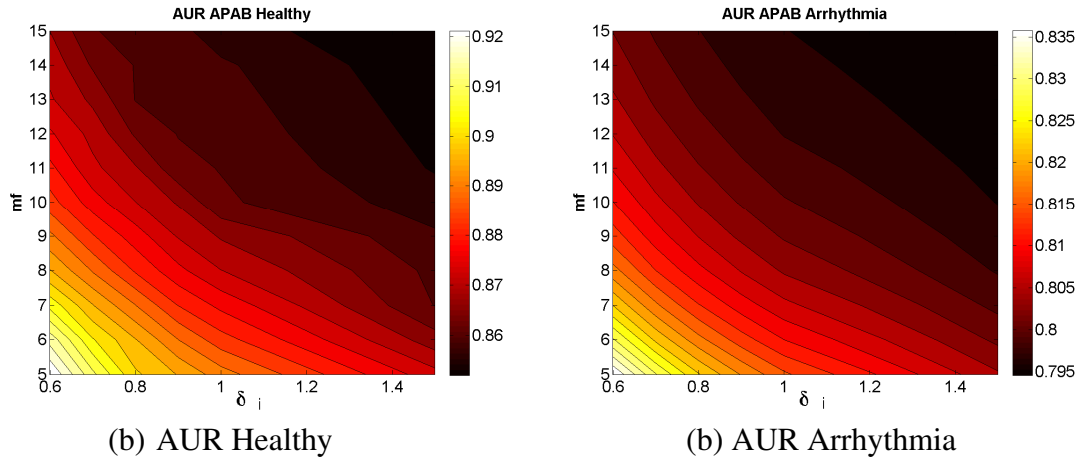


Figure D-1: AUR profile for APAB when m_f and δ_i vary

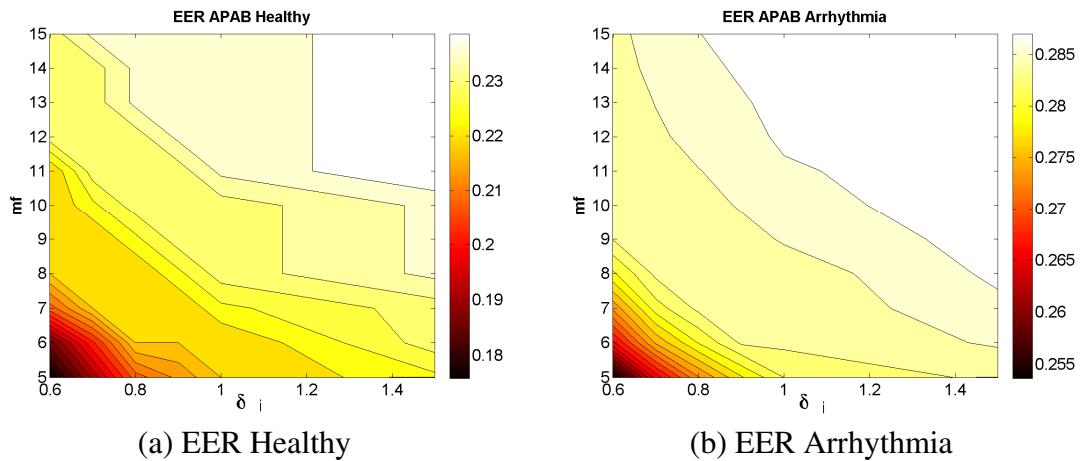
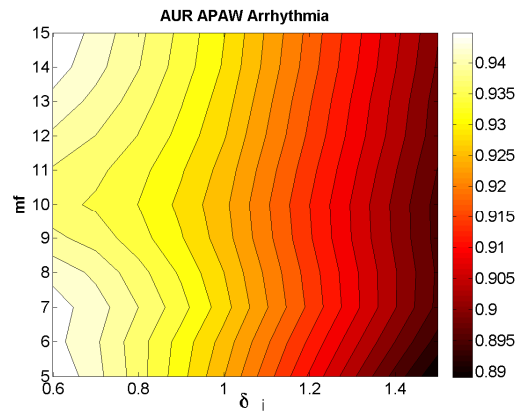
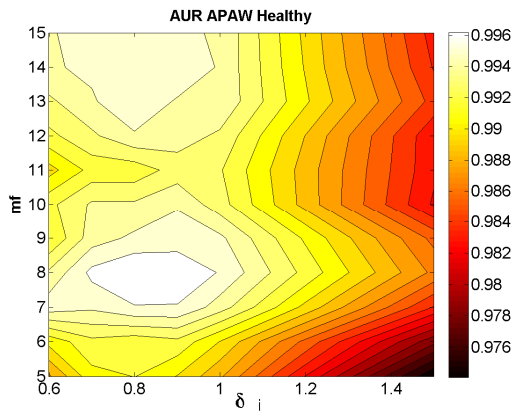


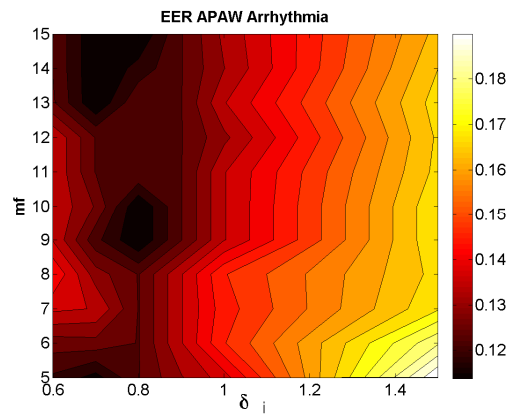
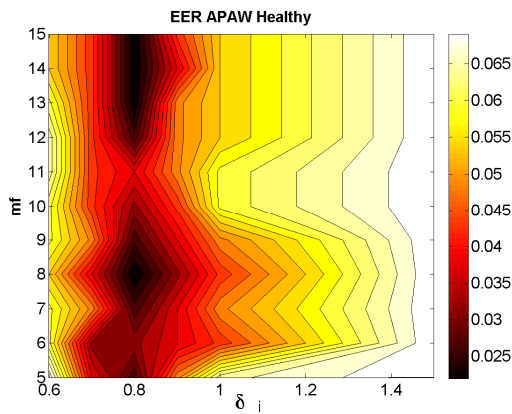
Figure D-2: EER profile for APAB when m_f and δ_i vary



(b) AUR Healthy

(b) AUR Arrhythmia

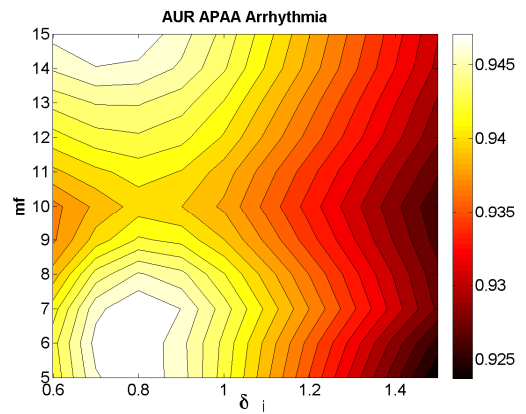
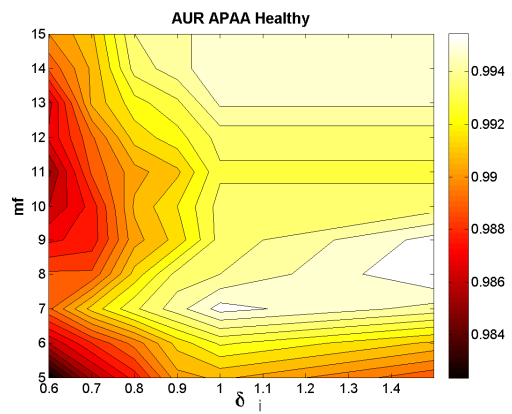
Figure D-3: AUR profile for APAW when m_f and δ_i vary



(a) EER Healthy

(b) EER Arrhythmia

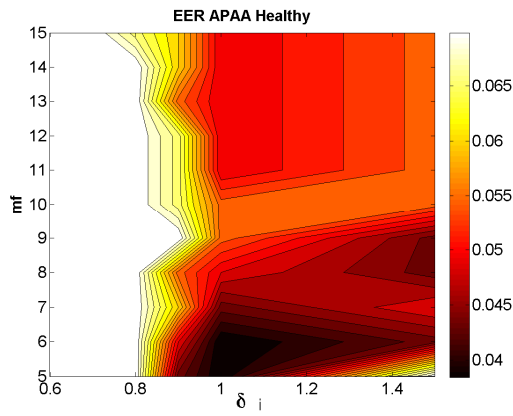
Figure D-4: EER profile for APAW when m_f and δ_i vary



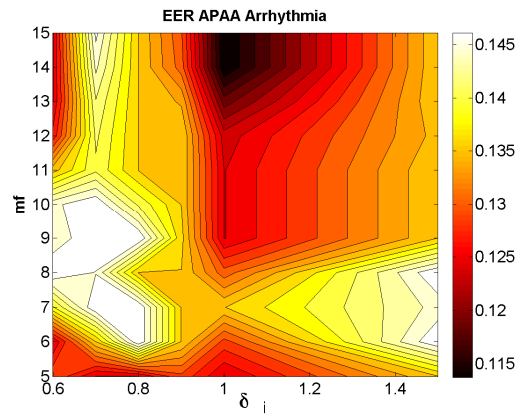
(b) AUR Healthy

(b) AUR Arrhythmia

Figure D-5: AUR profile for APAA when m_f and δ_i vary

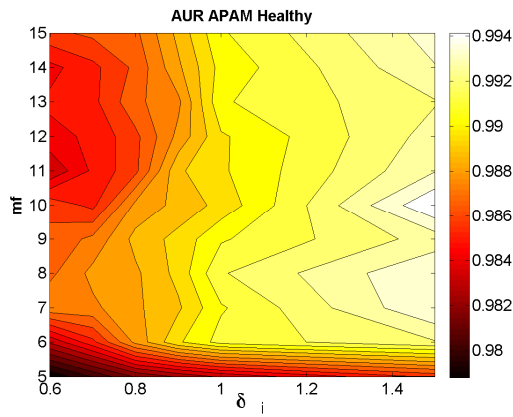


(b) EER Healthy

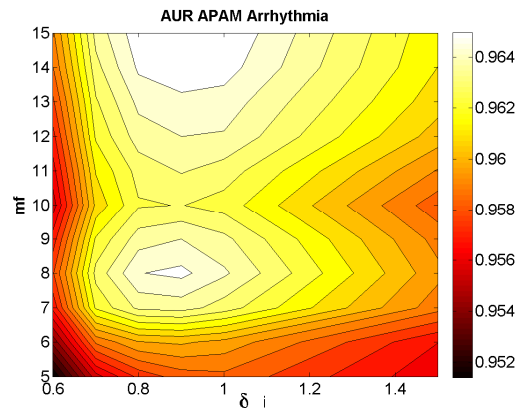


(b) EER Arrhythmia

Figure D-6: EER profile for APAA when m_f and δ_i vary

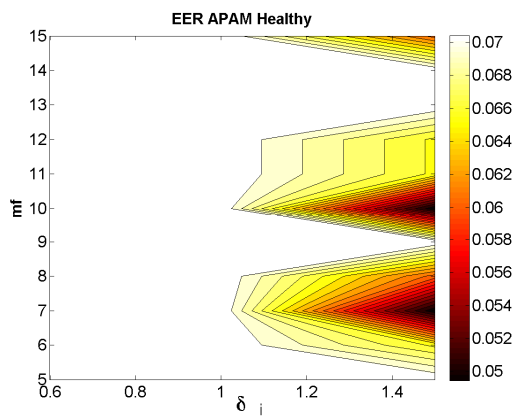


(c) AUR Healthy

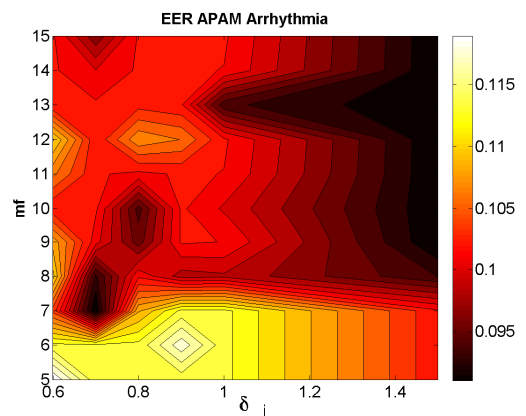


(b) AUR Arrhythmia

Figure D-7: AUR profile for APAM when m_f and δ_i vary

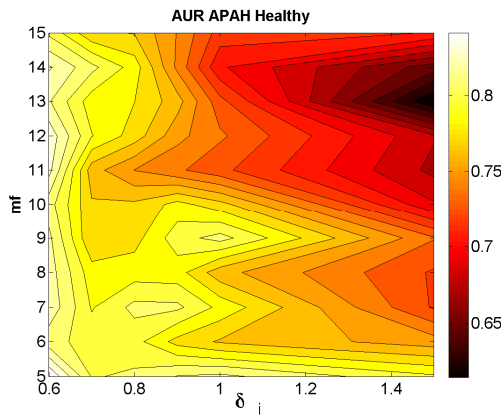


(d) EER Healthy

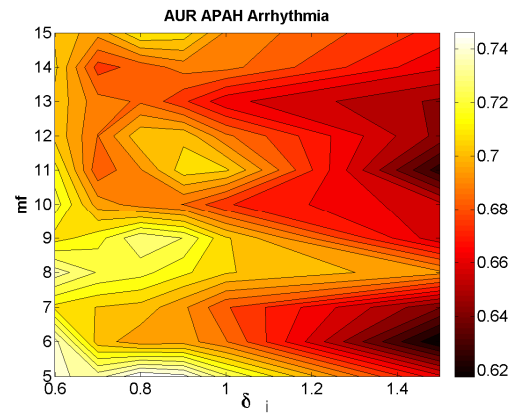


(b) EER Arrhythmia

Figure D-8: EER profile for APAM when m_f and δ_i vary

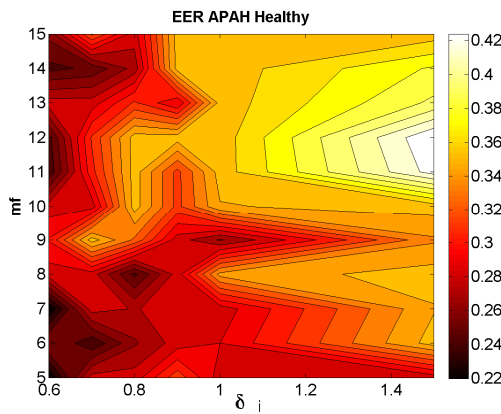


(e) AUR Healthy

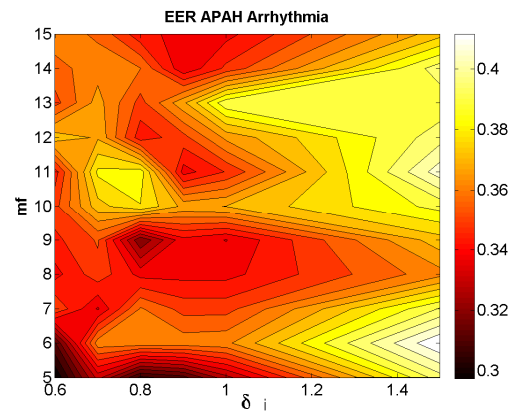


(b) AUR Arrhythmia

Figure D-9: AUR profile for APAA when m_f and δ_i vary

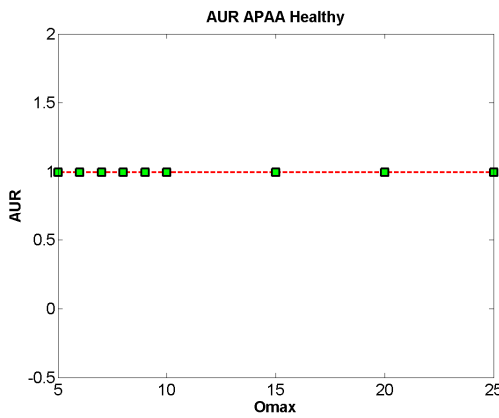


(f) EER Healthy

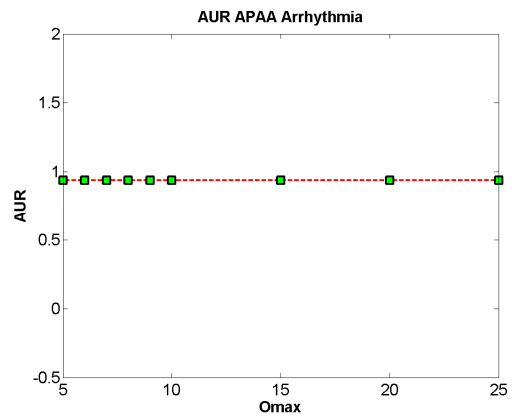


(b) EER Arrhythmia

Figure D-10: EER profile for APAA when m_f and δ_i vary

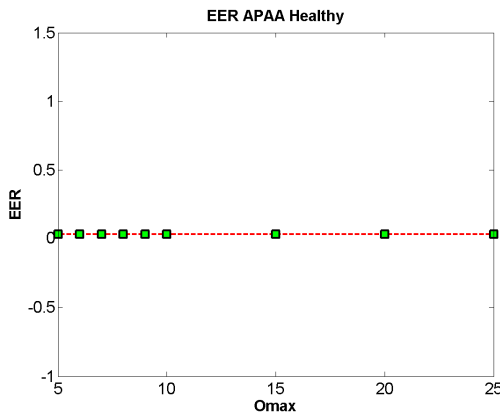


(c) AUR Healthy

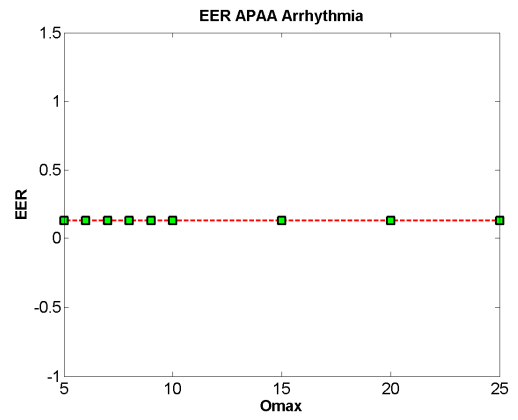


(b) AUR Arrhythmia

Figure D-11: AUR profile for APAA when O_{\max} and O_{\min} vary

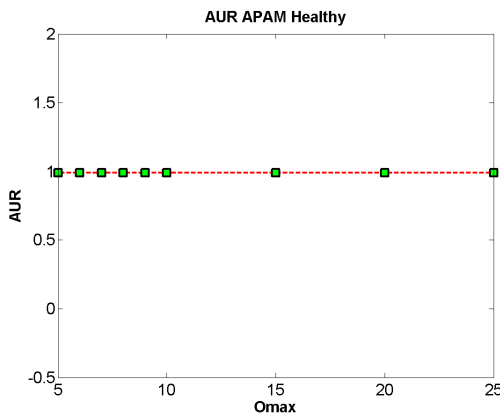


(d) EER Healthy

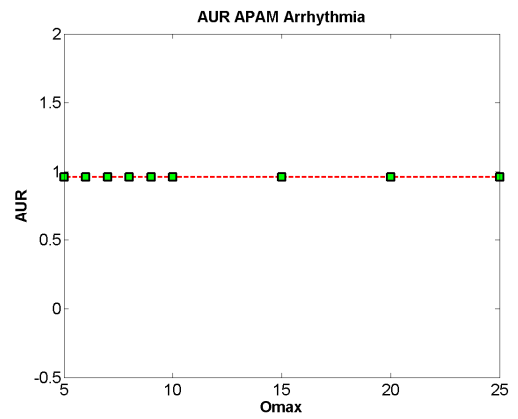


(b) EER Arrhythmia

Figure D-12: EER profile for APAA when O_{\max} and O_{\min} vary

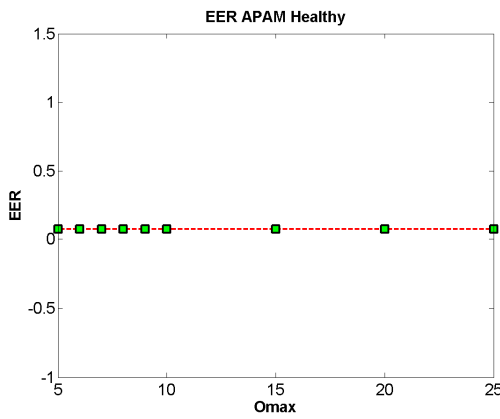


(b) AUR Healthy

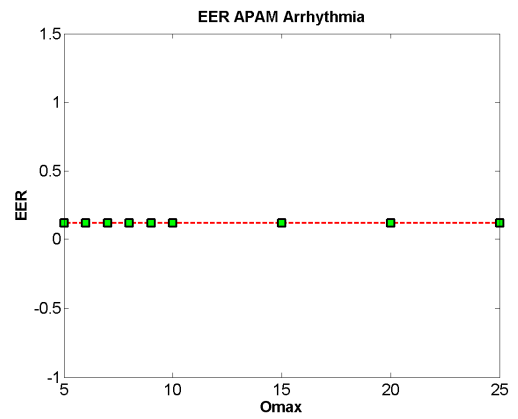


(b) AUR Arrhythmia

Figure D-13: AUR profile for APAM when O_{\max} and O_{\min} vary

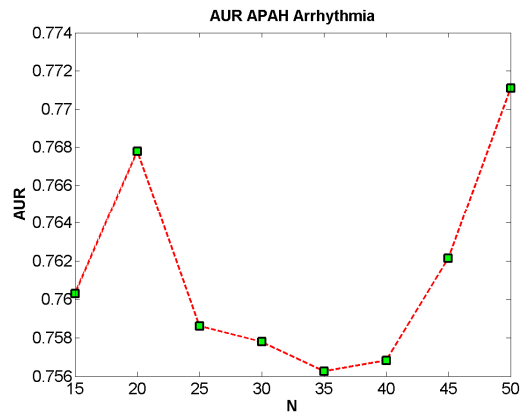
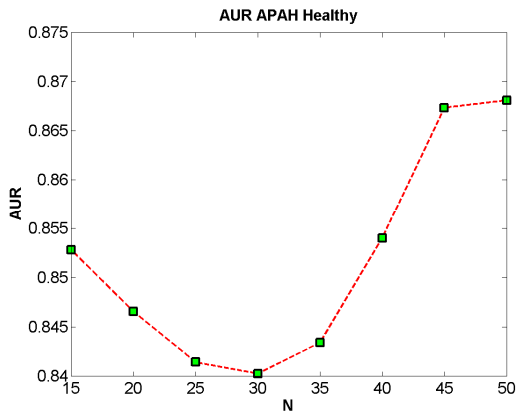


(a) EER Healthy



(b) EER Arrhythmia

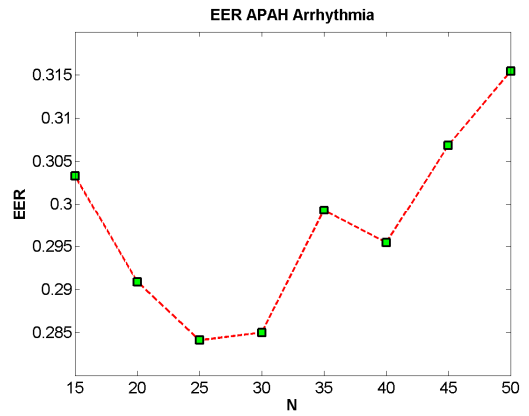
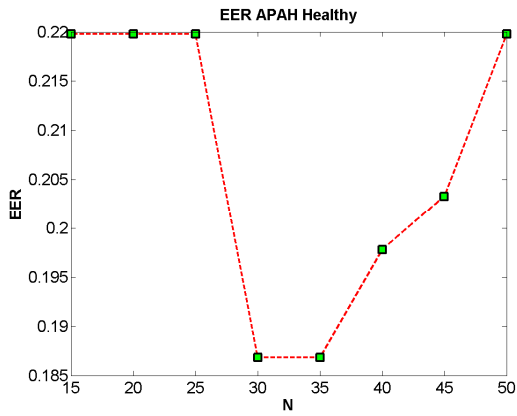
Figure D-14: EER profile for APAM when O_{\max} and O_{\min} vary



(c) AUR Healthy

(b) AUR Arrhythmia

Figure D-15: AUR profile for APAH when N varies



(d) EER Healthy

(b) EER Arrhythmia

Figure D-16: EER profile for APAH when N varies

E. Example of PA and APA performance on non biometric applications

The ECG recording requirements outlined in subsection 3.4.1 is reduced to only healthy subjects, the training and test database may come from the same recording and the ECG source may come from unpractical biometric leads (not limited to Lead I). These steps are necessary due to the difficulty of finding public ECG databases which meet the requirement in subsection 3.4.1. In this study, 58 healthy subjects from the Fantasia [131], Apnea [132] and MIT-BIH Normal Sinus Rhythm Database [3] are used. Each subject from these databases has their ECGs recording divided into 2 separate recordings. The first part of the recording is used to set up the training database while the second part of the recording is used to set up the test database. PAW and APAW is used to evaluate the performance of these databases..

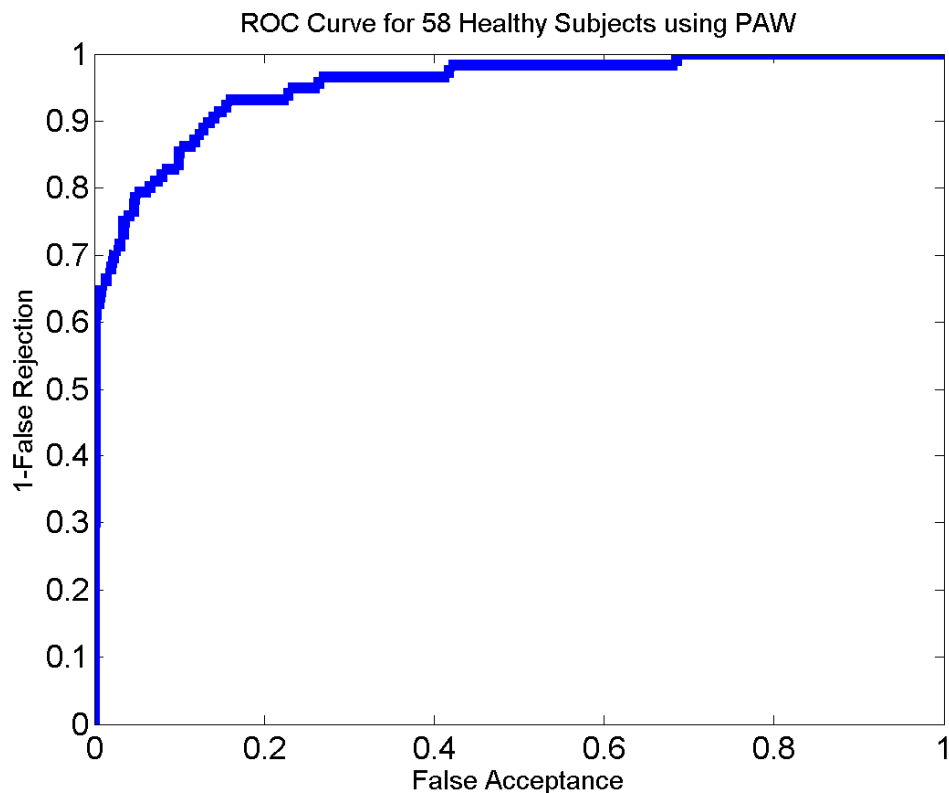


Figure E-1: ROC performance curve for 58 Healthy Subjects using PAW

The ROC curve for the 58 healthy subjects extracted using PAW is shown in Figure E-1. The m_f and m_i values to generate the feature vectors of the ROC curve are 25 and 1.5 respectively. From Figure E1, the AUR and EER values for these 58 healthy populations are 0.953 and 0.1210 respectively.

APAW is then used to evaluate the databases. The ROC curve for the 58 healthy subjects extracted using APAW is shown in Figure E-2. The δ_i and m_f are set to 0.6 and 7 respectively. From Figure E-1, the AUR and EER values for these 58 healthy populations are 0.948 and 0.1210 respectively.

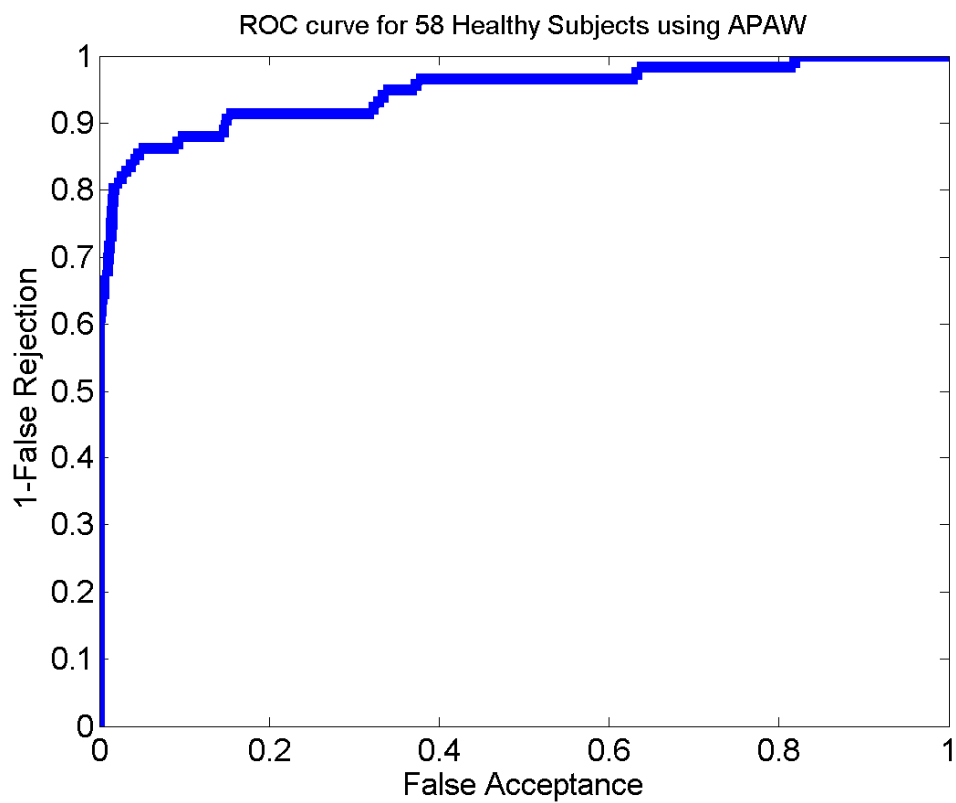


Figure E-2: ROC performance curve for 58 Healthy Subjects using APAW

REFERENCES

- [1] L. Gunn. "Skimming attacks at European ATMs rise 24%, although related losses fall 8%," 13 October, 2010; www.european-atm-security.eu.
- [2] G. Webster. "Biometric ATM gives cash via finger vein scan," 13 October, 2010; CNN articles.
- [3] A. Goldberger, L. Amaral, L. Glass *et al.*, "PhysioBank, PhysioToolkit, and PhysioNet: Components of a New Research Resource for Complex Physiologic Signals," *Circulation*, vol. 101, no. 23, pp. 215-220, 2000.
- [4] M. Faundez-Zanuy, "Biometric security technology," *IEEE Aerospace and Electronic Systems Magazine*, vol. 21, no. 6, pp. 15-26, 2006.
- [5] A. K. Jain, A. Ross, and S. Prabhakar, "An introduction to biometric recognition," *IEEE Transactions on Circuits and Systems for Video Technology*. vol. 14, no. 1, pp. 4-20, 2004.
- [6] A. Damato. "Biometric functionality," 08 September, 2011; <http://en.wikipedia.org/wiki/Biometrics>.
- [7] D. Gafurov, and E. Snekkenes, "Towards understanding the uniqueness of gait biometric," in 8th IEEE International Conference on Automatic Face & Gesture Recognition, 2008. FG '08. , 2008, pp. 1-8.
- [8] L. Lei, and D. Huichuan, "The Research of handwritten signatures," in IEEE International Symposium on IT in Medicine & Education, 2009. ITIME '09., 2009, pp. 1066-1069.
- [9] L. C. F. Araujo, L. H. R. Sucupira, Jr., M. G. Lizarraga *et al.*, "User authentication through typing biometrics features," *IEEE Transactions on Signal Processing*, , vol. 53, no. 2, pp. 851-855, 2005.
- [10] S. Furui, "Recent advances in speaker recognition," *Pattern Recognition Letter*, vol. 18, no. 9, pp. 859-872 September 1997.
- [11] S. Xiaoxin, and R. N. J. Veldhuis, "Grip-Pattern Verification for Smart Gun Based on Maximum-Pairwise Comparison and Mean-Template Comparison,"

- in 2nd IEEE International Conference on Biometrics: Theory, Applications and Systems, 2008. BTAS 2008. , 2008, pp. 1-5.
- [12] K.-M. L. Xudong Xie, “Facial expression recognition based on shape and texture,” *Pattern Recognition*, vol. 42, no. 5, pp. 1003-1011, May 2009.
- [13] E. P. Kukula, and S. J. Elliott, “Evaluation of a facial recognition algorithm across three illumination conditions,” *IEEE Aerospace and Electronic Systems Magazine*, vol. 19, no. 9, pp. 19-23, 2004.
- [14] S. Pankanti, S. Prabhakar, and A. K. Jain, “On the individuality of fingerprints,” *IEEE Transactions on Pattern Analysis and Machine Intelligence*, vol. 24, no. 8, pp. 1010-1025, 2002.
- [15] C. Yi, G. Parziale, E. Diaz-Santana *et al.*, “3D Touchless Fingerprints: Compatibility with Legacy Rolled Images,” in 2006 Biometrics Symposium: Special Session on Research at the Biometric Consortium Conference, 2006, pp. 1-6.
- [16] R. Sanchez-Reillo, C. Sanchez-Avila, and A. Gonzalez-Marcos, “Biometric identification through hand geometry measurements,” *IEEE Transactions on Pattern Analysis and Machine Intelligence*, vol. 22, no. 10, pp. 1168-1171, 2000.
- [17] W. W. Boles, and B. Boashash, “A human identification technique using images of the iris and wavelet transform,” *IEEE Transactions on Signal Processing*, vol. 46, no. 4, pp. 1185-1188, 1998.
- [18] H. Borgen, P. Bours, and S. D. Wolthusen, “Visible-Spectrum Biometric Retina Recognition,” in International Conference on Intelligent Information Hiding and Multimedia Signal Processing, 2008. IHHMSP '08 2008, pp. 1056-1062.
- [19] K. Nakajima, Y. Mizukami, K. Tanaka *et al.*, “Footprint-based personal recognition,” *IEEE Transactions on Biomedical Engineering*, vol. 47, no. 11, pp. 1534-1537, 2000.
- [20] L. Wang, G. Leedham, and S. Y. Cho, “Infrared imaging of hand vein patterns for biometric purposes,” *IET Computer Vision*, , vol. 1, no. 3-4, pp. 113-122, 2007.

- [21] L. Chih-Lung, and F. Kuo-Chin, "Biometric verification using thermal images of palm-dorsa vein patterns," *IEEE Transactions on Circuits and Systems for Video Technology*, vol. 14, no. 2, pp. 199-213, 2004.
- [22] S. Marcel, and J. D. R. Millan, "Person Authentication Using Brainwaves (EEG) and Maximum A Posteriori Model Adaptation," *IEEE Transactions on Pattern Analysis and Machine Intelligence*, vol. 29, no. 4, pp. 743-752, 2007.
- [23] C. Miyamoto, S. Baba, and I. Nakanishi, "Biometric person authentication using new spectral features of electroencephalogram (EEG)," in International Symposium on Intelligent Signal Processing and Communications Systems, 2008. ISPACS 2008. , 2009, pp. 1-4.
- [24] R. Hoekema, G. J. H. Uijen, and A. van Oosterom, "Geometrical aspects of the inter-individual variability of multilead ECG recordings," in Computers in Cardiology 1999, 1999, pp. 499-502.
- [25] L. Green, R. Lux, C. Haws *et al.*, "Effects of age, sex and body habitus on QRS and ST-T potential maps of 1100 normal subjects," *Circulation*, vol. 71, no. 2, pp. 244-253, 1985.
- [26] M. Faundez-Zanuy, J. Fierrez-Aguilar, J. Ortega-Garcia *et al.*, "Multimodal biometric databases: an overview," *Aerospace and Electronic Systems Magazine, IEEE*, vol. 21, no. 8, pp. 29-37, 2006.
- [27] S. A. Shaikh, and C. K. Dimitriadis, "My fingers are all mine: Five reasons why using biometrics may not be a good idea," in International Symposium on Biometrics and Security Technologies, 2008. ISBAST 2008, 2008, pp. 1-5.
- [28] N. Abhishek, N. Karthik, and J. A. K, "Biometric Template Transformation: A Security Analysis," in Proceedings of SPIE, Electronic Imaging, Media Forensics and Security XII.
- [29] A. Ross, and A. Jain, "Introduction to Biometric," *Handbook of Biometric*: Springer, 2008.
- [30] D. S. Wilks, "Multivariate Statistic - Euclidean Distance," *Statistical Methods in the Atmospheric Sciences*, p. 462, Amsterdam, Netherlands: Elsevier Inc, 2011.

- [31] Jiawei Han, M. Kamber, and J. Pei, "Dissimilarity of Numeric Data : Minkowski Distance," *Data Mining: Concepts and Techniques* pp. 72-73, Waltham, USA: Morgan Kaufmann Publishers, 2011.
- [32] A. R. Webb, "Measures of dissimilarity," *Statistical pattern recognition*, p. 421, West Sussex, England: John Wiley & Sons Ltd, 2002.
- [33] C. Preisach, H. Burkhardt, L. S. Thieme *et al.*, "Canberra distance- based similarity," *Data analysis, machine learning and applications*, p. 7, Berlin: Springer, 2008.
- [34] N. T. Nguyen, C.-G. Kim, and A. Janiak, "Performance Comparison of Similarity Measurements for Database Correlation Localization Method," *Intelligent Information and Database Systems*, p. 455, Berlin: Springer, 2011.
- [35] P.-N. Tan, M. Steinbach, and V. Kumar, "Introduction to Data Mining," p. 500: Addison-Wesley, 2005.
- [36] R. Zhu, Y. Zhang, B. Liu *et al.*, "Image Segmentation Based on FCM with Mahalanobis Distance," *Information Computing and Application*, p. 207, New York: Springer Berlin Heidelberg, 2010.
- [37] E. W. Weisstein. "Correlation Coefficient - From MathWorld--A Wolfram Web Resource.," October, 2011; <http://mathworld.wolfram.com/CorrelationCoefficient.html>.
- [38] T. Fawcett, "An introduction to ROC analysis," *Pattern Recognition Letters*, vol. 27, pp. 861-874, 2006.
- [39] A. J. Mansfield, and J. L. Wayman, "Best Practices in Testing and Reporting Biometric Devices," *Centre for Mathematics and Scientific Computing, National Physical Laboratory, Teddington, Middlesex*, August 2002.
- [40] A. P. Bradley, "The use of the area under the ROC curve in the evaluation of machine learning algorithms," *Pattern Recognition*, vol. 30, no. 7, pp. 1145-1159, 1997.
- [41] J. Heuser. "Electrical conduction system of the heart," 07 September, 2011; http://en.wikipedia.org/wiki/Electrical_conduction_system_of_the_heart.
- [42] D. Martin, "Components of the normal EKG waveform," *The Complete Study Guide To Learning The Electrocardiogram*, pp. 9-11, Surprise, Arizona: Mind-Forge Publishing, 2007.

- [43] N. M. Arzeno, D. Zhi-De, and P. Chi-Sang, "Analysis of First-Derivative Based QRS Detection Algorithms," *Biomedical Engineering, IEEE Transactions on*, vol. 55, no. 2, pp. 478-484, 2008.
- [44] J. Pan, and W. J. Tompkins, "A Real-Time QRS Detection Algorithm," *Biomedical Engineering, IEEE Transactions on*, vol. BME-32, no. 3, pp. 230-236, 1985.
- [45] N. V. Boulgouris, K. N. Plataniotis, and E. M. Tazanakou, "The Heartbeat : The Living Biometric," *Biometrics: theory, methods and application*, p. 436, Canada: John Wiley & Sons, Inc, 2010.
- [46] J. J. Goldberger, and J. Ng, "Formation of a Template for ECG Analysis: Identification of Fiducial Points," *Practical Signal and Image Processing in Clinical Cardiology*, pp. 125-126, London: Springer, 2010.
- [47] P. Laguna, R. Jan, E. Bogatell *et al.* "ECGPUWAVE," 08 September, 2009; <http://www.physionet.org/physiotools/wag/ecgpuw-1.htm>.
- [48] A. Goldberger, L. Amaral, L. Glass *et al.* "ECGPUWAVE," 08 September, 2009; <http://physionet.org/>.
- [49] P. Laguna, "New Electrocardiographic Signal Processing Techniques: Application to Long-term Records," Science Faculty, University of Zaragoza, 1990.
- [50] W. M. H. W. Mahmud, and M. B. Malarvili, "Comparative Analysis of Preprocessing Techniques for Quantification of Heart Rate Variability," *5th Kuala Lumpur International Conference on Biomedical Engineering 2011*, H.-N. Ting, ed., pp. 415-419: Springer, 2011.
- [51] P. W. Macfarlane, A. V. Oosterom, O. Pahlm *et al.*, "ECG Instrumentation : Application and Design (Safety Requirements for Electrodes)," *Comprehensive Electrocardiology*, pp. 459-461, London: Springer-Verlag, 2011.
- [52] K. M. Lewis, and K. A. Handal, "The ECG and the 12-Lead System," *Analysis of the 12-lead ECG*, pp. 9-18, Canada: Delmar Thomson Learning, 2000.
- [53] W. Allyn. "AHA Diagnostic ECG Electrode Placement," 09 September, 2010;

http://www.welchallyn.com/documents/Cardiopulmonary/Electrocardiographs/PC-Based%20Exercise%20Stress%20ECG/poster_110807_pcxerecg.pdf.

- [54] M. B. Conover, "The 12 Electrocardiogram Leads," *Understanding Electrocardiography*, pp. 3-7, Missouri: Mosby, 2003.
- [55] T. Moukabary, "Willem Einthoven (1860-1927) : Father of electrocardiography," *Cardiology Journal*, vol. 14, no. 3, pp. 316-317, 2007.
- [56] F. Sufi, I. Khalil, and J. Hu, "ECG Based Authentication," *Handbook of Information and Communication Security*, P. Stavroulakis and M. Stamp, eds., pp. 310-330, Berlin Heidelberg: Springer Verlag, 2010.
- [57] National_Research_Concil, "The evaluation of forensic DNA evidence," *The Evaluation of Forensic DNA Evidence*, p. 161, United States of America: National Academy Press, 1998.
- [58] T. Pilkington, R. Barr, and C. Rogers, "Effect of conductivity interfaces in electrocardiography," *Bulletin of Mathematical Biology*, vol. 30, no. 4, pp. 637-643, 1968.
- [59] D. N. Masica, M. D. B. J. Maron, and L. J. Krovetz, "Racial variations in the childhood electrocardiogram: Preliminary observations " *American Heart Journal*, vol. 84, no. 2, pp. 153, 1972.
- [60] P. S. Rao, M. K. Thapar, and R. J. Harp, "Racial variations in electrocardiograms and vectorcardiograms between black and white children and their genesis. ," *Journal of electrocardiology*, vol. 17, no. 3, pp. 239, 1984.
- [61] A. van Oosterom, R. Hoekema, and G. J. H. Uijen, "Geometrical factors affecting the interindividual variability of the ECG and the VCG," *Journal of electrocardiology*, vol. 33, pp. 219-227, 2000.
- [62] Yongjin Wang, F. Agrafioti, D. Hatzinakos *et al.*, "Analysis of Human Electrocardiogram for Biometric Recognition," *EURASIP Journal on Advances in Signal Processing*, vol. 2008, no. 148658, pp. 1-11, 2008.
- [63] G. Wuebbeler, R. Bousseljot, D. Kreiseler *et al.* "Human Verification by heart beat signals,"
<http://www.berlin.ptb.de/8/84/842/BIOMETRIE/842biometrie.html>.

- [64] E. B. Zeisler, and L. N. Katz, "Studies of the electrical field of the heart. I. Invariants of the electrocardiogram," *American Heart Journal*, vol. 8, no. 5, pp. 676-681, 1933.
- [65] M. Raju. "Heart-Rate and EKG Monitor Using the MSP430FG439," 11 October 2009; <http://focus.ti.com/general/docs/litabsmultiplefilelist.tsp?literatureNumber=slla280a>.
- [66] T. W. Shen, W. J. Tompkins, and Y. H. Hu, "One-lead ECG for identity verification," in *Engineering in Medicine and Biology*, 2002. 24th Annual Conference and the Annual Fall Meeting of the Biomedical Engineering Society EMBS/BMES Conference, 2002. Proceedings of the Second Joint, 2002, pp. 62-63 vol.1.
- [67] A. D. C. Chan, M. M. Hamdy, A. Badre *et al.*, "Wavelet Distance Measure for Person Identification Using Electrocardiograms," *Instrumentation and Measurement, IEEE Transactions on*, vol. 57, no. 2, pp. 248-253, 2008.
- [68] L. Biel, O. Pettersson, L. Philipson *et al.*, "ECG analysis: a new approach in human identification," *IEEE Transactions on Instrumentation and Measurement*, vol. 50, no. 3, pp. 808-812, 2001.
- [69] M. Kyoso, and A. Uchiyama, "Development of an ECG identification system," in *Engineering in Medicine and Biology Society*, 2001. Proceedings of the 23rd Annual International Conference of the IEEE, 2001, pp. 3721-3723 vol.4.
- [70] S. A. Israel, J. M. Irvine, A. Cheng *et al.*, "ECG to identify individuals," *Pattern Recognition*, vol. 38, no. 1, pp. 133-142, 2005.
- [71] F. Agrafioti, and D. Hatzinakos, "ECG Based Recognition Using Second Order Statistics," in *Communication Networks and Services Research Conference*, 2008. CNSR 2008. 6th Annual, 2008, pp. 82-87.
- [72] S.-C. Fang, and H.-L. Chan, "Human identification by quantifying similarity and dissimilarity in electrocardiogram phase space," *Pattern Recognition*, vol. 42, no. 9, pp. 1824-1831, 2009.

- [73] Y. Gahi, M. Lamrani, A. Zoglat *et al.*, “Biometric Identification System Based on Electrocardiogram Data,” in *New Technologies, Mobility and Security*, 2008. NTMS '08., 2008, pp. 1-5.
- [74] Y. Jianchu, and W. Yongbo, “A wavelet method for biometric identification using wearable ECG sensors,” in *Medical Devices and Biosensors*, 2008. ISSS-MDBS 2008. 5th International Summer School and Symposium on, 2008, pp. 297-300.
- [75] R. Palaniappan, and S. M. Krishnan, “Identifying individuals using ECG beats,” in *2004 International Conference on Signal Processing and Communications*, 2004. SPCOM '04, 2004, pp. 569-572.
- [76] K. N. Plataniotis, D. Hatzinakos, and J. K. M. Lee, “ECG Biometric Recognition Without Fiducial Detection,” in *2006 Biometrics Symposium: Special Session on Research at the Biometric Consortium Conference*, 2006, pp. 1-6.
- [77] S. Saechia, J. Koseeyaporn, and P. Wardkein, “Human Identification System Based ECG Signal,” in *IEEE Region 10 TENCON 2005* 2005, pp. 1-4.
- [78] T. W. Shen, W. J. Tompkins, and Y. H. Hu, "One-lead ECG for identity verification." pp. 62-63 vol.1.
- [79] G. Wübbeler, M. Stavridis, D. Kreiseler *et al.*, “Verification of humans using the electrocardiogram,” *Pattern Recognition Letters*, vol. 28, no. 10, pp. 1172-1175, 2007.
- [80] F. Agrafioti, and D. Hatzinakos, “Fusion of ECG sources for human identification,” in *Communications, Control and Signal Processing*, 2008. ISCCSP 2008. 3rd International Symposium on, 2008, pp. 1542-1547.
- [81] Y. Can, M. T. Coimbra, and B. V. K. V. Kumar, “Investigation of human identification using two-lead Electrocardiogram (ECG) signals,” in *Biometrics: Theory Applications and Systems (BTAS)*, 2010 Fourth IEEE International Conference on, 2010, pp. 1-8.
- [82] S. Chauhan, A. Arora, and A. Kaul, “A survey of emerging biometric modalities,” in *International Conference and Exhibition on Biometrics Technology*, India, 2012, pp. 213-218.

- [83] D. P. Couthinho, A. L. N. Fred, and M. A. T. Figueiredo, "One-lead ECG based personal identification using ziv-merhaz cross parsing," in 20th International Conference on Pattern Recognition (ICPR), 2010, pp. 3858-3861.
- [84] M. Homer, J. M. Irvine, and S. Wendelken, "A model-based approach to human identification using ECG," in Proceedings of SPIE, , Orlando Florida, USA, 2009, pp. 7306.
- [85] J. M. Irvine, B. K. Wiederhold, L. Gavshon *et al.*, "Heart Rate Variability : a new biometric for human identification," in International Conference on Artificial Intelligence (ICAI 2001), Las Vegas, Nevada, USA, 2001, pp. 1106–1111.
- [86] R. Matta, J. K. H. Lau, F. Agrafioti *et al.*, "Real-time continuous identification system using ECG signals," in Electrical and Computer Engineering (CCECE), 2011 24th Canadian Conference on, 2011, pp. 1313-1316.
- [87] B. Nasri, M. Guennoun, and K. El-Khatib, "Using ECG as a measure in biometric identification systems," in Science and Technology for Humanity (TIC-STH), 2009 IEEE Toronto International Conference, 2009, pp. 28-33.
- [88] T. W. Shen, and W. J. Tompkins, "Biometric Statistical Study of One-Lead ECG Features and Body Mass Index (BMI)," in Engineering in Medicine and Biology Society, 2005. IEEE-EMBS 2005. 27th Annual International Conference of the, 2005, pp. 1162-1165.
- [89] T. W. Shen, W. J. Tompkins, and Y. H. Hu, "Implementation of a on-lead (ECG) human identification system on a normal population," *Journal of Engineering and Computer Innovations*, vol. 2, no. 1, pp. 12-21, January 2011, 2011.
- [90] N. Venkatesh, and S. Jayaraman, "Human electrocardiogram for biometrics using DTW and FLDA," in 20th International Conference on Pattern Recognition, 2010, pp. 3838-3841.
- [91] W. Wei, W. Honggang, M. Hempel *et al.*, "Secure Stochastic ECG Signals Based on Gaussian Mixture Model for e-Healthcare Systems," *Systems Journal, IEEE*, vol. 5, no. 4, pp. 564-573, 2011.

- [92] N. Abhishek, N. Karthik, and J. A. K, "Biometric Template Transformation: A Security Analysis."
- [93] M. Li, and S. Narayanan, "Robust ECG biometrics by fusing temporal and cepstral information," in 20th International Conference on Pattern Recognition, 2010, pp. 1326-1329.
- [94] J. L. C. Loong, S. K.S, R. Besar *et al.*, "A new approach to ECG biometric systems : A comparative Study between LPC and WPD," in Wprld Academy of Science, Engineering and Technology, 2010, pp. 759-764.
- [95] A. Lourenco, H. Silva, and A. L. N. Fred, "Unveiling the biometric potential of finger-based ECG signals," *Computational Intelligence and Neuroscience*, vol. 2011, pp. 8 (Article ID 720971), 2011.
- [96] M. Tawfik, and T. Kamal, "Human identification using QT signal and QRS complex of the ECG," *The online Journal on Electronics and Electrical Engineering*, vol. 3, no. 1, pp. 383-387, 2011.
- [97] M. Tawfik, H. Selim, and T. Kamal, "Human Identification using time normalized (QT) signal and the QRS complex of the ECG," in 7th International Conference of Communication System Networks and Digital Signal Processing July 2010, pp. 755-759.
- [98] G. B. Moody, and R. G. Mark, "The impact of the MIT-BIH Arrhythmia Database," *Engineering in Medicine and Biology Magazine, IEEE*, vol. 20, no. 3, pp. 45-50, 2001.
- [99] A. Taddei, G. Distante, M. Emdin *et al.*, "The European ST-T Database: standard for evaluating systems for the analysis of ST-T changes in ambulatory electrocardiography," *European Heart Journal*, vol. 13, pp. 1164-1172, 1992.
- [100] J. Simon, and K. Conring. "Physikalisch-Technische Bundesanstalt (PTB) database," 10 Desember, 2009; http://www.ptb.de/index_en.html.
- [101] T. W. Shen, "Applied ECG biometric technology for disability population," in Proceedings of the 2nd International Convention on Rehabilitation Engineering & Assistive Technology, 2008, pp. 103-107.

- [102] Y. Wang, F. Agraftoti, D. Hatzinakos *et al.*, "Analysis of human electrocardiogram for biometric recognition," *EURASIP Journal on Advances in Signal Processing*, vol. 2008, no. 148658, 2008.
- [103] O. Boumbarov, Y. Velchev, and S. Sokolov, "ECG personal identification in subspaces using radial basis neural networks," in *Intelligent Data Acquisition and Advanced Computing Systems: Technology and Applications*, 2009. IDAACS 2009. IEEE International Workshop on, 2009, pp. 446-451.
- [104] Y. Wan, and J. Yao, "A neural network to identify human subjects with electrocardiogram signals," in *Proceedings of the World Confress on Engineering and Computer Science (WCECS 2008)*, San Francisco, USA, 2008, pp. 13-16.
- [105] Y. N. Singh, and P. Gupta, "ECG to Individual Identification," in *Biometrics: Theory, Applications and Systems*, 2008. BTAS 2008. 2nd IEEE International Conference on, 2008, pp. 1-8.
- [106] Y. N. Singh, and P. Gupta, "Biometric method for human identification using electrocardiogram," in *Proceedings of the 2nd IAPR/ IEEE International Conference on Biometric*, Seoul, Korea, 2009.
- [107] E. F. T. K. Sang, "Memory-Based Shallow Parsing," *Journal of Machine Learning Research*, vol. 2, pp. 559-594, 2002.
- [108] Barbara G. Tabachnick, and L. S. Fidell, "Using Multivariate Statistics," pp. 339-350: Allyn and Bacon, 2001.
- [109] W. Yongjin, K. N. Plataniotis, and D. Hatzinakos, "Integrating Analytic and Appearance Attributes for Human Identification from ECG Signals," in *2006 Biometrics Symposium: Special Session on Research at the Biometric Consortium Conference*, 2006, pp. 1-6.
- [110] G. Jiexin, F. Agraftoti, H. Mohammadzade *et al.*, "ECG for blind identity verification in distributed systems," in *Acoustics, Speech and Signal Processing (ICASSP)*, 2011 IEEE International Conference on, 2011, pp. 1916-1919.
- [111] S. Suppappola, and S. Ying, "Nonlinear transforms of ECG signals for digital QRS detection: a quantitative analysis," *Biomedical Engineering, IEEE Transactions on*, vol. 41, no. 4, pp. 397-400, 1994.

- [112] L. Wang, G. Leedham, and S. Y. Cho, "Infrared imaging of hand vein patterns for biometric purposes," *IET Computer Vision*, vol. 1, no. 3-4, pp. 113-122, 2007.
- [113] S. I. Safie, J. J. Soraghan, and L. Petropoulakis, "Pulse Active Bit (PAB) feature extractor for ECG biometric authentication," in *Systems, Signals and Image Processing (IWSSIP)*, 2011 18th International Conference on, 2011, pp. 1-4.
- [114] S. I. Safie, J. J. Soraghan, and L. Petropoulakis, "ECG biometric authentication using Pulse Active Width (PAW)," in *Biometric Measurements and Systems for Security and Medical Applications (BIOMS)*, 2011 IEEE Workshop on, 2011, pp. 1-6.
- [115] S. I. Safie, J. J. Soraghan, and L. Petropoulakis, "Pulse Active Mean (PAM): A PIN supporting feature extraction algorithm for doubly secure authentication," in *Information Assurance and Security (IAS)*, 2011 7th International Conference on, 2011, pp. 210-214.
- [116] S. I. Safie, J. J. Soraghan, and L. Petropoulakis, "Electrocardiogram (ECG) Biometric Authentication Using Pulse Active Ratio (PAR)," *Information Forensics and Security, IEEE Transactions on*, vol. 6, no. 4, pp. 1315-1322, 2011.
- [117] S. I. Safie, J. J. Soraghan, and L. Petropoulakis, "Pulse Active Ratio (PAR): A new feature extraction technique for ECG biometric authentication," in *Signal and Image Processing Applications (ICSIPA)*, 2011 IEEE International Conference on, 2011, pp. 16-21.
- [118] ECGPUWAVE, "[http://www.physionet.org/.](http://www.physionet.org/)"
- [119] E. Billauer. "Peak detection using MATLAB , <http://www.billauer.co.il/peakdet.html>," 2010.
- [120] S. I. Safie, J. J. Soraghan, and L. Petropoulakis, "ECG Based Biometric for Doubly Secure Authentication," in *19th European Signal Processing Conference, EUSIPCO 2011, Barcelona, 2011*, pp. 2274-2278.
- [121] Lachlan Gunn. "Would you use biometric technology at an ATM?," June, 2011; <http://www.finextra.com/community/fullblog.aspx?blogid=4419>

- [122] Link. "PIN Change," 5 December 2011; <http://www.link.co.uk/Cardholders/Pages/PINchange.aspx>.
- [123] M. Bond, and P. Zielinski, *Decimalisation table attacks for PIN cracking*, University of Cambridge, 2003.
- [124] Webster, John G.; , "Reducing Motion Artifacts and Interference in Biopotential Recording," *Biomedical Engineering, IEEE Transactions on* , vol.BME-31, no.12, pp.823-826, Dec. 1984.
- [125] Huhta, James C.; Webster, John G.; , "60-Hz Interference in Electrocardiography," *Biomedical Engineering, IEEE Transactions on* , vol.BME-20, no.2, pp.91-101, March 1973.
- [126] Van Alste, J. A.; Schilder, T. S.; , "Removal of Base-Line Wander and Power-Line Interference from the ECG by an Efficient FIR Filter with a Reduced Number of Taps," *Biomedical Engineering, IEEE Transactions on* , vol.BME-32, no.12, pp.1052-1060, Dec. 1985
- [127] Zhi-Dong Zhao; Yu-Quan Chen; , "A New Method for Removal of Baseline Wander and Power Line Interference in ECG Signals," *Machine Learning and Cybernetics, 2006 International Conference on* , vol., no., pp.4342-4347, 13-16 Aug. 2006.
- [128] J Slocum, E Byrom, L McCarthy, A Sahakian, and S Swiryn "Computer detection of atrioventricular dissociation from surface electrocardiograms during wide QRS complex tachycardias" *Circulation*, vol 72, pp 1028-1036, 1985.
- [129] Thakor, Nitish V.; Webster, John G.; Tompkins, Willis J.; , "Estimation of QRS Complex Power Spectra for Design of a QRS Filter," *Biomedical Engineering, IEEE Transactions on* , vol.BME-31, no.11, pp.702-706, Nov. 1984
- [130] S. Reza, "The open-source electrophysiological toolbox", Shiraz University, 1st April 2012; <http://www.oset.ir/>.
- [131] Iyengar N, Peng C-K, Morin R, Goldberger AL, Lipsitz LA. Age-related alterations in the fractal scaling of cardiac interbeat interval dynamics. *Am J Physiol* 1996;**271**:1078-1084

- [132] T Penzel, GB Moody, RG Mark, AL Goldberger, JH Peter. [The Apnea-ECG Database](#). *Computers in Cardiology* 2000;27:255-258.
- [133] Thakor, N.V.; Zhu, Y.-S.; , "Applications of adaptive filtering to ECG analysis: noise cancellation and arrhythmia detection," *Biomedical Engineering, IEEE Transactions on* , vol.38, no.8, pp.785-794, Aug. 1991
- [134] Xue, Q.; Hu, Y.H.; Tompkins, W.J.; , "Neural-network-based adaptive matched filtering for QRS detection," *Biomedical Engineering, IEEE Transactions on* , vol.39, no.4, pp.317-329, April 1992.